UNIVERSITY OF BORÅS
SCIENCE FOR THE PROFESSIONS

Modular textile-enabled bioimpedance system for personalized health monitoring applications

JAVIER FERREIRA GONZÁLEZ

Doctoral Thesis

Royal Institute of Technology, KTH
School of Technology and Health
Stockholm, Sweden 2017

Technical University of Madrid, UPM
School of Telecommunications
Systems and Engineering
Madrid, Spain 2017

ISBN 978-91-7729-377-4
ISSN 1653-3836
ISRN/KTH/STH/2017:6-SE
TRITA-STH Report 2017:6

Royal Institute of Technology, KTH
School of Technology and Health
SE-100 44 Stockholm
SWEDEN

University of Borås, UB
Faculty of Care Science, Work Life and Social Welfare
SE-501 90 Borås
SWEDEN

Technical University of Madrid, UPM
School of Telecommunications Systems and Engineering
ES-28031 Madrid
SPAIN

Dedicated to my family,
friends and Evelyn

Abstract - English

A growing number of factors, including costs, technological advancements, ageing populations, and medical errors, are leading industrialized countries to invest in research on alternative solutions to improve their health-care systems and increase patients' quality of life. Personal health systems (PHS) examplify the use of information and communication technologies that enable a paradigm shift from the traditional hospital-centered healthcare delivery model toward a preventive and person-centered approach. PHS offer the means to monitor a patient's health using wearable, portable or implantable systems that offer ubiquitous, unobtrusive bio-data acquisition, allowing remote monitoring of treatment and access to the patient's status. Electrical bioimpedance (EBI) technology is non-invasive, quick and relatively affordable technique that can be used for assessing and monitoring different health conditions, *e.g.*, body composition assessments for nutrition. When combined with state-of-the-art advances in sensors and textiles, EBI technologies are fostering the implementation of wearable bioimpedance monitors that use functional garments for personalized healthcare applications. This research work is focused on the development of wearable EBI-based monitoring systems for ubiquitous health monitoring applications. The monitoring systems are built upon portable monitoring instrumentation and custom-made textile electrode garments. Portable EBI-based monitors have been developed using the latest material technology and advances in system-on-chip technology. For instance, a portable EBI spectrometer has been validated against a commercial spectrometer for total body composition assessment using functional textile electrode garments. The development of wearable EBI-based monitoring units using functional garments and dry textile electrodes for body composition assessment and respiratory monitoring has been shown to be a feasible approach. The availability of these measurement systems indicates progress toward the real implementation of personalized healthcare systems.

Keywords: personal healthcare system • electrical bioimpedance • wearable • pervasive • portable • monitoring • body composition • chronic kidney disease • wireless sensor • ubiquitous • instrumentation

Sammanfattning - Svenska

Ett flertal faktorer, såsom stigande kostnader, tekniska framsteg, en åldrande befolkning, etc. har fått de industrialiserade länderna att investera i forskning kring alternativa lösningar för att förbättra hälso- och sjukvårdssystemen och därmed öka patienternas livskvalitet. Personliga hälso- och sjukvårdssystem (PHS) är exempel på informations- och kommunikationsteknik som möjliggör ett paradigmskifte från den traditionella sjukhuscentrerade vårdmodellen mot en strategi av personcentrering och förebyggande. PHS erbjuder möjlighet att övervaka en patients hälsa med hjälp av bärbara, portabla eller implanterbara system som för icke-påverkande insamling av fysiologiska signaler överallt. Detta medger fjärrövervakning av behandling och patientstatus. Elektrisk bioimpedans (EBI) teknik är en icke-invasiv, snabb och relativt billig teknik som kan användas för att bedöma och övervaka olika hälsotillstånd, t ex uppskatta kroppssammansättning. I kombination med state-of-the-art framsteg inom sensorer och smarta textilier, stödjer EBI teknik införandet av bärbara bioimpedansmonitorer som använder funktionella plagg i personbaserade vårdapplikationer. Denna forskning fokuserar på utveckling av bärbara EBI baserade övervakningssystem för hälsoövervakningstillämpningar. Övervakningssystemen bygger på bärbara övervakningsinstrument och textila elektroder insydda i kläderna. Bärbara EBI-baserade monitorer har utvecklats med hjälp av den senaste materialteknologi och framsteg inom system-on-chip-teknik. Exempelvis, har en bärbar EBI spektrometer utvärderats mot en kommersiell spektrometer för bedömning kroppssammansättning med användning av ett textilelektrodplagg. Utvecklingen av bärbara EBI baserade övervakningsenheter som använder funktionella plagg och torra textila elektroder för bedömning av kroppssammansättning och för andningsövervakning har visat sig tillhandahålla en genomförbar lösning. Tillgången på sådana mätsystem erbjuder klara steg fram emot det faktiska utnyttjandet i personliga vårdsystem.

Nyckelord: Personliga hälso- och sjukvårdssystem • elektrisk bioimpedans • bärbar • genomträngande • portabel • övervakning • kroppssammansättning • kronisk njursjukdom • omgivnings bistå levande • trådlös sensor • allestädes närvarande

Resumen - Español

Los países industrializados se enfrentan a numerosos retos relacionados con el mantenimiento y la mejora de calidad de sus sistemas de atención médica. Algunos de los retos más acuciantes en estos países están relacionados con el control de costes, la integración de avances tecnológicos, el envejecimiento de la población o la detección y minimización de errores en la práctica clínica. Dada la importancia de hacer frente a estos retos, se está realizando una gran inversión en el desarrollo de soluciones alternativas a las prácticas tradicionales, de forma que se facilite una atención médica más aceptable para los pacientes y con unos costes asumibles por la sociedad. Los sistemas de salud personal (PHS, por sus siglas en inglés) examinan el uso de tecnologías de información y comunicación para crear y potenciar un cambio paradigmático desde el modelo tradicional de atención sanitaria centrado en el hospital hacia un enfoque preventivo y centrado en la persona. Los PHS ofrecen los medios para monitorizar la salud de un paciente utilizando sistemas portables, portátiles o implantables en el paciente. Estos sistemas habilitan la adquisición ubicua y discreta de todo tipo de datos con relevancia clínica, incluidos datos biológicos del paciente, permitiendo la monitorización remota del tratamiento y el acceso al estado actual del paciente. Una de las tecnologías aplicables a los PHS es la tecnología de bioimpedancia eléctrica (EBI). La EBI es una técnica no invasiva, rápida y asequible que puede usarse para evaluar y monitorizar diferentes condiciones de salud como la composición corporal del paciente con fines nutricionales. Cuando estas técnicas se combinan con avances de última generación en sensores y textiles, las tecnologías resultantes habilitan la implementación de sistemas de monitorización de bioimpedancia portátiles e integrados en prendas funcionales para aplicaciones de atención médica personalizadas. Este trabajo de investigación se centra en el desarrollo de sistemas de monitorización basados en sistemas de bioimpedancia portátiles para aplicaciones de monitorización de salud ubicuas. Los sistemas de monitorización, desplegados en forma de instrumentación portátil y prendas textiles funcionales como sensores, se han desarrollado utilizando las últimas tecnologías de materiales y los avances en la tecnología de sistemas sobre chip. En concreto, un espectrómetro EBI portátil ha sido validado contra un espectrómetro comercial para la evaluación de la composición corporal total usando prendas funcionales que incorporan electrodos textiles. Se ha demostrado la validez de este tipo de sistemas, junto a textiles funcionales actuando como electrodos, en la evaluación de la composición corporal o la monitorización de las funciones respiratorias. La disponibilidad de estos sistemas de medida indica el progreso hacia la implementación real de sistemas de salud personalizados.

Palabras clave: sistemas de monitorización personales • bioimpedancia eléctrica • usable • portátil • monitorización • composición corporal • enfermedad renal crónica • sensor inalámbrico • omnipresente

Preface

This PhD research has been conducted as part of a double PhD degree with agreement between the School of Technology and Health (STH) at the Royal Institute of Technology (KTH) in Stockholm, Sweden and the School of Telecommunications Systems and Engineering (ETSIST) at the Technical University of Madrid (UPM) in Spain.

This research was performed at the University of Boras (UB) in Sweden under the supervision of Professor Kaj Lindecrantz from KTH, Professor Fernando Seoane from KTH and UB in Sweden; and Dr. Ivan Pau de la Cruz from UPM in Spain.

Acknowledgments

I would like to express my sincere gratitude to my supervisors and mentors Professor Kaj Lindecrantz, Professor. Fernando Seoane and Dr. Ivan Pau de la Cruz, for their support during my research studies and the development of this thesis work.

I want to express special gratitude to all friends and workmates that I have encounter during the Swedish chapter of my life. I thank my fellow work mates Ruben Buendia, Juan Carlos Marquez, Martin Bohlen, Jorge Ferreira, David Ayllon, Reza Atefi, Charlie Wand and Farhad Abtahi, for all those working discussions, fikas and necessary parties. Also, I thank all my Spanish friends, specially Teresita's friends ; Jose Luis, Ahinoa, Vanesa, Emilio, Beatriz and their respective life partners, also Nocilla's team; Alberto, Pipete, Pablo, Morales, Nacho and Carlitos , and with special mention to my dear friend Rene Manzanas.

Last but not least, I would especially like to thank my parents Daniel Ferreira and Catalina González as well as my brother Pablo for their guidance and support throughout my life. In addition, I would like to mention Sonaiska Barber, Jenny, Uwe, Christian, Brenda and little Jorinde for their unconditional support and fun moments. Finally, I would like to express my deepest gratitude to my girlfriend Evelyn Lebis for her love, patience and never ending support.

Muchas gracias a todos!

Thank you very much to all!

Tack så mycket alla!

Javier Ferreira

December, 2016

List of appended papers

This thesis includes the following appended papers, which will be referred to and numbered using Roman numerals. The complete papers are attached as appendices at the end of this document.

Paper I ***"An analog front-end enables electrical impedance spectroscopy system on-chip for biomedical applications"***, F. Seoane, **J. Ferreira**, J. J. Sanchez *et al. Journal Physiological Measurement,* Vol. 29, S267-S278, 2008. [J1]

Paper II ***"AD5933-based spectrometer for electrical bioimpedance applications"***, **J. Ferreira**, F. Seoane, A. Ansede Peña *et al.*, *Published in Journal of Physics: Conference Series Vol. 224, doi:10.1088/1742-6596/224/1/012011 and presented at the XIVth International Conference on Electrical Bioimpedance & XIth Electrical Impedance Tomography, Florida, 2010. [C1]*

Paper III ***"AD5933-based electrical bioimpedance spectrometer; towards textile-enabled applications"***. **J. Ferreira**, F. Seoane, and K. Lindecrantz. *33rd Annual International Conference of the IEEE Engineering in Medicine and Biology Society, Boston, USA 2011*. [C4]

Paper IV ***"A handheld and textile-enabled bioimpedance system for ubiquitous body composition analysis. An initial functional validation"***, J. Ferreira, I. Pau, K. Lindecrantz, *et al.* IEEE Journal on Biomedical and Health Informatics, DOI 10.1109/JBHI.2016.2628766, 2016, [J6]

Paper V ***"Portable bioimpedance monitor evaluation for continuous impedance measurements. Towards wearable plethysmography applications"***. **J. Ferreira**, F. Seoane, and K. Lindecrantz. 35st Annual International Conference of the IEEE Engineering in Medicine and Biology Society, EMBS, Osaka, Japan, 2013. [C9]

Paper VI ***"Wearable biomedical measurement systems for assessment of mental stress of combatants in real time"***. F. Seoane, I. Mohino-Herranz, **J. Ferreira** *et al.* Sensors, vol. 14, no. 4, pp. 7120-7141, 2014 [J3]

Paper VII ***"Assessment of mental, emotional and physical stress through analysis of physiological signals using smartphones"***. I. Mohino-Herranz, R. Gil-Pita**, J. Ferreira**, *et al.* Sensors 2015, 15(10), 25607-25627; doi:10.3390/s151025607. [J5]

Division of work between authors: Each author's contribution at different stages of the reported studies is described in the following paragraphs.

Paper I ***"An analog front-end enables electrical impedance spectroscopy system on-chip for biomedical applications"***

Ferreira, Sanchez, Bragos and Seoane contributed to the experimental design and idea. Data acquisition was executed by Ferreira and Sanchez. Data analysis was performed by Ferreira, Sanchez and Seoane. The study was reported by Bragos and Seoane.

Paper II ***"AD5933-based spectrometer for electrical bioimpedance applications"***

Ferreira developed the analog front end used for the experiment and Ansede, Ferreira and Seoane contributed to the design of the study. Data acquisition was carried out by Ansede. Data analysis was performed by Ansede and Ferreira and reported by Ferreira and Seoane.

Paper III ***"AD5933-based electrical bioimpedance spectrometer; towards textile-enabled applications"***

Ferreira designed and implemented the bioimpedance spectrometer used for the experiments. Ferreira and Seoane contributed to the data acquisition and data analysis. The study was reported by Ferreira.

Paper IV ***"A handheld and textile-enabled bioimpedance system for ubiquitous body composition analysis. Initial functional validation"***

Ferreira designed the experiment and performed the data acquisition and data analysis. The study was reported by Ferreira and reviewed by Seoane, Pau and Lindecrantz.

Paper V ***"Portable bioimpedance monitor evaluation for continuous impedance measurements. Towards wearable plethysmography applications"***

Ferreira designed the experiment and performed the data acquisition and data analysis. The study was reported by Ferreira and reviewed by Seoane and Lindecrantz.

Paper VI ***"Wearable biomedical measurement systems for assessment of mental stress of combatants in real time"***

Ferreira developed the monitoring devices, Ferreira and Seoane developed the monitoring textile garments. The validations measurements were performed by Alvarez, Ayllón, Llerena and Gil-Pita. The data analysis, report and review were performed by all the authors.

Paper VII ***"Assessment of mental, emotional and physical stress through analysis of physiological signals using smartphones"***

Ferreira developed the monitoring devices, and Ferreira and Seoane developed the monitoring textile garments. The validation measurements were performed by Mohino-Herranz and Gil-Pita. The data analysis, report and review were performed by all the authors.

Other scientific contributions

The following publications have been developed in connection with this research work but are not included in this thesis:

"Textile electrode straps for wrist-to-ankle bioimpedance measurements for body composition analysis. Initial validation and experimental results"

J. C. Marquez, **J. Ferreira**, F. Seoane *et al.* 32nd Annual International Conference of the IEEE Engineering in Medicine and Biology Society, Buenos Aires, Argentina, 2010. [C3]

"The challenge of the skin-electrode contact in textile-enabled electrical bioimpedance, measurements for personalized healthcare monitoring applications".

F. Seoane, J. C. Marquez, **J. Ferreira,** *et al.* Biomedical Engineering, Trends in Materials Science, A. N. Laskovski, ed., p. 564, ISBN: 978-953-307-513-6, 2011. [B1]

"Adaptive frequency distribution for electrical bioimpedance spectroscopy measurements"

F. Seoane, **J. Ferreira**, R. Buendia *et al.* 34th Annual International Conference of the IEEE Engineering in Medicine and Biology Society, San Diego, USA, 2012, pp. 562-565. [C6]

"Strechable circuit board technology enabling seamless textile-electronic integration for electrical muscle stimulation therapy"

F. Seoane, J. Gawell, **J. Ferreira**; *et al.* IDTechEx Printed Electronics USA, Santa Clara, USA, 2012. [C7]

"Bioimpedance-based wearable measurement instrumentation for studying the autonomic nerve system response to stressful working conditions"

J. Ferreira, R. Buendia, L. Alvarez *et al.* XV. International Conference on Electrical Bio-Impedance (ICEBI) and XIV. Conference on Electrical Impedance Tomography (EIT), Heilbad Heiligenstadt , Germany, 2013. [C8]

"Sensorized garments and textrode-enabled measurement instrumentation for ambulatory assessment of the autonomic nervous system response in the ATREC project"

F. Seoane**, J. Ferreira**, L. Alvarez, *et al.* Journal of Sensors 2013, 13(7), 8997-9015; doi:10.3390/s130708997. [J2]

"Utilizing smart textiles-enabled sensorized toy and playful interactions for assessment of psychomotor development on children"

M. Vega-Barbas, I. Pau, J. Ferreira, *et al.* Journal of Sensors, Volume 2015 (2015), Article ID 898047, 9 pages. [J4]

Table of contents

Abbreviations and symbols

Abbreviations

AFE	*Analog front end*
BCA	*Body composition analysis*
BIS	*Bioimpedance spectroscopy*
BMI	*Body mass index*
BZM	*Bioimpedance module*
CKD	*Chronic kidney disease*
CT	*Computed tomography*
CVC	*Current to voltage converter*
DDS	*Direct digital synthesis generator*
DEXA	*Dual energy X-ray absorptiometry*
DFT	*Discrete Fourier transform*
EBI	*Electrical bioimpedance*
EBIS	*Electrical bioimpedance spectroscopy*
EC	*Extra cellular*
ECF	*Extra cellular fluid*
FFM	*Fat free mass*
GND	*Ground potential*
HD	*Haemodialysis*
HHD	*Home haemodialysis*
IC	*Intra cellular*
ICF	*Intra cellular fluid*
ICT	*Information and communication technologies*
INA	*Instrumentation amplifier*
LC	*Lung composition*
LPF	*Low pass filter*
MRI	*Magnetic resonance imaging*
NLLS	*Non-linear least square*
PD	*Peritoneal dialysis*
PGA	*Programmable gain amplifier*
PHS	*Personalized healthcare system*
RR	*Respiration rate*
SMT	*Surface mount technology*

SoC	*System-on-chip*
SPP	*Serial port profile*
STD	*Standard deviation*
TBC	*Total body composition*
TBW	*Total body water*
TEB	*Thoracic electrical bioimpedance*
Textrode	*Textile electrode*
TOST	*Two one side equivalence test*
TRS	*Total right side*
VCV	*Voltage to current converter*

Symbols

Symbol	***Units***	***Meaning***
ω	*rad/s*	*Angular frequency*
α	-	*Dimensionless Cole parameter alpha*
τ	*sec*	*Relaxation time constant*
C_m	*farads*	*Membrane capacitance*
ECF	*liters*	*Extra cellular fluid content*
f_C	*Hz*	*Characteristic frequency*
H	*cm*	*Body height*
ICF	*liters*	*Intra cellular fluid content*
R_∞	*Ω*	*Resistance at infinite frequency*
R_0	*Ω*	*Resistance at zero frequency*
R_e	*Ω*	*Resistance extracellular medium*
R_i	*Ω*	*Resistance intracellular medium*
TBW	*liters*	*Total body water content*
W	*kg*	*Body weight*
Z_{ep}	*Ω*	*Electrode polarization impedance*
Z_{TUS}	*Ω*	*Impedance of the tissue under study*
ρ	*Ω·m*	*Electrical resistivity*
σ	$(\Omega \cdot m)^{-1}$	*Electrical conductivity*

Chapter 1

Introduction

A growing number of factors including aging populations and sedentary life styles, are increasing the demands on healthcare systems around the world (Zhaurova 2008, Owen, Sparling et al. 2010, Nations 2012). For example, in the European Union, over six countries had healthcare expenditures that exceeded 10% of their gross domestic product (GDP), while for the United States, healthcare expenditures were over 16% of the GDP, as reported in 2012 (Squires 2012, EuroStat 2015). Healthcare costs are rising substantially to levels such that further measures need to be taken to maintain healthcare service quality and sustainability.

Many initiatives within the European Union are targeting a paradigm shift from the traditional reactive hospital-centered approach toward a proactive, patient-oriented and self-managed approach, which could help to improve service quality, contribute to sustainability and reduce costs. For example, as of 2014, 97% of healthcare costs in the European Union were spent on treatment, with only 3% invested in prevention (Alliance 2014).

Managing and caring for patients with chronic diseases accounts for over 75% of healthcare costs in developed countries. For instance, in Spain, up to 80% of the total healthcare cost is dedicated to supplying services for managing chronic diseases, such as cardiovascular disease, kidney disease, diabetes and cancer. Half of the Spanish population, approximately 20 million, is suffering from at least one chronic disease, and at ages above 65 years the average amounts to four chronic diseases (Guerrero 2015).

For example, one of the most resource demanding diseases is chronic kidney disease (CKD), with morbidity of up to 12% of the population, and with more than 50% of patients being elderly patients and showing signs of different stages of this disease. Chronic kidney disease leads to a gradual and irreparable loss of renal function, known as end-stage renal disease (ESRD), where patients must undergo kidney replacement therapy through either periodic dialysis treatment or kidney transplantation. Although CKD is not common enough to be considered as a worldwide public health threat, it has reached epidemic proportions, with 10-12% of the population showing some signs of renal malfunction (Jha, Garcia-Garcia et al. 2013).

The latest technological advances in fields such as information and communication technologies (ICT), dialysis equipment or sensor technologies have enabled improvements in CKD treatment therapies (Diamantidis and Becker 2014) and the transition from conventional in-center hemodialysis to home-based dialysis treatments (Neuman 2012). Peritoneal dialysis (PD) and home hemodialysis (HHD) are life-saving home-based renal replacement treatments that, compared to conventional in-center hemodialysis (HD), provide similar long-term patient survival, fewer life-style restrictions, *e.g.* a more liberal diet, and more flexibility in terms of treatment location (Beard 2013).

Dialysis removes metabolic toxic waste and excess fluid (Henning 2007), with the target of replacing the compromised renal function of the patient (Drukker, Parsons et al. 1983). Fluid balance, also known as dry weight or euvolemic state, is an important goal of dialysis treatment (Kushner, de Vries et al. 1996), and assessing the dry weight value is critical for achieving a good therapeutic outcome (Wystrychowski and Levin 2007). Even for doctors in a clinical setting, accurate assessment of dry weight is currently a challenge (Miguel 2010). Consequently, at home, CKD patients should benefit from tools enabling the close monitoring of volume control (Van Biesen, Williams et al. 2011) for maintaining their proper fluid balance and treatment quality.

Personal healthcare solutions (PHS) offer the means to follow a patient's health using wearable, portable or implantable systems. These systems offer ubiquitous, unobtrusive biomedical data acquisition for the purpose of obtaining important information about the patient's health status and providing feedback to the patient to assist in disease prevention, treatment and lifestyle management. PHS provide health professionals with comprehensive monitoring and diagnostic data that will help them to improve their diagnoses and offer more effective care to their patients. PHSs are formed from different elements; typical PHS comprise the following elements: biomedical sensors, which could be wearable, portable or implantable; communications interfaces such as wireless technologies; signal processing; and artificial intelligence to assist professionals or patients with decision making and knowledge management. The use of PHS provides continuous health monitoring, disease management and ambient assisted living, which is expected to offer continuity of care, to improve a patient's quality of life and streamline healthcare. The monitoring of physiological signals with portable, unobtrusive and ubiquitous measurement devices is an essential component for the proliferation of home health monitoring applications as they allow remote access to patient status and treatment monitoring.

The monitoring applications of bioimpedance technology have proven it to be a useful, inexpensive and non-invasive daily-use monitoring technique for impedance cardiography (Van De Water, Miller et al. 2003), skin cancer detection (Aberg, Nicander et al. 2004) and monitoring nutrition status (Moissl, Wabel et al. 2006), among others. In the case of body composition assessment (BCA), the use of electrical bioimpedance spectroscopy (EBIS) methods (Buendia, Seoane et al. 2015) has been proven to be useful for monitoring the distribution of different body fluid compartments, such as total body water (TBW), extracellular (ECF) and intracellular (ICF) fluids, and fat mass (FT). For instance, patients suffering from CKD tend to accumulate excess fluids in the extracellular compartment, and EBIS methods have been used to assess the euvolemic state and to estimate the amount of fluid that should be removed by ultrafiltration (Kuhlmann, Zhu et al. 2005, Davies and

Davenport 2014). In most EBI-based applications, the measurements are performed by trained personal at a clinic or hospital a few times a week; therefore, the feasibility of EBI measurements for home-based monitoring applications has not been yet fully studied.

1.1 Objectives

The aim of this doctoral thesis work is to research new technologies that could facilitate the implementation of wearable monitoring sensors, which could be integrated in functional textile garments for the development of personal health system monitoring solutions. The wearable sensors are used to monitor biological signals, such as electrocardiogram, temperature, respiratory function or bioimpedance-related signals. These portable monitoring devices are designed to be unobtrusive and ubiquitous, and are specifically designed to work with dry textile electrode sensors and to be integrated seamlessly into functional textile garments for daily use.

The main goal of these research studies has been identified as follows:

> *Enable the development of novel wearable EBI-based monitoring solutions that could foster the proliferation of personalized health monitoring applications*

More specifically, this research work was initially focused on the development of a bioimpedance portable monitor that uses dry textile electrodes incorporated into functional garments to monitor body fluid distribution and that could enable the implementation of novel EBI-based PHS in , for example, patients who suffer from chronic kidney disease (CKD) and who require the maintenance of an euvolemic state through homecare dialysis.

According to the aforementioned requirements, and to evaluate this concept, two main research questions (RQ) have been identified:

> *RQ1: Could a custom-made wearable/portable bioimpedance spectrometer for ubiquitous personal health monitoring applications achieve the measurement performance of existing clinical measuring devices?*

Based on the previous research question, focusing on home-based EBI monitoring applications, the following research question has been formulated:

> *RQ2: Could the development of textile electrode-based garments in combination with the developed EBI spectroscopy monitor be used for continuous monitoring applications with similar measurement performance as existing clinical monitoring devices?*

During the course of this research, a new set research questions based on the results obtained from the developed EBIS monitoring system were formulated to

enable other types of EBI solutions. These research questions are described as follows:

> *RQ3: How feasible is to modify the developed EBI spectroscopy system for its use in EBI-based plethysmography applications?*

Based on the previous research question, focusing on home-based monitoring applications the following research question has been formulated:

> *RQ4: Could the development of textile electrode-based garments in combination with the developed EBI plethysmography unit be used for continuous monitoring applications?*

These research questions have been investigated in this dissertation work, and the research tasks performed herein were aimed at exploring the measurement performance of a small and portable custom-made EBI monitoring system that performed as well as commercial equipment at using textile electrodes with bioimpedance systems to monitor body fluids and at developing PHS as feasible option for bioimpedance technology and functional textile garments.

Although the goal of this research studies is to enable monitoring on PHS using functional textile garments, the personal healthcare system platform as such has not been implemented in this work; instead, only the first steps regarding the development of the monitoring instrumentation and functional textile garments have been validated. However, the obtained results have enabled the integration of the monitoring systems in dedicated PHS for monitoring fluid consumption specifically, the MySleeve project, which is introduced in the following sections.

1.2 Methodology

The research work performed in this doctoral thesis has been carried out following the scientific method in many of the developments and experiments done, where a hypothesis was formulated, tested and validated, and at the same time, the conclusion was used to reformulate newer hypotheses.

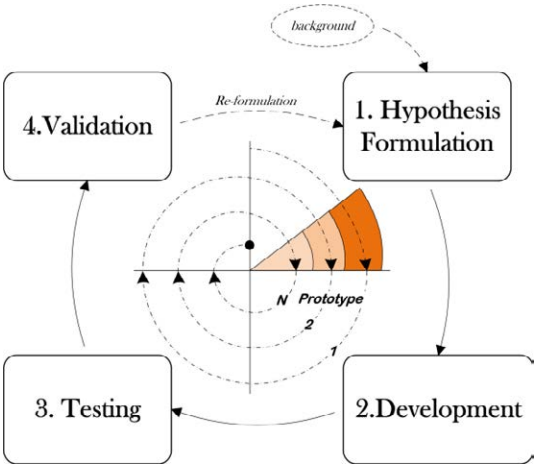

Figure 1.1 Spiral research methodology model

The following general four stages, as shown in Figure 1.1, were used in the development of this research work to answer the formulated research questions:

1. Hypothesis formulation: based on the identified problems, assertions, observations, previous experiments and background information, a hypothesis is formulated.
2. Development stage: covers all the experimental and prototype developments that are needed to perform the experiment.
3. Testing stage: the experiment is carried out, and data are collected for future analysis and verification.
4. Validation stage: observations and collected data are used for validation and drawing conclusions based on initial hypothesis.

Due to the complexity of the final solution, smaller tasks were developed to answer the formulated research questions partially and could help to progress toward the final solution; for instance, the development of an EBI monitoring system was covered in several iteration loops, where smaller system parts were first evaluated and used to implement the next iteration that could lead to a successful device development solution. Therefore, this research work was performed following a spiral implementation methodology, where, according to Figure 1.1, the results of previous experiments were used to reformulate and redefine the final solution, and several iterations were performed until a satisfactory solution was achieved.

1.3 Thesis outline

This doctoral dissertation is divided into a total of six chapters, and seven appended publications at the end of this document. Following this first chapter, Chapter 2 provides a brief introduction to personalized health solutions, electrical bioimpedance technology and some of the more relevant EBI monitoring applications. Chapter 3 describes the materials used for the development of the portable monitoring systems, including the measurement instrumentation, the dry textile electrode materials and the system requirements. The results obtained in this

research work are summarized in Chapter 4, which is divided into two sections. The first section of Chapter 4 covers the implementation results for the portable bioimpedance spectrometer and textile garments used for body composition assessments. The second section in Chapter 4 presents the results obtained for the wearable EBI monitor system used for plethysmography applications, covering the validation tests and functional textile garment description. In Chapter 5, the results are discussed and used to draw conclusions. Finally, Chapter 6 alphabetically lists all the references used in this doctoral dissertation.

Chapter 2

Background

2.1 Personalized health monitoring systems

Personal health systems (PHS) exemplify the use of information and communication technologies (ICT) and other technologies to enable a paradigm shift from the traditional reactive hospital centered healthcare delivery model toward a preventive, proactive and person centered model that could help to reduce costs, improve service quality and contribute to sustainability.

The use of ICT as a tool for enhancing the quality, accessibility and efficiency of healthcare systems has been supported extensively by the European Commission since the launch of the eEurope 2002 action plan (European Commission 2000). For instance, the European project *PHS2020* (Codagnone 2009) was focused on identifying existing healthcare gaps and proposing a number of research roadmaps to turn PHS into a reality. Within the *PHS2020* project and with the collaboration of many experts, the following definition of PHS was elaborated:

Personal health systems assist in the provision of continuous, quality controlled, and personalised health services to empowered individuals regardless of location. They consist of:

a) *Ambient and/or body (wearable, portable or implantable) devices, which acquire, monitor and communicate physiological parameters and other health related context of an individual (e.g., vital body signs, biochemical markers, activity, emotional and social state, environment);*
b) *Intelligent processing of the acquired information and coupling of it with expert biomedical knowledge to derive important new insights about individual's health status.*
c) *Active feedback based on such new insights, either from health professionals or directly from the devices to the individuals, assisting in diagnosis, treatment and rehabilitation as well as in disease prevention and lifestyle management.*

The underlying PHS concept is to empower individual health responsibility while targeting a paradigm shift from the traditional reactive hospital-centered healthcare approach toward a proactive and patient-oriented approach.

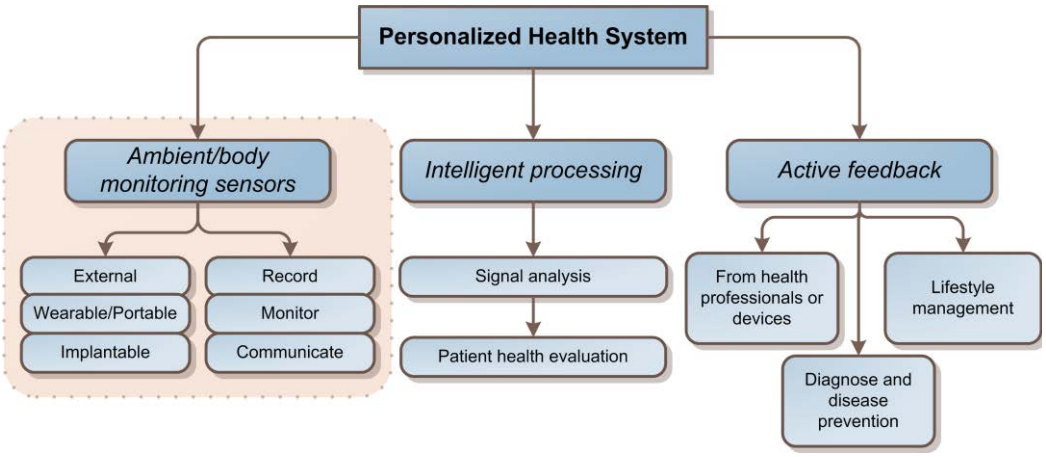

Figure 2.1 Personalized health system component diagram.

This PHS definition, represented in Figure 2.1, provides a good approach to identify and frame all of the different elements that are normally present in these types of health monitoring solutions.

Monitor sensors are an essential part of any PHS, since they are responsible for providing the patient health data that will be used by the signal processing unit to evaluate the patient health status. Some of the main functions of the monitoring sensor are to record, display and transfer the patient data to the storage and processing unit. The storage unit can be situated locally in a patient terminal or externally in a healthcare server. Depending on the size and integration level, the monitoring sensors can be categorized as portable, wearable or implantable. The intelligent processing unit is responsible for using the measured sensor data and appling the selected signal analysis algorithms in order to provide the right information that will help with evaluating the patient health status. The active feedback unit is in charge of representing the processed information that can be used to assist in diagnosis or treatment, as well as to help with disease prevention and lifestyle management.

A typical example of a personal health system solution is represented in Figure 2.2, where all the aforementioned elements of PHS are represented, as well as the flow of sensor information from the user to the healthcare server, and the feedback information from the caregivers to the user.

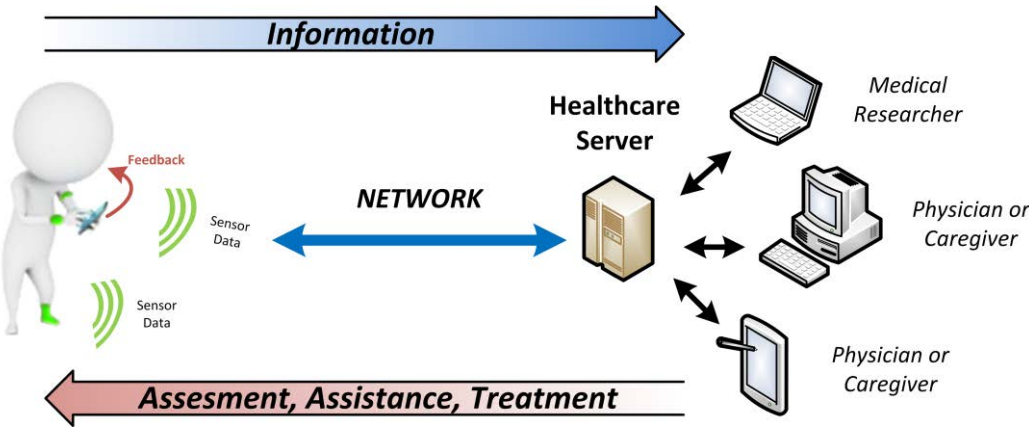

Figure 2.2 Pesonal health system architecture diagram example.

Notwithstanding the potential benefits of PHS applications, there are currently still barriers that hinder the deployment of eHealth solutions. New action plans from the European Commission, such as *the eHealth Action Plan 2012-2020* (European Commission 2012) and the publication from *C. Fernandez-Llatas et. al.*(Fernandez-Llatas, Martinez-Romero et al. 2016) are targeting the identification of barriers and making recommendations for the successful implementation of eHealth applications.

An important aspect for the successful implementation of PHS is system standardization since the personal health system solutions will be deployed in many different scenarios, countries and healthcare systems. Hence, the Continua Health Alliance (Continua Health Alliance 2012) and the white paper resulting from the *HeartCycle* Project (Lekka, Reiter et al. 2008) seek to identify different recommendations that need to be followed for a successful standardization of PHS. The *HeartCycle* document gives an overview of the current certification procedures for PHS in Europe, identifying major gaps and drafting recommendations. Nevertheless, to realize the potential of eHealth applications, designing new elements to be used in a personal health system solution will require the standardization, quality assurance and interoperability of systems.

2.1.1 Monitoring sensors

A sensor is defined as a device that detects some type of input from the physical environment and then provides a corresponding output. The physical input could be in the form of light, heat, motion, pressure, electricity, etc.

In biomedical applications, sensors are selected to obtain any physiological or other health related parameters of an individual that could be used to clinically assist in diagnosis, treatment, disease prevention and lifestyle management. The range of biological signals that can be obtained is very broad, but some of the most popular biological signals used are enumerated as follows:

- Biopotential signals, such as electrocardiography (ECG), which monitors the electrical activity of the heart, electroencephalography (EEG) , which

monitors the electrical activity of the brain, or electromyography (EMG), which is used to monitor the electrical activity of muscle tissue.

- Optical measurements, such as photoplethismography (PPG), which is used to monitor blood flow volume changes.
- Bioimpedance measurements, which are used to characterize biological tissues.
- Concentration, amount or presence of biochemical substances, which can be used to monitor any sign of disease or other abnormality.

Monitoring sensing devices used in biomedical application are typically composed of sensing, processing and output functional modules, as well as the power unit. The sensing unit is responsible for translating the physical signal into an electrical one that the processing unit could use. The processing unit is responsible for reading the electrical signal from the sensing unit and, performing some kind of signal processing to transfer the data to the output module. The processing unit is normally implemented by a microprocessor unit running a small piece of software to handle all the functions, including sensor signal acquisition, data processing and data transmission. The main purpose of the output unit is to either store, display, transfer or perform a specific function depending on the measured signal and application.

A continuous glucose monitor (CGM) device, as shown in Figure 2.3, is an example of a biomedical monitoring device that periodically monitors blood glucose levels and accordingly activates an insulin pump to maintain proper glucose levels. In adition, all the measurements and pump action data can be displayed or stored in the device for future use.

Figure 2.3 Continuous glucose monitoring system by Medtronic, image source (Medtronic 2016)

In addition to fulfilling the standards for patient electrical safety (International Electrotechnical Commission 2010) and the Medical Devices Directives (European Commission 2007), other requirements must be considered for the successful development of PHS monitoring devices, including usability, trustworthiness, system maintenance and system interoperability.

2.2 Electrical bioimpedance technology

Biological tissue is mainly composed of cells and fluids. For example, in the human body, muscle tissue consists of long and tubular cells called myocytes, which contract to produce force. The cell is considered the basic structural and functional unit of all biological organisms, and it may exist as an independent unit of life under certain conditions. Generally, a cell is encompassed by a lipid bilayer membrane, known as the cell membrane, which isolates the intracellular (IC) medium from the extracellular (EC) medium. The IC space contains the cell organelles, the cell nucleus and other cell components. The EC space surrounding the cells is divided into two major sub compartments: the interstitial fluid and blood plasma. Due to the existence of free ions, *e.g.*, sodium (Na^+), potassium (K^+), chlorine (Cl^-), protein ions , *etc.*, in the IC and EC mediums, biological tissue can be considered as an electrolyte with passive and active electrical properties. Regarding passive electrical properties, the IC and EC mediums are considered as ionic conductors, and together with the non-conducting dielectric lipid cell membrane, they behave as a capacitor.

Early studies of biological tissues and electricity contributed to the discovery and characterization of electrical properties of tissue (Fricke and Morse 1925, Schwan 1957). Based on the assumption that the cells are suspended in the EC medium with conductive electrical properties*, H. Fricke* presented the electrical equivalent model of blood cells. This model, apart from being precise, has been fully recognized and extensively used with acceptable results. Fricke's representation model is shown in Figure 2.4.c, where R_e represents the resistance of the extra cellular medium, R_i the resistance of the IC medium and C_m represents the capacitance of the cell membrane. From Fricke's model in Figure 2.4, it is clear that if an external current is applied, the current will flow through different paths depending on the current frequency value. At low frequencies, the current will flow mainly through the EC medium. At higher frequencies, the modelled cell membrane capacitor will act as a shunt, allowing the current to flow through the IC and EC mediums.

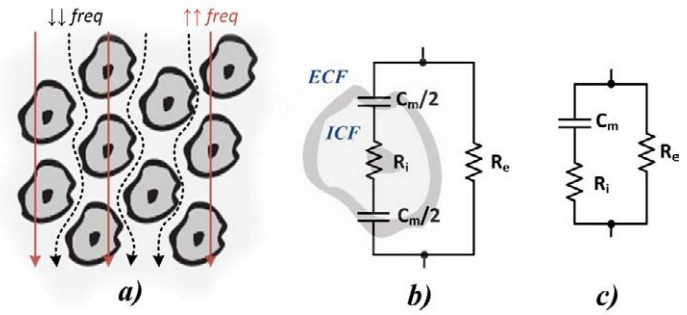

Figure 2.4 Fricke's cell suspension electrical model and its circuit representation.

Although Fricke's circuit model is a good model for a suspension of cells, it is less accurate for the more complex structures that constitute the human body. Other models, such as the Cole equation (Cole 1940), have been proposed and used, which shows a better agreement with the empirical data. Currently, the Cole model is used

in several EBI applications for tissue characterization such as in body composition analysis (BCA).

The passive electrical properties of biological tissue exhibit a certain dependency on the frequency of an externally applied electrical field. The conductivity (σ) and permittivity (ε) are passive electric properties of biological tissue that are expressed as a function of the frequency. The conductivity indicates how easily free charges move through a medium and is related to the conductance. The permittivity is the measure of the resistance that is encountered when an electric field is formed in a dielectric medium and is also expressed as the ability to permit storage of electric energy in a dielectric medium; this measurement is related to the conductance.

The impedance of biological tissue varies with the frequency, and four main specific dispersions windows have been identified: α, β, δ and γ (Schwan 1994, Schwan 1999). The α dispersion window, between 1 mHz up to a 1 kHz, and β dispersion window, between 1 kHz and 100 MHz, are quite relevant for clinical applications because within these dispersion windows is where most changes in the electric properties of human tissue occur, such as the accumulation of fluids or changes in cell structure due to a medical condition.

2.2.1 Bioimpedance measurements

The electrical impedance of a material is the opposition that the material offers to the flow of electrical charges through it. For materials of biological origin the term electrical bioimpedance (EBI) is used. To characterize the electrical tissue properties, an external energy source is needed; in EBI measurements, the source of energy is either an injected current or a voltage applied to the biological material through a set of electrodes. The resulting voltage or current is measured, and the impedance is obtained by applying Ohm's law equation, see Equation (2.1) where ω is the frequency in [rad/s].

$$Z_{(\omega)} = \frac{V_{(\omega)}}{I_{(\omega)}} \qquad (2.1)$$

Depending on the EBI application, there are two methods to obtain the impedance value: by exciting with a controlled current or with a controlled voltage. Each method has its own advantages and disadvantages (Grimnes and Martinsen 2008), but the most widely used technique involves a controlled current for excitation and measures the resulting voltage. The excitation current should be chosen to comply with the IEC-60601-1 standard for ensuring patient safety and electrical currents (IEC 2010).

2.2.2 Measurement electrode configuration

A typical EBI measurement requires two-, three- or four-contact points (Grimnes and Martinsen 2008) to measure the voltage and current values.

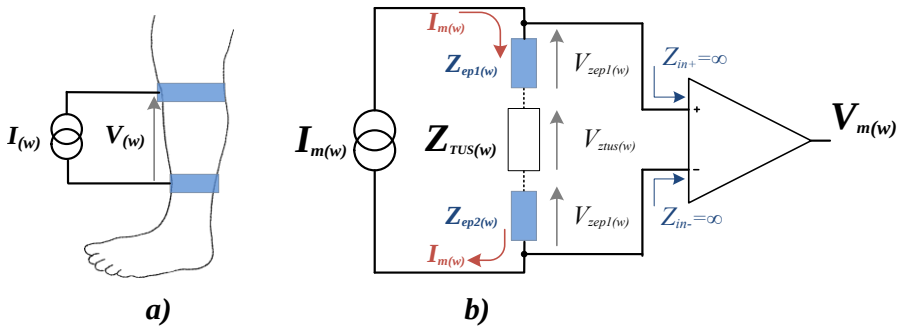

Figure 2.5 Bipolar EBI measurement configuration (a) and equivalent measurement circuit (b).

In a 2-electrode or bipolar EBI measurement, two electrodes are used to inject the current, and the same electrodes are used to sense the resulting voltage. In Figure 2.5, an example of an EBI bipolar configuration measurement of the lower part of the leg is displayed in (a), and the general bipolar configuration equivalent electrical circuit is shown in (b), where $I_{m(w)}$ is the constant current, $Z_{ep1(w)}$ and $Z_{ep2(w)}$ are the electrode polarization impedances, $Z_{tus(w)}$ is the measured impedance and $V_{m(w)}$ is the voltage obtained from the differential amplifier. The measured impedance can be expressed in terms of its equivalent electric circuit equation, as shown in Equation (2.2).

$$Z_{m\_2e(\omega)} = \frac{V_{m(\omega)}}{I_{m(\omega)}} = \frac{V_{zep1(\omega)} + V_{ztus(\omega)} + V_{zep2(\omega)}}{I_{m(\omega)}} \qquad (2.2)$$

Since the electrical current flows through the sensing electrodes, the voltage drop across $Z_{ep1(w)}$ and $Z_{ep2(w)}$ is included in the measured voltage together with the voltage over $Z_{tus(w)}$. Assuming that the electrode polarization impedances are approximately equal, the measured impedance equation $Z_{m\_2e(w)}$ is shown in Equation (2.3).

$$Z_{m\_2e(\omega)} = \frac{V_{m(\omega)}}{I_{m(\omega)}} = \frac{I_{m(\omega)} \cdot \left(2 \cdot Z_{ep(\omega)} + Z_{tus(\omega)}\right)}{I_{m(\omega)}} = 2 \cdot Z_{ep(\omega)} + Z_{tus(\omega)} \qquad (2.3)$$

For a 4-electrode or tetrapolar configuration, two electrodes are used to inject the current, and two electrodes are used to sense the resulting voltage. In Figure 2.6, a tetrapolar EBI measurement of the lower part of the leg is shown in (a), and a typical tetrapolar electrical circuit is displayed in (b). In Figure 2.6 (b), the impedances of the electrodes used to inject the current are $Z_{ep1(w)}$ and $Z_{ep2(w)}$, and the impedances of the electrodes used to sense the voltage are $Z_{ep3(w)}$ and $Z_{ep4(w)}$. The impedance is calculated according to Equation (2.4).

$$Z_{m\_4e(\omega)} = \frac{V_{m(\omega)}}{I_{m(\omega)}} = \frac{V_{zep3(\omega)} + V_{ztus(\omega)} + V_{zep4(\omega)}}{I_{m(\omega)}} \qquad (2.4)$$

Assuming an ideal differential amplifier, the measured impedance can be expressed by Equation (2.5).

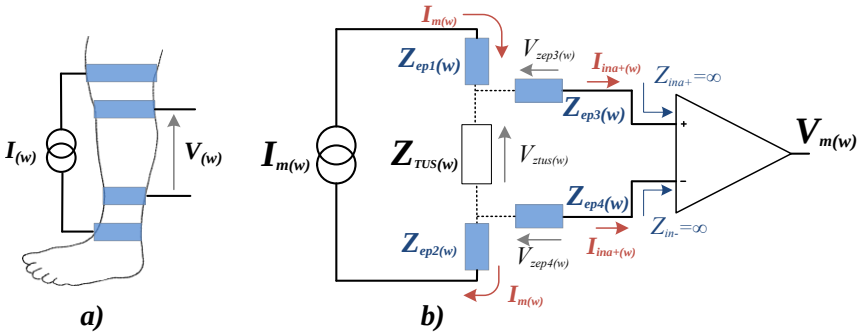

Figure 2.6 Tetrapolar EBI measurement configuration (a) and equivalent measurement circuit (b).

$$Z_{m\_4e(\omega)} = \frac{I_{m(\omega)} \cdot Z_{tus(\omega)}}{I_{m(\omega)}} = Z_{tus(\omega)} \qquad (2.5)$$

Since the input impedances Z_{ina+} and Z_{ina-} of an ideal differential amplifier are infinite, the currents and the voltages over the electrode polarization impedances $Z_{ep3(w)}$ and $Z_{ep4(w)}$ are equal to zero; therefore, the measured impedance $Z_{m(w)}$ is equal to $Z_{tus(w)}$. This advantage over a bipolar configuration makes the tetrapolar configuration the most commonly used configuration.

2.2.3 Impedance estimation methods

There are several possible methods to estimate the bioimpedance values after the voltage-current signals have been obtained. These methods include fast Fourier transform (FFT) techniques, sine correlation methods (Pallas-Areny and Webster 1993), gain-phase detectors (Yuxiang, Jue et al. 2006) and lock-in amplifiers.

One of the most widely used impedance estimation techniques is the sine correlation method, also named quadrature demodulation, and its functional block diagram is depicted in Figure 2.7. The injected current signal $I_{m(t)}$, typically a single sine waveform, flows through the unknown impedance Z. Then, the resulting voltage signal $V_{m(t)}$ is multiplied by the in-phase and in-quadrature components from the injected current signal that will be averaged and multiplied by a calibration factor, either a_{Re} or a_{Im}, in order to obtain the real $Re_{Z(t)}$ and imaginary $Im_{Z(t)}$ impedance component values.

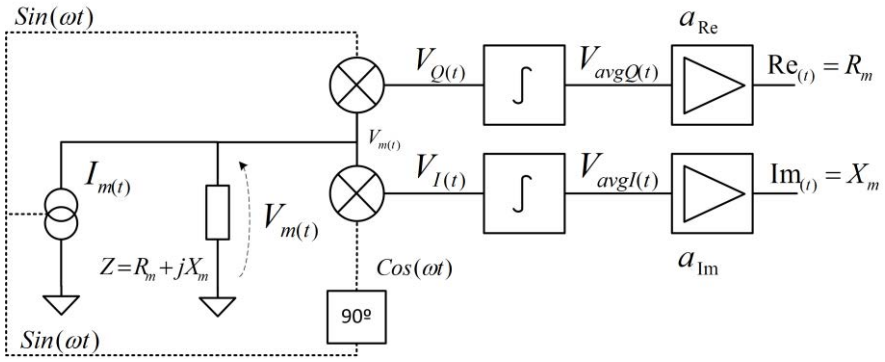

Figure 2.7 Sine correlation estimation method block diagram.

The sine correlation estimation technique could be implemented using only analog circuitry, but typically, some of the analog signals are digitally converted using digital-to-analog converter (DAC) or analog-to-digital converter (ADC), so that some of the mathematical operations could be digitally performed by a processor, and digitally stored for future use (Pallas-Areny and Webster 1993, Yuxiang, Jue et al. 2006). Typically, the injecting current signal $I_{m(t)}$ will be digitally generated and converted by a DAC, the resulting voltage signal $V_{m(t)}$ will be digitally sampled by an ADC and the rest of the operations will be performed digitally by a processor. One method to characterize the electric properties over a frequency range is to use a single frequency excitation signal at a time to obtain the impedance components; this procedure is repeated while incrementing the excitation frequency each time to perform a frequency sweep (Pallàs-Areny and Webster 2001).

Another commonly used impedance estimation method, named multi-sine or chirp excitation, uses a complex excitation signal that is formed by the summation of n-signals at different frequencies, (Bragos, Blanco-Enrich et al. 2001, Sanchez, Vandersteen et al. 2012). Compared to the single excitation signal method, these new methods have the advantage of performing the impedance characterization in less time.

2.2.4 The skin-electrode interface

Electrodes constitute an interface between the electronic currents from electronic measuring instrumentation and the ionic currents that flow in biological tissues. Normally, a non-invasive skin electrode is made of a metal conductor, *e.g.* silver, and an electrolytic gel, *e.g.* silver-chloride, that it is applied in the skin surface, as shown in Figure 2.8. This type of electrodes is categorized as a non-invasive electrode.

Human skin is composed of three primary layers: the epidermis, the dermis and the hypodermis, also called the subcutaneous layer. The epidermis is the primary barrier between the outside world and the interior of the body and is mainly composed of dead cells that act as a dielectric membrane that is semi-permeable to ions. The dermis and subcutaneous layers are beneath the epidermis and contain

some biological components, such as hair follicles, sweat glands or blood vessels, that behave as ionic conductors.

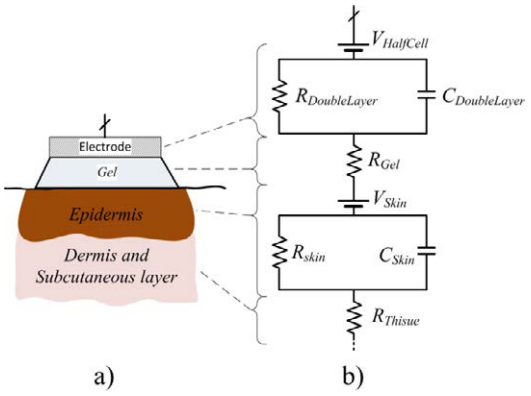

Figure 2.8 The skin-electrode interconnection layers (a) and the electrical equivalent model (b).

The electrodes used for EBI measurements are normally non-invasive and are placed on the skin surface. In Figure 2.8, the different electrode-skin layers (a) and the equivalent circuit model (b) are illustrated. Each skin layer has an equivalent electrical model (Neuman 2009). C_{skin} and R_{skin} represent the electrical behaviour of the epidermis, and R_{thisue} corresponds to resistance formed by the dermis and subcutaneous layer. Conventional skin electrodes are provided with an electrolyte gel layer that enables the transfer of ionic currents and are modelled by the resistance R_{gel}, while the electrode-electrolyte interface is represented by $C_{DoubleLayer}$ and $R_{DoubleLayer}$, as shown in Figure 2.8.b. The elements $V_{HalfCell}$ and V_{skin} are generated by the accumulation of charges between the layers; this effect is known as the "Helmholtz double layer" effect.

The term dry electrode refers to an electrode that does not incorporate any type of electrolytic interface, such as the gel layer in Figure 2.8. Typically, when comparing gel electrodes and dry electrodes with the same contact area, the dry electrodes exhibit higher electrode-skin contact impedance due to the lack of any electrolytic medium between the electrode and the skin. This high electrode-skin contact impedance is reduced after the electrode has been applied and the skin starts sweating allowing ions present in the sweat to function as an electrolytic interface.

Advances in textile materials, conductive yarns and coatings have enabled the development and validation of textile electrodes for biomedical applications, including for EBI measurements (Medrano, Beckmann et al. 2007, Beckmann, Neuhaus et al. 2010, Marquez, Seoane et al. 2013), surface electromyography (EMG) measurements (Finni, Hu et al. 2007) and electrocardiography (ECG) measurements (Pola and Vanhala 2007).

Factors such as the textile structure, textile conductive materials, and skin hydration status may affect textile electrode performance, and their influence must be taken in consideration when textile electrodes are used. The proliferation of the use of textile electrodes, together with improvements in their performance, are

enabling a handful of novel and emerging applications, such as those in the field of home healthcare and personal health systems, since they can be integrated into functional garments.

As shown in the previous section, the skin-electrode impedance polarization can play an important role in the estimation of the impedance $Z_{tus(w)}$, especially for 2- and 3-electrode configurations. EBI measurement errors may be present due to several factors, such as the use of non-ideal electronic instrumentation, the presence of high electrode polarization impedance, the influence of stray capacitances or the presence of other types of artifacts (Bogónez-Franco, Nescolarde et al. 2009, Buendía, Bogónez-Franco et al. 2012).

Therefore, to minimize all the possible measurement artifacts, the selection of electrode shape, material, and textile structure as well as design of the electronic instrumentation must be taken in the consideration for the successful development of an EBI measuring system.

2.3 Bioimpedance-based monitoring applications

Bioimpedance technology and its monitoring applications have been proven a useful, affordable, harmless and non-invasive daily-use monitoring technique in applications such as impedance cardiography (Van De Water, Miller et al. 2003, Bernstein, Henry et al. 2012), skin cancer detection (Aberg, Nicander et al. 2004) or monitoring nutrition status (Moissl, Wabel et al. 2006), among others. In the case of body composition assessment (BCA), the use of bioimpedance spectroscopy (EBIS) methods (Buendia, Seoane et al. 2015) has been proven to be useful for monitoring the distribution of different body fluid compartments, such as total body water (TBW), extracellular (ECF) and intracellular (ICF) fluids, and fat mass (FT). For instance, patients suffering from chronic kidney disease (CKD) tend to accumulate excess fluids in the extracellular compartment, and EBIS methods have been used to assess the euvolemic state and to estimate the amount of fluid that should be removed by ultrafiltration (Kuhlmann, Zhu et al. 2005, Davies and Davenport 2014).

The following sections will cover some EBI applications that are relevant to this dissertation work; specifically, the use of spectral EBI measurements for the estimation of body composition values and the use of continuous EBI measurements for the evaluation of TEB measurements for respiration.

2.3.1 Bioimpedance-based body composition assessment

Using EBI technology to estimate body composition assessment is a quick, inexpensive and non-invasive measurement procedure compared with clinical methods such as magnetic resonance imaging (MRI), computed tomography (CT) or dual energy X-ray absorptiometry (DEXA). These clinical methods are often used as references or "gold standards" for BCA since they offer better accuracy and consistency but they require expensive equipment only located in clinics or hospitals, as well as being combined with invasive techniques, which make these methods unsuitable for daily continuous monitoring applications.

The use of a combination of EBI spectroscopy measurements, Cole modelling and Hanai mixture theory has become one of the most common approaches to estimate BCA parameters (Van Loan, Withers et al. 1993, De Lorenzo, Andreoli et al. 1997, Jaffrin and Morel 2008, Matthie 2008).

The Cole function (Cole 1940), see Equation (2.6), is a complex non-linear function that models and experimentally fits EBI measurements in the *β dispersion* range, from several kHz to several hundreds of MHz. The equation is defined by four parameters: R_0, R_∞, α, and τ, as well as the independent variable ω, which represents the natural frequency.

$$Z_{(w)} = R_\infty + \frac{R_0 + R_\infty}{1 + (j\omega\tau)^\alpha} \qquad (2.6)$$

In Equation (2.6), the parameter R_0 represents the resistance at zero frequency, which contains information about the conductivity of the EC medium; R_∞ represents the resistance at high frequency, which includes information about the conductivity of both mediums, the EC and the IC; the parameter τ is the relaxation time constant, which is the inverse of the natural frequency, $\tau = 1/\omega_c$; and α is a dimensionless parameter.

To obtain the four Cole parameters, the measurement data are fitted with the Cole function using mathematical methods that find the Cole parameters that approximate the experimental data as close as possible. One implemented method is to fit the data to the semicircle in the impedance plane (Kun and Peura 1999); this method offers a good estimation of R_0, R_∞ and α , but the estimation of the parameter τ is less accurate because this method does not account for the frequency information of the EBI measurements. The non-linear least square (NLLS) fitting method is also used extensively to fit the Cole model in different planes, such as magnitude plane or the imaginary plane, and has shown good results compared with other fitting methods for the estimation of the Cole parameters for BCA applications (Buendia, Gil-Pita et al. 2011, Nordbotten, Tronstad et al. 2011).

Measurements of total body composition, also called total right side (TRS), are taken using a tetrapolar configuration and placing the electrodes on the right side between the wrist and the ankle, as shown in Figure 2.9, with the subject lying in the supine position. The measurement from EBI spectroscopy is fitted with the Cole function, and the obtained parameters R_0 and R_∞ are used to obtain the intracellular fluid and extracellular fluid resistances.

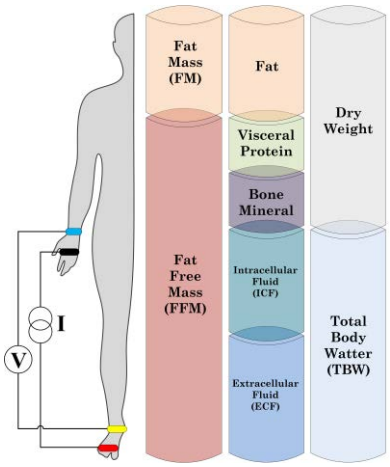

Figure 2.9 Total right side EBI measurement configuration (left) and compartmental model of the human body (right).

One of the most widely accepted approaches to estimate the ECF content from TRS EBI measurements is the method of *De Lorenzo et al.* (De Lorenzo, Andreoli et al. 1997). It is based on Hanai's mixture conductivity theory (Hanai 1968), see Equation (2.7).

$$ECF = K_e \cdot \left(\frac{H^2 \cdot \sqrt{W}}{R_e}\right)^{2/3} \qquad (2.7)$$

In Equation (2.7), the ECF parameter is in *liters*, H is the height in *cm*, W is the weight in *kg*, R_e is the resistance of the ECF equation in *ohms*, and K_e is a dimensionless constant that depends on the shape factor of the human body, which is considered as the sum of 5 cylinders. Experimental studies suggest that the constant K_e is equal to $K_{e\_m}=0.306$ for males and $K_{e\_f}=0.316$ for females (Van Loan, Withers et al. 1993).

The ICF volume is calculated as proposed by *De Lorenzo et al* (De Lorenzo, Andreoli et al. 1997) and depicted in Equation (2.8). In this equation, R_i is the resistance of the ICF, K_p is resistivity ratio of the ICF and ECF, and is equal to $K_{p\_m}=3.82$ for males and $K_{p\_f}=3.40$ for females.

$$\left(1 + \frac{ICF}{ECF}\right)^{5/2} = \frac{R_e + R_i}{R_i} \cdot \left(1 + K_p \frac{ICF}{ECF}\right) \qquad (2.8)$$

A new approach by *Moissl et al.* (Moissl, Wabel et al. 2006) proposes a correction of Hanai's theory for the calculation of ICF and ECF by considering the effect of body mass index (BMI). Therefore, the ICF and ECF can be obtained by Equations (2.9) and (2.10).

$$ECF_{BCS} = k_{ECW} \cdot \left(\frac{H^2 \cdot \sqrt{W}}{R_e}\right)^{2/3} \quad (2.9)$$

$$ICF_{BCS} = k_{ICW} \cdot \left(\frac{H^2 \cdot \sqrt{W}}{R_i}\right)^{2/3} \quad (2.10)$$

Where, k_{ECW} and k_{ICW} are functions of BMI and can be obtained as follows.

$$k_{ECW} = \frac{0.188}{BMI} + 0.2883 \quad (2.11)$$

$$k_{ICW} = \frac{5.8758}{BMI} + 0.4194 \quad (2.12)$$

This new approach suggested by *Moissl et al.* (Moissl, Wabel et al. 2006) was obtained through a cross-validation study on 152 test subjects, where EBI spectroscopy measurements were compared with dilution methods. The ECF was obtained with a precision of *0.4±1.41 liters* compared with the dilution methods.

Another method suggested by *Jaffrin M. Y. et. al.* (Jaffrin and Morel 2008) is used to estimate TBW from the FFM, by applying EBIS analysis and DEXA measurements. The TBW is obtained using Equations (2.13)and (2.14) as follows.

$$TBW = k_t \left(\frac{H^2 \cdot \sqrt{W}}{R_\infty}\right)^{2/3} \quad (2.13)$$

$$k_t = \left(\frac{K_b \cdot \rho_{\infty n}}{\sqrt{D_b}}\right)^{2/3} \quad (2.14)$$

In Equation (2.14), K_b is the shape factor, which has a value of 4.3, $\rho_{\infty n}$ is the resistivity, which is equal to 104.3 Ω·m for men and 100.5 Ω·m for women, and D_b is the body density, which has a value of 1.05. In this approach, the total body water can be obtained by adding the ICF and the ECF. The fat free mass can be obtained by an empirical relationship, which states that 73.2% of the FFM is water (Van Loan, Withers et al. 1993, Jaffrin and Morel 2008), as expressed in Equation (2.15).

$$FFM = {TBW}/{0.732} \quad (2.15)$$

2.3.2 Continuous impedance measurements

The use of EBI technology for respiration function monitoring is one of the earliest non-invasive monitoring applications of EBI measurements and is commonly known as impedance pneumography (IP). During the Apollo XI mission in 1969, NASA was already using IP to monitor the breathing of the astronauts. Since

then, EBI technology has improved to a great extent and can accurately correlate with volume estimations obtained from spirometers (Ernst, Litvack et al. 1999). The respiratory volume and flow signal extracted from IP during tidal breathing contains pathological signs of chronic obstructive pulmonary disease (COPD), cystic fibrosis, and asthma, among others. In impedance cardiography (ICG), thoracic impedance (TEB) is measured in combination with electrocardiography (ECG) measurements to evaluate the hemodynamics of the heart (Woltjer, Bogaard et al. 1996) by combining information from the electrical ECG signals and the TEB measurements.

Continuous impedance measurements are always performed using the same excitation frequency and obtaining EBI measurements periodically at constant time intervals. Compared to impedance spectroscopy measurements where the impedance measurement is obtained over a frequency analysis range, in continuous impedance measurements an EBI signal is obtained over a time period. Time-related signal processing methods, such as filters or threshold detectors, are used to extract valuable information from the continuous impedance measurements.

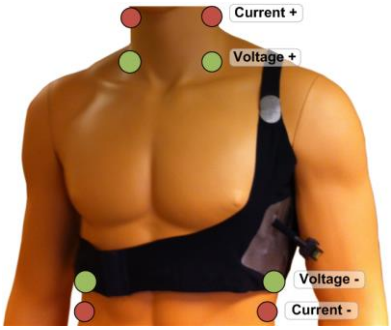

Figure 2.10 Tetrapolar lateral spot electrode measurement configuration for TEB measurements.

For instance, measurements for ICG applications are taken using a tetrapolar configuration, and placing the electrodes in either a lateral spot electrode configuration (Woltjer, Bogaard et al. 1996), as shown in Figure 2.10, or a whole body approach. Typically, an alternating current between 0.5 mA to 4 mA with a single frequency between 50 kHz up to 100 kHz is used to obtain the thoracic impedance. Since blood is as twice as conductive as muscle tissue and several times more conductive than other types of tissue (Geddes and Baker 1967), TEB measurements often contain impedance changes due to heartbeat, blood flow and chest muscle movements, among other factors. ICG measurements could provide beat-to-beat cardiovascular information when TEB measurements are combined with ECG measurements (Woltjer, Bogaard et al. 1996).

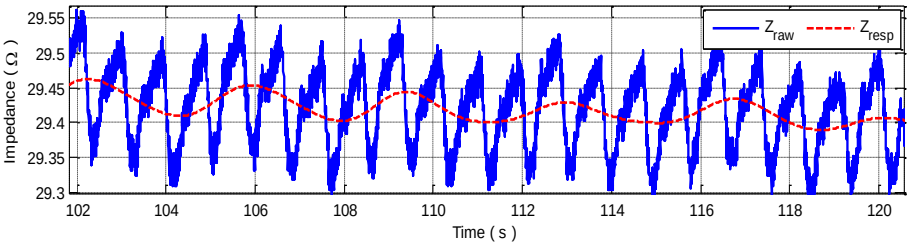

Figure 2.11 Section of a TEB measurement of raw impedance magnitude signal (Zraw) and impedance respiration signal (Zresp).

For example, in Figure 2.11, part of a TEB measurement signal obtained using the lateral spot electrode configuration is displayed. The blue continuous trace represents the measured EBI raw signal Z_{raw}, and the red dotted trace represent the respiration component Z_{resp} . These data were extracet after using a low pass filter with a cutting frequency at 10 Hz where the respiration cycle can be seen.

Chapter 3

Materials and methods

This chapter introduces the materials and the methods used for the implementation of the EBI-based monitoring solutions presented in this work. The first part introduces the AD5933 chip, a novel system-on-chip (SoC) impedance network analyzer from Analog Devices Inc. (Analog Devices Inc. 2005), as well as the custom analog front end (AFE) that enables the AD5933 to perform EBI measurements. In the following section, the SFB7 EBI spectrometer from ImpediMed (ImpediMed 2011) is described. The following section describes the types of measuring electrodes used, including commercial gel electrodes, as well as the smart textile materials used for the development of custom sensing garments incorporating textile electrodes. Finally, the last section introduces a list of system requirements used for the development of EBI-based wearable monitoring solutions.

3.1 The system-on-chip impedance network analyzer

Advances in electronics and semiconductor technology have enabled the integration of modular electronic systems into SoC solutions that are fostering the implementation of compact and low-power electronic solutions. The novel SoC impedance network analyzer AD5933 was released back in 2005 by Analog Devices Inc. (Analog Devices Inc. 2005), and for a long time it was the only SoC solution that incorporated all the necessary functional components to perform impedance measurements over a frequency range in a single chip solution using a bipolar measurement configuration. A few years later, in 2011, Analog Devices Inc. released the ADAS100 analog-front-end chip, which incorporated a 5-electrode ECG module and impedance unit that enabled it to perform continuous impedance measurements for respiration and heart monitoring. In 2012, Texas Instruments Inc. released a system-on-chip named AFE4300 that incorporated a weight scale and body composition measurement unit, which could perform single-point EBI measurements up to a frequency of 100 kHz using a tetrapolar electrode configuration. This dissertation work has explored the potential of the AD5933 SoC for the implementation of EBI monitoring devices.

The AD5933 SoC from Analog Devices Inc. (Analog Devices Inc. 2005) allows the carrying out of impedance measurements using a two-lead measurement configuration with a frequency range from 1 kHz to 100 kHz, an impedance dynamic range from 1 kΩ to 10 MΩ and a system accuracy of 0.5%. It is equiped with a serial I2C interface to control the internal functions and to retrieve the impedance measurement data. The AD5933 uses the sine correlation estimation method, also referred to as the single-point discrete Fourier transform (DFT), to obtain the real and imaginary impedance values. The AD5933 is able to operate with a single power supply between 2.7 v and 5.5 v, consumes only 33 mW at 3.3 v and has dimensions equal to 8x6x2 mm (Analog Devices Inc. 2005).

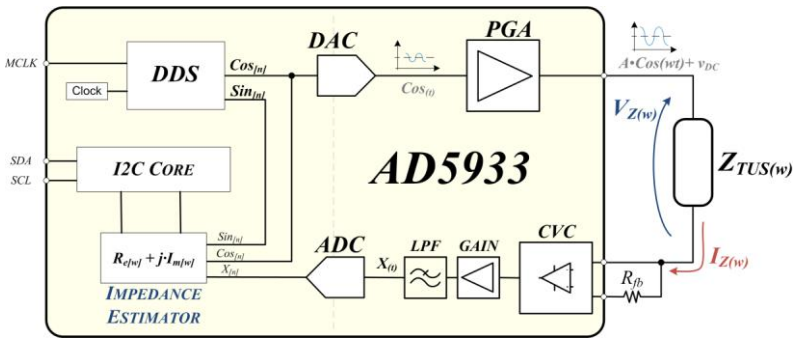

Figure 3.1 SoC AD5933 impedance network analyser block diagram.

The main AD5933 functional blocks are depicted in the diagram shown in Figure 3.1 and listed below:

- *The stimulation stage* comprises a direct digital synthesizer (DDS), which generates the digital sine waves, which can be configured for a specific impedance excitation frequency, denoted as w_n; a 12-bit digital-to-analog converter (DAC) and a programmable gain amplifier (PGA), which adapts the generated voltage applied to the impedance $Z_{TUS}(w)$.
- *The receiver stage* comprises a current-to-voltage converter (CVC), a voltage amplifier, an antialiasing low pass filter (LPF) and a 12-bit analog-to-digital converter (ADC). The receiver stage will adapt and convert the flowing current through $Z_{TUS}(w)$ into a voltage that will be fed to the following stage.
- *The impedance estimation stage* obtains 1024 sample points of the signals generated by the DDS module, $cos[w_n \cdot n]$ and $sin[w_n \cdot n]$, and the digitalized input signal $x_{[n]}$, in order to estimate the real and imaginary impedance values using DFT, as shown in Equations (3.1) to (3.3).
- *The chip control stage* comprises the I2C core module responsible for controlling all the chip functions and storing the measurement results, among other functions; check the AD5933 datasheet for further details.

To characterize the impedance over a frequency analysis range, the AD5933 uses the frequency sweep technique; thus, each time a single frequency point is obtained, the excitation frequency is increased incrementally, and this sequence is repeated until all the frequency spectrum points are obtained. For each frequency, the AD5933 will obtain 1024 samples of the output and input signals to estimate the

real and imaginary impedance component values and will perform 1024-point single frequency DFT analysis, also denoted as the previously introduced sine correlation method.

$$X_{(w_n)} = \sum_{n=0}^{1023} \left(x_{[n]} * (cos[w_n \cdot n] - j * sin[w_n \cdot n]) \right) = Re_{(w_n)} - j \cdot Im_{(w_n)} \quad (3.1)$$

$$Re_{(w_n)} = \sum_{n=0}^{1023} x_{[n]} * \cos[w_n \cdot n] \quad (3.2)$$

$$Im_{(w_n)} = \sum_{n=0}^{1023} x_{[n]} * \sin[w_n \cdot n] \quad (3.3)$$

To obtain the impedance magnitude and phase values, the estimated real and imaginary components need to be adjusted by a previously obtained calibration factor; check the datasheet for the complete operation procedure (Analog Devices Inc. 2005). The calibration factor is determined by performing a frequency sweep over a sample with a known impedance value; the manufacturer suggests using a middle single-point or two-point calibration method with a resistor.

There are several factors that make the AD5933 SoC unsuitable for the acquisition of EBI measurements, detailed as follows:

- Bipolar measurement configuration. As previously covered, in a two-lead measurement configuration, the electrode impedance polarization is also included in the measured impedance; for that reason, spectral characterization applications are basically avoided.
- Voltage-driven measurement. This makes it very difficult to have control over the injected current. This problem constitutes a safety hazard since the injected current can be bigger than the values establish by the electrical safety standard IEC 606011 (IEC 2010).
- The dynamic impedance range. It is between 1 kΩ to 10 MΩ, and most EBI measurements are below 1 kΩ. An application note suggests that lower impedances could be measured using an additional external operational amplifier with a voltage-driven and with bipolar configuration.
- The excitation voltage. This requires a DC voltage level to operate with a single power supply, leading to the polarization of the electrodes and the biological tissues and thus constituting a safety hazard.

3.1.1 Custom analog-front-end

As covered in the previous section, the AD5933 SoC is not suitable for EBI applications; therefore, an AFE interface is needed to ensure that these factors are minimized. The suggested AFE interface (*PAPER I*) (Seoane, Ferreira et al. 2008) will modify the AD5933 voltage-controlled bipolar measurements into a current-controlled tetrapolar configuration, which ensures patient safety and is capable of

measuring impedances below 1 kΩ, as would be expected in most tissues found in the human body.

The suggested AFE, along with the functional blocks, is depicted in Figure 3.2. Note that the interface electrodes impedances between the AFE and the Z_{TUS} are not present in this figure. The functional block diagram of the AFE based on the following two functional units:

- *Voltage to current converter.* The output voltage from the AD5933 is filtered by a high pass filter (HPF) in order to remove the DC component; the HPF output drives a voltage-to-current converter that generates a current, which is injected into the tissue under study (TUS) impedance.
- *Current to voltage converter.* The voltage across the impedance Z_{TUS} is sensed by an instrumentation amplifier (INA) that will amplify the measured voltage $V_{Z(w)}$, and add the DC voltage expected by the AD5933 input circuitry. The INA-generated voltage will be converted to a current signal and fed to the AD5933 input pins.

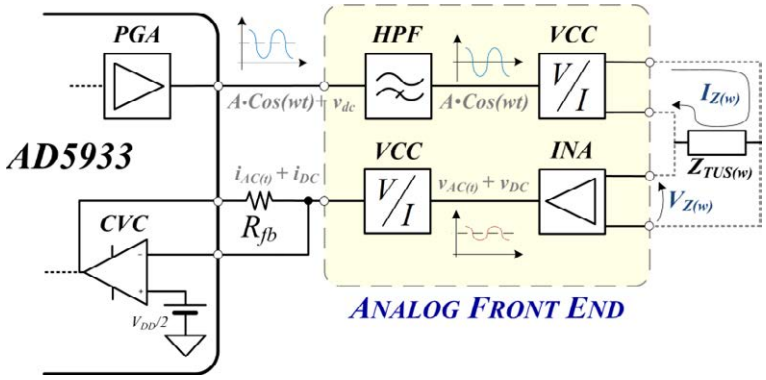

Figure 3.2 Block diagram for the custom analog-front-end.

The implementation and validation of the suggested AFE will be covered in the following sections. The electrical components used for the implementation of the AFE functional blocks are selected to ensure their proper performance when using textile-based electrodes and are designed to be operated in low-power and low-voltage applications.

SFB7 ImpediMed Specifications	
Size	190x 130 x 110 mm
Weight	1 kg
Impedance range	10 – 1100 Ω
Frequency range	4 kHz – 1 MHz
Num. frequencies	256
Interfaces	Display, Ethernet, Infrared
Power	Li-ion battery
Runtime	3 hours

Figure 3.3 SFB7 EBI spectrometer from Impedimed Ltd specifications.

3.2 The SFB7 EBI spectrometer unit

The SFB7 unit manufactured by ImpediMed (ImpediMed 2011) is a portable EBI spectrometer that can perform single EBI channel tetra polar bioimpedance measurements with up to 256 frequencies between 4 kHz and 1000 kHz for the analysis of bioimpedance-based body composition parameters such as TBW, ICF, ECF or FFM, among others. The SFB7 spectrometer is CE and FDA approved as a class II medical device.

The device performs a tetrapolar EBI spectroscopy measurement in approximately one second and provides the EBI spectral raw data and the calculated body composition parameters, which are obtained using Cole modelling and Hanai mixture theory (ImpediMed 2011). The measurements are obtained using the tetrapolar configuration and proprietary ImpediMed gel electrodes.

The SFB7 unit is equipped with a touch screen display, infrared and Ethernet connections for measurement transfer, and and internal battery for portable operations. The SFB7 unit is also provided with Windows-based software that allows the transfer of data from the unit to a PC, the visualization of the measurements and the possibility of performing offline data processing if needed; see Figure 3.3 for a list of the more relevant SFB7 specifications and actual device appearance.

In this work, the SFB7 unit is considered to be the “gold standard” or reference measurement equipment for tetrapolar EBI spectroscopy measurements. Therefore, measurements obtained with the SFB7 and any developed prototypes will be used to evaluate the performance of the solutions presented in this work.

3.3 Electrodes for EBI measurements

The performances of the developed prototypes are tested using several electrodes solutions, mainly 3M™ Red Dot™ repositionable gel electrodes and custom-made textile electrode garments based on silver-coated P130+B textile fabric from Shieldex Technik-Tex.

Figure 3.4 3M™ Red Dot™ repositionable monitoring electrode (left) and functional straps with incorporated textile electrodes for TRS EBI measurements (right).

The 3M™ Red Dot™ repositionable monitoring electrode, shown on the left side of Figure 3.4, belongs to the category of non-polarizable silver-silver chloride (Ag/AgCl) gel electrodes, which allows the transfer of charges at the skin-electrode interface with minimal voltage generation. The electrodes are composed of a conductive and sticky electrolytic gel in contact with the skin and an electrically conductive snap button to facilitate the connection with the electronic instrumentation. The electrode construction is designed to target many applications, such as telemetry, Holter monitoring or at intensive care units, allowing a low profile and conformability characteristics.

The custom-made functional textile electrode garments, such as the one shown in the left side of Figure 3.4 used for TRS EBI measurements (Ferreira, Seoane et al. 2011, Márquez Ruiz 2013), were custom made using conventional textile fabric and a silver-coated conductive inner fabric that functions as a dry electrode. In this research, several kinds of functional textile electrode garments are designed basedon this silver-coated conductive fabric and other textile materials.

The conductive fabric material is the model P130+B, a synthetic wrap-knitted silver-coated fabric from the manufacturer Shieldex Technik-Tex. P130+B is made of 78% polyamide and 22% elastomer and coated with 99% conductive silver particles with a total resistivity below of 2 Ω/sq. To ensure optimal contact between the conductive fabric to the skin surface, an intermediate foam material layer is always used. To facilitate electrical connection to the measurement instrumentation, conductive male snap buttons are used and electrically connected to the conductive textile electrode material. In addition, a folded conductive textile fabric, in the form of a border tag, has been used as an electrical connection to evaluate the performance of different electrical connections. The outer electrode layer is made of conventional textile materials, such blue synthetic wrap-knitted or neoprene fabric,

which is also equipped with Velcro fasteners to allow a quick placement and removal procedure.

For the development of the custom-made functional textile garments, some requirements were previously identified, such as the proper selection of textile materials to provide the most comfort while using and wearing the garment, and the design of the garment to keep the electrodes in the most effective position, as well as to produce a comfortable, natural and easy-to-place garment for self-managed daily-use monitoring applications.

3.4 EBI-based monitoring system requirements

The requirements for an EBI-based wearable monitoring system have been kept very general regarding of any specific EBI application. Therefore, critical factors such as usability, wearability, and system integration are not specifically targeted in this research work, even though do they are taken in consideration in the prototype designs. The first objective is to ensure the proper measurement performance while at the same time meeting some of the requirements for personal health system monitoring solutions.

The EBI-monitoring systems are designed to be easily reconfigured for a specific EBI application; thus, the instrumentation can be customized to perform impedance measurements over different dynamic impedance ranges, *e.g.,* in total body composition or segmental measurements, by means of adjusting the different instrumentation voltage gains.

This thesis covers the development of EBI-based wearable monitoring systems that are able to perform EBI measurements using functional textile electrode garments for the development of personal health system monitoring solutions. Therefore, some of the identified system requirements are as follows:

- *System accuracy.* The implemented EBI monitoring system should exhibit an equivalent performance as EBI spectrometers currently used in clinical practice, *e.g.,* SFB7 from ImpediMed Inc.
- *Patient electrical safety*. The device must fulfil the requirements for patient electrical safety imposed by the IEC 60601 standard (IEC 2010).
- *Portability/Wearabilty*. The device should be small, lightweight, and battery operated, thus enabling its integration for wearable and home-care applications.
- *Dry textile electrodes*. The measurement instrumentation should be designed to perform measurements using dry textile electrodes.
- *Wireless communications*. To control and transfer data to a standard master unit, such as a PC or a mobile device.

The choice of electronic materials and components for the implementation of the EBI monitoring unit is based on the previously listed requirements; therefore factors such as power consumption, chip dimensions and printed electronic circuit technology are key elements for the device implementation.

Chapter 4

Implementation and validation results

This chapter is divided in two sections. The first one presents the results for an EBI monitoring system for BCA applications, and the second presents the results for a monitoring system for ECG and EBI-based plethysmography applications. On each section the developed hardware, textile-based garments and measurements results are covered.

4.1 Wearable EBIS monitoring system for BCA applications

The first tests (PAPER I and PAPER II) performed were designed in order to evaluate the analog-front-end (AFE) accuracy, which enables the acquisition of EBI measurements by the AD5933 SoC. While performing measurements over 2R1C electrical circuits, the maximum relative error obtained in all cases (PAPER II) was below 4%, and in the case of the total body composition measurements, the resistance relative error was below 1%.

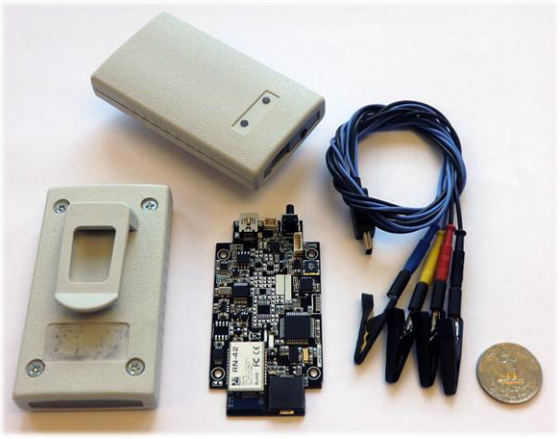

Figure 4.1 The custom-made portable EBI monitor.

Table 4.1 Technical comparison of the ImpediMed SFB7, the Fresenius BCM and the implemented AD-EBIS monitor

	SFB7 ImpediMed	*BCM Fresenius*	*AD-EBIS*
Size (mm)	190x 130 x 110	170 x 110 x 270	90 x 50 x 17
Weight (grams)	1000	2000	70
Frequency Range	4 kHz – 1 MHz	5 kHz – 1 MHz	5 kHz – 273 kHz
Discrete Frequencies	256	50	134
Interfaces	Ethernet/Infrared	Smart Card	Bluetooth 2.1 SPP
Power Supply	Li-ion Battery	Li-ion Battery	Li-ion Battery
Runtime	3 hours	5 hours	3 hours

After the first AD5933+AFE EBI accuracy evaluations were done, the development of a portable unit was carried out following the system requirements previously introduced, while using surface mount technology (SMT) components and the best available materials, which allow its integration in a reduced size unit for portable EBI measurements. In parallel, research regarding functional textile garments incorporating textile electrodes was carried out, and the results are also covered in this chapter.

The developed portable spectrometer unit (named AD-EBIS) based on the proposed AD5933+AFE is shown in Figure 4.1, and the specifications for the actual device are listed as follows:

- *EBI frequency range:* from 5 kHz to 270 kHz, with a maximum of 512 discrete points.
- *Injecting current:* equal to 100 μA_{rms} DC free.
- *Communication interface:* standard Bluetooth 2.1 wireless communications.
- *Power supply:* Li-ion battery powered, with up to 3 h of continuous measurements.
- Provided with a user button, an acoustic speaker and two LED indicators.
- Size of 90 x 50 x 17 mm and a total weight of 70 g.

Table 4.1 displays a comparison of the physical and electrical properties for the designed AD-EBIS and the commercial SFB7 spectrometer from ImpediMed and BCM spectrometer from Fresenius.

4.1.1 AD-EBIS spectrometer monitoring unit

The general functional block diagram of the designed AD-EBIS unit is shown in Figure 4.2. The following sections include detailed descriptions of each functional module.

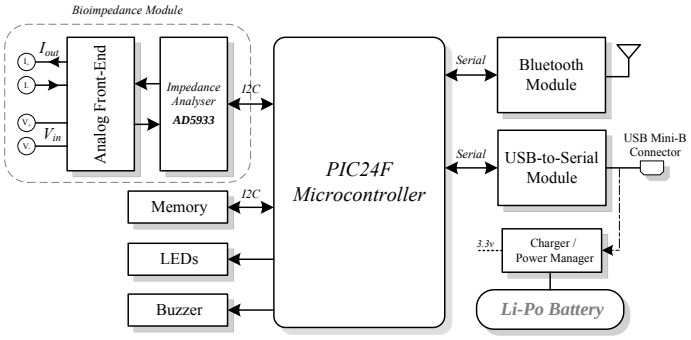

Figure 4.2 Block diagram for the custom AD-EBIS portable unit.

4.1.1.1 Microcontroller unit

The main modular unit is a PIC24F microcontroller from Microchip Inc., which contains the firmware that controls the functions and modules of the AD-EBIS unit. The PIC24FJ256GB106 microcontroller was chosen for its powerful set of peripherals and low-power functions especially designed for portable applications.

The AD-EBIS firmware was developed using high level ANSI C programing and Microchip MPLAB C30 compiler. The PIC24F firmware implements all high-level functions to perform both impedance measurement and wireless data retrieval. The impedance measurements are stored temporally in the internal RAM memory for posterior transmission using the Bluetooth protocol. The AD-EBIS is connected wirelessly to a Windows-based custom application to retrieve the measurements and store them for future processing. The measurement files containing the frequency and real and imaginary parts of the EBI measurements are stored in readable text format.

4.1.1.2 The AD5933 impedance analyser

The AD5933 was connected using a serial I2C port configured with a frequency clock of 400 kHz and an external clock oscillator circuit of 16 MHz with a frequency stability of ±50 PPM. The output voltage range was set to 1.98 $v_{p\text{-}p}$ with a DC bias of 1.5 *v.* The recommended AD5933 impedance frequency range is from 1 kHz to 100 kHz (Analog Devices Inc. 2005), but it can be reprogrammed for frequencies up to 450 kHz (PAPER II).

4.1.1.3 The analog-front-end

As described in the previous sections, the AFE is implemented in two stages: a voltage-to-current conversion stage and an input current-to-voltage conversion stage, as shown in Figure 3.2 in Chapter 3. The AFE has been implemented with 1% precision resistors and 5% tolerance capacitors, using SMT components with form factor 0603.

The high pass filter was implemented as a second order unit gain Sallen-Key topology, and with a cut frequency f_c=0.97 Hz and quality factor of 0.67. The voltage-to-current converter was implemented with an operational amplifier in a transadmittance amplifier configuration. The voltage to current converter gain was

set to 133 $\mu A_p/v$, yielding an injecting current of approximately 100 $\mu A_{RMS.}$ The instrumentation amplifier (INA) was configured with a gain of 7 v/v, and the selected INA has a CMR of 120 dB, offset voltage of 50 μV and quiescent current of 700 μA.

The AD-EBIS is calibrated using a multipoint calibration method with 2R1C electrical components with 1% precision tolerance, where the calibration factor is obtained for each impedance excitation frequency and stored in the internal memory. To achieve the highest possible precision, floating point variables are used.

4.1.1.4 Wireless communications

The system is provided with standard Bluetooth communication implementing the serial profile port (SPP), which emulates RS-232 serial cable communications. The RN42 commercial module from Robin Networks Inc. is used (RobinNetworks 2013) as this Bluetooth module represents the best available option in terms of power consumption and space requirements for the implementation of a portable unit, while also being availabe as a fully qualified Class 2 Bluetooth 2.1 + EDR module.

The RN-42 module is configured in slave mode with encrypted communications and password pairing protection enabled; therefore the AD-EBIS unit can be used only by an authorized Bluetooth master device.

4.1.1.5 User interfaces

The AD-EBIS is equipped with a user button to switch the unit on and off, two LED indicators to display the battery and Bluetooth status, an acoustic buzzer indicator, and an enhanced mini-B female USB connector used either to charge the battery or to connect the measuring leads.

The enhanced mini USB connector supports the standard USB communications pins and has an extra line of 5 pins in the bottom part of the connector, for other type of communications used for the measuring leads in the AD-EBIS. The electrode cable assembly uses an enhanced mini-b male USB connector that only allows connection to an enhanced mini-b female USB connector, avoiding the connection of the electrode cable to other USB mini-B compatible devices. Using the same USB port for charging and measuring, eliminates the risk of performing measurements while the unit is connected to a power supply to charge the battery (IEC 2010).

4.1.2 Initial AD-EBIS spectrometer unit performance tests

The performance of the AD-EBIS system (PAPER II) was evaluated against that of the SFB7 spectrometer by performing a set of 30 complex EBI measurements representing a typical TRS impedance values using 2R1C circuits with 1% precision tolerance. The AD5933 frequency analysis range was extended up to 450 kHz (PAPER II), so the impedance spectra from 5 kHz up to 450 kHz were obtained with both spectrometers and the absolute measurement errors were calculated.

The average resistance and reactance measurement spectra are shown in Figure 4.3.a. Both devices display a good performance, with only a slight deviation at high

frequencies, *i.e.* those higher than 250 kHz, being present in the reactance part for the AD-EBI spectrometer.

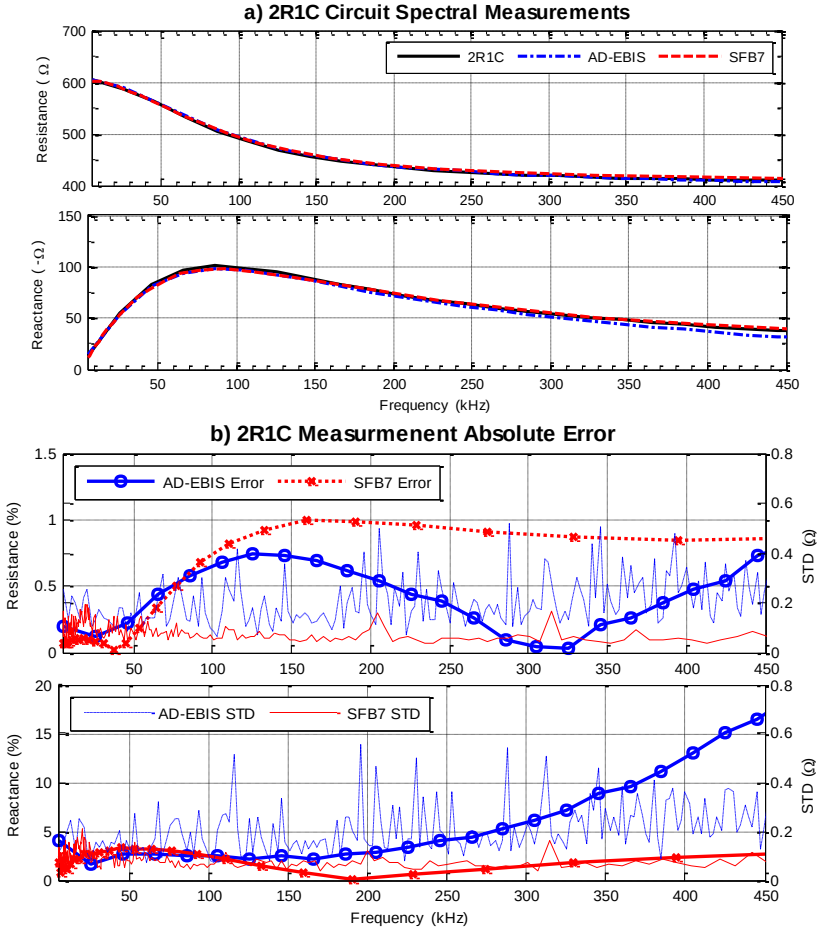

Figure 4.3 2R1C spectral measurement (a), and 2R1C absolute error and STD absolute error (b) (PAPER II)

The resistance and reactance absolute errors are displayed in the left axis and thicker traces in Figure 4.3.b. The AD-EBIS exhibits a maximum error equal to 0.75%, which is lower than the maximum error of 1% obtained with the SFB7 spectrometer. In the reactance part, the AD-EBIS has an error greater than 5% above approximately 270 kHz, while the SFB7 has a maximum error below 4% for the whole frequency range. The standard deviations (STD) are also displayed in the right axis and thinner traces in the same figure, and the SFB7 exhibits a lower value standard deviation than the AD-EBIS, but in both cases, the maximum STD are below 0.5 Ω.

4.1.3 Total right side monitoring system for BCA applications

Several textile electrode garments prototypes used for bioimpedance-based BCA applications have been developed and tested (Marquez, Ferreira et al. 2010,

Ferreira, Seoane et al. 2011, Ferreira, Pau et al. 2016), and the results obtained from the tests of each prototype helped to redefine and improve the measurement performance of the textile-based electrode garments while validating their use in combination with the AD-EBIS unit for personalized EBI-based monitoring applications.

4.1.3.1 Total right side textile-based electrode garments

The latest custom-made textile-based electrode garments for total bioimpedance analysis between the wrist and the ankle are shown in Figure 4.4 (PAPER III). The measurement garment set is built upon two separate pieces: one for the ankle-foot and one for the wrist-hand, as shown in Figure 4.4 *a* and *b,* respectively.

Figure 4.4 Textile electrode garments for TRS EBI measurements placement in the ankle-foot (a) and wrist- hand (b)

The garments were built upon the Sensiplats® commercial supporting bandages manufactured by Horizonte Textil GmbH. On each garment piece, two electrical isolated electrodes, marked as a_i and a_v respectively in Figure 4.5, are added to provide current injection and voltage sensing,. The textile electrodes are manufactured using the Shieldex P130+B biocompatible silver-based conductive fabric from Statex and an intermediate 3 mm foam layer to provide mechanical pressure between the conductive fabric and the subject's skin. Each textile electrode is equipped with a conductive snap button and conductive textile flaps, facilitating the electrical connection with the EBI measurement equipment.

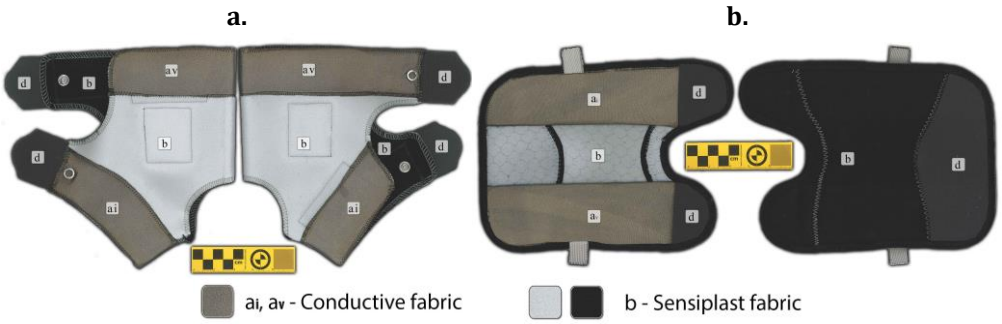

Figure 4.5 Inner and outer surfaces of the functional textile electrode garments for TRS EBI measurements, ankle-foot (left) and wrist-hand (right) (PAPER III).

The conductive areas for the ankle- foot garment are 102 cm^2 for the injecting current electrode and 132 cm^2 for the voltage sensing electrode; for the wrist- hand garment, the conductive areas are 99 cm^2 for the injecting current electrode and 88 cm^2 for the voltage sensing electrode. In the following section the EBI measurement performance of the textile electrodes is addressed.

4.1.3.2 TRS EBI Measurement results

Initial validations (PAPER II) between the AD-EBIS and the reference spectrometer SFB7 were performed in which TRS EBI measurements were obtained from three healthy subjects using the dry textile electrode garments. The measurements were used to evaluate the AD-EBIS measurement performance and upper frequency limit error for three frequencies ranges: 5-100 kHz, 5-200 kHz and 5-450 kHz. The complex EBI measurements obtained with both devices displayed similar results, but the AD-EBIS measurements had a visible deviation in the bioimpedance reactance part, as observed from the results in Figure 4.3.

Table 4.2 Total mean relative difference for the AD5933-EBIS against SFB7 Cole parameters in the frequency range 5-450 kHz.

Frequency Range	R_0 (%)	R_∞ (%)	f_C (%)
5-100 kHz	0,06	0,10	2,33
5-200 kHz	0,19	0,64	1,71
5-450 kHz	0,49	0,99	6,76

In Table 4.2, the mean absolute difference error for the Cole parameters R_0, R_∞ and f_C obtained from the AD-EBIS measurements with different frequency ranges against those obtained from the SFB measurements in the reference frequency range of 5-450 kHz are shown. The estimations of R_0 and R_∞ are very similar with a difference value below 1%, but the estimation of the characteristic frequency f_C has a higher deviation. This deviation in f_C could be due to the deviation in the reactance

part of the AD-EBIS bioimpedance and the applied fitting method, which uses the real and imaginary parts to extract the Cole parameters.

In more recent tests (PAPER III), the set of textile-based electrode garments introduced in section 4.1.3.1 were tested using the AD-EBIS and SFB7 spectrometer to obtain TRS EBI measurements from seven subjects wearing the textile-based electrode garments. These measurements were obtained following a detailed measurement protocol. The average TRS EBI measurements obtained with each device and from each subject are shown in Figure 4.6. The measurement differences between the devices and between the subjects are minimal; there are some cases, *i.e.,* subjects 2, 3 and 5, where a deviation at high frequencies can be observed.

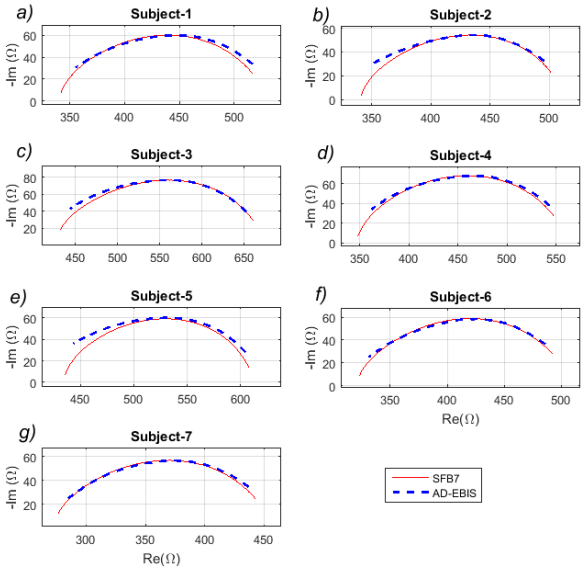

Figure 4.6 Average TRS resistance vs. reactance measurement plots for each subject with both spectrometers (PAPER III)

The TRS EBI measurements were used to obtain the Cole and BCA parameters R_0, R_∞, *ECF* and *ICF*. In Figure 4.7, the Cole and BCA parameter correlation plots for all the subject measurements with both spectrometers are shown, from which Lin's concordance correlation coefficient (CCC) and the linear regression equations are also calculated. The linear regression results indicate that there is an equivalence between the spectrometers with a constant average difference of 16.3 Ω for R_0, 9.3 Ω for R_∞, 0.4 liters for *ECF* and 1.1 liters for *ICF*.

The TOST test, which was calculated for the Cole parameters R_0 and R_∞ between devices at a probability level of 0.05, revealed that the maximum error for statistical equivalence was below 3.02% for both Cole parameters, with mean values equal to 2.1 % for R_0 and 1.9 % for R_∞.

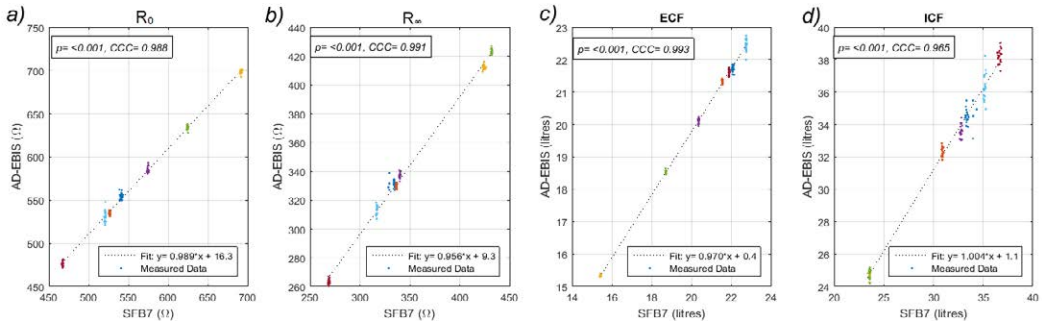

Figure 4.7 Correlation plots of SFB7 vs. AD-EBIS for R_0, R_∞, ECF and ICF for all subjects (PAPER III)

To evaluate the textile electrode garment performance, the electrode-skin contact impedance (Z_{ep}) was obtained with both devices on each subject. The averaged impedance magnitude plot for Z_{ep}, in which the original frequency analysis range is used, is shown in Figure 4.8. As shown in the figure, for most of the subjects, the electrode-skin contact impedance is on average below 500 Ω for low frequencies and decreases down to 20 Ω at higher frequencies, indicating good electrode-skin contact impedance for the subjects with both spectrometers.

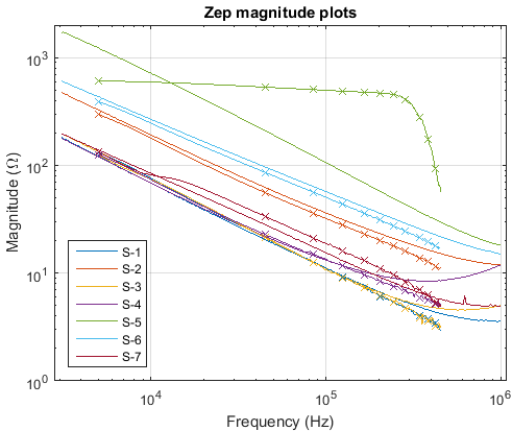

Figure 4.8 Textile electrode-skin contact impedance spectrum plots for each subject with the SFB7 spectrometer solid trace, and AD-EBIS solid-dotted trace. (PAPER III)

In the same experiment, a set of measurements were performed on two subjects, Subject 1 and Subject 3, to evaluate the electrode polarization and impedance shift during a resting period at the beginning of the experiment. After setting the textile electrode garments, EBI spectroscopy measurements were recorded every 20 s during the resting period, and the Cole parameters R_0, R_∞, f_c and α were calculated.

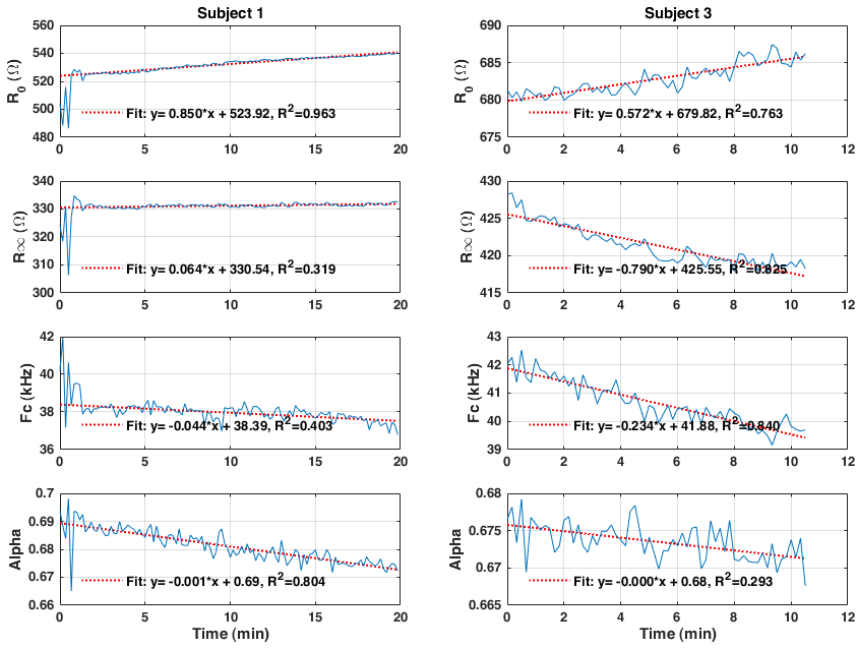

Figure 4.9 Cole parameter plots extracted from TRS continuous measurements for subjects 1 and 3 during the resting period, of 20 minutes and 10 minutes, respectively. Measurements were performed with the SFB7 spectrometer with a measurement interval of 10 seconds. (PAPER III)

In Figure 4.9, the Cole parameter plots and linear regression values are shown for both subjects. It is worth nothing that the resting period for Subject 1 was extended by an additional 10 minutes to obtain more measurements. For Subject 1, there is a visible transitory effect within the first two minutes for all the Cole parameters that then stabilizes with a constant drift over time, but in the case of Subject 3, this transitory effect is not present. The impedance value of R_0 during the resting period increases by 17 Ω, equal to 3.2 %, for Subject 1 and 12 Ω, equals to 1.7 %, for Subject 3, while the impedance value of R_∞ decreases by 16 Ω for Subject 3 and remains almost constant for Subject 1.

4.1.4 Textile-based EBI system for limb edema monitoring

A similar measurement setup, which was based on the AD-EBIS unit and a custom-made ankle-foot textile-based electrode garment for assessing fluid balance in the lower limb has been developed.

4.1.4.1 Ankle-foot textile-based electrode garment

A textile-based electrode garment for focal EBI measurements in the ankle-foot area, which is shown in Figure 4.10, was developed to monitor edema in the lower limb (To be published).

Figure 4.10 Textile electrode garment for focal ankle-foot EBI measurements

The ankle-foot electrode garment is equipped with four electrical isolated electrode areas placed in the inner side; as shown in Figure 4.11. The garment is custom built using 4 mm neoprene fabric, Shieldex P130+B electrode conductive fabric, 3 mm foam fabric, snap buttons for measurement instrumentation connection and Velcro fasteners, similar to the TRS textile electrodes introduced in section 4.1.3.1.

Figure 4.11 Inner surfaces of the ankle-foot textile electrode garment.

The conductive areas for the finger electrode area, as shown in Figure 4.11.a, are 64 cm^2 for the injecting current electrode and 95 cm^2 for the voltage sensing electrode; for the ankle electrode area, as shown in Figure 4.11.b, the conductive areas are 134 cm^2 for the injecting current electrode and 110 cm^2 for the voltage sensing electrode.

4.1.4.2 *Focal EBI measurements results*

The developed monitoring system based on the AD-EBIS unit and the ankle textile electrode garment, in combination with other state-of-the-art monitoring sensors, was used in the clinical study MySleeve (To be published). The MySleeve study aimed at validating a personalized healthcare solution to ensure better adherence of dialysis patients to fluid restriction by providing direct feedback information on fluid intake to the patient through the use of state-of-the-art monitoring systems. The MySleeve study was coordinated by the Department of Smart Medical Devices for Cardiovascular Healthcare at the University of Eindhoven and in collaboration with the University Hospital Catharina Ziekenhuis in Eindhoven under the European project DoChange (DoChange 2016).

The portable bioimpedance system, based on the AD-EBIS unit and the ankle textile electrode introduced in the previous sections, was used, as well as other motnitoring sensors, by CKD patients undergoing dialysis treatment and requiring daily bioimpedance measurements. Fron every bioimpedance measurement session, a set of 10 EBI spectroscopy measurements were obtained, and transmitted to the hospital data center for future processing.

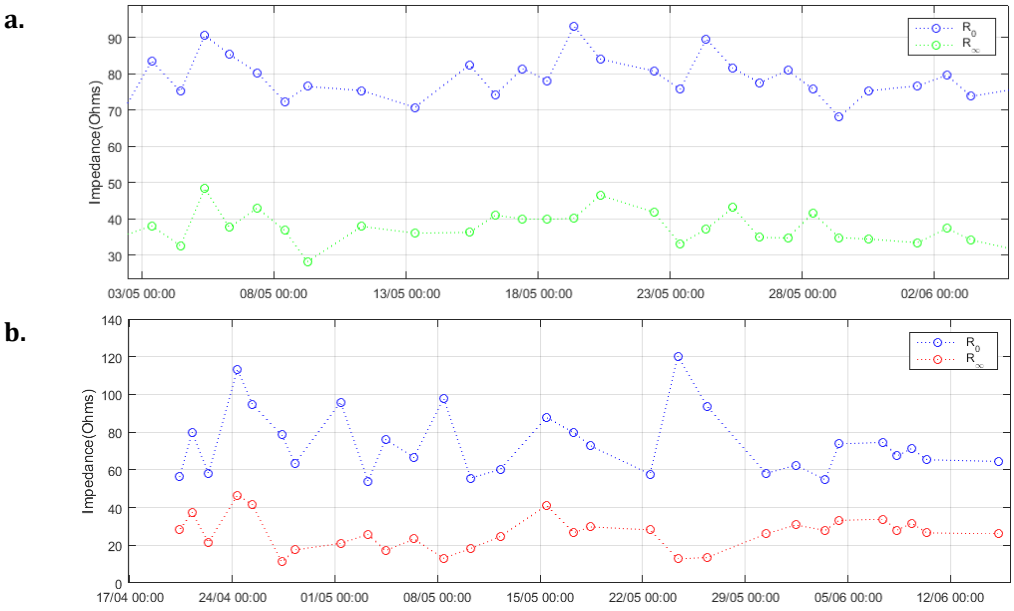

Figure 4.12 Cole parameters R_0 and R_∞ for the MySleeve Ankle AD-EBIS measurements, for patients ID10 (a) and ID18 (b) (To be published).

Some of the preliminary data for two subjects collected by the AD-EBIS system (To be published) are shown in Figure 4.12, where the average Cole parameters R_0 and R_∞ are obtained and plotted for each measurement session every day.

It is expected that the value of R_0 decreases as the patient accumulates waste fluids in the extracellular space, known as the interdialytic period, and after the patient goes through dialysis and extra waste fluids are removed, and it is predicted that the value of R_0 will increase, these types of changes have been reported

previously (Anand, Doan et al. 2012) and were observed in the data collected by the AD-EBIS monitoring system.

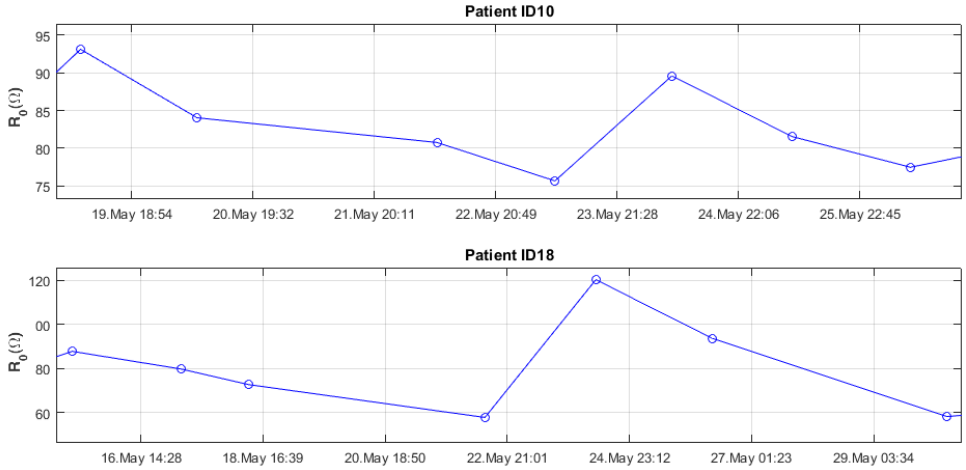

Figure 4.13 Set of Ankle AD-EBIS measurements for patients ID10 (a) and ID18(b) during MySleeve study (To be published).

These cycles, as reported by (Anand, Doan et al. 2012), can be observed in the MySleeve collected data shown in Figure 4.13. These interdialytic period changes could be clearly observed for patient ID10 between 18/05 and 29/05, and for patient ID18, between 15/05 and 05/06; further data analysis will be carried out in combination with data from other sensors (To be published). An automatic analysis performed on the dynamics of R_0 for patient ID10 detected 17-18 dialysis interdialytic periods in a time span of 69 days, which suggests that dialysis was performed approximately every 3.6 to 3.9 days.

4.2 Wearable EBI monitoring system for plethysmography applications

This section presents the studies on exploring other possible uses for the developed AD-EBIS spectrometer unit by performing fast continuous single frequency EBI measurements for EBI-based plethysmography monitoring applications, such as respiration monitoring or impedance cardiography.

The AD-EBIS spectrometer unit is optimized to perform measurements for EBI values below 100 Ω, such as those typically found in EBI plethysmography applications. The injecting current was configured to 400 μA_{RMS} and the voltage sensing instrumentation amplifier gain was increased to 26 v/v. The AD-EBIS firmware was modified to perform the continuous impedance measurements and, in real time, transmit the data wirelessly to a computer.

4.2.1 AD-EBIS validation for continuous impedance measurement

The maximum continuous impedance estimation frequency and the system measurement performance error, as well as TEB measurements in one subject, were assessed using the AD-EBIS unit and 3M gel electrodes (PAPER IV).

The maximum impedance estimation time measured was on average 1.79 ms, equivalent to a maximum impedance estimation frequency of approximately 550 Hz, using an injecting impedance signal frequency equal to 100 kHz. The system measurement performance was evaluated over 2R1C circuit components obtaining a maximum magnitude measurement error of 0.26% with STD of 0.04 Ω for a total of 30 s.

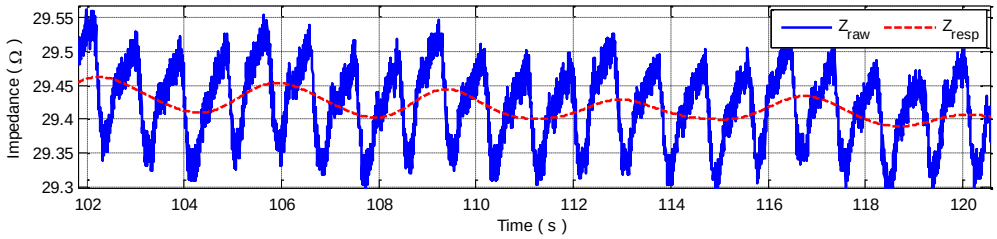

Figure 4.14 Raw impedance magnitude signal (Zraw) and impedance respiration signal (Zresp) (PAPER IV).

In the TEB measurement Z_{raw} over 23 s shown in Figure 4.14, the continuous trace Z_{raw} represents the raw impedance measurement and the dashed trace Z_{resp} represents the respiration component obtained from the low pass filtered Z_{raw} signal. In the signal Z_{raw} , the cardiac and respiratory non-stationary components can be observed as well as a high frequency signal due to the extimation error of the AD5933 SoC.

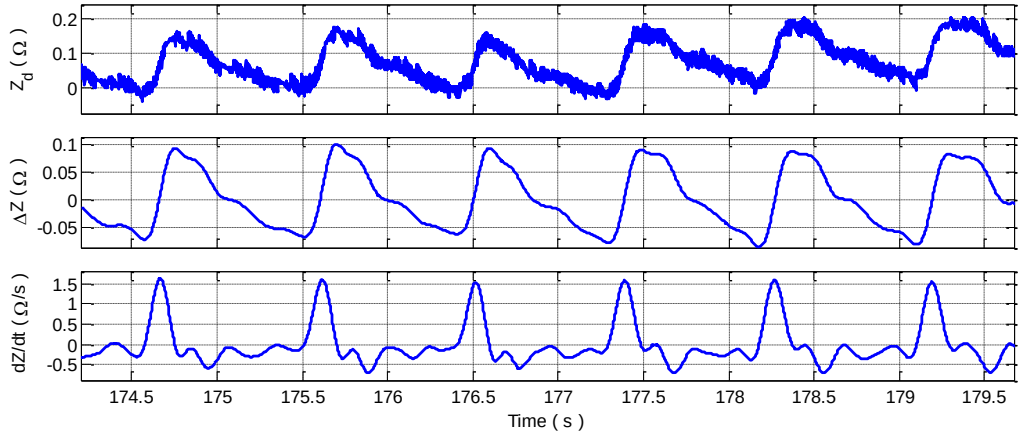

Figure 4.15 Detrended impedance magnitude (Zd), filter impedance magnitude (ΔZ) and first derivative (dZ/dt) plots (PAPER IV).

To evaluate the performance for impedance cardiography analysis, the signal Z_{raw} was processed (Bernstein 2010). In Figure 4.15, the detrended impedance signal Z_d, the filtered cardiac signal ΔZ and its first derivative d_Z/d_t are shown for a 6 s of Z_{raw} signal. The beat-to-beat interval extracted from the plots is approximately 0.91 s, corresponding to a heart rate of 66 bpm. Some impedance cardiography values can be extracted from the plots, such as the increment difference for the ΔZ signal of 0.17 Ω, the peak value for d_Z/d_t of 1.5 Ω/s and the baseline thoracic impedance value of 27.6 Ω.

After the successful results obtained from the continuous impedance measurement validation tests, a new modular EBI-based monitoring hardware, incorporating an ECG measurement unit, and aimed at reducing the hardware size was developed that could be reconfigured for the development of EBI-based monitoring applications and that even could be integrated into a wearable single piece monitoring garment solution. This modular hardware is introduced and validated in the following sections.

4.2.2 The BZM; an ECG and EBI monitoring hardware module

A modular EBI-based monitoring hardware, named as BZM module, was developed, in which all the electronics components were fitted into a reduced size PCB module, as shown in Figure 4.16.b. The BZM is a one-module solution that incorporates a tetrapolar EBI measuring unit, identical to the AD-EBIS unit, a 1-lead ECG front-end and a microcontroller that can be firmware reconfigured to use it in several EBI-based monitoring applications; Figure 4.16.b shows the actual size of the unit.

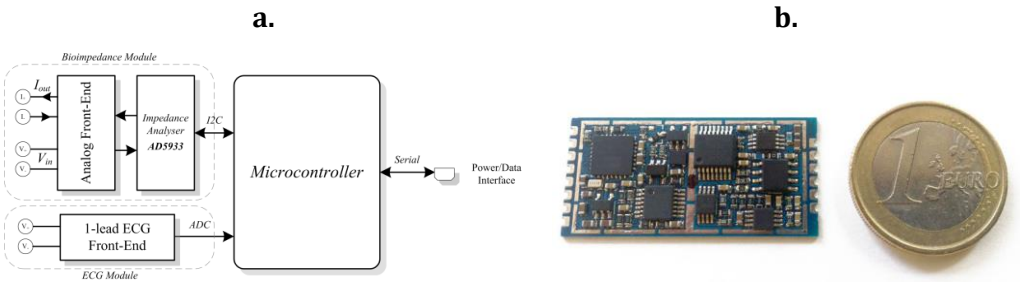

Figure 4.16 Block diagram for the BZM module unit (a) and its physical appearance (b)

The achieved BZM specifications are listed as follows:

- Reduce size module of 38x18x3 mm.
- Tetrapolar EBI measurement unit that can be firmware reconfigured as;
  - EBI spectrometer, with a measurement frequency range of 5-270 kHz
  - Continuous EBI monitor, with a sampling frequency up to 550 Hz
- 1-Lead ECG measurement unit, with a sampling frequency up to 1 kHz.
- High-performance low-power microcontroller.
- Standard digital asynchronous serial communication interface port.

- 3 v low-power operation voltage.
- Maximum measuring power consumption of 40 mA at 3 v.

The EBI functional module comprises the same components as the AD-EBIS monitoring unit and therefore inherits all the measurement performance covered in the previous sections. The 1-lead two electrodes ECG front-end is based on the topology suggested by (Merritt, Nagle et al. 2009) but without the driven right leg circuitry. The ECG module is provided with a gain of 400 v/v and filter cut-off frequencies f_{HP} = 0.04 Hz and f_{LP} = 150 Hz. The microcontroller used is a Microchip high-performance 16-bit digital signal controller dsPIC33FJ128GP802 that performs all the module functions and is controlled by standard asynchronous serial communications running at 115.2 kbps.

This module has been developed as a general reconfigurable platform to be used in different custom monitoring devices where the communications protocol, type of measurement storage, battery power options, and device shape-size, among other characteristics, could be tailored depending the monitoring application and textile garment solution selected.

4.2.3 Wearable monitoring system for thoracic EBI and ECG measurements

This section covers the developed monitoring prototype units, textile electrode garments and measurement tests performed for the ECG and thoracic EBI signals measurements.

4.2.3.1 Portable ECG and EBI monitoring unit

Two sets of wearable device prototypes designed for ECG and EBI-based plethysmography monitoring applications were designed (PAPERS V and VI) based on the developed BZM monitoring module.

The first prototype version (PAPER V), named ECGZ, was developed to record ECG and TEB signals on an on-board micro-SD memory card for offline signal processing. The ECGZ device was provided with an internal Li-ion battery, the BZM monitoring module, a battery charger and a microcontroller. The device has dimensions equal to 50x35x20 mm and is provided with a 4 GB micro-SD memory card and an 800 mAh battery that allows continuous recording of ECG and EBI signals for up to 5 hours.

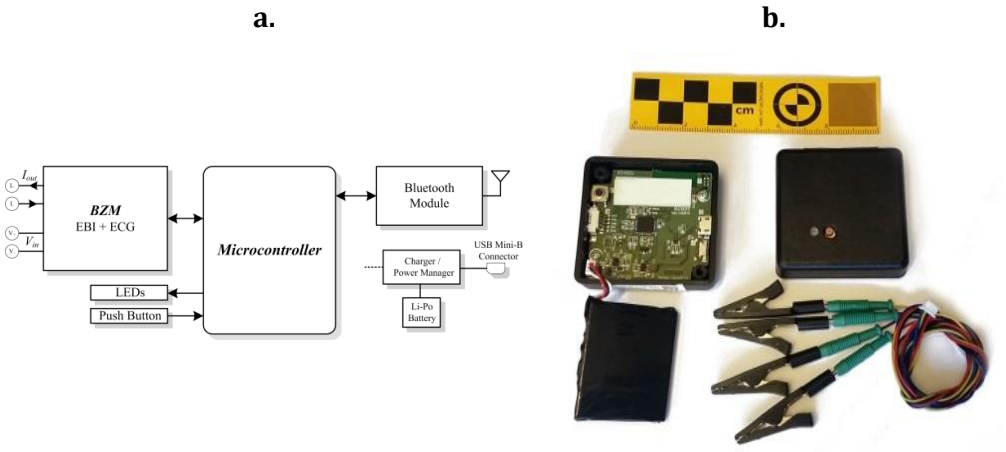

Figure 4.17 Block diagram (a) and physical appearance (b) of the custom ECGZ2 portable unit

The latest monitoring unit for ECG and EBI-base plethysmography monitoring applications (PAPER VI), named as ECGZ2, is shown in Figure 4.17.b. The ECGZ2 unit is developed using the same hardware technology previously used in the AD-EBIS and ECGZ units and is divided into four basic functional blocks: the BZM monitoring unit, the RN41 Bluetooth communication unit from Robin Networks Inc., a power manager unit and a microchip microcontroller, as shown in Figure 4.17.a. The measurements are transmitted in real time wirelessly in a data packet form. The ECG measurements are performed at a sampling frequency of 250 Hz, and the EBI measurements are performed at a sampling frequency of 100 Hz with an EBI excitation frequency of 100 kHz. The device dimensions are 50x50x15 mm, and it is equipped with a 900 mAh Li-ion battery that enables the unit to run up to 4 hours of continuous ECG and EBI measurements.

4.2.3.2 Thoracic textile electrode garments

The first textile electrode garment prototype for thoracic measurements (PAPER V) is built as a set of reconfigurable textile patch electrodes and elastic straps. The repositionable electrodes are built using the Shieldex P130+B conductive fabric from Statex, an intermediate 3 mm foam layer, snap buttons for electrical connection and have an approximate electrode conductive area of 25 cm^2. The electrodes can be positioned along a set of stretchable straps provided with holes for the electrodes (PAPER V). A total of 6 textile electrodes are used: two for the 1-lead ECG measurements and four for the EBI measurements. This textile electrode garment is developed to allow the repositioning of the electrodes on the subject's chest area in order to measure the different cardiac potentials and impedance changes.

The latest textile electrode garment prototype for thoracic ECG and EBI measurements (PAPER VI) is shown in Figure 4.18 and Figure 4.19. The garment is built as one piece and includes a textile pocket to hold the ECGZ2 monitoring unit, as shown in Figure 4.18.a. The electrodes are connected through a cable that hidden in between the garment fabrics and a connector is used so that the unit can be easily detached.

The garment is fully custom-made using raw textile materials as follows, and as shown in Figure 4.19:

- The garment main body fabric is made of stretchable black spandex
- The chest perimeter is provided with an elastic band of 55 mm
- The four electrodes are made from Shieldex P130+B fabric, with a conductive area of 24 cm^2.
- A 3 mm foam fabric layer is used between the elastic band and the conductive fabric.
- Cables are used to interconnect the electrodes and to connect them to the monitoring device and are hidden between the garment fabrics.
- Black hook-and-eye bra-type fasteners are used.

Figure 4.18 Thoracic textile electrode garment placement; front view (a), back view (b) and monitoring device placement (a) (PAPER V).

The outer electrodes, marked as a_i in Figure 4.19, are used for EBI current injection and the inner electrodes, marked as a_v in Figure 4.19, are used to sense voltage for the EBI measurements and for the 1-lead ECG measurements.

Figure 4.19 Thoracic textile electrode garment inner side (PAPER V).

Overall, the textile electrode garment (PAPER VI) was designed to offer comfort and usability while ensuring good placement and grip for the accurate acquisition of measurements during daily activities.

4.2.3.3 Thoracic EBI and ECG measurements results

The measurements tests (PAPERS V and VI) were performed in collaboration with the Spanish armed forces and the University of Alcala in Spain under the project "Assessment in Real Time of the Stress of Combatants" (ATREC) which aims to enable real-time assessment of mental stress via of non-invasive wearable monitoring devices (Seoane, Ferreira et al. 2013, Seoane, Mohino-Herranz et al. 2014, Mohino-Herranz, Gil et al. 2015).

The first results (PAPER V) were obtained using the ECGZ unit and the repositionable electrode garments for the acquisition of ECG and thoracic EBI measurements to extract the subject cardiac and respiratory components. A total of 12 monitoring systems composed by the ECGZ and textile electrode straps, among other monitoring systems, were used in the first project stage to determine which biological signals are better biomarkers for the assessment of stress. The first validation tests were performed on several subjects wearing the monitoring system. In Figure 4.20, ECG and TEB measurements recorded over 60 s are shown. The obtained ECG recording, as shown in Figure 4.20.a, showed a good cardiac signal, where during the breath holding period from second 60 to second 80, the ECG showed a stable output. For the respiration EBI-based recording, as shown in Figure 4.20.b, the respiration pattern could be seen as the impedance increased and decreased with the respiration cycle.

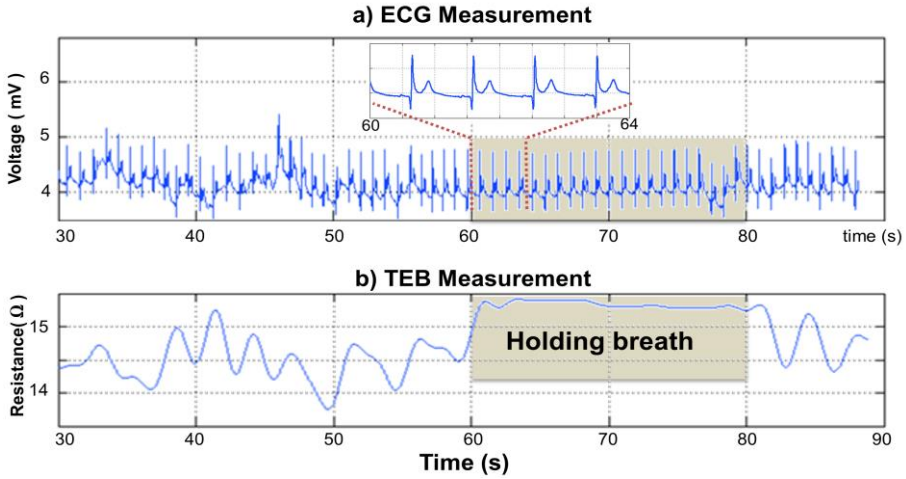

Figure 4.20 A time period of ECG recording (a) and thoracic EBI recording (b) (PAPER V).

The latest results (PAPER V), obtained during the second stage of the ATREC, used the monitoring system based on the ECGZ2, which was described in section 4.2.3.1, and the vest textile electrode garment, which was described in section 4.2.3.2. In this case, the measurements were transmitted to an Android mobile phone running a custom app that extracted real-time parameters from the ECG and TEB measurements. The ATREC system was tested following a protocol while performing activities during several scenarios; the first one was used to classify the type of activity performed with a 21.2% probability of error, the second scenario was used to classify three different emotional states with a probability of error equal to 4.8%, and in the last scenario the system was used to distinguish between low

mental load and mental overload with a probability error of 32.2%. The results were obtained as part of an initial system validation stage to determine if the system was capable of performing the tasks in real time. Future efforts are being directed at decreasing the probability of error while classifying the activities and mental load of different subjects.

Chapter 5

Discussion and conclusions

This chapter is divided in two main sections where the results obtained in this research work are discussed against the formulated research questions. In adition, a section for the conclusions is included at the end of this chapter.

5.1 EBIS monitoring system for BCA applications

The first validation results indicated that the SoC impedance spectrometer AD5933, in combination with the proposed analog front end can indeed perform EBI measurements in the frequency range from 5 kHz to 100 kHz. The spectral measurement errors obtained while measuring over 2R1C circuits were generally low, *e.g.,* in the worst case studied in PAPER II, the error was below 4%. The first results confirmed the viability of the implementation of a portable EBI monitoring unit using the presented instrumentation.

The implemented EBI portable spectrometer unit, the AD-EBIS, has dimensions of 90x50x17 mm, a weight of only 70 grams and equipped with standard Bluetooth communications and internal batteries. These portable features, compared with other commercial devices, *e.g.,* SFB7 or BCM in Table 4.1, make the developed portable bioimpedance spectrometer more suitable for applications where the size and weight are important factors, such as in wearable and portable monitoring applications.

The spectral plots obtained with the developed AD-EBIS measuring 2R1C circuits, as shown in Figure 4.3, indicated that the spectrometer can perform accurate impedance measurements well above other upper frequency limits previously reported, such as 100 kHz in (Seoane, Ferreira et al. 2008, Ferreira, Seoane et al. 2010) and 200 kHz in (Bogónez-Franco, Bayés-Genís et al. 2010). The AD-EBIS exhibits a good accuracy compared with the reference spectrometer SFB7 on 2R1C measurements, showing a smaller error in the resistance spectrum measurements but a noticeable error in the reactance spectrum at frequencies above 270 kHz.

5.1.1 EBI BCA measurements

The obtained results show the feasibility of performing accurate TRS EBI spectroscopy measurements using dry textile electrodes for Cole parameter estimation and BCA applications.

Despite the clear deviation observed in the reactance spectrum at high frequencies for 2R1C, as shown in Figure 4.3, the Cole parameter estimation performed on the EBIS data measured up to 450 kHz with the AD-EBIS produces very similar values for R_0 and R_∞ as those estimated from the EBIS measurement performed with the SFB7 spectrometer. The differences observed in the estimation of the Cole parameters, R_0 and R_∞, using the AD-EBIS are below 1% compared with the parameters obtained with the SFB7 reference spectrometer, as shown in Table 4.2.

For the assessment of body fluid distribution, the most common approach to estimate the Cole parameters is to fit the EBI spectral data to a depressed semicircle, therefore using only the resistance and reactance measurement data and ignoring the frequency information. This fitting approach is vulnerable to the reactance deviation present at high frequencies for the AD-EBIS; therefore the upper frequency must be limited to 270 kHz, where the phase error has an acceptable error value of 5%.

Currently, other methods proposed to estimate the Cole parameters using non-linear least quare (NLLS) iterative fitting, where the frequency information contained in the measurement is used (Ayllon, Seoane et al. 2009, Buendia, Gil-Pita et al. 2011). The method proposed by *Buendia et al.* suggest using the modulus of the Cole function as the function model used by NLLS fitting to extract the Cole parameters. Estimating the Cole parameters through this approach suggest the suitability of the portable AD-EBIS when using only the magnitude spectral data in the whole frequency range from 5 kHz to 450 kHz, where the maximum magnitude error value is below 1%.

Studies performed on the dependence of the limit of the upper frequency and the number of frequency points on the estimation of the Cole parameters for TBC measurements by *Buendia et al.* (Buendia, Gil-Pita et al. 2011) suggest that using a upper frequency limit of 250 kHz with a maximum of 16 frequency points produces similar Cole parameters estimation errors as using an upper frequency limit of 1 MHz with 256 frequency points. These results, combined with using NLLS with the modulus of the Cole function, suggest that the developed AD-EBIS spectrometer could perform measurements as accurate as commercial spectrometers, such as the SFB7, for the estimation of body fluid distribution.

Further results, as shown in Figure 4.7, revealed that for the Cole and BCA parameters obtained for seven subjects, there was a measurement bias between the data obtained by the AD-EBIS and the SFB7 ranging from 1.19% to 3.88% and a linear correlation relationship ranging from 0.995 to 0.998. The high value of the correlation coefficient together with the low bias values of 1.77% for R_0 and 1.71% for R_∞ suggest a high level of equivalence of the bioimpedance measurements. The statistical TOST equivalence test showed that the maximum error for statistical equivalence, obtained for a level of probability α=0.05, was below 3% for the Cole parameters R_0 and R_∞, guaranteeing their statistical equivalence within the values

expected for bioimpedance measurements according to (Piccoli, Pastori et al. 2005, Earthman, Wolfe et al. 2015).

Despite the statistical significance of the equivalence, the TOST values do not reflect clinical significance, because these concepts are very different. From a clinical significance perspective, considering that the body composition assessment by EBI spectroscopy analysis produces a disagreement with dilution methods in the range of 4.69% to 5.07% for total body water (Seoane, Abtahi et al. 2015), we foresee no practical impact in using any of the devices because the differences observed between them are smaller than the reported error range.

The measurements from two subjects performed during a resting period, as shown in Figure 4.9, indicated that after a short period of time, *i.e.*, below 2 minutes for Subject 1, the impedance measurements became stable, although there was a noticeable drift over the resting period for most of the parameter values for both subjects. As reported by other authors (Ismail and Leonhardt 2013), the internal physiological mechanisms of body fluid distribution are continuously adapting, as shown in Figure 4.9; for instance, during the resting period, the extracellular resistance parameter R_0 increases by 0.85 Ω/min, a value in agreement with the results reported by *Ismail et al.* in (Ismail and Leonhardt 2013) when subjects changed their position from standing to supine. These and other factors, such as body posture, ambient temperature and food intake, will impact the body fluid balance estimation, potentially leading to inaccuracies when analyzing EBIS measurements for assessments of body composition. These factors must be taken in consideration, and detailed measurement protocols must be used. Furthermore, additional studies on the dynamics of body fluid distribution should be performed, emphasizing their impact on the analysis of EBIS measurements for body composition assessment. It is likely that such time-related fluid dynamics could partially contribute to the differences observed in the results shown in Figure 4.7, i.e., 1.19% for ECF and 3.88% for ICF.

The achieved portable AD-EBIS features, measurement performance over 2R1C electrical model circuits and EBI measurements using textile electrodes in garments allow the initially formulated research questions RQ1 and RQ2 to be answered.

5.1.2 Textile electrode performance

The magnitude values of the electrode-skin contact impedance obtained with the TRS textile electrode garments using both EBI spectrometers were very similar, and they in fact exhibited very low magnitude values, as shown in Figure 4.8. Performing EBIS measurements with low electrode-skin contact impedance increases the robustness of EBIS measurements by minimizing the source of errors, such as the influence of stray capacitances (Scharfetter, Hartinger et al. 1998).

Dry textile electrodes are expected to have high electrode-skin contact impedance, mainly due to the poor contact interface, which sometimes can be improved by scrubbing and applying conductive electrode gel, thus reducing the impedance of the interface. In the case of the presented dry textile electrode garments, the contact impedance was very low, mainly due to the high electrode contact area of, on average, 105 cm^2, which is 10 times larger than the typical size of

commercial Ag/AgCl gel electrodes. In addition, the presence of measurement artifacts was minimized, as the only deviations visible in the impedance plots were at high frequencies for subjects 2, 3 and 5, as shown in Figure 4.6. These deviations may be a result of the presence of electrode impedance mismatch errors due to the different electrode contact areas in the textile electrode garments (Buendía, Bogónez-Franco et al. 2012).

These results prove that indeed, EBI measurements can be performed using the developed AD-EBIS unit and dry textile electrodes incorporated into functional garments, answering formulated research question RQ2.

5.2 EBI monitoring system for plethysmography applications

The first performance tests on 2R1C circuits shows that the AD-EBIS unit could perform single frequency continuous impedance measurements for a maximum interval frequency of 550 Hz with a magnitude error below 0.26%. The obtained TEB signal Z_{raw} plotted in Figure 4.14 exhibits good measurement performance without requiring any kind of signal preprocessing. In Z_{raw} the cardiac and respiratory components could be observed, and in addition, certain high frequency content is also noticed, mainly due to the AD5933 impedance estimation error among other external factors. The obtained respiratory and cardiac signals demonstrated good performance, as shown in Figure 4.15, enabling the possibility of the unit being used for applications such as respiratory flow (Seppa, Viik et al. 2010), respiratory volume changes (Ernst, Litvack et al. 1999), swallowing function by impedance pharyngography (Kusuhara, Nakamura et al. 2004), respiration monitoring (Mohino-Herranz, Gil et al. 2015) thoracic ICG (Kubicek 1969, Ferreira, Seoane et al. 2013) or brachial impedance interrogation (Bernstein, Henry et al. 2012, Bernstein, Henry et al. 2015).

The developed BZM module, which incorporates the instrumentation for measuring EBI continuous impedance and 1-lead ECG biopotential and a stand-alone microprocessor to carry out all complex measurement procedures, presents novel features, suggesting its use as a generic and yet versatile EBI-based monitoring module that, through its reconfigurable capabilities, can be used to implement custom tailored wearable monitoring solutions, as shown several times in (Seoane, Ferreira et al. 2013, Abtahi, Berndtsson et al. 2014, Seoane, Mohino-Herranz et al. 2014, Zhang, Freund et al. 2016). Even though the monitoring systems based n the BZM unit have not been yet validated against any clinical monitoring system, the obtained measurements showed good results, as seen in Figure 4.15 and Figure 4.20.

The development of the BZM module, the actual implementation of the ECGZ2 monitoring unit and the development of the measurement and monitoring solutions using sensorized garments with textile electrodes provide a definitive answer to research questions RQ3 and RQ4.

5.3 Conclusions

The textile electrode garments have exhibited good measurement performance overall, but further studies regarding textile electrode degradation must be performed to establish their clinical reliability in home-based monitoring applications. For instance, information regarding the electrode-skin contact impedance value could be used as an indicator of electrode degradation performance over time, as well as an indicator of incorrect electrode placement. Studies of electrode area and construction must be carried out in the future to minimize the presence of electrode mismatch errors. The developed custom-made textile garments offer an easy, comfortable and reliable way to place measurement electrodes in the same location each time by an informal caregiver and even the patients themselves, which enables their possible use in self-managed and home-based monitoring environments.

The AD-EBIS spectroscopy monitoring unit offers some advantages for home-based monitoring usage not currently available within the commercial clinical bioimpedance instruments. The reduced dimensions and weight allows its possible integration in sensing garments to yield a single EBI monitoring unit for spectroscopy applications that achieves an equivalent measurement performance. Additionally, the capability for standard Bluetooth wireless communications facilitates the connectivity to many Bluetooth enabled devices, such as mobile devices, smart TVs and personal computers, offering an open EBI monitoring platform for the development of personal health system solutions.

The presented ECGZ2 unit and the BZM module enable the development of monitoring garments with incorporated instrumentation for personalized health monitoring. The developed BZM module has the potential for incorporating an EBI spectrometer and a continuous EBI and ECG monitor in the same module using the same hardware.

Nevertheless, the use of the developed EBI-based monitoring systems for the successful implementation of personalized healthcare solutions will require a further and deeper study of aspects such as system usability, user acceptance, measurement reliability or system maintenance, which should be covered in future studies.

5.4 Related projects

Some of the developed monitoring systems presented in this dissertation work have been, are being or will be used by other research groups in different monitoring applications, such as the presented MySleeve study in section 4.1.4. The following paragraphs will briefly introduce the related projects.

5.4.1 Health at work

We at work (We@Work) is a project founded by a grant from the European Institute of Innovation and Technology (EIT) Health, which started in January 2017 and is aiming to develop an integral tool for promoting and supporting a healthy and safe working life by exploiting the combination of ICT, big data analysis, wearable technologies and ergonomics. One of the personalized health monitoring solutions is based on a wearable measurement system build up by the presented ECGZ2 monitoring unit and a textile sensorized t-shirt to gather user biometric data. The monitoring data will be collected wirelessly by mobile gateways such as smartphones and tablets that will send the data to a cloud platform, *e.g.,* the Philips Health suite digital platform.

5.4.2 EBI-based swallowing sensing

At the University of Passau in Germany, the research group ACTLab within the framework of the SimpleSkin FET-OPEN project have been and are continuing developing tools to provide swallowing information using state-of-the-art sensors for therapy and dietary monitoring. Within the SimpleSkin project, ACTLab has developed a sensorized collar for assessment of swallowing function by impedance pharyngography as shown in (Zhang, Freund et al. 2016). This wearable measurement system incorporated four textile electrodes and the ECGZ2 monitoring unit for bioimpedance measurements, as well as a carbon-based pressure sensor.

5.4.3 Biofeedback

Pace breathing and heart rate variability (HRV) analysis are common aspects of biofeedback training (Lehrer, Vaschillo et al. 2000). In *Abtahi et al.* (Abtahi, Berndtsson et al. 2014) a real-time application running on an Android phone collects and processes the measurements recorded using wearable sensors to provide users with HRV parameters and respiration rate during pace breathing training sessions. The ECGZ2 unit and the sensorized textile electrode vest garment presented in this research work are used in (Abtahi, Berndtsson et al. 2014). In their publication, they use the system on eight healthy volunteers to evaluate the system performance and usability, resulting in a biofeedback game (Wollmann, Abtahi et al. 2016).

References

Aberg, P., I. Nicander, J. Hansson, P. Geladi, U. Holmgren and S. Ollmar (2004). "*Skin cancer identification using multifrequency electrical impedance – A potential screening tool*." IEEE Trans. Bio. Med. Eng. 51(12): 2097-2102.

Abtahi, F., A. Berndtsson, S. Abtahi, F. Seoane and K. Lindecrantz (2014). "*Development and preliminary evaluation of an Android based heart rate variability biofeedback system*." Conf Proc IEEE Eng Med Biol Soc 2014: 3382-3385.

Alliance, E. K. H. (2014). "*Is kidney disease really such an important issue for Europe?*", from www.ekha.eu.

Analog Devices Inc. . (2005). "*AD5933 Datasheet Document*." 2016, from http://www.analog.com/ad5933.

Anand, I. S., A. D. Doan, K. W. Ma, J. A. Toth, K. J. Geyen, S. Otterness, N. Chakravarthy, R. P. Katra and I. Libbus (2012). "*Monitoring changes in fluid status with a wireless multisensor monitor: results from the Fluid Removal During Adherent Renal Monitoring (FARM) study*." Congest Heart Fail 18(1): 32-36.

Ayllon, D., F. Seoane and R. Gil-Pita (2009). "*Cole equation and parameter estimation from electrical bioimpedance spectroscopy measurements - A comparative study*". Engineering in Medicine and Biology Society, 2009. EMBC 2009. Annual International Conference of the IEEE.

Beard, C. (2013). "*No place like home: Increasing access to home dialysis*", Cheshire and Merseyside Strategic Clinical Networks.

Beckmann, L., C. Neuhaus, G. Medrano, N. Jungbecker, M. Walter, T. Gries and S. Leonhard (2010). "*Characterization of textile electrodes and conductors using standardized measurement setups*." Physiological Measurement 31(2): 233.

Bernstein, D. P. (2010). "*Impedance cardiography: Pulsatile blood flow and the biophysical and electrodynamic basis for the stroke volume equations*." Journal of Electrical Bioimpedance 1: 2-17.

Bernstein, D. P., I. C. Henry, M. J. Banet and T. Dittrich (2012). "*Stroke volume obtained by electrical interrogation of the brachial artery: transbrachial electrical bioimpedance velocimetry*." Physiological Measurement 33(4): 629.

Bernstein, D. P., I. C. Henry, H. J. Lemmens, J. L. Chaltas, A. N. DeMaria, J. B. Moon and A. M. Kahn (2015). "*Validation of stroke volume and cardiac output by electrical interrogation of the brachial artery in normals: assessment of strengths, limitations, and sources of error*." J Clin Monit Comput 29(6): 789-800.

Bogónez-Franco, P., A. Bayés-Genís, J. Rosell and R. Bragós (2010). "*Performance of an implantable impedance spectroscopy monitor using ZigBee*." Journal of Physics: Conference Series 224(1): 012163.

Bogónez-Franco, P., L. Nescolarde, R. Bragós, J. Rosell-Ferrer and I. Yandiola (2009). "*Measurement errors in multifrequency bioelectrical impedance analyzers with and without impedance electrode mismatch*." Physiological Measurement 30(7): 573.

Bragos, R., R. Blanco-Enrich, O. Casas and J. Rosell (2001). "*Characterisation of dynamic biologic systems using multisine based impedance spectroscopy*". 18th Instrumentation and Measurement Technology Conference, Budapest, Hungary, IEEE.

Buendía, R., P. Bogónez-Franco, L. Nescolarde and F. Seoane (2012). "*Influence of electrode mismatch on Cole parameter estimation from Total Right Side Electrical Bioimpedance Spectroscopy measurements*." Medical Engineering & Physics 34(7): 1024-1028.

Buendia, R., R. Gil-Pita and F. Seoane (2011). "*Cole Parameter Estimation from the Modulus of the Electrical Bioimpeadance for Assessment of Body Composition. A Full Spectroscopy Approach.*" Journal of Electrical Bioimpedance 2: 72-78.

Buendia, R., R. Gil-Pita and F. Seoane (2011). "*Cole parameter estimation from total right side electrical bioimpedance spectroscopy measurements--influence of the number of frequencies and the upper limit*". 33rd Annual International Conference of the IEEE EMBS, Boston, Massachusetts USA.

Buendia, R., F. Seoane, K. Lindecrantz, I. Bosaeus, R. Gil-Pita, G. Johannsson, L. Ellegard and L. C. Ward (2015). "*Estimation of body fluids with bioimpedance spectroscopy: state of the art methods and proposal of novel methods*." Physiol Meas 36(10): 2171-2187.

Codagnone, C. (2009). "*PHS2020 - Reconstructing the Whole: Present and Future of Personal Health Systems*." from http://ec.europa.eu/information_society/newsroom/cf/itemlongdetail.cfm?item_id=5555.

Cole, K. S. (1940). "*Permeability and impermeability of cell membranes for ions.*" Quant. Biol. 8: 110–122.

Continua Health Alliance. (2012). "*The Continua Health Alliance*." from http://www.continuaalliance.org/.

Davies, S. J. and A. Davenport (2014). "*The role of bioimpedance and biomarkers in helping to aid clinical decision-making of volume assessments in dialysis patients*." Kidney Int 86(3): 489-496.

De Lorenzo, A., A. Andreoli, J. R. Matthie and P. Withers (1997). "*Predicting body cell mass with bioimpedance by using theoretical methods: a technological review*." J Appl Physiol 82(5): 1542-1558.

Diamantidis, C. J. and S. Becker (2014). "*Health information technology (IT) to improve the care of patients with chronic kidney disease (CKD)*." BMC Nephrol 15: 7.

DoChange. (2016). "*European Project - DoChange. Do cardiac health: advanced new generation ecosystem*." from http://www.do-change.eu/.

Drukker, W., F. M. Parsons and J. F. Maher (1983). "*Replacement of Renal Function by Dialysis. A textbook of dialysis*", Springer Netherlands.

Earthman, C. P., R. R. Wolfe and S. B. Heymsfield (2015). "*Dudrick Research Symposium 2015-Lean Tissue and Protein in Health and Disease: Key Targets and Assessment Strategies*." JPEN J Parenter Enteral Nutr.

Ernst, J. F., D. A. Litvack, D. L. Lozano, J. T. Cacioppo and G. G. Berntson (1999). "*Impedance pneumography: noise as signal in impedance cardiography*." Psychophysiology 36(3): 333-338.

European Commission. (2000). "*eEurope 2002 Action Plan*." from http://ec.europa.eu/information_society/eeurope/2002/index_en.htm.

European Commission. (2007). "*Medical Devices Directive 2007/47/EC*." from http://ec.europa.eu/enterprise/policies/european-standards/harmonised-standards/medical-devices/index_en.htm.

European Commission. (2012). "*eHealth Action Plan 2012-2020 - Innovative healthcare for the 21st century* ", from http://ec.europa.eu/information_society/newsroom/cf/itemdetail.cfm?item_id=9156.

EuroStat. (2015). "*Eurostat - Healthcare statistics in the European Union*." from http://ec.europa.eu/eurostat/statistics-explained/images/b/b6/Healthcare_statistics_YB2015.xlsx.

Fernandez-Llatas, C., A. Martinez-Romero, A. M. Bianchi, J. Henriques, P. Carvalho and V. Traver (2016). "*Challenges in personalized systems for Personal Health Care*". 2016 IEEE-EMBS International Conference on Biomedical and Health Informatics (BHI).

Ferreira, J., I. Pau, K. Lindecrantz and F. Seoane (2016). "*A handheld and textile-enabled bioimpedance system for ubiquitous body composition analysis. An initial functional validation*." Journal Biomedical Health Informatics.

Ferreira, J., F. Seoane, A. Ansede Peña and R. Bragos (2010). "*AD5933-Based Spectrometer for Electrical Bioimpedance Applications*". XIV International Conference on Electrical Bioimpedance & 11th Electrical Impedance Tomography. Gainesville, Florida, IOP Publishing.

Ferreira, J., F. Seoane and K. Lindecrantz (2011). "*AD5933-based electrical bioimpedance spectrometer. Towards textile-enabled applications*". 33rd Annual International Conference of the IEEE Engineering in Medicine and Biology Society. Boston, USA Conf Proc IEEE Eng Med Biol Soc. 5: 3282-3285.

Ferreira, J., F. Seoane and K. Lindecrantz (2013). "*Evaluation of a Portable SoC-based Bioimpedance System for Plethysmography Applications*". Medicinteknikdagarna. 1-2 October 2013, Stokholm, Sweden.

Finni, T., M. Hu, P. Kettunen, T. Vilavuo and S. Cheng (2007). "*Measurement of EMG activity with textile electrodes embedded into clothing*." Physiol Meas 28(11): 1405-1419.

Fricke, H. and S. Morse (1925). "*The Electric Resistance and Capacity of Blood for Frequencies Between 800 and 4.5 Million Cycles*." Journal of General Physiology 9: 153-167.

Geddes, L. A. and L. E. Baker (1967). "*The specific resistance of biological material--a compendium of data for the biomedical engineer and physiologist*." Med Biol Eng 5(3): 271-293.

Grimnes, S. and Ø. G. Martinsen (2008). "*Bioimpedance & Bioelectricity Basics*", Elsevier Ltd.

Guerrero, M. (2015). "*Soluciones para la gestión de la cronicidad*." from http://www.sedisa.net/documentos/Mon20150914744172015091 4InformeGestionCronicidadSEDISA.pdf.

Hanai, T. (1968). "*Electrical properties of emulsions.*" Emulsion Science.

Henning, M. R. (2007). "*Affecting Kt/V: An Analysis of Staff Interventions*." Dialysis & Transplantation 36(11): 584-601.

IEC. (2010). "*IEC 60601-1 - Medical electrical equipment - Part 1: General requirements for basic safety and essential performance*." from http://www.iec.ch/.

ImpediMed. (2011). "*Impedimed SFB7 - Home Web page*." Retrieved 2016, from https://www.impedimed.com/products/sfb7-for-body-composition/.

International Electrotechnical Commission. (2010). "*IEC 60601-1 - Medical electrical equipment - Part 1: General requirements for basic safety and essential performance*." from http://www.iec.ch/.

Ismail, A. H. and S. Leonhardt (2013). "*Simulating Non-Specific Influences of Body Posture and Temperature on Thigh-Bioimpedance Spectroscopy during Continuous Monitoring Applications*." Journal of Physics: Conference Series 434(1): 012008.

Jaffrin, M. Y. and H. Morel (2008). "*Body fluid volumes measurements by impedance: A review of bioimpedance spectroscopy (BIS) and bioimpedance analysis (BIA) methods*." Med Eng Phys 30(10): 1257-1269.

Jha, V., G. Garcia-Garcia, K. Iseki, Z. Li, S. Naicker, B. Plattner, R. Saran, A. Y. Wang and C. W. Yang (2013). "*Chronic kidney disease: global dimension and perspectives*." Lancet 382(9888): 260-272.

Kubicek, W. G. (1969). "*Development and evaluation of an impedance cardiographic system to measure cardiac output and other cardiac parameters*". Minneapolis, Minneapolis The University.

Kuhlmann, M. K., F. Zhu, E. Seibert and N. W. Levin (2005). "*Bioimpedance, dry weight and blood pressure control: new methods and consequences*." Curr Opin Nephrol Hypertens 14(6): 543-549.

Kun, S. and R. A. Peura (1999). "*Selection of measurement frequencies for optimal extraction of tissue impedance model parameters*." Medical & Biological Engineering & Computing 37(6): 699-703.

Kushner, R. F., P. M. de Vries and R. Gudivaka (1996). "*Use of bioelectrical impedance analysis measurements in the clinical management of patients undergoing dialysis*." The American Journal of Clinical Nutrition 64(3): 503S-509S.

Kusuhara, T., T. Nakamura, Y. Shirakawa, K. Mori, Y. Naomoto and Y. Yamamoto (2004). "*Impedance pharyngography to assess swallowing function*." J Int Med Res 32(6): 608-616.

Lehrer, P. M., E. Vaschillo and B. Vaschillo (2000). "*Resonant frequency biofeedback training to increase cardiac variability: rationale and manual for training*." Appl Psychophysiol Biofeedback 25(3): 177-191.

Lekka, E., H. Reiter, J. Luprano, R. Hammerschmidt and N. Maglaveras (2008). "*Personalized Health Certification Procedure White Paper. HeartCycle Project*".

Marquez, J. C., J. Ferreira, F. Seoane, R. Buendia and K. Lindecrantz (2010). "*Textile Electrode Straps for Wrist-to-Ankle Bioimpedance Measurements for Body*

Composition Analysis. Initial Validation and Experimental Results". 32nd Annual International Conference of the IEEE Engineering in Medicine and Biology Society. Buenos Aires, Argentina.

Marquez, J. C., F. Seoane and K. Lindecrantz (2013). "*Textrode functional straps for bioimpedance measurements-experimental results for body composition analysis*." European Journal of Clinical Nutrition 67(S1): S22-S27.

Márquez Ruiz, J. C. (2013). "*Sensor-Based Garments that Enable the Use of Bioimpedance Technology : Towards Personalized Healthcare Monitoring*". 6, Technology and Health, KTH Royal Institute of Technology.

Matthie, J. R. (2008). "*Bioimpedance measurements of human body composition: critical analysis and*." Expert Rev Med Devices 5(2): 239-261 LID - 210.1586/17434440.17434445.17434442.17434239 [doi].

Medrano, G., L. Beckmann, N. Zimmermann, T. Grundmann, T. Gries and S. Leonhardt (2007). "*Bioimpedance Spectroscopy with textile Electrodes for a continuous Monitoring Application*". 4th International Workshop on Wearable and Implantable Body Sensor Networks (BSN 2007).

Medtronic. (2016). "*Continuous Glucose Monitoring by Medtronic*." from http://www.medtronicdiabetes.com/treatments/continuous-glucose-monitoring.

Merritt, C. R., H. T. Nagle and E. Grant (2009). "*Fabric-based active electrode design and fabrication for health monitoring clothing*." IEEE Trans Inf Technol Biomed 13(2): 274-280.

Miguel, S. S. (2010). "*Haemodialysis dry weight assessment: A literature review*." Renal Society of Australasia Journal 6(1).

Mohino-Herranz, I., J. P. Gil, F. Ferreira, M. Rosa-Zurera and F. Seoane (2015). "*Assessment of Mental, Emotional and Physical Stress through Analysis of Physiological Signals Using Smartphones*." Sensors 15(10): 25607-25627.

Moissl, U. M., P. Wabel, P. W. Chamney, I. Bosaeus, N. W. Levin, A. Bosy-Westphal, O. Korth, M. J. Muller, L. Ellegard, V. Malmros, C. Kaitwatcharachai, M. K. Kuhlmann, F. Zhu and N. J. Fuller (2006). "*Body fluid volume determination via body composition spectroscopy in health and disease*." Physiol Meas 27(9): 921-933.

Nations, U. (2012). "*Population Ageing and the Non-communicable Diseases*", Department of Economic and Social Affairs, United Nations.

Neuman, M. (2012). "*Some bright spots for home dialysis*". Nephrology News & Issues.

Neuman, M. R. (2009). "*BIOPOTENTIAL ELECTRODES*". Medical Instrumentation Application and Design, Wiley.

Nordbotten, B. J., C. Tronstad, Ø. G. Martinsen and S. Grimnes (2011). "*Evaluation of algorithms for calculating bioimpedance phase angle values from measured whole-body impedance modulus*." Physiological Measurement 32(7): 755.

Owen, N., P. B. Sparling, G. N. Healy, D. W. Dunstan and C. E. Matthews (2010). "*Sedentary Behavior: Emerging Evidence for a New Health Risk*." Mayo Clinic Proceedings 85(12): 1138-1141.

Pallas-Areny, R. and J. G. Webster (1993). "*Bioelectric impedance measurements using synchronous sampling*." Biomedical Engineering, IEEE Transactions on 40(8): 824-829.

Pallàs-Areny, R. and J. G. Webster (2001). "*Sensors and Signal Conditioning*", A Wiley-Interscience publication.

Piccoli, A., G. Pastori, M. Guizzo, M. Rebeschini, A. Naso and C. Cascone (2005). "*Equivalence of information from single versus multiple frequency bioimpedance vector analysis in hemodialysis*." Kidney Int 67(1): 301-313.

Pola, T. and J. Vanhala (2007). "*Textile Electrodes in ECG Measurement*". Intelligent Sensors, Sensor Networks and Information, 2007. ISSNIP 2007. 3rd International Conference on.

RobinNetworks. (2013). "*RN-42 - Class 2 Bluetooth 2.1 + EDR module - Robin Networks Inc.*", from http://www.rovingnetworks.com/products/RN_42.

Sanchez, B., G. Vandersteen, R. Bragos and J. Schoukens (2012). "*Basics of broadband impedance spectroscopy measurements using periodic excitations*." Measurement Science and Technology 23(10): 105501.

Scharfetter, H., P. Hartinger, H. Hinghofer-Szalkay and H. Hutten (1998). "*A model of artefacts produced by stray capacitance during whole body or segmental bioimpedance spectroscopy*." Physiological Measurement 19(2): 247-261.

Schwan, H. P. (1957). "*Electrical properties of tissue and cell suspensions*." Adv Biol Med Phys 5: 147-209.

Schwan, H. P. (1994). "*Electrical properties of tissues and cell suspensions: mechanisms and models*". Proceedings of 16th Annual International Conference of the IEEE Engineering in Medicine and Biology Society, Baltimore, MD, USA, IEEE.

Schwan, H. P. (1999). "*The Practical Success of Impedance Techniques from an Historical Perspective*." Ann N Y Acad Sci 873 1-12.

Seoane, F., S. Abtahi, F. Abtahi, L. Ellegard, G. Johannsson, I. Bosaeus and L. C. Ward (2015). "*Mean Expected Error in Prediction of Total Body Water: A True Accuracy Comparison between Bioimpedance Spectroscopy and Single Frequency Regression Equations*." Biomed Res Int 2015: 656323.

Seoane, F., J. Ferreira, L. Alvarez, R. Buendia, D. Ayllón, C. Llerena and R. Gil-Pita (2013). "*Sensorized Garments and Textrode-Enabled Measurement Instrumentation for Ambulatory Assessment of the Autonomic Nervous System Response in the ATREC Project*." Sensors 13(7): 8997-9015.

Seoane, F., J. Ferreira, J. J. Sanchez and R. Bragos (2008). "*An Analog front-end enables electrical impedance spectroscopy system on-chip for biomedical applications*." Physiological Measurement 29(6): S267-278.

Seoane, F., I. Mohino-Herranz, J. Ferreira, L. Alvarez, R. Buendia, D. Ayllon, C. Llenera and J. P. Gil (2014). "*Wearable biomedical measurement systems for assessment of mental stress of combatants in real time*." Sensors 14(4): 7120-7141.

Seppa, V., J. Viik and J. Hyttinen (2010). "*Assessment of pulmonary flow using impedance pneumography*." IEEE Trans Biomed Eng 57(9): 2277-2285.

Squires, D. A. (2012). "*Explaining high health care spending in the United States: an international comparison of supply, utilization, prices, and quality*." Issue Brief (Commonw Fund) 10: 1-14.

Van Biesen, W., J. D. Williams, A. C. Covic, S. Fan, K. Claes, M. Lichodziejewska-Niemierko, C. Verger, J. Steiger, V. Schoder, P. Wabel, A. Gauly, R. Himmele and B. C. M. s. g. on behalf of the Euro (2011). "*Fluid Status in Peritoneal Dialysis*

Patients: The European Body Composition Monitoring (EuroBCM) Study Cohort." PLoS ONE 6(2): e17148.

Van De Water, J. M., T. W. Miller, R. L. Vogel, B. E. Mount and M. L. Dalton (2003). "*Impedance cardiography: the next vital sign technology?*" Chest 123(6): 2028-2033.

Van Loan, M., P. Withers, J. Matthie and P. L. Mayclin (1993). "*Use of bio-impedance spectroscopy (BIS) to determine extracellular fluid (ECF), intracellular fluid (ICF), total body water (TBW), and fat-free mass (FFM).* ." Human Body Composition In Vivo Methods, Models, and Assessments: 4.

Woltjer, H. H., H. J. Bogaard, G. J. Scheffer, H. I. van der Spoel, M. A. Huybregts and P. M. de Vries (1996). "*Standardization of non-invasive impedance cardiography for assessment of stroke volume: comparison with thermodilution*." Br J Anaesth. 77(6): 748-752.

Wollmann, T., F. Abtahi, A. Eghdam, F. Seoane, K. Lindecrantz, M. Haag and S. Koch (2016). "*User-Centred Design and Usability Evaluation of a Heart Rate Variability Biofeedback Game*." IEEE Access 4: 5531-5539.

Wystrychowski, G. and N. W. Levin (2007). "*Dry weight: sine qua non of adequate dialysis*." Adv Chronic Kidney Dis 14(3): e10-16.

Yuxiang, Y., W. Jue, Y. Gang, N. Feilong and H. Ping (2006). "*Design and preliminary evaluation of a portable device for the measurement of bioimpedance spectroscopy*." Physiological Measurement 27(12): 1293.

Zhang, R., M. Freund, O. Amft, J. Cheng, B. Zhou, P. Lukowicz, S. Fernando and P. Chabrecek (2016). "*A generic sensor fabric for multi-modal swallowing sensing in regular upper-body shirts*". Proceedings of the 2016 ACM International Symposium on Wearable Computers. Heidelberg, Germany, ACM: 46-47.

Zhaurova, K. (2008). "*Genetic Causes of Adult-Onset Disorders*." Nature Education 1 1(49).

Annex I – Scientific publications

PAPER I

An analog front-end enables electrical impedance spectroscopy system on-chip for biomedical applications

Fernando Seoane, Javier Ferreira, Juan Jose Sanchez *et al.*

Published in Journal of Physiological Measurement, Vol. 29, S267-S278, 2008

IOP PUBLISHING PHYSIOLOGICAL MEASUREMENT

Physiol. Meas. **29** (2008) S267–S278 doi:10.1088/0967-3334/29/6/S23

An analog front-end enables electrical impedance spectroscopy system on-chip for biomedical applications

Fernando Seoane[1,2], **Javier Ferreira**[1], **Juan José Sanchéz**[1] **and Ramon Bragós**[3]

[1] School of Engineering, Medical Electronics Group, University College of Borås, Borås 50190, Sweden
[2] Department of Signals and Systems, Division of Biomedical Engineering, Chalmers University of Technology, Gothenburg 41296, Sweden
[3] Department of Electronic Engineering, Technical University of Catalonia, Barcelona 08034, Spain

E-mail: fernando.seoane@hb.se

Received 30 November 2007, accepted for publication 12 May 2008
Published 11 June 2008
Online at stacks.iop.org/PM/29/S267

Abstract

The increasing number of applications of electrical bioimpedance measurements in biomedical practice, together with continuous advances in textile technology, has encouraged several researchers to make the first attempts to develop portable, even wearable, electrical bioimpedance measurement systems. The main target of these systems is personal and home monitoring. Analog Devices has made available AD5933, a new system-on-chip fully integrated electrical impedance spectrometer, which might allow the implementation of minimum-size instrumentation for electrical bioimpedance measurements. However, AD5933 as such is not suitable for most applications of electrical bioimpedance. In this work, we present a relatively simple analog front-end that adapts AD5933 to a four-electrode strategy, allowing its use in biomedical applications for the first time. The resulting impedance measurements exhibit a very good performance in aspects like load dynamic range and accuracy. This type of minimum-size, system-on-chip-based bioimpedance measurement system would lead researchers to develop and implement light and wearable electrical bioimpedance systems for home and personal health monitoring applications, a new and huge niche for medical technology development.

Keywords: electrical bioimpedance spectroscopy, system-on-chip, four-electrode method

(Some figures in this article are in colour only in the electronic version)

1. Introduction

The continuous progress of medical applications of electrical bioimpedance spectroscopy (EBIS) (Aberg *et al* 2005, Moissl *et al* 2006, Caduff *et al* 2006), combined with recent advances in textile electrode technology (Pacelli *et al* 2006, Paradiso and De Rossi 2006), enable the development of bioimpedance-based measurement systems for home monitoring (Medrano *et al* 2007, Vuorela *et al* 2007) and personal monitoring (Scheffler *et al* 2003).

Traditionally, wearable systems for on-body measurements have focused on the acquisition of biosignals and activity monitoring, in the line of the EU project Wealthy IST-2001-37778 (Paradiso *et al* 2004). The European Commission has specifically supported several textile-based healthcare projects, e.g. BIOTEX IST-2004-016789, CONTEXT IST-2004-027291, MERMOTH FP6-IST-508272, MyHeart IST-2002-507816, OFSETH IST-2005-027869, PROETEX IST-2004-026987 and STELLA FP6-IST-028086. Currently, it is possible to find commercial products for personal healthcare monitoring, e.g. Lifeshirt® of Vivometrics® and adiSTAR® of Adidas.

Often the acquired signals are ECG and heart rate with electrodes, movement with accelerometers and respiration rate with piezoelectric and/or inductive sensors. EBI has not been among the typical measurements for monitoring until recently. Initially, EBI measurements target the respiration activity rate by impedance pneumography (Paradiso and De Rossi 2006, Seppä *et al* 2007), heart failure by impedance cardiography (Amft and Habetha 2007) and even body composition by bioelectrical impedance analysis (Hännikäinen *et al* 2007). Nowadays it is possible to find a commercially available, single-frequency ambulatory bioimpedance monitor for cardiac assessment: AIM-8 manufactured by Bio-Impedance Technology, Inc.

A concise review of wearable systems for physiological measurements can be found in Hännikäinen *et al* (2007). For comprehensive and detailed information about healthcare applications of smart textiles, see Van Langenhove (2007).

AD5933 is the first commercially available impedance network analyzer implemented in a single integrated circuit, and it allows us to take an important step from portable to wearable applications. The complexity of the impedance measurement system is reduced to basically one integrated circuit plus additional analog circuitry for signal conditioning, to meet the requirement for electrical bioimpedance (EBI) applications.

AD5933 alone is not suitable for EBI measurements on patients, or for several EBI applications, due to several factors, e.g. dc excitation, a voltage-driven system with large output impedance and a two-electrode system. In this work, we propose and validate the addition of an analog front-end (AFE) to fully adapt the AD5933 circuit to a four-electrode strategy. In this way, the deflection signal is adapted for on-body measurements. The resulting system is a multifrequency measurement system with very few ICs which is suitable for wearable applications.

2. Methodology

2.1. Materials

The core of the measurement system is the impedance network converter integrated circuit AD5933. The impedance measurement system by itself is the evaluation board for the AD5933 circuit provided by Analog Devices Inc., the EVAL-5933EB[4].

[4] See www.analog.com.

The AFE is implemented with general application op-amp circuits, instrumentation amplifiers and voltage references. An adaptation circuit for measurements of small impedance has been used as recommended by Analog Devices.

The software used to control AD5993 and display the impedance measurements is provided with the evaluation board. This software application has been adapted for correct four-electrode operation with Visual Basic 6.0.

All the documentation related to the AD5933 evaluation board, schematics, user manual and software is available at the Analog Devices Inc. website.

2.2. Accuracy test

Impedance measurements have been performed on pure resistive loads as well as on a 2R-1C series circuit; note the absence of physical electrodes or any equivalent dummy. The measurements have been done with and without the AFE in the frequency range from 5 kHz to 100 kHz.

To study the error performance and its dependence on the load dynamic range, a pure resistive load has been measured at 10 kHz and its deviation from the theoretical value has been calculated. The value of the working load has been changed from 50 Ω to 1.6 kΩ.

To study the frequency performance of the measurement system, the 2R-1C series circuit has been used as a measurement load, measuring both resistance and reactance.

2.3. Four-electrode validation

To validate the proper implementation of the four-electrode technique, impedance measurements have been performed on a 2R-1C series circuit phantom. The measurements have been done by modeling the electrodes with an equivalent electrical circuit. The electrode-equivalent circuits have been connected in series with the phantom and the four leads, for both injection and measurement. The elements and values of the equivalent circuit have been selected to model the effect of the electrode polarization impedance, Z_{EP}.

3. Electrical bioimpedance instrumentation

Electrical bioimpedance measurements are most often performed as deflection measurements by measuring the response of the system to an external electrical excitation (Pallàs-Areny and Webster 2001). Current is injected in the tissue under study (TUS) and the voltage drop caused in the load is measured or, reciprocally, the voltage is applied to the TUS and the correspondingly caused current through the TUS is measured. In either case, a generator for the excitation signal is required as well as a sensing stage to measure the response of the TUS.

Once the response to the excitation in voltage or current is measured by the system, the next step in an impedance measurement system is the impedance estimation process. This functional block estimates the complex impedance from the electrical measurements obtained, and there are several approaches to implementing this function. Sine correlation and Fourier analysis are choices often selected.

The electrodes are a critical element of an EBI measurement system; they function as an electronic-to-ionic interface between the electronic conductor in the measurement leads and the ionic conductor in the load, i.e. biological tissue. This interface can be described as a parallel circuit of a variable resistance R_E and a variable capacitance C_E; in addition, there is also a variable voltage source U_{EP} at the interface, as depicted in figure 1. The electrode impedance as well as the skin–electrode contact impedance can influence the impedance

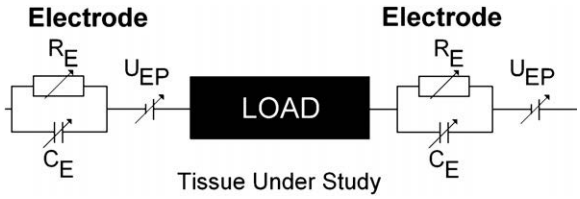

Figure 1. Equivalent model for the electrical interface, ionic–electronic, responsible for the electrode impedance Z_{EP} and its connection with the working load.

measurement to a very great extent, especially when the measurement setup is implemented as a two-electrode system.

In the two-electrode method, the same pair of electrodes is used to excite and to measure the response of the tissue. Therefore the impedance of the electrode, see figure 1, will be added to the impedance of the load. For instance if current is injected and voltage is measured, then the voltage measurement will contain the voltage drop caused in the TUS as well as the voltage drop caused in C_E and R_E.

The four-electrode method is a robust electrode setup that reduces the influence of the electrode impedance and the skin–electrode contact impedance. This method uses a pair of electrodes to excite the TUS and a different pair of electrodes to measure the response. In the case of current excitation, electrical current does not flow through the sensing electrodes because of the high input impedance of the differential amplifiers. Therefore, the sensed voltage does not contain any voltage drop caused by C_E and R_E (Pallàs-Areny and Webster 2001).

3.1. AD5933 impedance converter

AD5933 is a two-electrode impedance measurement system, with a large dynamic range of the measurement load. According to the datasheet, AD5933 is able to measure loads ranging from 1 kΩ to 1 MΩ, although the auxiliary resistor connected to the input feedback resistor (RFB) should be tailored for the specific range.

The AD5933 integrated circuit contains all the necessary elements to implement a fully integrated impedance spectrometer—in this case, a waveform generator, a voltage source output, a current measurement input, a Fourier-based impedance estimator and even a serial communication port. See figure 2.

Note that the impedance estimation method is based on the Fourier analysis decomposition of both the reference signal and the measurement signal. In this case the reference signal represents the applied voltage, while the measurement signal represents the current through the measurement load. The DFT block provides the result as the ratio of reference over measurement, i.e. *volts over amperes*, thus impedance in Ω, as indicated in (1). In this manner, the REAL and IMAGINARY registers contain resistance and reactance information, respectively:

$$\frac{\text{REFERENCE SIGNAL}}{\text{MEASUREMENT SIGNAL}} = \frac{V_{OUT}(\omega)}{I_{IN}(\omega)} = Z(\omega) \quad (\Omega). \tag{1}$$

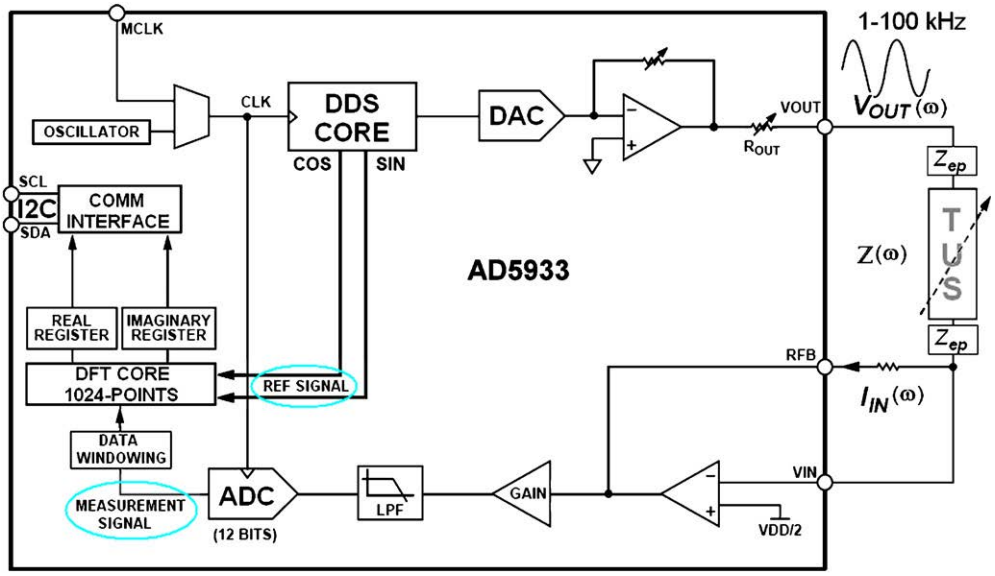

Figure 2. The functional block diagram of AD5933 for measurements of bioimpedance.

3.2. AD5933 as a bioimpedance device

The first point to note is that the AD5933 circuit is a two-electrode impedance measurement device. This fact by itself limits severely the range of application of usage, e.g. applications of spectral characterization are basically discarded since the impedance measurement obtained will also contain the electrode polarization impedance as well as the electrode–skin impedance.

Another important limitation of AD5933 is a safety issue: the voltage output contains a dc level, dc_{bias}, which is different from the dc level at V_{in}, namely $V_{dd/2}$. This imbalance produces a dc voltage across the electrodes and the TUS, introducing dc current in the TUS, which can be a health hazard for the patient.

Moreover, AD5933 is a voltage-driven measurement system without any control over the injected current. This might be a safety hazard issue since the injected current can be larger than the limits set by IEC-60601.

Most often, values of EBI measurements fall within the range of tens or hundreds of Ohms than in the range of thousands of ohms. According to the specifications in the datasheet, the lower limit of AD5933 is 1 kΩ. This fact might be an additional limitation, depending on the application, to performing measurements of bioimpedance.

Nevertheless, AD5933 can perform measurements of loads below 1 kΩ when the output voltage is attenuated by an op-amp in inverting configuration as indicated in figure 3.

3.3. Analog front-end specifications

The AFE must guarantee that the impedance measurement system is totally adapted to perform reliable four-electrode measurements of EBI according to the following specifications.

(i) The electrical safety of the patient must be ensured.
(ii) The dynamic range of measurement must be as expected in a human body.
(iii) The AFE must operate at any frequency supported by AD5933.

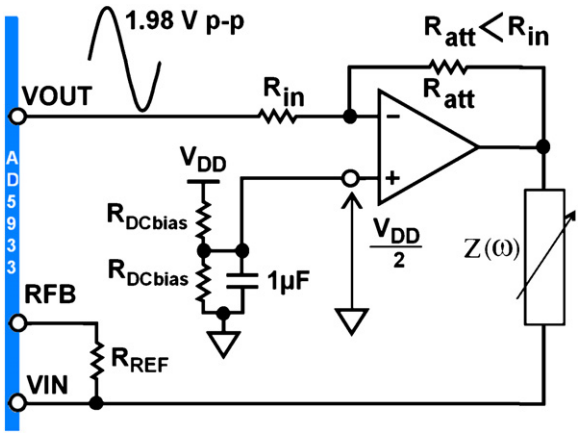

Figure 3. Attenuation circuit to adapt AD5933 for measurements of small impedance. The circuit proposed by Analog Devices in the datasheet of the evaluation board for AD5933. Note that 1.98 Vpp is the output for AD5933 functioning in Range 1 operation mode. Note that the resistive values used for implementing the circuit are 1 kΩ and 4.13 kΩ for R_{att} and R_{in} respectively, and the op-amp was TL082.

In order to achieve the aforementioned requirements, besides having an excitation and sensing ports totally independent of each other, i.e. four-electrode measurement setup, the AFE must block the flow of dc current through the TUS while simultaneously ensuring that the value of the ac current complies with the safety regulations imposed by IEC-60601. All these must be provided by the AFE while keeping the signal input and output signals of the AD5933 circuit within operational levels, i.e. avoiding current or voltage saturation.

3.4. System function and interfaces

The AFE is an interface between AD5933 and the TUS. As such, it must have the proper input and output stages to seamlessly interconnect to each of them. For a better understanding of the following description, it is advised to follow the block diagram depicted in figure 4.

In short, we could consider the AFE as a combination of two voltage-to-current converters (V2CC), one in the direction from AD5933 to the TUS and another from the TUS to AD5933.

Since AD5933 applies voltage and expects a current flowing into its RFB input, the AFE interfacing with AD5933 has a voltage input and a current output. The current source output expressly generates the current resulting from the ratio of V_{out} and the impedance of the TUS, which is the current expected by AD5933 at the RFB input.

At the TUS side, the AFE has a current source as output while the input is a differential voltage measurement channel. The current source excites the TUS with an adjustable current. In this case, a current of 350 μA rms has been selected, thus fully complying with IEC-60601 for measurements above 3.5 kHz.

In essence, the AFE operation can be described as follows: after the removal of the dc bias component from the voltage output of AD5933 with a high-pass filter at the input of the first V2CC. The ac voltage from V_{out} drives a voltage-controlled current source (VCCS) injecting an ac current I_{out} into the TUS. Note that I_{out} is directly proportional to V_{out}. The ac current I_{out} causes a voltage drop at the TUS, which is sensed by the second V2CC and, since the voltage drop at the TUS drives the second V2CC, an ac current proportional to the voltage drop in the

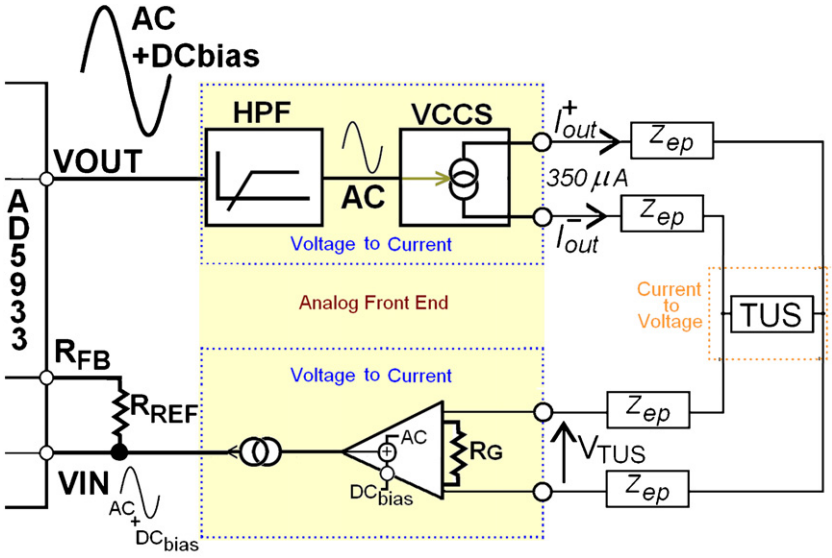

Figure 4. Functional block diagram of the proposed and implemented analog front-end.

TUS is generated. Finally, a dc component is added to the ac current generated. This added dc component is equivalent to dc_{bias} originally removed from V_{out}. Note that the total gain introduced by the cascade combination of both V2CC together with the resistor R_{REF} at the input RFB sets the upper limit of the load dynamic range:

$$V_{DAC\_max} \geqslant R_{REF} \times g_{m2} \times g_{m1} \times V_{out} \times Z_{TUS\_max}. \tag{2}$$

Even when carefully selecting the transconductance functions g_{m1} and g_{m2} of the V2CCs in (3), the total gain of the AFE can be set to 1. The AFE introduces a critical change in the impedance estimation process implemented by AD5933. Originally, AD5933 implemented the impedance estimation by performing the quotient of a voltage signal over a current signal, assigned to the reference signal and the measurement signal respectively. The AFE modifies such signal assignation in such a way that the operation performed by AD5933 is the quotient between a current signal over a voltage signal, i.e. amperes over volts, corresponding with the admittance of the measurement load instead. This issue has to be considered by the software application when handling the estimated immitance data:

$$\frac{\text{REFERENCE SIGNAL}}{\text{MEASUREMENT SIGNAL}} = \frac{V_{OUT}(\omega)}{I_{IN}(\omega)} = \frac{I_{load}(\omega)/g_{m1}}{g_{m2} \times I_{load}(\omega) \times Z(\omega)} = \frac{1}{Z(\omega)} \times \frac{1}{g_{m2} \times g_{m1}} = Y(\omega). \tag{3}$$

4. Performance results

4.1. Accuracy

The performance of the EBI measurement system can be observed in figures 5 and 6. Figure 5 contains the measurement error obtained at 10 kHz for measurements of resistive loads with both measurement arrangements, as follows.

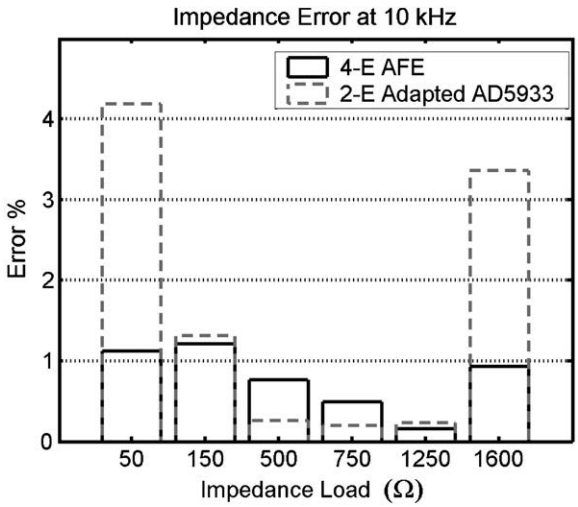

Figure 5. Impedance measurement error for measurements at 10 kHz with both measurement arrangements. Note that the calibration has been done with a resistive load of 1000 Ω.

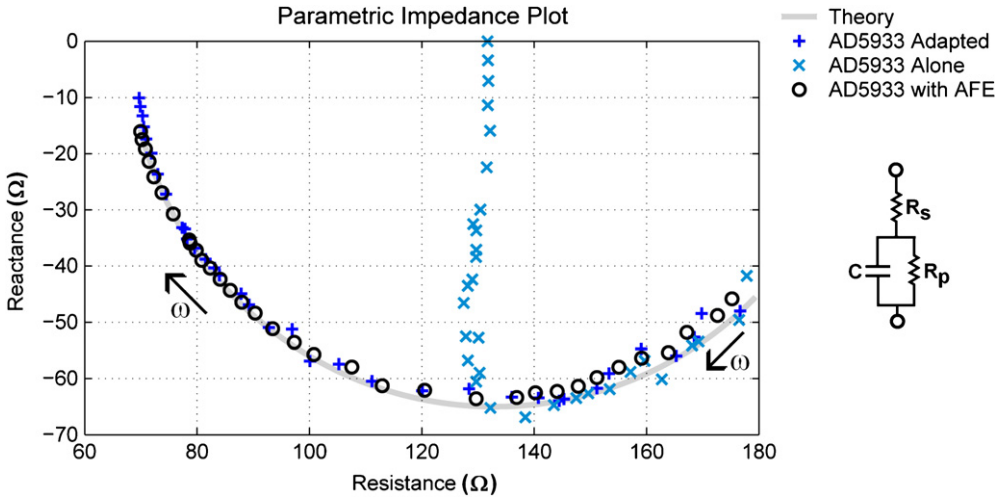

Figure 6. Parametric impedance plot of theoretical and measured values of a series 2R-1C circuit. $R_s = 68\ \Omega$, $R_p = 130\ \Omega$ and $C = 100$ nF. Frequency range: 5–100 kHz. Note that since the TUS used in this measurement is an electrical phantom, there is no electrode polarization impedance present, Z_{EP}.

(i) Four-electrode setup using the AFE. The bar is plotted with discontinuous trace.
(ii) Two-electrode setup using the attenuation circuit described in figure 3. The bar is plotted with solid trace.

In general, the measurement error is kept very low for most of the impedance range, especially for values near the calibration value, 1000 Ω.

In figure 6, the parametric plot reactance versus resistance contains the impedance values of a 2R-1C series model. For comparison, the measurements obtained with AFE, without

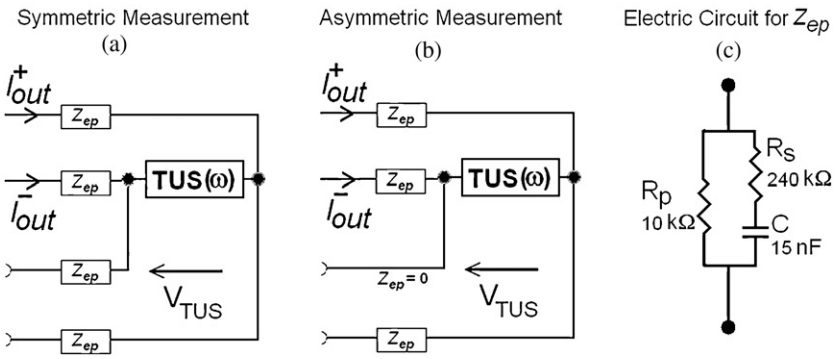

Figure 7. A lead imbalance experiment to test the proper implementation of the four-electrode method.

AFE and with the attenuation circuit are plotted together with the theoretical value. Note that the electrical series circuit is the measurement load as such, and therefore there is no electrode polarization impedance of any kind present in these measurements.

It is easy to note, in the impedance plots in figure 6, the remarkable agreement between the theoretical values and the measurement done with the AFE, especially at high frequencies. Note that the frequency range of the measurement is 5–100 kHz, increasing clockwise as indicated in the plots.

In figure 6, it is also possible to observe that the measurements performed with AD5933 and the attenuator circuit do not match the theoretical values as well as those with the AFE.

Another significant result to remark is the asymptotic behavior of the measurements performed with AD5933 alone. These measurements apparently indicate the lower limit of the impedance measurement range.

4.2. Electrode polarization avoidance

The effect of electrodes has been modeled by adding impedances to the measurement leads. The goal pursued with the addition of these impedances is to simulate the effect of the electrode polarization impedance Z_{ep}. The electrode model used for this experiment is depicted in figure 7(c). Impedance measurements have been done with two different setups: symmetric and asymmetric, as depicted in figures 7(a) and (b) respectively, and the results of the corresponding measurements are plotted in the impedance parametric plot in figure 8. The plot contains the value of the measurements, dotted trace and discontinuous trace for the symmetric case and the asymmetric case, respectively, and for comparison the theoretical value of the measurement load is plotted with the continuous trace.

5. Discussion

5.1. On the application of AD5933 for electrical biomedical impedance

The reported measurements strongly indicate that the AD5933 impedance converter by itself cannot be used for any application EBIS where proper electrical characterization is needed. This result was expected, since AD5933 performs two-electrode measurements only.

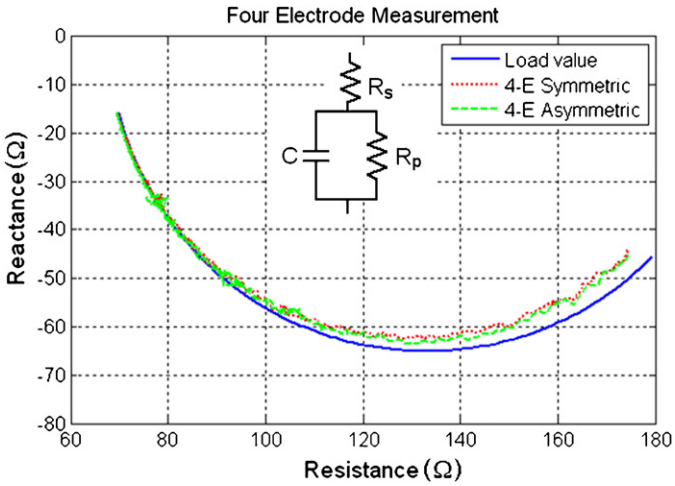

Figure 8. The parametric impedance plot of a series 2R-1C circuit. $R_s = 68\ \Omega$, $R_p = 130\ \Omega$ and $C = 100$ nF, with impedance in leads modeling the effect of electrodes. Frequency range: 5–100 kHz. Note that the value for the capacitor in the theoretical calculations is the nominal value, while the value for the resistors R_s and R_p is the value measured at measured dc.

In addition to this limitation, the excitation signal generated by AD5933 is not dc free and the signal is injected by a voltage source. An important consequence of the voltage excitation is that the current through the load is dependent on the impedance value of the load as well as on the electrode polarization impedance. Since the value of the working load, mostly the electrode polarization impedance, can change with time, the current through the tissue can exceed the limit imposed by IEC-60601.

Another important limitation regarding the voltage source of AD5933 is that its minimum output impedance, R_{out}, is 200 Ω. Such a value is very high for a voltage source, especially when the working load can be very small, as in electrical bioimpedance applications.

Moreover, apparently AD5933 cannot measure loads smaller than 130 Ω approximately. See figure 6. This lower limit is related to the voltage source, R_{out} of 200 Ω and 5.8 mA Vpp of the ac output current. With a maximum current of 5.8 mA and a voltage source providing around 1.9 Vpp, the minimum load is approximately 330 Ω, including 200 Ω of R_{out}. This might not be a limitation in practice, since in a bioimpedance application the presence of the electrodes will increase the value of the working load.

5.2. Frequency performance with a whole single dispersion capacitive system

The measurements obtained with the proposed measurement system and the theoretical values agree significantly well in the whole frequency range. In this frequency range, we should not expect large parasitic effects in RC dummy circuits. Nevertheless, in a wearable application the measurement scenario is much more hostile, and the existence of parasitic capacitances might ruin the measurements. AD5933 has a built-in function for calibration, but at this point it is unknown to what extent such a feature will contribute to minimizing this type of negative effect.

5.3. Accuracy performance and load dependence

The reported experimental results indicate that the introduction of an external AFE does not significantly worsen AD5933. As expected, the results suggest that the best performance

is obtained when the measurement load approximates to the calibration load. In a typical application of electrical bioimpedance, the target load will have a dynamic range much smaller than the impedance range considered in these tests. Therefore it is most likely that the impedance measurement system will be able to keep, for each specific application, the high accuracy reported in figure 5.

5.4. Four-electrode setup

The four-electrode technique is successfully implemented with the AFE, as the measurements with simulated electrodes and particularly the asymmetric test show. The only source of concern is the observed deviation of both measurements at low frequencies from the theoretical value. This deviation may be due to the fact that the theoretical value for the circuit is calculated with the nominal value and not with the real value of the test components. The circuit overcomes the intrinsic limitation of the two-electrode structure of the AD5933 device. Note that measurements with the original two-electrode setup of AD5933 would have produced impedance values in the range of several kΩ, including the impedance of the electrode equivalent model (Ferreira and Sanchez 2007).

5.5. Limitations

The only foreseen limitation for this type of device is the upper limit frequency. A maximum high frequency of 100 kHz is not enough for certain EBI applications, especially when the purpose of the measurement is to characterize the full beta dispersion. In the datasheets provided by Analog Devices, the option to measure above 100 kHz is considered. We have not tested the performance of AD5933 above the recommended frequency range in this work because the objective of the work was to adapt AD5933 for EBI measurements.

Regarding safety issues of the AFE due to the excitation current, the implemented solution as such can be used to measure EBI at frequencies down to 3.5 kHz, complying with IEC-60601. Simply by adjusting the transconductance of the first VCCS in the AFE, the output current can be adjusted to perform measurements of EBI at lower frequencies.

6. Conclusions

The analog front-end proposed in this paper complies with the initial requirements. It implements a complete four-electrode measurement system, and completely adapts AD5933 for electrical bioimpedance measurements. This achievement is obtained by the addition of very few ICs, in essence only two, and a few passive components. This simple analog front-end, in combination with the unique system-on-chip impedance spectrometer, reduces the size and complexity of the electronics of an EBI measurement system.

The development of wearable home-monitoring devices can benefit to a very large extent from such reduction in size and complexity, while it allows the implementation of EBI measurement systems with target sizes similar to mobile phones or even watches. The availability of such minimal monitoring devices would contribute substantially to spreading the use of EBI measurement for home monitoring and wearable applications.

References

Aberg P *et al* 2005 Non-invasive and microinvasive electrical impedance spectra of skin cancer—a comparison between two techniques *Skin Res. Technol.* **11** 281–6

Amft O and Habetha J 2007 *Smart Textiles for Medicine and Healthcare. Materials, Systems and Applications* ed L Van Langenhove (Cambridge, UK: Woodhead Publishing) pp 275–301

Caduff A *et al* 2006 Non-invasive glucose monitoring in patients with diabetes: a novel system based on impedance spectroscopy *Biosens. Bioelectron.* **22** 598–604

Ferreira J and Sanchez J J 2007 Electrical bioimpedance measurement system for limb edema monitoring *Master Thesis* School of Engineering, University College of Borås p 104

Hännikäinen J, Vuorela T and Vanhala J 2007 Physiological measurements in smart clothing: a case study of total body water estimation with bioimpedance *Trans. Inst. Meas. Control* **29** 337–54

Medrano G *et al* 2007 Bioimpedance spectroscopy with textile electrodes for a continuous monitoring application *4th Int. Workshop on Wearable and Implantable Body Sensor Networks (BSN 2007)* pp 23–8

Moissl U M *et al* 2006 Body fluid volume determination via body composition spectroscopy in health and disease *Physiol. Meas.* **27** 921–33

Pacelli M, Loriga G, Taccini N and Paradiso R 2006 Sensing fabrics for monitoring physiological and biomechanical variables: e-textile solutions *Medical Devices and Biosensors, 2006. 3rd IEEE/EMBS Int. Summer School* pp 1–4

Pallàs-Areny R and Webster J G 2001 *Sensors and Signal Conditioning* (New York: Wiley-Interscience)

Paradiso R and De Rossi D 2006 Advances in textile technologies for unobtrusive monitoring of vital parameters and movements *Engineering in Medicine and Biology Society, 2006. EMBS '06. 28th Annual Int. Conf. IEEE (New York)* pp 392–5

Paradiso R, Loriga G and Taccini N 2004 Wearable health care system for vital signs monitoring *MEDICON 2004 (Naples)*

Scheffler M, Hirt E and Caduff A 2003 Wrist-wearable medical devices: technologies and applications *Med. Dev. Technol.* **14** 26–30

Seppä V P, Väisänen J, Kauppinen P K, Malmivuo J and Hyttinen J 2007 Measuring respirational parameters with a wearable bioimpedance device *ICEBI* (Graz: Springer)

Van Langenhove L 2007 *Smart Textiles for Medicine and Healthcare. Materials, Systems and Applications* (Cambridge, UK: Woodhead Publishing)

Vuorela T, Seppä V P, Vanhala J and Hyttinen J 2007 Wireless measurement system for bioimpedance and ECG *12th Int. Conf. on Electrical Bio-Impedance* ed H Scharfetter and R Merwa (Graz: Springer)

PAPER II

AD5933-based spectrometer for electrical bioimpedance applications

Javier Ferreira, Fernando Seoane, Antonio Ansede Peña *et al.*

Published in Journal of Physics: Conference Series Vol. 224, doi:10.1088/1742-6596/224/1/012011 and presented at the XIVth International Conference on Electrical Bioimpedance & XIth Electrical Impedance Tomography, Florida, 2010

AD5933-based Spectrometer for Electrical Bioimpedance Applications

J. Ferreira[1], F. Seoane[1,2], A. Ansede[1,3] and R. Bragos[3]

[1] School of Engineering, University of Borås, SE-501 90 Borås, SWEDEN

[2] Department of Signal & Systems, Chalmers University of Technology, SE-41296, Gothenburg, SWEDEN

[3] Department of Electronic Engineering. Universitat Politècnica de Catalunya. Campus Nord, C-4. Jordi Girona 1-3. 08034, Barcelona. SPAIN

E-mail: fernando.seoane@hb.se

Abstract. To build an Electrical Bioimpedance (EBI) spectrometer using the Impedance Measurement System-On-Chip AD5933 together with a 4-Electrode Analog Front End (4E-AFE) has been proven practicable. Such small measurement devices can make possible several new applications of EBI technology, especially when combined with functional textiles, which can enable wearable applications for personal health and home monitoring. After the implementation and functional validation of the 4E-AFE-enabled spectrometer, the next natural step is to validate for which EBI applications the 4E-AFE-enabled system is suitable. To test the applicability of this novel spectrometer on several EBI applications, 2R1C equivalent models have been experimentally obtained and impedance spectroscopy measurements have been performed with the system under study and with the SFB7 EBI spectrometer manufactured by ImpediMed. The 2R1C circuit parameters have been estimated with the BioImp software from the spectra obtained with both EBI spectrometers and the estimated values have been compared with the original values used in each circuit model implementation. The obtained results indicated that the 4E-AFE-enabled system cannot beat the performance of the SFB7 in accuracy but it performs better in preciseness. In any case the overall performance indicates that the 4E-AFE-enabled system can perform spectroscopy measurements in the frequency range from 5 to 100 kHz.

1. Introduction

Over recent years, advances in different technological fields like electronics, physics and materials have made possible to embed complex functional systems into a single integrated circuit producing the System-on-Chip technology. As a result of such technological advances a whole impedance spectrometer is available on a single integrated circuit: the AD5933 [1] from Analog Devices. Such a level of integration together with advances made in textile technology, especially in the development of textile electrodes suitable for applications of Electrical Bioimpedance (EBI) [2], might enable wearable applications for personal health and home monitoring based in EBI measurements.

In this work the performance of a custom-made EBI spectrometer based on the AD5933 in combination with a 4-electrode Analog Front End [3] is evaluated when measuring 3 different

impedance loads modeling three typical EBI applications: Total Body Composition (TBC), Respiration Rate (RR) and Lungs Composition (LC), also known as Pulmonary Edema [4] .

2. Materials and Methods

2.1. Spectrometers and 2R1C models

Two different spectrometers have been used in this work: the ImpediMed SFB7 and a custom-made device based in the AD5933 in combination with an analog front-end to enable 4-electrode impedance measurements [3].

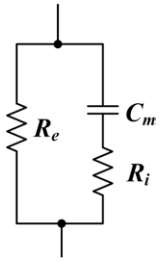

Figure 1. 2R1C parallel bridge model

The measurements have been performed on a 2R1C parallel electrical model representing biological tissue, see Figure 1. The values of the model parameter to build the 2R1C models, R_e, R_i and C_m, were extracted from experimental EBI measurements with the software BioImp [5]. The 2R1C have been build to produce an impedance complex spectrum similar to experimental impedance spectra obtained in the aforementioned applications. The resistors used in the model belong to the E-24 series and a potentiometer was used to trim the values of the circuit parameters, see Table 1, to obtain the intended impedance spectrum.

Table 1. 2R1C Modeling for TBC, RR and LC EBI Applications.

EBI Application	Electrical Equivalent 2R1C Values		
	R_e (Ω)	R_i (Ω)	C_m (nF)
TBC	917.5	665.4	3.42
RR	58.5	25.58	75.7
LC	81.5	22.15	47.7

2.2. Methods

Using both impedance spectrometers, 100 impedance measurements were performed in the frequency range 5 to 100 kHz on each experimentally-based 2R1C circuit model. For each EBI application the average complex spectrum from the measurements was obtained for each of the impedance spectrometers. A comparison between the resistance and the reactance spectra obtained from each spectrometer has been done.

Using the software BioImp applied on the measured impedance spectra obtained with each of the spectrometers, the value of the 2R1C circuit parameters was estimated and the obtained estimation error was studied to perform a comparison between the SFB7 and the AD5933-based spectrometer.

3. Results

3.1. Spectral Measurements

The reactance and resistance spectra from the impedance measurements for the different EBI applications are plotted in Figure 2. As it is denoted in all the spectral plots, the spectra obtained with both devices are perfectly overlapped for both the resistance and the reactance. Only a small deviation at high frequency can be observed on the reactance of for TBC and RR on Figure 2.b) and 2.d) respectively.

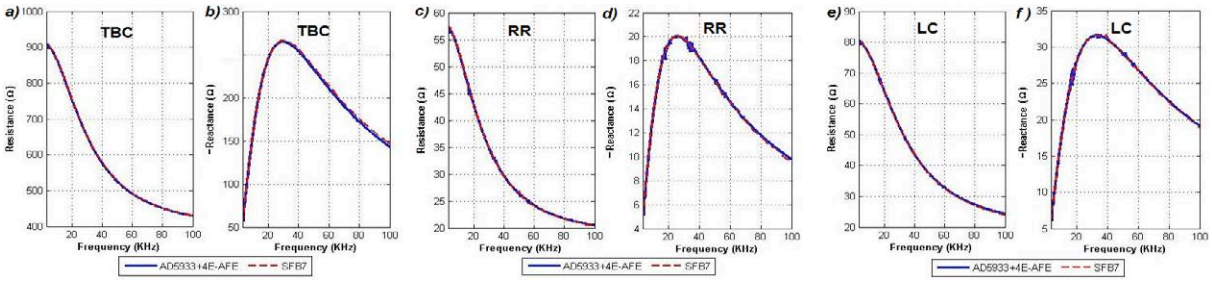

Figure 2. Resistance and reactance spectrum plots from the measurements obtained with the AD5933-based spectrometer in continuous and SFB7 in dashed trace, respectively.

3.2. 2R1C Circuit Parameters Estimation

The average values estimated for the 2R1C parameters from the impedance measurements obtained with both spectrometers are indicated in Table 2. For each of the applications, the relative differences respect the real values of the circuit components, as indicated in Table 1, are indicated by the relative error. The Standard Deviation obtained with both spectrometers for the estimation of each of the parameters is also indicated. For all the applications and all the parameters with the exception of the estimation of C_m for TBC, the SFB7 exhibit a smaller error than the AD5933-based spectrometer. Regarding to the Standard Deviation, it is the AD5933-based spectrometer the one that presents lower values for each of the parameters and all three applications.

Table 2. Error and Accuracy on 2R1C Parameters Estimation, SFB7 vs. AD5933+4E-AFE

EBI Application		TBC		RR		LC	
Parameter		SFB7	AD+AFE	SFB7	AD+AFE	SFB7	AD+AFE
R_e	Average Value (Ω)	917,88	914,15	58,33	57,89	81,37	81,07
	Standard Deviation	0,1594	0,0423	0,0177	0,0077	0,0193	0,0131
	Relative Error	0,04%	0,36%	0,29%	1,03%	0,16%	0,53%
R_i	Average Value (Ω)	664,49	676,3	25,60	26,00	22,25	22,95
	Standard Deviation	0,5540	0,1280	0,0493	0,0238	0,0498	0,0193
	Relative Error	0,14%	1,64%	0,08%	1,63%	0,44%	3,63%
C_m	Average Value (nF)	3,34	3,37	74,56	74,08	46,67	46,28
	Standard Deviation	0,0009	0,0003	0,0444	0,0181	0,0149	0,0117
	Relative Error	2,22%	1,47%	1,50%	2,14%	2,16%	2,97%

4. Discussion

The spectral plots obtained with both spectrometers show that the AD5933-based spectrometer with the 4-electrode enabling front-end produced complex impedance spectra that are almost exact to the spectra obtained with the SFB7.

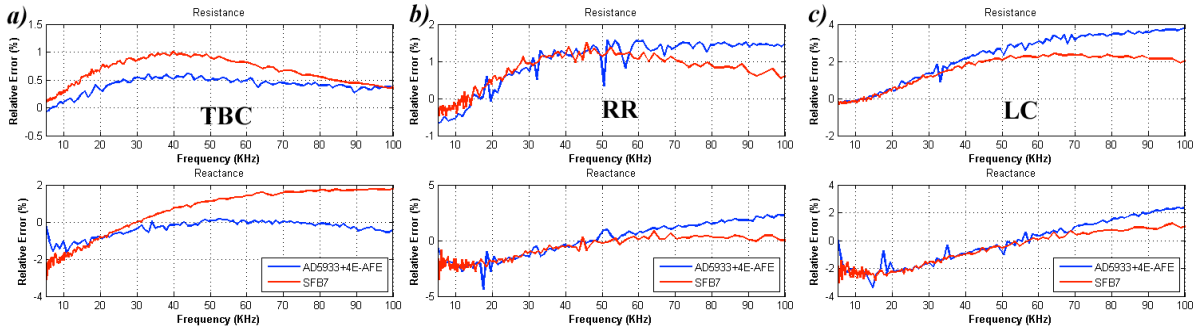

Figure 3. Relative measurement error in the resistance and the reactance obtained for the measurements with both EBI spectrometers for the three applications under study: TBC, RR and LC in a),b) and c) respectively

The analysis of the error data provided by Table 2 and Figure 3, suggest that the SFB7 presents a better accuracy than the AD5933-based spectrometer. In any case the estimation errors produced with both devices are generally low.

In the other hand according to Table 2, the preciseness shown by the custom-made impedance spectrometer based on the AD5933 is higher than the preciseness obtained with the SFB7. Both dispersions and errors obtained with both equipments are small compared with the high variability of the clinical measurements. E.g. in the measuring of Lungs Circulate Air Volume [5] the error measured with a neumotacometer and with Electrical Impedance Tomography (EIT) is around 20%, compared with the worst case studied in this work for RR the error drops below 4%.

5. Conclusion

The good complex spectroscopy performance exhibited by the AD5933-based spectrometer as well as the high accuracy and precision exhibited for the 2R1C model parameter estimation, which is critical in applications of total body composition assessment [6], strongly supports that EBI spectrometers based in SOC solutions like the AD5933 can be use in typical EBI applications like body composition analysis, respiration rate and pulmonary edema.

The reduced size of the AD5933, its small power consumption [7] together with the availability of off-the-shelf Bluetooth solutions indicate that the implementation of portable applications of EBI is close, even wearable if combined with textile garments [8] and electrodes [2].

6. References

[1] Analog Devices *AD5933 Product web site*. Accessed on 2010-01-15; Available from: http://www.analog.com/en/AD5933/productsearch.html.

[2] Márquez JC *et al*. 2009 Textile Electrodes in Electrical Bioimpedance Measurements - A Comparison with Conventional Ag/AgCl Electrodes *in Conf Proc IEEE Eng Med Biol Soc*, **1**: p. 4816-9

[3] Seoane F *et al*. 2008 An analog front-end enables electrical impedance spectroscopy system on-chip for biomedical applications. *Physiol. Meas.* **29**(6): p. S267-78.

[4] Mayer M *et al*. 2005 Monitoring of lung edema using focused impedance spectroscopy: a feasibility study. *Physiol. Meas.* **26**: p. 185-92.

[5] Ansede A 2009 A Feasibility Study of the Suitability of an AD5933-based Spectrometer for EBI Applications *Master Thesis Series* University of Borås.

[6] De Lorenzo A *et al.* 1997 Predicting body cell mass with bioimpedance by using theoretical methods: a technological review *J Appl. Physiol.* **82**(5): p. 1542-1558.

[7] Macias R 2009 Towards Wearable Spectroscopy Bioimpedance Applications Power Management for a Battery Driven Impedance Meter *Master Thesis Series* University of Borås.

[8] MyHeart IST 2002-507816. *Project web site* Accessed on 2010-01-15; Available from: http://www.hitech-projects.com/euprojects/myheart.

PAPER III

AD5933-based electrical bioimpedance spectrometer; towards textile-enabled applications

Javier Ferreira, Fernando Seoane, and Kaj Lindecrantz

Published and presented at the 33rd Annual International Conference of the IEEE Engineering in Medicine and Biology Society, Boston, USA 2011

33rd Annual International Conference of the IEEE EMBS
Boston, Massachusetts USA, August 30 - September 3, 2011

AD5933-Based Electrical Bioimpedance Spectrometer. Towards Textile-Enabled Applications

J. Ferreira, *Student Member IEEE,* F. Seoane, *Member IEEE,* and K. Lindecrantz, *Member IEEE.*

***Abstract*— Advances on System-On-Chip and Textile technology allows the development of Textile-enabled measurement instrumentation. Textile Electrodes (Textrodes) have been proven reliable for performing Electrical Bioimpedance Spectroscopy (EBIS) measurements, and the availability of a integrated circuit impedance spectrometer, the AD5933, has allowed the implementation of small size EBIS spectrometers.**

In this work an AD5933-based spectrometer has been implemented, and its performance on 2R1C circuits and for tetrapolar total right side EBIS measurements has been compared against the commercially available spectrometer SFB7. The study has been focused on the working upper frequency range and the estimation of the Cole parameters required for assessment of body fluid distribution: R_0 and R_∞. The results indicate that AD5933-based spectrometer implemented in this work can perform accurate impedance measurements well above the upper limits recommended in the datasheet. The AD5933-EBIS presents a good performance compared with the SFB7 on the 2R1C circuit and the total right side measurements, showing a smaller error in the resistance spectrum and small deviation error in the reactance when measuring over 270 kHz. The comparison on the Cole parameters estimation obtained with the SFB7 and the AD5933-based spectrometer exhibit a difference below 1% for the estimation of R_0 and R_∞. Consequently the overall measurement performance shown by the implemented AD5933-based spectrometer suggests its feasible use for EBIS measurements using dry Textrodes. This is of special relevance for the proliferation of EBI-based personalized health monitoring systems for patients that require to monitor the distribution of body fluids, like in dialysis.

I. Introduction

Technological improvements in System-on-Chip technology have enabled the integration of complex functional systems into a single integrated circuit. As a result a complete impedance spectrometer is available on a single integrated circuit: AD5933 manufactured by Analog Devices [1]. Its availability in combination with a 4-Electrode Analog Front End (4E-AFE) [2] has allowed the development of a complete Electrical Bioimpedance Spectrometer (EBIS). The performance of the AD5933-based EBIS has been tested on electrical 2R1C-circuits for several Electrical Bioimpedance (EBI) applications [3], validating its potential use on EBI applications like Body Composition Assessment (BCA).

Recent developments in conductive textile fabrics and electrode technology have allowed the implementation of Textile electrodes (Textrodes) garments for EBI-based measurements for BCA [4-5] and cardiovascular monitoring [6].

The BCA parameters indicating the amount of Extra-Cellular (ECF), Intra-Cellular (ICF) and Total Body Fluid (TBF) [7] are obtained from the estimation of the resistance value at DC and infinite frequency, known as Cole parameters R_0 and R_∞. The broader the frequency range of the obtained EBI measurement spectrum, the better the accuracy of the estimations of the Cole parameters will be. Therefore the frequency limits of the EBI measurement play an important role in the correct estimation of the BCA parameters.

According to the datasheet [1], the AD5933 spectrometer recommended frequency analysis is from 1 to 100 kHz with a system accuracy below 0.5%, but in reality the device allows to perform impedance measurements up to 500 kHz. The availability of such EBI spectrometer together with the proper textrode garment would allow the implementation of BCA monitoring systems for home applications [8].

In this work, the measurement performance of a custom made AD5933-based EBI spectrometer using dry Textrodes is studied, with typical experimental EBI measurements for BCA from the point of view of the estimation of R_0 and R_∞ and with special attention to the upper frequency limit. The work is based in a comparative study between the AD5933-based EBI spectrometer and a commercially available spectrometer: the ImpediMed SFB7.

II. Materials and Methods

A. EBI Spectrometers

Two EBI spectrometers have been used in this work: the ImpediMed SFB7 and a custom made AD5933-EBIS.

The SFB7 [9] performs tetrapolar measurements in the frequency range from 4 kHz to 1000 kHz, and it has been used as a golden standard.

The AD5933-EBIS is based the AD5933 Impedance

Manuscript received April 15, 2011.

J. Ferreira is with the School of Engineering at the University of Borås, 501 90 SWEDEN and the School of Technology and Health at Royal Institute of Technology, SE-141 52 Huddinge, SWEDEN (javier.ferreira@hb.se)

F. Seoane is with the School of Engineering at the University of Borås, 501 90 SWEDEN and the School of Technology and Health at Royal Institute of Technology, SE-141 52 Huddinge, SWEDEN. (fernando.seoane@hb.se).

K Lindecrantz is with the School of Technology and Health at Royal Institute of Technology, SE-141 52 Huddinge, SWEDEN. (kaj.lindecrantz@sth.kth.se)

Fig.1 Textrode garment prototype placement.

Network Analyzer as impedance core, and performs also tetrapolar measurements implementing the 4E-AFE introduced in [2] . The upper frequency limit was incremented up to 450 kHz just by programming the AD5933 registers to do so. The AD5933-based EBIS is battery driven and uses Bluetooth technology to control and transfer the measurements to a PC station.

A. *Measurement Textrodes*

A custom designed Textrode garment, see Fig.1, has been used to perform Total Right Side EBI measurements [10]. The textrode is based on two pieces: one for the hand-wrist and other for the foot-ankle both incorporating two separate conductive textile areas used as electrodes for current injection and voltage sensing.

The garment has Velcro fasteners and snap-button connectors. The outer layer is made of synthetic wrap knitted fabric and an intermediate foam layer assures good skin-electrode contact. The inner surface is made of conductive Shieldex® Fabric P130+B. The Shieldex® fabric is a two dimension stretchable conductive fabric based on Silver Plated (99% pure silver) and with a raw material constitution of 78% Polyamide and 22% Elastomer.

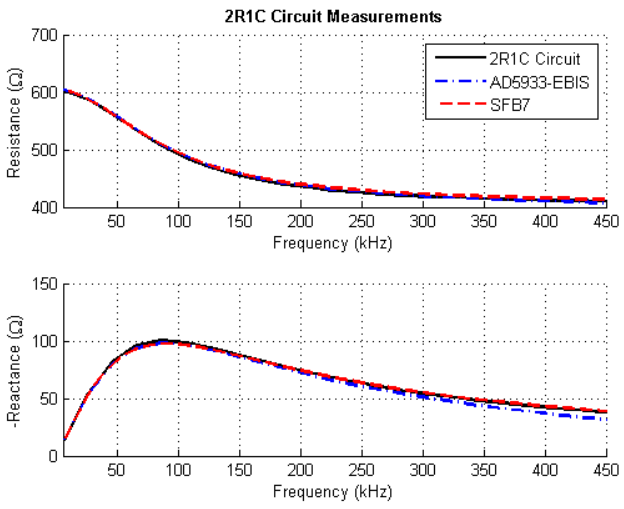

Fig.2 Impedance Measurements on 2R1C circuit with SFB7

B. *2R1C and EBIS Measurements*

Using both spectrometers EBIS measurements were taken on a 2R1C circuit dummy, and Total Right Side (TRS) [11] on three healthy subjects lying supine in a resting state. The 2R1C circuit model was implemented with a resistor of 1.21 kΩ in series with a 1 nF capacitor, both in parallel with a resistor of 604 Ω, all components with a 0.1% precision. A set of 30 complex EBI spectroscopy measurements were taken for each subject with the textrode garment. In the case of the 2R1C circuit, 20 measurements were taken.

C. *Spectrum Analysis and Cole parameters estimation*

The complex impedance spectra have been compared in the frequency range 5 – 450 kHz, for both circuit and TRS measurements. In addition the Cole parameters, R_0, R_∞ and f_C, have been estimated from the TRS EBI spectra using the three frequency ranges: 5-100 kHz, 5-200 kHz and 5-450 kHz. The estimation of the Cole parameters have been estimated using Impedimed Bioimp Software, the Cole parameter estimation has been performed with the TD compensation option disabled.

III. Results

A. *2R1C Circuit Measurements*

The average resistance and reactance spectra from the 2R1C circuit measurements are plotted in Fig. 2. Both devices present a good performance, but the reactance spectrum obtained with the AD5933-EBIS exhibits a slight deviation at high frequencies.

The Absolute error for the Resistance and the Reactance spectra is shown in Fig. 3 with a doted and cross marker line for the AD5933-EBIS and SFB7 respectively. The AD5933-EBIS presents a lower error value in the resistance spectra compared to the SFB7. In the Reactance plot, the AD5933-EBIS presents an error greater than 5% above 270 kHz approximately; while SFB7 has an error lower than 4% for

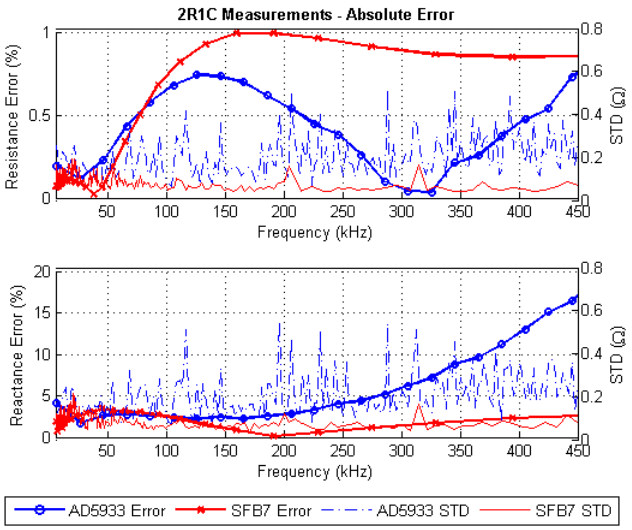

Fig.3 Absolute Error and STD for 2R1C circuit measurements.

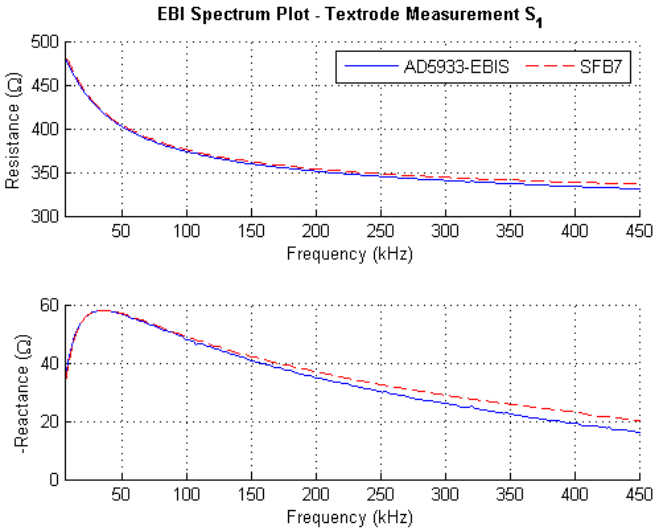

Fig. 4 Resistance and Reactance TRS spectrum plots for Subject 1 with SFB7 and AD5933 EBIS.

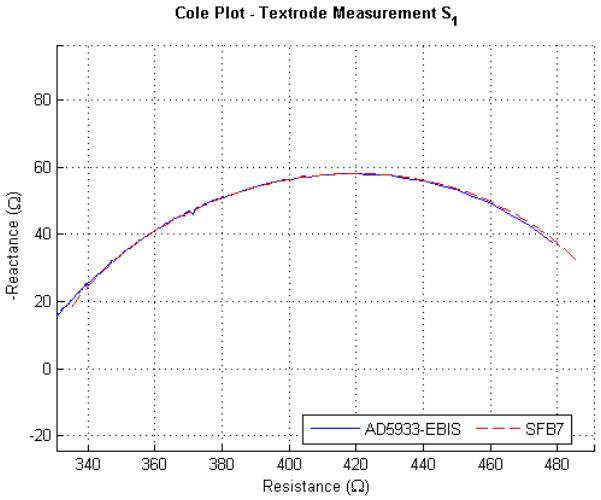

Fig.5 Impedance Plot for EBI TRS measurement on Subject 1.

the complete frequency range. In the same figure the Standard Deviation (STD) for the 2R1C measurements is shown for both devices, the SFB7 presents lower STD compared with the AD5933-EBIS. In both cases the STD stays below 0.5 Ω.

B. Spectral Measurement

The complex EBIS measurements obtained with both spectrometers were very similar for the three subjects, exhibiting the same underestimation on the reactance spectrum at high frequencies as observed in the 2R1C circuit measurements. The averaged resistance and reactance spectrum for Subject 1 is shown in the Fig. 4. The resistance spectrum presents a slight difference at frequencies above 200 kHz. In the case of the reactance spectrum the differences is more noticeable and increasing with the frequency.

The impedance plot for EBIS measurements Subject 1 is shown in Fig. 5. The impedance plots obtained with both devices are nearly similar, making difficult to trace some difference between them.

C. Cole Parameter Estimation

The estimated values for the Cole parameters are shown in Table I. This table provides the average values for the Cole parameters estimations obtained with the BioImp Software from the EBI measurement performed on each subject with both spectrometers. The values estimated from the measurements taken with both spectrometers in the frequencies ranges of 5-100 kHz and 5-200 kHz are very similar. In Table II it is possible to observe the mean difference among the three subjects for each of the parameters, and for each of the three frequency ranges. Notice that for R_0 *and* R_∞ the difference is kept below 1.2%, in the frequency range of 5-450 kHz, the difference on the Cole parameters it is slightly larger but it is still relatively very small

In Table I and Table II it is possible to observe that the deviation produced on the estimation of characteristic frequency, f_C, it is slightly larger than in the cases for R_0 and R_∞.

Table III shows the Mean Absolute Deviation between the estimation of the Cole parameter obtained with the SFB7 using the 5-450 kHz frequency range and the value for the Cole parameters estimated from the measurements taken with the AD5933-EBIS for the 3 frequency ranges. In the table it is possible to observe that the difference for R_0 and R_∞ is smaller than 1%.

TABLE I
COLE PARAMETERS ESTIMATION

Frequency (kHz)	Device	R_0 (Ω)			R_∞ (Ω)			f_C (kHz)		
		S_1	S_2	S_3	S_1	S_2	S_3	S_1	S_2	S_3
5-100	*AD5933*	510,4	566,9	546,3	325,0	399,5	338,7	35,0	37,7	25,0
	SFB7	509,6	562,8	546,4	328,2	402,4	344,9	35,7	38,0	25,5
5-200	*AD5933*	511,8	567,9	547,8	322,8	397,6	337,0	35,2	37,9	25,2
	SFB7	511,1	564,0	547,7	324,8	399,4	342,7	36,5	38,9	25,7
5-450	*AD5933*	514,2	568,8	549,5	320,9	396,8	336,1	37,4	40,5	28,4
	SFB7	511,9	564,5	547,9	323,3	398,4	342,4	36,2	38,3	25,5

TABLE II
TOTAL MEAN RELATIVE DIFFERENCE

Frequency Range	R_0 (%)	R_∞ (%)	f_C (%)
5-100 kHz	0,29	1,18	1,55
5-200 kHz	0,29	0,92	2,67
5-450 kHz	0,49	0,99	6,76

TABLE III
TOTAL MEAN RELATIVE DIFFERENCE FOR THE AD5933-EBIS

Frequency Range	R_0 (%)	R_∞ (%)	f_C (%)
5-100 kHz	0,06	0,10	2,33
5-200 kHz	0,19	0,64	1,71
5-450 kHz	0,49	0,99	6,76

IV. DISCUSSION

The close resemblance between the impedance spectra obtained from the 2R1C circuit indicate that the AD5933-EBIS can indeed perform accurate impedance measurement well above other upper limits previously reported, 100 kHz

in [2-3] and 200 kHz in [12]. The deviation in the reactance spectrum observed with increasing frequency might be related with that fact the load for the initial calibration was just a resistance, among other factors. A deeper study about the elements influencing in the accuracy and preciseness of the AD5933 is being done.

Despite the clear deviation observed in the reactance at high frequencies, the Cole parameter estimation performed from EBIS data measured up to 450 kHz produce very similar values for R_0 and R_∞ to those estimated from the EBIS measurement performed with the SFB7. This is due to the fact that the semicircular plot produced by the EBIS measurements taken with both spectrometers are almost identical, and since the curve fitting to the Cole function implemented by the Bioimp software fits the EBIS data in the impedance plane, it is expected that similar impedance plots will produce similar values for R0 and R∞. The estimation of the Cole parameters depend on the curve fitting approach implemented. Since the resistance spectrum obtained with spectrometers are very similar, the use of other estimation algorithms based in the resistance spectrum only, such as the one in [13], would also produce precise estimations for R_0 and R_∞.

Since the estimation of the body fluid distribution from EBIS data currently depend only on the estimates of R_0 and R_∞ [7], it is very likely that the AD5933-EBIS spectrometer in combination with the Textrode garment would be useful for BCA applications. A clinical study comparing the performance of several commercial EBIS meters with the AD5933-EBIS is schedule to be performed shortly.

V. Conclusions

The results obtained show the feasibility to obtain accurate TRS EBIS measurements using the custom made AD5933-EBIS with dry Textrodes for Cole parameter and BCA estimation.

The AD5933 EBIS presents a good performance compared with the SFB7 on the 2R1C measurements, showing a smaller error in the resistance spectrum measurement but a noticeable error in the reactance spectrum at frequencies above 270 kHz. On the other hand, the difference observed in the estimation of the Cole parameters, R_0 and R_∞ using the AD5933 EBIS is below 1% when compared with the values estimated from a commercial EBIS meter like the SFB7.

The availability of Textrode garments and reduced size spectrometers like the AD5933-EBIS used in this work will enable the implementation of EBI-based personalized health monitoring systems for body fluid distribution. Such systems could play an important role improving the quality life of chronic kidney disease patients requiring dialysis for example.

References

[1] A. Devices. "AD5933 Datasheet Document," http://www.analog.com/static/imported-files/data_sheets/AD5933.pdf.

[2] F. Seoane, J. Ferreira, J. J. Sanchéz *et al.*, "Analog Front-End Enables Electrical Impedance Spectroscopy System On-Chip for Biomedical Applications," *Physiol. Meas.* , vol. 29 pp. S267-S278, 2008.

[3] J. Ferreira, F. Seoane, A. Ansede Peña *et al.*, "AD5933-Based Spectrometer for Electrical Bioimpedance Applications," in International Conference on Electrical Bioimpedance, Gainesville, Florida, 2010.

[4] J. C. Marquez, J. Ferreira, F. Seoane *et al.*, "Textile Electrode Straps for Wrist-to-Ankle Bioimpedance Measurements for Body Composition Analysis. Initial Validation & Experimental Results," in IEEE EMBC 2010, Buenos Aires, Argentina, 2010.

[5] J. C. Marquez, F. Seoane, E. Välimäki *et al.*, "Comparison of Dry-Textile Electrodes for Electrical Bioimpedance Spectroscopy Measurements.," in ICEBI2010, Gainesville, 2010.

[6] J. Muehlsteff, O. Such, and R. Willmann, "The Role of Technology for Non-Invasive Cardiovascular Monitoring in the Future Exemplified," *World Congress on Medical Physics and Biomedical Engineering, September 7 - 12, 2009, Munich, Germany*, pp. 388-391, 2009.

[7] M. Y. Jaffrin, and H. Morel, "Body fluid volumes measurements by impedance: A review of bioimpedance spectroscopy (BIS) and bioimpedance analysis (BIA) methods," *Medical Engineering & Physics*, vol. 30, no. 10, pp. 1257-1269, 2008.

[8] F. Zhu, G. Wystrychowski, T. Kitzler *et al.*, "Application of bioimpedance techniques to peritoneal dialysis," *Contrib Nephrol*, vol. 150, pp. 119-28, 2006.

[9] "Impedimed SFB7 - Home Web page," 2011-06-15; http://www.impedimed.com/products/sfb7-for-body-composition/sfb7-for-europe.htm.

[10] J. C. Marquez, and F. Seoane, "Textrode Garment for Bioimpedance Measurements. Experimental Results for Body Composition Analysis," *To be submitted in 2011*, 2011.

[11] U. G. Kyle, I. Bosaeus, A. D. De Lorenzo *et al.*, "Bioelectrical impedance analysis—part II: utilization in clinical practice," *Clinical nutrition (Edinburgh, Scotland)*, vol. 23, no. 6, pp. 1430-1453, 2004.

[12] P. Bogonez-Franco, and et al., "Performance of an implantable impedance spectroscopy monitor using ZigBee," *Journal of Physics: Conference Series*, vol. 224, no. 1, pp. 012163.

[13] D. Ayllon, F. Seoane, and R. Gil-Pita, "Cole equation and parameter estimation from electrical bioimpedance spectroscopy measurements - A comparative study." pp. 3779-3782.

PAPER IV

A handheld and textile-enabled bioimpedance system for ubiquitous body composition analysis. An initial functional validation

Javier Ferreira, Ivan Pau, Kaj Lindecrantz, *et al.*

Published at the IEEE Journal on Biomedical and Health Informatics, DOI 10.1109/JBHI.2016.2628766, 2016

A handheld and textile-enabled bioimpedance system for ubiquitous body composition analysis. An initial functional validation

Javier Ferreira[1, 2, 3,*], *Member, IEEE*, Iván Pau[3], Kaj Lindecrantz[1, 4], *Member, IEEE,* and Fernando Seoane[1, 2], *Senior Member, IEEE*

Abstract — In recent years, many efforts have been made to promote a healthcare paradigm shift from the traditional reactive hospital-centered healthcare approach towards a proactive, patient-oriented and self-managed approach that could improve service quality and help reduce costs while contributing to sustainability. Managing and caring for patients with chronic diseases accounts over 75% of healthcare costs in developed countries. One of the most resource demanding diseases is chronic kidney disease (CKD), which often leads to a gradual and irreparable loss of renal function, with up to 12% of the population showing signs of different stages of this disease. Peritoneal dialysis and home haemodialysis are life-saving home-based renal replacement treatments that, compared to conventional in-center hemodialysis, provide similar long-term patient survival, less restrictions of life-style, such as a more flexible diet, and better flexibility in terms of treatment options and locations. Bioimpedance has been largely used clinically for decades in nutrition for assessing body fluid distributions. Moreover, bioimpedance methods are used to assess the overhydratation state of CKD patients, allowing clinicians to estimate the amount of fluid that should be removed by ultrafiltration. In this work, the initial validation of a handheld bioimpedance system for the assessment of body fluid status that could be used to assist the patient in home-based CKD treatments is presented. The body fluid monitoring system comprises a custom-made handheld tetrapolar bioimpedance spectrometer and a textile-based electrode garment for total body fluid assessment. The system performance was evaluated against the same measurements acquired using a commercial bioimpedance spectrometer for medical use on several voluntary subjects. The analysis of the measurement results and the comparison of the fluid estimations indicated that both devices are equivalent from a measurement performance perspective, allowing for its use on ubiquitous e-healthcare dialysis solutions.

Index Terms— bioimpedance, body composition, electrodes, garment, home care, instrumentation, personalized healthcare, proactive care, self-managed care, sensor, textiles, wearable, wireless

[1]School of Technology and Health, KTH, Huddinge, Sweden. E-Mail: javierfg@kth.se (J.F), kaj.lindecrantz@sth.kth.se (K.L.)

[2]Department of Acute and Prehospital Care, and Medical Technology. University of Borås, Sweden. E-Mail: fernando.seoane@hb.se (F.S)

[3]Department of Telematics and Electronics, Technical University of Madrid, UPM, Madrid, Spain. E-Mails: ivan.pau@upm.es (I.P)

[4]Department of Clinical Science, Intervention and Technology, Karolinska Institute, 14186 Stockholm, Sweden. kaj.lindecrantz@sth.kth.se (K.L.)

[*]Corresponding author; e-mail: javierfg@kth.se

I. Introduction

Factors, such as aging populations, sedentary life-styles and increased life expectancies, are raising the demands of the healthcare system [1-3]. For example, in the European Union, over six countries exceeded 10% of the gross domestic product (GDP) in healthcare expenditures, while for the United States, healthcare expenditures were over 16% of the GDP as reported in 2012 [4, 5]. Healthcare costs are rising substantially to levels such that further measures need to be taken to maintain service quality and sustainability.

Many initiatives within the European Union are targeting a paradigm shift from the traditional reactive hospital-centered approach toward a proactive, patient-oriented and self-managed approach that could help to reduce costs, improve service quality and contribute to sustainability. For instance, in the European Union, 97% of healthcare costs are spent on treatment, with only 3% invested in prevention [6].

Managing and caring for patients with chronic diseases accounts over 75% of the healthcare costs in developed countries. For instance, in Spain, up to 80% of the total healthcare cost is dedicated to supplying service for managing chronic diseases such as cardiovascular, kidney, diabetes or cancer among others. Half of the Spanish population, approximately 20 million, is suffering from at least one chronic disease, and at ages above 65 years the average amounts to four chronic diseases [7].

One of the most resource demanding diseases is chronic kidney disease (CKD) with up to 12% of the population and more than 50% are elderly patients showing signs of different stages of this disease. Chronic kidney disease leads to a gradual and irreparable loss of renal function, known as end stage renal disease (ESRD), where patients must undergo kidney replacement therapy through either periodic dialysis treatment or kidney transplantation. CKD is not common enough to be considered a worldwide public health threat, but indeed it has reached epidemic proportions with 10-12% of the population showing some signs of renal malfunction [8].

With the latest technological advances in fields such as information and communication technologies, dialysis equipment or sensor technologies have enabled the improvement of CKD treatment therapies [9] and the transition of conventional in-center hemodialysis to home-

based dialysis treatments [10]. Peritoneal dialysis (PD) and home hemodialysis (HHD) are life-saving home-based renal replacement treatments that, compared to conventional in-center hemodialysis (HD), provide similar long-term patient survival, less restrictions of life-style, such as a more liberal diet, and better flexibility in terms of treatment location [11].

Dialysis removes metabolic toxic waste and excess of fluid [12], aiming to replace the compromised renal function of the patient [13]. Fluid balance, also known also as dry weight or the euvolemic state, is an important goal of dialysis treatment [14], and assessing the dry weight value is critical for achieving a good therapeutic outcome [15]. Even in a clinical setting for doctors, accurate assessment of dry weight is currently a challenge [16]. Consequently at home, CKD patients should benefit from tools enabling the close monitoring of volume control [17] for keeping their proper fluid balance.

Bioimpedance technology and its monitoring applications have been proven useful as a non-invasive monitoring technology for daily use in applications such as impedance cardiography [18, 19], skin cancer detection [20] or monitoring nutrition status [21], among others. In the case of body composition assessment (BCA), the use of bioimpedance spectroscopy (EBIS) methods [22] have been proven to be useful for monitoring the distribution of different body fluid compartments, such as total body water (TBW), extracellular (ECF) and intracellular (ICF) fluids, and fat mass (FT), among others. For instance, patients suffering CKD tend to accumulate excess fluids in the extracellular compartment, and EBIS methods have been used to assess the euvolemic state and to estimate the amount of fluid that should be removed by ultrafiltration [23, 24].

Aligned with [17] and stepping towards a solution for supporting fluid assessment at home, in this work, a bioimpedance system for the assessment of body fluid status and its initial validations are presented. The body fluid monitoring system is composed of a custom-made handheld tetrapolar bioimpedance spectrometer and a textile-based electrode garment for total body fluid assessment. The complete monitoring system was designed to be operated by end users with minimal expertise, to minimize electrode placement errors, and to ensure clinical measurement reliability. The system components are described, and its performance is compared against a commercial impedance spectrometer while performing measurements on voluntary subjects using the same textile-based electrode garment.

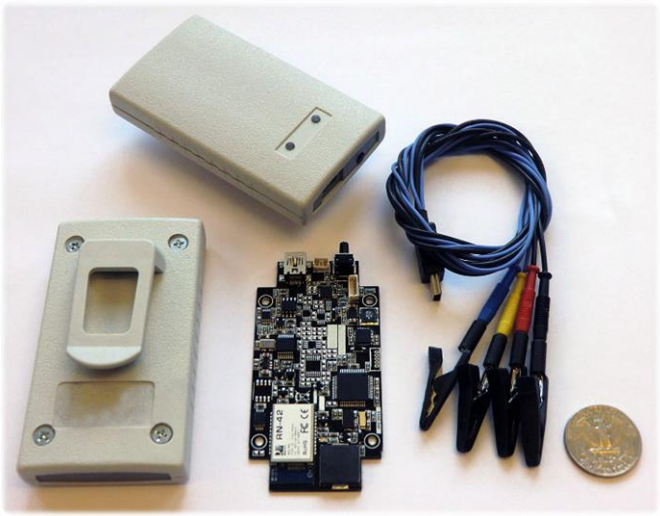

Fig. 1. The custom-made EBIS monitor, named AD-EBIS.

II. Materials

A. Bioimpedance Spectrometers

All the measurements obtained with the custom made Electrical BioImpedance (EBI) spectrometer are compared against the same measurements obtained with the commercial EBI spectrometer SFB7 manufactured by ImpediMed Ltd. In this study, the SFB7 is considered as reference measurement equipment or the "golden standard". The SFB7 performs EBI spectroscopy measurements for BCA in a tetrapolar configuration from 4 kHz up to 1 MHz, and with 256 discrete frequency points logarithmically distributed.

1) Custom-made handheld bioimpedance spectrometer; AD-EBIS

The developed spectrometer, named AD-EBIS, is a portable-standalone tetrapolar bioimpedance spectrometer that includes an internal processing unit, a battery and wireless communications, among other components. The AD-EBIS spectrometer is shown in Fig. 1, and the achieved specifications are listed as follows:

- Size of 90 x 50 x 17 mm and a total weight of 70 g
- Measurement frequency range: from 5 kHz to 270 kHz, with up to 512 discrete points
- Injecting measurement current: 100 µArms DC free
- Wireless communication: standard Bluetooth 2.1 providing an SSP profile
- Power supply: Li-ion battery that provides up to 2 h of continuous measurements
- User interfaces: user button, acoustic indicator and two LED indicators
- Designed to comply with the electrical patient safety regulations specified by IEC 60601

The block diagram of the AD-EBIS spectrometer is shown in Fig. 2. The core of the spectrometer is a low-power high-performance microcontroller that controls the unit and the

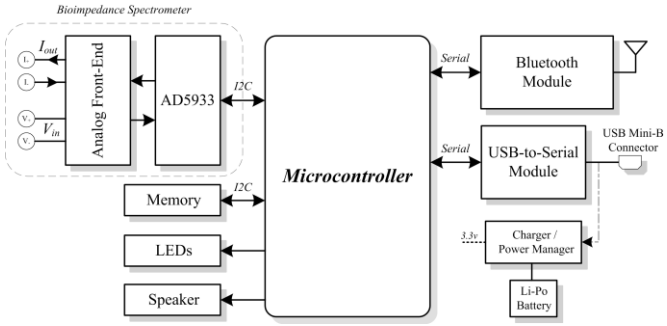

Fig. 2. AD-EBIS EBIS unit block diagram.

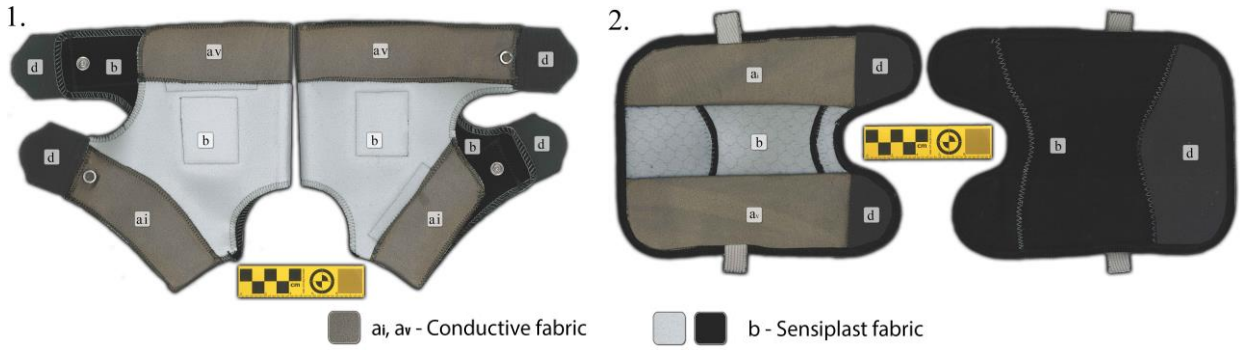

Fig. 3. Inner and outer surfaces of the functional textile electrode garment for foot-ankle (1) and hand-wrist (2).

bioimpedance measurement sequence and wirelessly transfers the data to a host for further processing. The AD-EBIS main functional blocks are the bioimpedance spectrometer module, the wireless communication module, user interfaces and a battery power management unit.

a) The bioimpedance spectrometer module

The bioimpedance spectrometer module has been previously presented by the authors [25, 26]. The AD5933 is connected using the serial I2C port configured with a frequency clock of 400 kHz and an external clock oscillator circuit of 16 MHz. The recommended AD5933 impedance frequency range is 1 kHz to 100 kHz, but it can be programmed for frequencies up to 450 kHz [26]. The AD-EBIS unit is calibrated using a multipoint calibration method using a 2R1C electrical circuit dummy, and the obtained calibration factor is stored in the memory module. To achieve the highest possible precision, floating point variables were used in the microcontroller firmware.

b) Wireless communications

Fig. 4. Textile electrode garment placement in the foot-ankle (1) and hand-wrist (2).

The system includes standard Bluetooth 2.1 communication, implementing a serial profile port (SPP), which emulates standard serial cable RS-232 communications. The commercial module RN42 from Microchip Technology Inc. is used. This Bluetooth module provides a good compromise in terms of power consumption and compact dimensions while being offered as a fully certified Class 2 Bluetooth 2.1 module. The module RN-42 was configured in slave mode using encrypted communications and password pairing protection, and therefore the AD-EBIS unit can be used only by an authorized Bluetooth master device. The Bluetooth master device in this study was a PC running Windows 7 and a custom application to collect the impedance measurements for further data analysis and BCA parameter extraction.

c) User interfaces

The AD-EBIS is provided with a user button to switch the unit on and off, two LED indicators to display the system, the battery and the Bluetooth status, and an acoustic indicator. The unit is provided with one enhanced mini-B female USB connector for battery charging and also used for the connection of the bioimpedance tetrapolar measuring leads. The enhanced mini USB connector supports standard USB communications and has an extra line of 5 pins in the bottom part of the connector for other types of communications, which is used for the measurement leads of the AD-EBIS unit. The electrode cable assembly uses an enhanced mini-b male USB connector, which only allows for connection to an enhanced mini-b female USB connector, and thus does not allow for connection of the measuring electrode cable leads to another standard USB mini-b device. Using the same USB port for charging and measuring eliminates the risk of performing measurements while the unit is connected to a non IEC-60-601 compliant charging power supply.

B. Custom-made textile electrode garments for body composition analysis

The custom-made electrode garments were designed to provide tetrapolar bioimpedance measurement between the wrist and the ankle for total body composition bioimpedance analysis. They were built upon elbow and ankle commercial

TABLE I – TRS EBI MEASUREMENT PROTOCOL PROCEDURE

Steps	*Description*
1	Inform the subject about the experiment, obtain the signed consent document, and assign a random subject identification to be used for naming the stored data.
2	Obtain subject height and weight.
3	Clean the electrode area, ankle and wrist, with alcohol gel and place the textile electrode garments.
4	*Resting time period*; allow the subject to lie in supine position for 10 minutes. During this time prepare the spectrometers and input the necessary setup data.
5	*SFB7 measurements*; obtain a set of 20 EBI measurements.
6	*Zep SFB7 measurements*; perform a three-electrode EBI measurement for skin-electrode impedance extraction.
7	*AD-EBIS measurements*; obtain a set of 20 EBI measurements.
8	*Zep AD-EBIS measurements*; perform a three-electrode EBI measurement for obtaining skin-electrode impedance.

supporting bandages Sensiplast® manufactured by Horizonte Textil GmbH. The original bandages were modified to provide two separate electrode areas on each garment for current injection and voltage sensing, marked in Fig. 3, as a_i and a_v respectively. The textile electrodes, denoted by the darker grey areas in Fig. 3 and marked as a_i and a_v, were built using biocompatible silver-based conductive Shieldex P130+B fabric from Statex and an intermediate 3 mm foam layer to provide mechanical pressure on the conductive electrode fabric against the subject's skin.

The conductive fabric P130+B is a synthetic wrap knitted fabric made of 78% polyamide, 22% elastomer and plated with 99% conductive silver, which provides a surface resistivity lower than 2 Ω/square. The conductive areas for the foot-ankle garment are 102 cm^2 for the injecting current electrode and 132 cm^2 for the voltage sensing electrode; for the hand-wrist garment; the conductive areas are 99 cm^2 for the injecting current electrode and 88 cm^2 for the voltage sensing electrode. Fig. 3.1 shows the inner side of the foot-ankle garment construction and Fig. 3.2 shows the inner and outer sides for the hand-wrist garment construction. Snap button connectors were provided on each electrode area to enable the connection of the measuring cable using crocodile clips. The textile electrode garment placement is shown in Fig. 4, where the garment in Fig. 4.2 is placed on the right hand, and the garment in Fig. 4.1 is placed on the right foot.

III. METHODS

A. Experimental measurement setup

The EBI TRS measurements were performed at the research laboratory for Medical Textile-Electronics at the University of Borås in Sweden. The measurements were approved by the regional ethics committee of Gothenburg with ethical approval number 274-11. A measurement protocol was followed, and a written document explaining the experiment and measurement protocol was delivered to the seven male participants to obtain their signed consent. The weights of each subject were obtained in the laboratory using A&D medical scale model UC-321PBT and the height was obtained using a wall-mounted meter. The measurement protocol was performed in the following steps as described in Table I.

TABLE II – ANTHROPOMETRIC SUBJECT DATA

Subject	*Age (years)*	*Height (cm)*	*Weight (kg)*	*BMI ($kg \times m^{-2}$)*
1	30	175	104	33.9
2	30	181	80	24.4
3	34	170	65	22.5
4	34	179	84	26.2
5	27	179	77	24.0
6	36	176	103	33.2
7	36	172	81	27.4
		Mean ± STD		
	32.4 ± 3.4	176 ± 4	84.8 ± 14.1	27.4 ± 4.5

For each of the seven male subjects, a set of 20 EBI measurements were performed with each device and using the same measurement textile electrode garments presented in Section II.b, while using a total right side (TRS) tetrapolar EBI measurement configuration between the right wrist and the right ankle.

B. Measurement data analysis

The measurements with each spectrometer were transferred into a computer and imported to MATLAB software for further processing. Because each device performs the bioimpedance measurements with a different frequency range and frequency distribution, to avoid any Cole parameter estimation errors and to ensure equal measurement performance comparison between devices, the obtained impedance spectra of each device was adjusted to have a common frequency resolution and frequency range [27].

a) Body composition data analysis

First, the SFB7 EBI spectroscopy measurements were frequency limited between 5 – 274 kHz with a total of 177 frequency points. Second, the frequency point distribution for the AD-EBIS measurements was interpolated, using the MATLAB function "*interp1*", so the AD-EBIS measurements had the same logarithmic distribution as the SFB7 measurements. Cole parameters R_{zero} and R_{inf} were obtained by mathematically fitting the EBIS measurement data of both spectrometers to the impedance magnitude part of the Cole equation [28] using MATLAB non-linear least squares (NLSS) fitting functions.

The body composition parameters were obtained using the *Van Loan* method [29] and *De Lorenzo* formulas [30]. The parameters *ECF* and *ICF* were calculated using the Cole parameters R_{zero} and R_{inf}, the anthropometric subject data and the body composition formulas, as given by (1) and (2).

$$ECF = K_e \cdot \left(\frac{H^2 \cdot \sqrt{W}}{R_e}\right)^{2/3} \quad (1)$$

In (1), *ECF* is the extra cellular fluid in *liters*, *H* is the height in centimeters, R_e is the extracellular resistance in *Ohms*, W is the weight in kilograms and K_e a body shape factor dimensionless constant[30].

$$\left(1 + \frac{ICF}{ECF}\right)^{5/2} = \frac{R_e + R_i}{R_i} \cdot \left(1 + K_p \frac{ICF}{ECF}\right) \quad (2)$$

In (2), *ICF* is the intracellular fluid in *liters*, R_i is the intracellular resistance in *Ohms*, and *Kp* is a body shape factor dimensionless constant [30].

The EBI spectrum plots of resistance vs. reactance were obtained for each subject with each spectrometer. Bland-Altman and Correlation plots of the Cole parameters, R_{zero} and R_{inf}, and well as *ECF* and *ICF* were used to compare the performance among the spectrometers. The two one-side t-test (TOST) [31, 32] was used to test equivalence and also to verify that the mean difference between the two spectrometers was at least equal to or below the 2-3% error present in the precision of an impedance measurement [33].

$$t_{TOST} = \frac{(\mu_{AD-EBIS} - \mu_{SFB7}) - \varepsilon_{ERROR}}{\sqrt{\frac{{\sigma_{AD-EBIS}}^2}{n_{AD-EBIS}} + \frac{{\sigma_{SFB7}}^2}{n_{SFB7}}}} \quad (3)$$

The TOST is defined as follows: assuming $\mu_{AD\text{-}EBIS}$ as the test group mean, μ_{SFB7} as the reference group mean, $\sigma_{AD\text{-}EBIS}$ and σ_{SFB7} their respective standard deviations, ε_{ERROR} as the accepted error, and the null hypothesis of non-equivalence defined as $H_{01}: \mu_{AD-EBIS} - \mu_{SFB7} \leq \varepsilon_{ERROR}$ and $H_{02}: \mu_{AD-EBIS} - \mu_{SFB7} \geq \varepsilon_{ERROR}$, the null hypothesis H01 is rejected if $t_{TOST} \geq t_{critical}$ and the null hypothesis H02 is rejected if $-t_{TOST} \geq t_{critical}$.. The t_{TOST} value is calculated using (3), and $t_{critical}$ was obtained for a level of probability of 0.05.

b) *Electrode-skin contact impedance*

After performing the TRS EBI measurements with each spectrometer, a three-electrode EBI measurement was performed, as given by steps 6 and 8 in Table I. The injecting current electrode lead was electrically connected to the sensing voltage electrode in the wrist electrode garment. The electrode-skin contact impedance was obtained by subtracting the averaged TRS measurements and the average of the three-electrode EBI measurements. The electrode-skin contact impedance spectrum was used to compare the textile electrode performance and the impedance differences obtained with each spectrometer.

c) *Impedance evolution during resting time period*

Sets of TRS EBI measurements for two subjects were obtained during the resting time period, as given by step 4 in Table I, to analyze the stabilization and evolution of the measured impedance during this period. The resting period was increased by 10 min only for the first subject, for a total of 20 minutes to evaluate the impedance progression over a longer period of time. For these two subjects and during the whole resting period, one TRS EBI measurement was performed every 10 seconds using only the SFB7 spectrometer, obtaining a total of 120 TRS measurements for the first subject and 60 TRS measurements for the other subject. The Cole parameters R_{zero}, R_{inf}, F_c and *Alpha* [29] were obtained and used to visualize the impedance evolution during the resting time.

IV. MEASUREMENT RESULTS

Following the measurement protocol in Table I, TRS EBI measurements were performed on seven healthy male human volunteers. All the EBI measurements between steps 5 and 8 in Table I were performed continuously with a total measurement time of approximately 3 minutes. Their anthropometric data can be found in Table II.

The averaged original TRS EBI measurements for each of the two devices and for each subject are shown in Fig. 5, where the impedance plot resistance vs. reactance is displayed. The measurement difference for all the subjects between the two devices is minimal. There is a visible deviation at high frequencies for subjects 2, 3 and 5, as shown in subplots *b*, *c* and *e* in Fig. 5 respectively.

After processing the EBI measurements, the Cole and BCA parameters, R_{zero}, R_{inf}, *ECF* and *ICF*, were calculated. In Fig. 6, the Bland-Altman plots for the Cole and BCA parameters are shown, where each subplot displays the difference between the values obtained with the SFB7 and AD-EBIS devices. As observed in the figure, most samples were within 95% of the agreement limits, ± 1.96 of the standard deviation of the difference, while there is an average difference of 10 Ω for R_{zero}, 6 Ω for R_{inf}, 0.25 liters for *ECF* and -1.2 liters for *ICF*, with relative errors of 1.77% for R_{zero}, 1.71% for R_{inf}, 1.19%

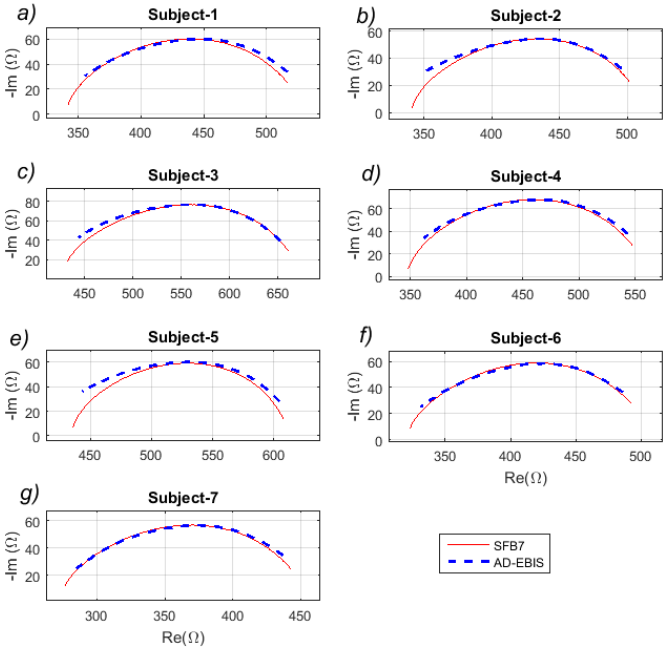

Fig. 5. TRS average resistance vs. reactance plots for each subject with both spectrometers.

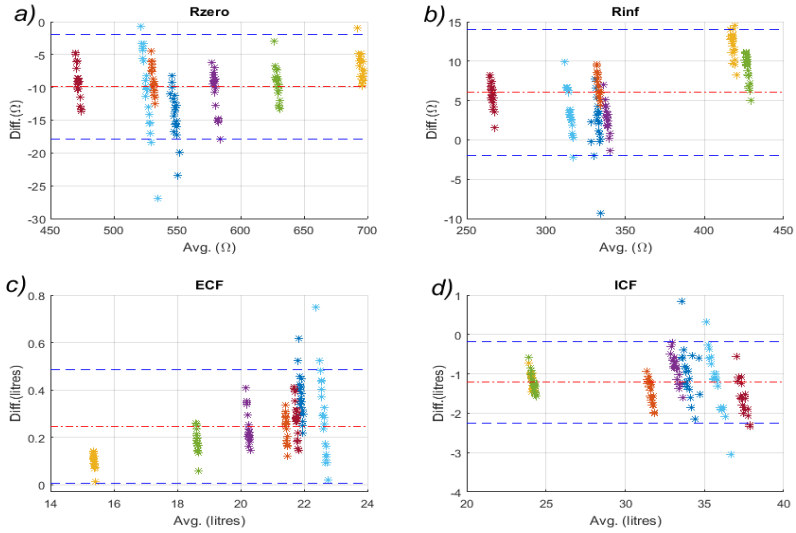

Fig. 6. R_{zero} in *(a)*, R_{inf} in *(b)*, ECF in *(c)* and ICF in *(d)* Bland-Altman plots for all the measurements of SFB7 vs. AD-EBIS

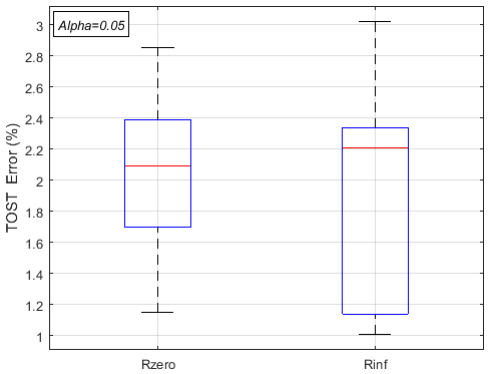

Fig. 7. Maximum error for statistical TOST equivalence for the Cole parameters R_{zero} and R_{inf}, obtained for a level of probability of alpha=0.05.

for *ECF* and 3.88% for *ICF*.

The box plot results for the maximum error for statistical equivalence obtained with the TOST test [31, 32] for Cole parameters R_{zero} and R_{inf} for all the subjects are shown in Fig. 7. The plot shows that for both Cole parameters, with a probability level of 0.05, the maximum error for statistical equivalence is below 3.02%, with mean values equal to 2.1% for R_{zero} and 1.9% for R_{inf}.

As shown in Fig. 8, the Cole and BCA parameters were used to display correlation plots for all the subjects between each device. For each subplot, the linear regression and Lin's concordance correlation coefficient (CCC), were obtained, and the results are displayed inside each plot. As the linear regression results indicate, there is an equal relationship between the measurements of both devices, with average constant differences of 16.3Ω for R_{zero}, 9.3Ω for R_{inf}, 0.4 liters for *ECF* and 1.1 liters for *ICF* between the two devices.

The electrode-skin contact impedance (Z_{ep}) was calculated for each subject, and the averaged impedance magnitude plot is shown in Fig. 9, where the continuous trace represents the original data measured by the SFB7 and the continuous dotted trace represents the original data from the AD-EBIS. For most of the subjects and for devices, the textile electrode-skin contact impedance Z_{ep} is below 500 Ω at low frequencies and reaches approximately 20 Ω at higher frequencies. The impedance values of the Z_{ep} spectra are very well paired among subjects and spectrometers, except for the measurements performed on subject 5 with the AD-EBIS device.

For subjects 1 and 3, a continuous set of impedance measurements were recorded during the resting period by collecting a single EBIS measurement every 20 seconds, as given by step 4 in the protocol described in Table I. The Cole parameters during the resting period are displayed in Fig. 10, where R_{zero} and R_{inf} denote the impedance at low and high frequencies respectively in Ohms, F_c denotes the characteristic frequency in kilo hertz, and alpha the dimensionless Cole parameter. In addition, a linear data fitting was performed on each parameter, and the results are displayed in the bottom part of each subplot. For Subject 1, there was a transitory period of approximately two minutes, where the impedance values oscillate, and after two minutes the values stabilize. As observed in Fig. 10, there is a continuous drift over time for all the calculated Cole parameters for both subjects; for example,

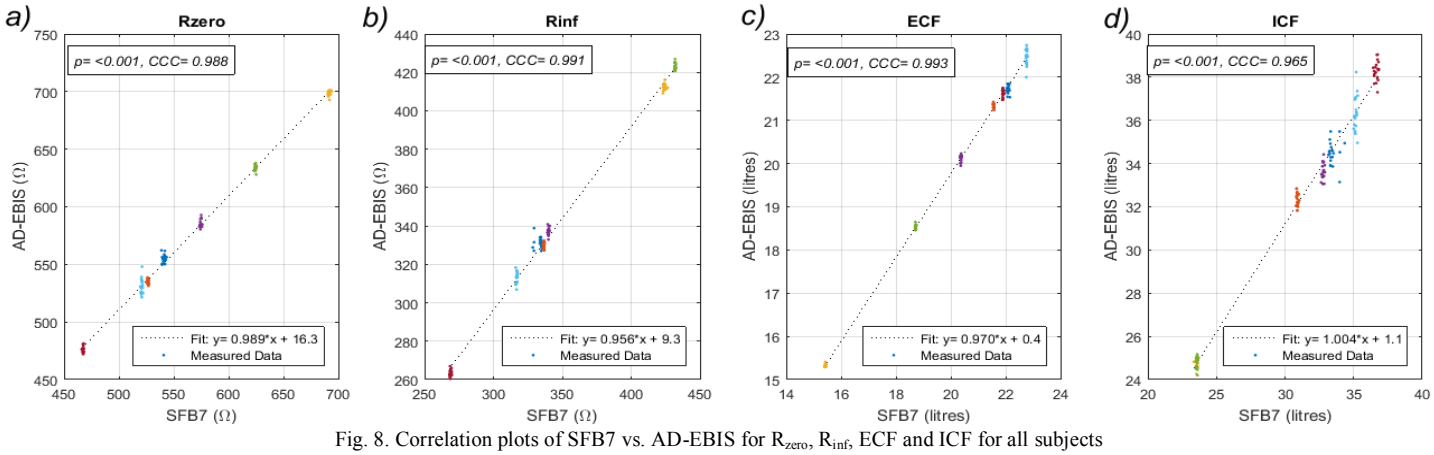

Fig. 8. Correlation plots of SFB7 vs. AD-EBIS for R_{zero}, R_{inf}, ECF and ICF for all subjects

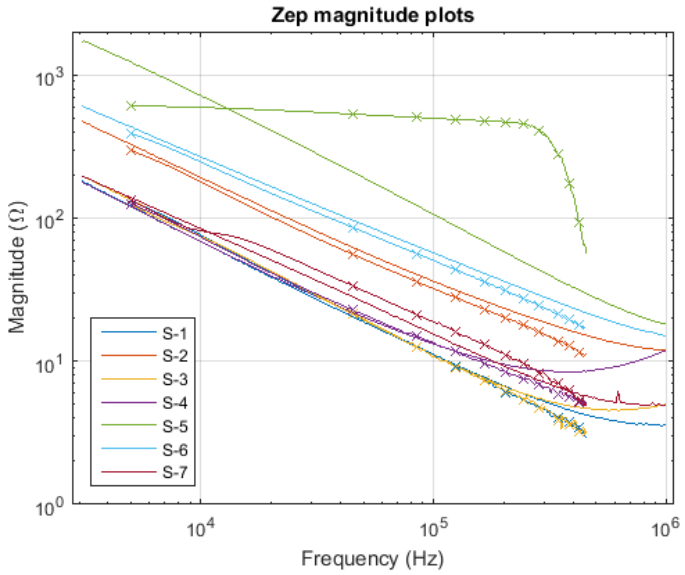

Fig. 9. Textile electrode-skin contact impedance spectrum plots for each subject with the SFB7, solid trace, and AD-EBIS, solid-dotted trace.

during the resting period, there is an impedance increment on R_{zero} of 17Ω or 3.2% for subject 1 during 20 minutes, and 12Ω or 1.7% for subject 3 during 10 minutes, while R_{inf} decreases by 16Ω for subject 3, but remains almost constant for subject 1.

V. Discussion

The electrode-skin contact impedance magnitude values obtained using both EBI spectrometers were very similar and had with very low magnitudes. Performing EBIS measurements with low electrode-skin contact impedance increases the robustness of EBIS measurements by minimizing the source of errors, such as the influence of stray capacitances, as indicated in [34-36].

Dry textile electrodes are expected to have high electrode-skin contact impedance mainly due to the poor contact interface, which sometimes it is reduced by scrubbing and applying conductive electrode gel to improve the interface. In the case of the presented dry textile electrode garments, the contact impedance was very low, mainly due to the high electrode contact area, on average 105 cm^2, which is 10 times higher compared to commercial Ag/AgCl gel electrodes. In addition, the presence of measurement artifacts was minimal, as only deviations in the impedance plots at high frequencies for subjects 2, 3 and 5 were visible, as shown in Fig. 5. Such deviations may be as a result of the presence of electrode impedance mismatch errors due to the different electrode contact areas in the textile electrode garments.

The measurement performance of the developed EBI spectrometer, AD-EBIS, showed an equivalent performance as that of the commercial EBI spectrometer, SFB7. The spectrum plots obtained with both devices were quite similar among all of the subjects in the comparable frequency range. The observed slight differences were in agreement with the values previously reported by the authors in [26], where a small deviation was reported at high frequencies between the SFB7 and the same bioimpedance core module used in the presented AD-EBIS unit.

Beyond the simple measurement comparison and focusing on the Cole characterization of the spectral measurements, further mathematical analyses revealed a bias ranging from 1.19% to 3.88%, and a linear correlation relationship ranging from 0.995 to 0.998 for the Cole and BCA parameters obtained for all the subjects between the measurements of both spectrometers.

The high value of the correlation coefficient together with the low bias values of 1.77% for R_{zero} and 1.71% for R_{inf} suggest a high level of equivalence of the bioimpedance measurements. The statistical TOST equivalence test showed that the maximum error for statistical equivalence, obtained for a level of probability of α=0.05, was below 3% for the Cole parameters R_{zero} and R_{inf}, guaranteeing their statistical equivalence within the values expected for bioimpedance measurements according to [33, 37].

Despite the statistical significance of the equivalence the TOST values do not reflect clinical significance, because those concepts are very different. From a clinical significance perspective, considering that the body composition assessment approaches used currently clinically worldwide are associated with average prediction errors between 4.69% and 5.07% for total body water [38], and because the differences observed between devices are smaller than this error range, we foresee no practical impact in using any of the devices.

The measurements performed during the resting time on two subjects indicated that after a short period of time, below 2 minutes for subject 1, the impedance measurements became stable although there was a noticeable drift over the resting time period for most of the parameter values for both subjects. As reported by other authors [39], the internal physiological mechanisms of body fluid distribution is continuously adapting, as shown in Fig. 10; for instance during the resting time, the extracellular resistance parameter R_{zero} increases 0.85Ω/min, and similar results were reported in [39] for when subjects change their position from standing to supine. These and other factors, such as body posture, ambient temperature or food intake, will impact the body fluid balance estimation, potentially leading to inaccuracies when analyzing EBIS measurements for assessment of body composition, and such factors must be taken in consideration and detail measurement protocols must be used. Furthermore, additional studies on the dynamics of body fluid distribution should be performed, emphasizing the impact on the analysis of EBIS measurements for body composition assessment. It is likely that such time-related fluid dynamics could partially contribute to the differences observed in this publication, i.e., 1.19% for *ECF* and 3.88% for *ICF*.

Bioimpedance technology is becoming a useful tool for clinicians to assess overhydration in CKD patients [40, 41]. Paradoxically, while the use of body composition monitors , such as the BCM from Fresenius GMBH, is spreading within in-center dialysis, home-based dialysis patients, who are at a greater risk of overhydration [42, 43], cannot benefit from such assessments of body fluid balance through bioimpedance

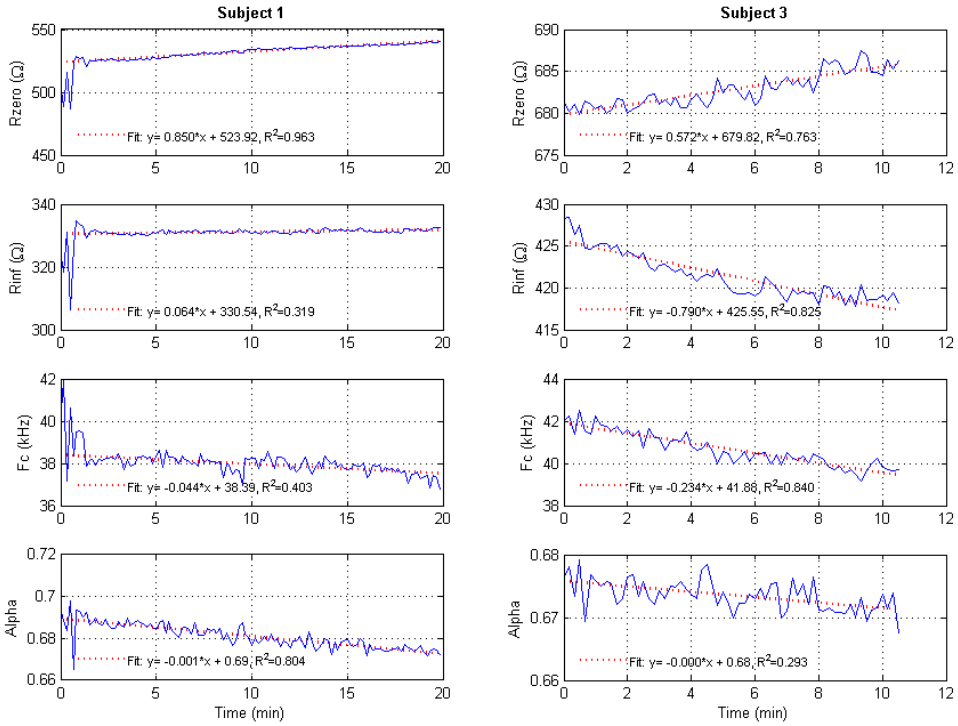

Fig. 10. Cole parameter plots extracted from TRS continuous measurements for subjects 1 and 3 during resting time, 20 minutes and 10 minutes respectively. Measurements performed with SFB7 spectrometer with measurement interval of 10 seconds.

technology.

A critical aspect in the treatment quality of PD and HHD, especially at home, is the ability of patients to actively monitor their therapy by daily recording multiple parameters, such as weight, fluid removal quantity and blood pressure with a monthly follow-up by a dialysis specialist. Adding the prototyped textile electrode straps and the Bluetooth enabled AD-EBIS handheld spectrometer to home monitoring weight and blood pressure, such as in [44], to develop an e-health solution for supporting dialysis at home would be relatively straight-forward.

There is a need for new e-health solutions that can assist and enable a paradigm shift in the care of CKD patients, thereby facilitating the anticipated increase in the number of patients choosing available home-based homecare therapies. Increasing the proportion of home-based dialysis patients would have an enormous impact on all aspects of point-of-care of CKD patients, and would contribute to the sustainability of the current healthcare system.

VI. Conclusion and Ongoing Work

The current developed garments exhibited good measurement performance, but further studies regarding textile electrode degradation must be performed to establish its clinical reliability in home-based monitoring applications. For instance, information regarding the electrode-skin contact impedance value could be used as an indicator of electrode degradation performance over time. The developed custom-made textile garment offers an easy, comfortable and reliable way to place the measurement electrodes in the same location each time by the subjects themselves, which enables its possible use in self-managed and home-based monitoring environments. The presented EBI monitoring system offers some advantages, for home-based monitoring use compared to other clinical bioimpedance spectrometer solutions, as the presented electrode garment solution minimizes electrode connection and placement errors, it has reduced dimensions and weight that allow for its possible integration in the electrode garment to yield a single measuring unit, and it incorporates standard Bluetooth wireless communications that allow it the connectivity to many Bluetooth devices, such as mobile devices, smart TVs and personal computers.

Currently, a similar measurement setup based on the presented AD-EBIS unit and a custom-made ankle textile electrode garment for assessing fluid balance is being used as a part of monitoring system in the MySleeve study. This study aims to achieve better adherence to fluid restriction by providing direct feedback and information on fluid intake and balance to the patient through the use of state-of-the-art monitoring systems. The MySleeve study is being coordinated by the Department of Smart Medical Devices for Cardiovascular Healthcare at the University Eindhoven, in collaboration with University Hospital Catharina Ziekenhuis in Eindhoven, within the European project DoChange.

References

[1] U. Nations, *Population Ageing and the Non-communicable Diseases*, Department of Economic and Social Affairs, United Nations, 2012.

[2] N. Owen, P. B. Sparling, G. N. Healy *et al.*, "Sedentary Behavior: Emerging Evidence for a New Health Risk," *Mayo Clinic Proceedings,* vol. 85, no. 12, pp. 1138-1141, 2010.

[3] K. Zhaurova, "Genetic Causes of Adult-Onset Disorders," *Nature Education 1,* vol. 1, no. 49, 2008.

[4] EuroStat. "Eurostat - Healthcare statistics in the European Union," http://ec.europa.eu/eurostat/statistics-explained/images/b/b6/Healthcare_statistics_YB2015.xlsx.

[5] D. A. Squires, "Explaining high health care spending in the United States: an international comparison of supply, utilization, prices, and quality," *Issue Brief (Commonw Fund),* vol. 10, pp. 1-14, May, 2012.

[6] E. K. H. Alliance. "Is kidney disease really such an important issue for Europe?," www.ekha.eu.

[7] M. Guerrero. "Soluciones para la gestión de la cronicidad," http://www.sedisa.net/documentos/Mon20150914744172015091 4InformeGestionCronicidadSEDISA.pdf.

[8] V. Jha, G. Garcia-Garcia, K. Iseki *et al.*, "Chronic kidney disease: global dimension and perspectives," *Lancet,* vol. 382, no. 9888, pp. 260-72, Jul 20, 2013.

[9] C. J. Diamantidis, and S. Becker, "Health information technology (IT) to improve the care of patients with chronic kidney disease (CKD)," no. 1471-2369 (Electronic), 20140115 DCOM-20140904, 2014.

[10] M. Neuman, "Some bright spots for home dialysis," *Nephrology News & Issues*, 2012.

[11] C. Beard, *No place like home: Increasing access to home dialysis*, Cheshire and Merseyside Strategic Clinical Networks, 2013.

[12] M. R. Henning, "Affecting Kt/V: An Analysis of Staff Interventions," *Dialysis & Transplantation,* vol. 36, no. 11, pp. 584-601, 2007.

[13] W. Drukker, F. M. Parsons, and J. F. Maher, *Replacement of Renal Function by Dialysis. A textbook of dialysis*, 2 ed., p.^pp. 967: Springer Netherlands, 1983.

[14] R. F. Kushner, P. M. de Vries, and R. Gudivaka, "Use of bioelectrical impedance analysis measurements in the clinical management of patients undergoing dialysis," *The American Journal of Clinical Nutrition,* vol. 64, no. 3, pp. 503S-509S, September 1, 1996, 1996.

[15] G. Wystrychowski, and N. W. Levin, "Dry weight: sine qua non of adequate dialysis," *Adv Chronic Kidney Dis,* vol. 14, no. 3, pp. e10-6, Jul, 2007.

[16] S. S. Miguel, "Haemodialysis dry weight assessment: A literature review," *Renal Society of Australasia Journal,* vol. 6, no. 1, 2010.

[17] W. Van Biesen, J. D. Williams, A. C. Covic *et al.*, "Fluid Status in Peritoneal Dialysis Patients: The European Body Composition Monitoring (EuroBCM) Study Cohort," *PLoS ONE,* vol. 6, no. 2, pp. e17148, 2011.

[18] J. M. Van De Water, T. W. Miller, R. L. Vogel *et al.*, "Impedance cardiography: the next vital sign technology?," *Chest,* vol. 123, no. 6, pp. 2028-33, Jun, 2003.

[19] D. P. Bernstein, I. C. Henry, M. J. Banet *et al.*, "Stroke volume obtained by electrical interrogation of the brachial artery: transbrachial electrical bioimpedance velocimetry," *Physiological Measurement,* vol. 33, no. 4, pp. 629, 2012.

[20] P. Aberg, I. Nicander, J. Hansson *et al.*, "Skin cancer identification using multifrequency electrical impedance – A potential screening tool," *IEEE Trans. Bio. Med. Eng.,* vol. 51, no. 12, pp. 2097-2102, 2004.

[21] U. M. Moissl, P. Wabel, P. W. Chamney *et al.*, "Body fluid volume determination via body composition spectroscopy in health and disease," *Physiol Meas,* vol. 27, no. 9, pp. 921-33, Sep, 2006.

[22] R. Buendia, F. Seoane, K. Lindecrantz *et al.*, "Estimation of body fluids with bioimpedance spectroscopy: state of the art methods and proposal of novel methods," *Physiol Meas,* vol. 36, no. 10, pp. 2171-87, Oct, 2015.

[23] S. J. Davies, and A. Davenport, "The role of bioimpedance and biomarkers in helping to aid clinical decision-making of volume assessments in dialysis patients," *Kidney Int,* vol. 86, no. 3, pp. 489-96, Sep, 2014.

[24] M. K. Kuhlmann, F. Zhu, E. Seibert *et al.*, "Bioimpedance, dry weight and blood pressure control: new methods and consequences," *Curr Opin Nephrol Hypertens,* vol. 14, no. 6, pp. 543-9, Nov, 2005.

[25] F. Seoane, J. Ferreira, J. J. Sanchez *et al.*, "An Analog front-end enables electrical impedance spectroscopy system on-chip for biomedical applications," *Physiological Measurement,* vol. 29, no. 6, pp. S267-78, 2008.

[26] J. Ferreira, F. Seoane, and K. Lindecrantz, "AD5933-based electrical bioimpedance spectrometer. Towards textile-enabled applications," in 33rd Annual International Conference of the IEEE Engineering in Medicine and Biology Society, Boston, USA 2011, pp. 3282-5.

[27] F. Seoane, J. Ferreira, R. Buendia *et al.*, "Adaptive frequency distribution for Electrical Bioimpedance Spectroscopy measurements," in 34th Annual International Conference of the IEEE Engineering in Medicine and Biology Society, San Diego, USA, 2012, pp. 562-565.

[28] K. S. Cole, "Permeability and impermeability of cell membranes for ions.," *Quant. Biol.,* vol. 8, pp. 110–122, 1940.

[29] M. Van Loan, P. Withers, J. Matthie *et al.*, "Use of bio-impedance spectroscopy (BIS) to determine extracellular fluid (ECF), intracellular fluid (ICF), total body water (TBW), and fat-free mass (FFM). ," *Human Body Composition In Vivo Methods, Models, and Assessments*, pp. 4, 1993.

[30] A. De Lorenzo, A. Andreoli, J. R. Matthie *et al.*, "Predicting body cell mass with bioimpedance by using theoretical methods: a technological review," *J Appl Physiol,* vol. 82, no. 5, pp. 1542-58, May, 1997.

[31] D. J. Schuirmann, "A comparison of the two one-sided tests procedure and the power approach for assessing the equivalence of average bioavailability," *J Pharmacokinet Biopharm,* vol. 15, no. 6, pp. 657-80, Dec, 1987.

[32] X. Dong, Y. Tsong, and M. Shen, "Equivalence tests for interchangeability based on two one-sided probabilities," *J Biopharm Stat,* vol. 24, no. 6, pp. 1332-48, 2014.

[33] A. Piccoli, G. Pastori, M. Guizzo *et al.*, "Equivalence of information from single versus multiple frequency bioimpedance vector analysis in hemodialysis," *Kidney Int,* vol. 67, no. 1, pp. 301-13, Jan, 2005.

[34] H. Scharfetter, P. Hartinger, H. Hinghofer-Szalkay *et al.*, "A model of artefacts produced by stray capacitance during whole body or segmental bioimpedance spectroscopy," *Physiological Measurement,* vol. 19, no. 2, pp. 247-261, May, 1998.

[35] R. Buendia, "Model Based Enhancement of Bioimpedance Spectroscopy Analysis: Towards Textile Enabled Applications," School of Technology and Health, KTH, Flemingsberg - Stockholm, 2011.

[36] R. Buendia, F. Seoane, and R. Gil-Pita, "Experimental validation of a method for removing the capacitive leakage artifact from electrical bioimpedance spectroscopy measurements," *Measurement Science and Technology,* vol. 21, no. 11, pp. 115802, 2010.

[37] C. P. Earthman, R. R. Wolfe, and S. B. Heymsfield, "Dudrick Research Symposium 2015-Lean Tissue and Protein in Health and Disease: Key Targets and Assessment Strategies," *JPEN J Parenter Enteral Nutr*, Dec 18, 2015.

[38] F. Seoane, S. Abtahi, F. Abtahi *et al.*, "Mean Expected Error in Prediction of Total Body Water: A True Accuracy Comparison between Bioimpedance Spectroscopy and Single Frequency Regression Equations," *Biomed Res Int,* vol. 2015, pp. 656323, 2015.

[39] A. H. Ismail, and S. Leonhardt, "Simulating Non-Specific Influences of Body Posture and Temperature on Thigh-Bioimpedance Spectroscopy during Continuous Monitoring Applications," *Journal of Physics: Conference Series,* vol. 434, no. 1, pp. 012008, 2013.

[40] R. Mamat, N. C. Kong, A. Ba'in *et al.*, "Assessment of body fluid status in hemodialysis patients using the body composition monitor measurement technique," *J Clin Nurs,* vol. 21, no. 19-20, pp. 2879-85, Oct, 2012.

[41] D. Marcelli, L. A. Usvyat, P. Kotanko *et al.*, "Body composition and survival in dialysis patients: results from an international cohort study," *Clin J Am Soc Nephrol,* vol. 10, no. 7, pp. 1192-200, Jul 7, 2015.

[42] R. A. Cader, H. A. Gafor, R. Mohd *et al.*, "Assessment of fluid status in CAPD patients using the body composition monitor," *J Clin Nurs,* vol. 22, no. 5-6, pp. 741-8, Mar, 2013.

[43] P. Lentini, M. de Cal, L. Zanoli *et al.*, "[The role of bioelectrical impedance in peritoneal dialysis]," *G Ital Nefrol,* vol. 30, no. 6, Nov-Dec, 2013.

[44] F. Seoane, M. A. Valero, A. Garcia-Perez *et al.*, "Implementation of an Open Telenephrology Platform to Support Home Monitoring."

PAPER V

Portable bioimpedance monitor evaluation for continuous impedance measurements. Towards wearable plethysmography applications

Javier Ferreira, Fernando Seoane and Kaj Lindecrantz

Published and presented at the 35st Annual International Conference of the IEEE Engineering in Medicine and Biology Society, EMBS
Osaka, Japan, 2013

Portable bioimpedance monitor evaluation for continuous impedance measurements. Towards wearable Plethysmography Applications

J. Ferreira, *Student Member IEEE*, F. Seoane, *Member IEEE*, and K. Lindecrantz, *Member IEEE.*

Abstract — Extensive applied research efforts in the last decade funded by the European Commission in functional textiles, textile electronic integration and monitoring technologies are targeting the proliferation of Personalized Health Monitoring Systems that could benefit the life quality of the patient as well as decrease the Health Care costs for society among other factors. The purpose of this paper is to study the capabilities of the system-on-chip Impedance Network Analyzer AD5933 to perform high speed single frequency continuous bioimpedance measurements. The theoretical maximum continuous impedance estimation time was determined, and the AD5933 with a custom 4-Electrode Analog Front-End (AFE) was used to determine the maximum continuous impedance estimation frequency as well as the system impedance estimation error when measuring a 2R1C electrical circuit model. Following, a Transthoracic Electrical Bioimpedance (TEB) measurement in a healthy subject was obtained using 3M gel electrodes in a tetrapolar lateral spot electrode configuration. The obtained TEB raw signal was filtered in MATLAB to obtain the respiration and cardiogenic signals, and from the cardiogenic signal the impedance derivative signal (dZ/dt) was also calculated. The results have shown that the maximum continuous impedance estimation rate is approximately 550 measurements per second with a magnitude estimation error below 1% on 2R1C-parallel bridge measurements. The displayed respiration and cardiac signals were exhibiting good performance, and they could be used to obtain valuable information in some plethysmography monitoring applications. The obtained results suggest that the AD5933-based monitor could be used for the implementation of portable and wearable Bioimpedance Plethysmography Applications, such as Impedance Cardiography. This combined with the results from research done in functional textile electrodes and garments might enable the implementation of Personalized Health Monitoring Applications in a relatively short time from now.

J. Ferreira and F. Seoane are with the School of Engineering at the University of Borås, 501 90 SWEDEN and the School of Technology and Health at Royal Institute of Technology, SE-141 52 Huddinge, SWEDEN (e-mail: javier.ferreira@hb.se and fernando.seoane@hb.se)

K Lindecrantz is with the School of Technology and Health at Royal Institute of Technology, SE-141 52 Huddinge, and Department of Clinical Science, Intervention, and Technology, Karolinska Institutet, 141 46 Stockholm, SWEDEN. (e-mail: kaj.lindecrantz@sth.kth.se)

I. INTRODUCTION

The application of Electrical Bioimpedance (EBI) technology for respiration function monitoring is one of the earliest non-invasive monitoring applications of EBI measurements and is commonly known as Impedance Pneumography (IP). Already in 1969, NASA used IP to monitoring the breathing of the astronauts during the Apollo XI mission. Since then, EBI technology has improved to a great extent and it can accurately correlate with volume estimations obtained from spirometers [1]. Respiratory volume and flow signal extracted from IP during tidal breathing contains pathological signs of Chronic Obstructive Pulmonary Disease (COPD), cystic fibrosis, or asthma among others. As a result of extensive applied research efforts in the last decade funded by the European Commission like, advances in textile and monitoring technology have produced textile sensors and measurement garments, which have enabled personalized health monitoring applications based in EBI measurements. Few years ago, Analog Devices introduced the first System-on-Chip (SoC) solution to perform complex impedance measurements named the AD5933 [2], and the development of an Analog-Front-End (4E-AFE) enabled the measurement of Bioimpedance using a tetrapolar configuration [3]. The AD5933 has been used successfully in applications like an Implantable Impedance Spectroscopy Monitor using Zigbee [4] or Body Composition Assessment using Textile Electrodes [5].

In this work, the performance of the AD5933+4E-AFE for continuous Impedance Measurements was evaluated for the implementation of ubiquitous Impedance Plethysmography Applications, such as Impedance Pneumography (IP) or Impedance Cardiography (ICG). The maximum continuous impedance estimation frequency and system performance error were assessed. Finally, the Thransthoracic Electrical Bioimpedance (TEB) in one subject using electrodes was recorded, and the signal was processed to obtain the respiration and cardiac signals.

II. MATERIALS

A. AD5933-Based Bioimpedance Measuring Device

The AD5933 from Analog Devices Inc. [2] is a SoC solution that incorporates all the necessary components to perform complex impedance measurements, and thanks to the tetrapolar Analog-front-End [3, 5], the AD5933 SoC can

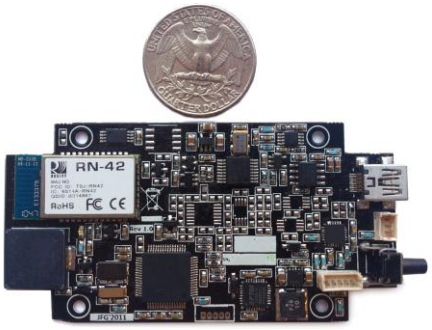

Figure 1 AD5933-EBIM Main Board.

perform Bioimpedance measurements in the range 5-270 kHz [5]. The AD5933-Based Bioimpedance Meter (AD5933-EBIM) used in this work it is a battery operated portable tetrapolar spectrometer controlled by a Microchip PIC24FJ microcontroller. It uses Bluetooth technology to transfers control messages and data between device and a PC station. The AD5933-EBIM dimensions are 50x90x15 mm, and 70 gr of weight including the battery and a plastic box.

1) *AD5933-EBIM Modifications*

The 4E-AFE has been modified to optimize the system for thoracic bioimpedance measurements. The injected current was configured to 400 μA_{RMS} and the input instrumentation amplifier gain to 26 v/v. The system was calibrated using a 2R1C circuit selected to model a typical thorax impedance response, formed by a resistor of 150 Ω 0.1% in series with a capacitor of 10nF 1%, both in parallel with a resistor of 75 Ω 0.1%, and the system was calibrated for the frequency points of 50, 100, 200, 300 and 400 kHz. The AD5933 SoC was programmed to have one settling time cycle, starting frequency equal to the analysis frequency, frequency increments equal to zero and number of increments equal to one [2]. The I2C clock was configured for a frequency of 400 kHz.

III. METHODS

A. *Theoretical Impedance Estimation Time*

The theoretical total sample time for a single measurement is calculated using the Equation 1, were $t_{AD5933Prot}$ is the time to perform all the I2C protocol instructions to read the registers and send the commands for the AD5933 chip, $t_{SetCycles}$ is the programed Settling Cycles Time and t_{ZConv} is the time for the AD5933 to estimate the Impedance values.

$$t_{SAMP} = t_{AD5933Prot} + t_{SetCycles} + t_{Z\,Conv} \quad (1)$$

The time t_{ZConv} is approximately 1 ms for a system clock of 16MHz [2]. The time $t_{AD5933Prot}$ is the total time to read the Impedance Value registers and send the repeat instruction time and the impedance status measurement check time. The time $t_{AD5933Prot}$ will depend how the AD5933 is accessed and also which I2C frequency clock is selected.

B. *Experimental Impedance Estimation Time*

The experimental impedance measurement estimation time was measured using a polling test program, which performs a continuous impedance measurement for a specific number of sample points, checking continuously the "Conversion-done" bit in the AD5933 status register in order to reach the maximum speed. After setting the AD5933 initial measurement configurations, the "Start-to-Measure" command is sent, and the program is continuously checking the conversion status bit to determinate if the impedance conversion has been done. When a conversion is done, the real and imaginary registers are read and a "Repeat-Frequency" command is sent. An output test pin is digitally toggled every time that a conversion is done, and with an oscilloscope the total impedance measurement time can be obtained. The total time for two sets of 10 and 100 sample points was obtained, using two impedance excitation frequencies, 50 kHz and 100 kHz.

C. *System Accuracy*

The system accuracy was evaluated for the measurement of a 2R1C circuit model formed by a resistor of 71.5 Ω 0.1% in series with a capacitor of 10 nF 1%, both in parallel with a resistor of 90.1 Ω 0.1%. The AD5933-EBIM was configured to perform a continuous impedance measurement in the 2R1C circuit for frequencies of 50, 100, 200, 300 and 400 kHz, recording a total of 30 seconds for each excitation frequency. The average magnitude and standard deviation were calculated, as well as the magnitude error for each excitation frequency.

D. *Thoracic Electrical Bioimpedance Measurements*

After obtaining the practical impedance estimation frequency, a set of 180 seconds of TEB measurement in one subject was obtained using an impedance sampling frequency of 400 Hz and an injecting impedance signal frequency of 100 kHz. The tetrapolar Lateral Spot Electrode Configuration [6] and repositionable EKG Ag/AgCl 3M Electrodes were used to perform the measurement while the patient was in sitting position and relaxed. The measurement was carried out under the Swedish ethical approval number 274-11.

The measurement was processed using MATLAB to obtain the respiration and cardiac signals. The respiration signal was obtained filtering the impedance magnitude signal using first a Low Pass FIR Filter at 10 Hz to eliminate the high frequency noise, and after a Low Pass Interpolated FIR filter [1] at 0.5 Hz. The Cardiac Signal (ΔZ) was obtained applying first a linear detrend and zero-mean function to the impedance magnitude signal, then that signal is filtered using a Band Pass FIR Filter with cut frequencies at 0.9 Hz and 7 Hz, also its first derivative signal (dZ/dt) was calculated.

IV. RESULTS

A. *Impedance Estimation Frequency tests*

The results for the impedance estimation time tests are shown in Table I. The maximum estimation time is similar for all the tests with an averaged value of 1.791ms, a maximum impedance estimation frequency of approximately 550 Hz. Using the Equation 1 and for an output frequency of

TABLE I IMPEDANCE ESTIMATION TIME RESULTS.

Z Freq.(kHz)	*Measurements (number)*	*Total Time (ms)*	*Z $F_{sampling}$ (Hz)*
50	10	17,98	556,2
50	100	179,10	558,3
100	10	17,94	557,4
100	100	179,11	558,3

50 kHz, the theoretical impedance sampling time gives a value of 1.895 ms, which it is very close to the measured time.

B. System Measurement performance

Table II shows the results for 30 seconds of measuring on a 2R1C circuit model. The magnitude error is low for all impedance excitation frequencies, with a maximum magnitude error of 0.26 % at 400 kHz. The maximum Standard Deviation (STD) was 0.04 Ω at 50 kHz.

C. TEB Results

A 23 seconds recording of the TEB signal Z_{raw} is shown in Figure 2. In the signal $Z_{raw,}$ the cardiac and respiratory components could be observed as well as high frequency content due to the AD5933 impedance estimation error. The filtered respiratory signal Z_{resp} is also displayed in Figure 2 with a dashed line. The respiration interval appears to be approximately 3.5 seconds per cycle, giving an average respiration rate of 17 breaths per minute.

The original detrended Impedance Signal (Z_d), the Cardiac Signal (ΔZ) and its first derivate (dZ/dt) are shown in Figure 3 for a sequence of 6 seconds of the original measurement. The beat-to-beat interval as extracted from the plots is approximately 0.91 seconds giving a heart rate of 66 beats per minute. Some parameters for Impedance Cardiography analysis [7] can be extracted from Figure 2 and Figure 3 such as the increment difference for ΔZ signal with a value of 0.17Ω, the peak value for dZ/dt which is 1.55 Ωs^{-1}, or the baseline thoracic impedance Z_0 value of 27.62 Ω.

V. DISCUSSION

The first performance tests over a 2R1C circuit shows that the AD5933-EBIM could perform continuous impedance measurement for a maximum frequency of 550 Hz and with a magnitude error below 0.26%. The difference between the theoretical and the practical value it could be due to AD5933 specifications where the parameter t_{ZConv} time is not well specified by the manufacturer or the current microcontroller code among other factors. Studies carried out by Schwan [8] suggest that the sampling frequency must be around 1 kHz, but most devices uses sampling frequencies around 500 Hz [9, 10].

TABLE II 2R1C MEASUREMENT PERFORMANCE RESULTS
SAMPLING FREQUENCY = 200HZ, MEASUREMENT TIME = 30S

Z $F_{measurement}$ (kHz)	*Impedance Magnitude*			
	Mean (Ω)	*STD (Ω)*	*Error (Ω)*	*Error (%)*
50	66,142	0,037	0,094	0,142
100	57,532	0,010	0,101	0,174
200	47,792	0,018	0,029	0,060
300	44,100	0,006	0,053	0,121
400	42,541	0,009	0,109	0,257

The obtained TEB signal Z_{raw} plotted in Figure 2 exhibit a good performance before any signal processing. In Z_{raw} the cardiac and respiratory components could be observed, also there is high frequency content due to the AD5933 impedance estimation error among other external factors. The obtained respiratory and cardiac signals displays good performance, enabling the possibility to be used in applications such as pulmonary flow [11], respiratory volume changes [1] or ICG assessment among others.

VI. CONCLUSIONS

The obtained results suggest that the AD5933-EBIM is suitable for continuous impedance Plethysmography Applications. These results together with the ability of AD5933-EBIM to perform spectroscopy measurements open new opportunities for several EBI applications where the tissue characterization and plethysmography applications are required.

The integration of the AD5933-EBIM with measuring garments could allow the development of novel Personalized Health Monitoring Applications for patients suffering diseases like COPD. Complementing the system with ECG recording synchronized with the TEB measurements and integrated it into a garment with textile electrodes [12] would constitute a novel approach towards wearable ICG monitoring devices.

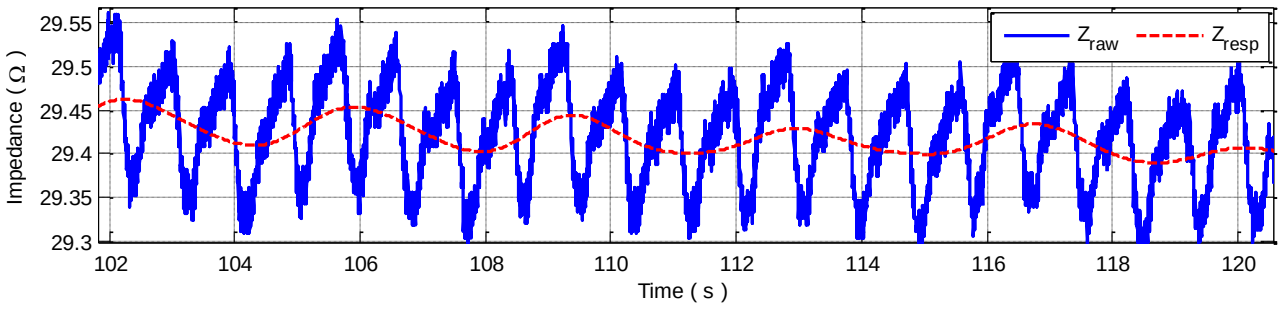

Figure 2 Raw Impedance Magnitude Signal (Z_{raw}) and Impedance Respiration signal (Z_{resp}).

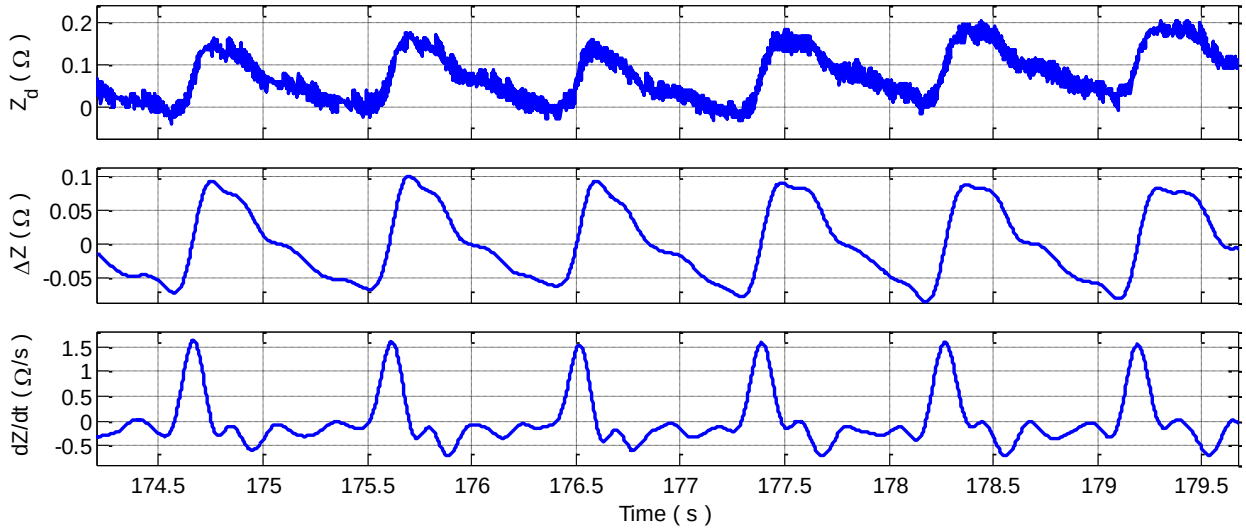

Figure 3 Detrended Impedance Magnitude (Z_d), Filter Impedance Magnitude (ΔZ) and First Derivative (dZ/dt) Plots.

VII. References

[1] D. A. Ernst Jm Fau - Litvack, D. L. Litvack Da Fau - Lozano, J. T. Lozano Dl Fau - Cacioppo *et al.*, "Impedance pneumography: noise as signal in impedance cardiography," *Psychophysiology,* vol. 36, no. 3, pp. 333-8, 1999.

[2] A. Devices. "AD5933 Datasheet Document," 2012; http://www.analog.com/ad5933.

[3] F. Seoane, J. Ferreira, J. J. Sanchéz *et al.*, "Analog Front-End Enables Electrical Impedance Spectroscopy System On-Chip for Biomedical Applications," *Physiol. Meas. ,* vol. 29 pp. S267-S278, 2008.

[4] P. Bogónez-Franco, A. Bayés-Genís, J. Rosell *et al.*, "Performance of an implantable impedance spectroscopy monitor using ZigBee," *Journal of Physics: Conference Series,* vol. 224, no. 1, pp. 012163, 2010.

[5] J. Ferreira, F. Seoane, and K. Lindecrantz, "AD5933-based electrical bioimpedance spectrometer. Towards textile-enabled applications." pp. 3282-5.

[6] H. H. Woltjer, H. J. Bogaard, G. J. Scheffer *et al.*, "Standardization of non-invasive impedance cardiography for assessment of stroke volume: comparison with thermodilution," *Br J Anaesth.,* vol. 77, no. 6, pp. 748-52., 1996.

[7] D. P. Bernstein, "Impedance cardiography: Pulsatile blood flow and the biophysical and electrodynamic basis for the stroke volume equations," *Journal of Electrical Bioimpedance,* vol. 1, pp. 2-17, 2010.

[8] H. P. Schwan, "Electrical Properties of Body Tissues and Impedance Plethysmography," *Medical Electronics, IRE Transactions on,* vol. PGME-3, pp. 32-46, 1955.

[9] C. Chia-Yin, H. Wei-Chih, and S. Liang-Yu, "Portable impedance cardiography system for real-time noninvasive cardiac output measurement." pp. 2072-2073 vol.5.

[10] P. Pandey V Fau - Pandey, and P. Pandey, "Cancellation of respiratory artifact in impedance cardiography," no. 1557-170X (Print), 20070206 DCOM- 20121002, 2005.

[11] J. Seppa Vp Fau - Viik, J. Viik J Fau - Hyttinen, and J. Hyttinen, "Assessment of pulmonary flow using impedance pneumography," *IEEE Trans Biomed Eng,* vol. 57, no. 9, pp. 2277-85, 2010.

[12] J. C. Marquez Ruiz, F. Seoane, and K. Lindecrantz, "Textrode-enabled Transthoracic Electrical Bioimpedance Measurements : Towards Wearable Applications of ImpedanceCardiography," *Journal of Electrical Bioimpedance*, 2013.

PAPER VI

Wearable biomedical measurement systems for assessment of mental stress of combatants in real time

Fernando Seoane, Inma Mohino-Herranz, Javier Ferreira *et al.*

Published in Sensors 2014, vol. 14, no. 4, pp. 7120-7141

Sensors **2014**, *14*, 7120-7141; doi:10.3390/s140407120

OPEN ACCESS

sensors

ISSN 1424-8220

www.mdpi.com/journal/sensors

Article

Wearable Biomedical Measurement Systems for Assessment of Mental Stress of Combatants in Real Time

Fernando Seoane [1,2,*], Inmaculada Mohino-Herranz [3], Javier Ferreira [1,2], Lorena Alvarez [3], Ruben Buendia [2], David Ayllón [3], Cosme Llerena [3] and Roberto Gil-Pita [3]

[1] School of Engineering, University of Borås, SE-50190 Borås, Sweden; E-Mail: javierfg@kth.se

[2] School of Technology and Health, Royal Institute of Technology, SE-14152, Stockholm, Sweden; E-Mail: rubenbl@kth.se

[3] Department of Signal Theory and Communications, University of Alcala, ES-28871, Madrid, Spain; E-Mails: inmaculada.mohino@edu.uah.es (I.M.-H.); lorena.alvrezp@uah.es (L.A.); david.ayllon@uah.es (D.A.); cosme.llerena@uah.es (C.L.); roberto.gil@uah.es (R.G.-P.)

* Author to whom correspondence should be addressed; E-Mail: fernando.seoane@hb.se; Tel.: +46-33-435-4444; Fax: +46-33-435-4008.

Received: 2 January 2014; in revised form: 31 March 2014 / Accepted: 15 April 2014 / Published: 22 April 2014

Abstract: The Spanish Ministry of Defense, through its Future Combatant program, has sought to develop technology aids with the aim of extending combatants' operational capabilities. Within this framework the ATREC project funded by the ―Coincidente" program aims at analyzing diverse biometrics to assess by real time monitoring the stress levels of combatants. This project combines multidisciplinary disciplines and fields, including wearable instrumentation, textile technology, signal processing, pattern recognition and psychological analysis of the obtained information. In this work the ATREC project is described, including the different execution phases, the wearable biomedical measurement systems, the experimental setup, the biomedical signal analysis and speech processing performed. The preliminary results obtained from the data analysis collected during the first phase of the project are presented, indicating the good classification performance exhibited when using features obtained from electrocardiographic recordings and electrical bioimpedance measurements from the thorax. These results suggest that cardiac and respiration activity offer better biomarkers for assessment of stress than speech, galvanic skin response or skin temperature when recorded with wearable biomedical measurement systems.

Keywords: bioimpedance; GSR; heart rate; mental stress; non-invasive measurements; textile electrodes; speech analysis; multimodal signal processing

1. Introduction

The Spanish Future Combatant Program (ComFut) developed by the Spanish Ministry of Defense pursues the integration of technology aids for the combatant with the aim of including not only intelligence facilities, geographical information systems or improved ballistics, but also systems able to analyze the physical and psychological state of the individual. With the aim of extending operational capability, the combatant must be not only by physically ready, but also mentally trained, which encompasses from stress management to dream deprivation. In this issue, information supported by augmented reality systems and real time monitoring of biometrics can be used to improve the mental capabilities of the future combatant.

In this framework, this paper presents the ATREC project funded by the "Coincidente" Spanish program of the Ministry of Defense, which aims at analyzing the use of biometrics and real time monitoring of combatant stress levels. This is a novel and multidisciplinary objective, since it includes the combination of wearable sensors, signal processing, pattern recognition and psychological analysis of the obtained information.

1.1. The ATREC Project

ATREC is the acronym for the Spanish project name "Análisis en Tiempo Real del Estrés del Combatiente" (Real-Time Analysis of the Stress of the Combatant). The main objective of the project is to set up a complete system to assess in real time the emotional, physical and mental stress load of a combatant during combat. It is based on the use of wearable measurement systems for the acquisition of non-invasive physiological measurements and wireless communication. Figure 1 shows a diagram of the whole system.

The project is divided in two main stages or phases. In a first phase, the ATREC project aims at identifying indicators suitable for monitoring Autonomous Nervous System (ANS) activity that can feasibly be acquired by customized wearable instrumentation. In this stage a set of sensorized garments has been implemented for performing non-invasive recording of several physiological variables. These variables include galvanic skin response (GSR), body temperature, electrocardiogram (ECG), thoracic electrical bioimpedance (TEB), and voice recording for speech analysis. In order to carry out this stage, a system prototype has been designed and implemented, and it has been used in a set of controlled stress experiments with a wide number of subjects. The prototype system is based on several different measurement systems that combined with different sensorized garments has allowed changes in the position and modalities of the different sensors, generating a wide number of possible measurement configurations.

In a second phase, a final prototype has been implemented allowing the measurement of the selected most important measurements, with the final configuration of the sensors. It consists in a

uniform vest that embeds all the electronics and signal processing algorithms to assess and represent the different stress levels in both the soldier and command displays.

Figure 1. System overview of the full system aimed to be implemented during the ATREC project integrating sensorized garments, wireless communication and wearable computing for real-time assessment.

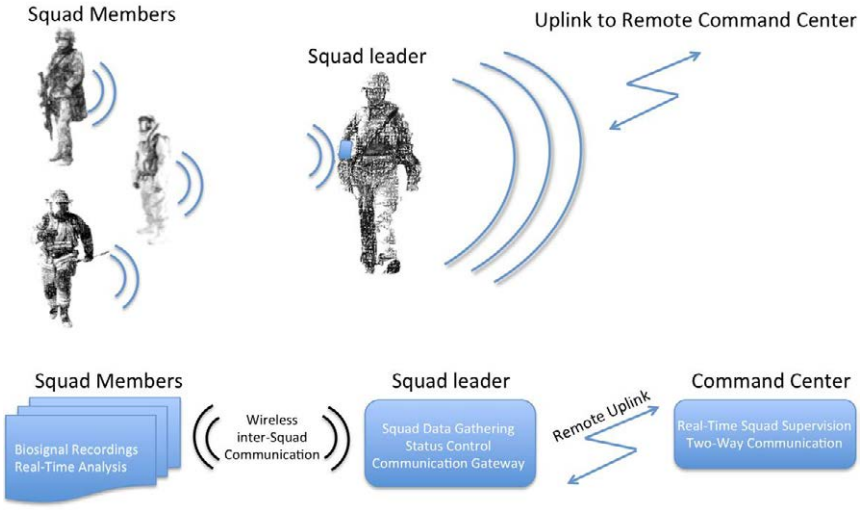

This manuscript is mainly focused on the work done during the first phase, the one targeting the selection of the main biomedical parameters for assessment of mental stress and workload. The second phase addresses the construction of sensorized vest and, its validation and the usability study is out of the scope of this manuscript and it will be described elsewhere.

1.2. Wearable Biomedical Measurement Systems

Advances in the fields of electronics and instrumentation technology, together with novel textile materials and novel textile-electronic integration technics have boosted the development and implementation of sensorized garments for wearable biomedical measurement systems [1], specially in the last decade.

As a result of extensive and numerous research efforts, several wearable and textile-enable monitoring systems for the performance of non-invasive measurements have been designed and implemented like a sensorized chest strap for cardiopulmonary activity status during emergencies [2], a sensorized vest incorporating fully woven textile sensors for monitoring ECG and respiration rate [3] or the HeartCycle Sensorized vest for detection of cardiogenic pulmonary edema [4]. A comprehensive listing of wearable biomedical measurement systems is available in [1].

Moreover, leaving aside research project prototypes, currently it is possible to find commercially available wearable sensing technologies for several different applications, ranging from simple wearable heart rate (HR) monitors for fitness, e.g., the Polar heart rate strap [5], to body worn multiparametric measurement systems, e.g., the EQ02 life monitor manufactured by Equivital [6] or the nECG shirt L1 developed by nuubo which is designed to measure ECG [7].

Available wearable biomedical measurement systems and the respective enabling technologies allow the development of solutions not only for personalized health monitoring applications e.g.,

management of chronic patients and home-care, but also for personal protective equipment for workers operating in dangerous and stressful conditions e.g., soldiers, firemen, bomb-squad members, *etc.*

1.3. Non-Invasive Assessment of Mental Stress

The brain and the spinal cord comprise the central nervous system (CNS), which through the Autonomic Nervous System (ANS) and peripheral innervation of organs and glands controls the heart's electrical activity, gland secretion, blood pressure, and respiration function among others to preserve the homeostasis of the organism, i.e., the human body in this case. The ANS is responsible for enabling and controlling the reaction of the body to external and internal stimuli. Such a control function is performed through the two branches of the ANS: The Sympathetic Nervous System (SNS) and the Parasympathetic Nervous System (PNS). Analysis of ANS activity regarding SNS and PNS is a common practice for assessing stress [8].

Evaluation of ANS activity can be performed by recording and analysing several physiological variables: heart rate [9], respiration rate (RespR) [10], ElectroEncephaloGraphical (EEG) activity [11], skin galvanic response (GSR) [12,13] and skin temperature [14].

The analysis of a speaker's speech can provide information about cognitive and affective task workloads as well as performance levels [15,16]. Interpersonal oral communication includes both verbal and paraverbal information that allows the communication of emotions and feelings [17]. Therefore, speech analysis if combined with the sensor-based detection process may improve the final performance of the stress detection system. In this line the aforesaid first phase of the ATREC project also includes the use of voice recordings for further speech analysis.

1.4. Sensorized Garments and Instrumentation for Assessment of ANS Activity.

The available literature indicates that most of the wearable systems made for assessment of ANS activity have targeted the study of emotional, cognitive, physical arousal mental status and stress [12,18–28]. Nevertheless several wearable devices and sensorized garments have been implemented and used to record physiological variables to study the response of the ANS during stressful tasks in a non-invasive manner through, e.g., parameters from cardiac activity, GSR dynamics, skin temperature and RespR [10,13,29,30].

The sensorized garments manufactured for recording such relevant physiological variables are mostly chest straps [5,6,31–33] and t-shirts [7,20,21,34–40] aiming to record respiration and heart activity and gloves [20–23], glove-like devices [19,24,25] and wrist-bands [26–28,41] for recording GSR and temperature.

Since the turn of the century, sensorized gloves, gloves-like systems and wristbands have been used for obtaining GSR recordings and performing electrodermal response studies. With the passage of time the level of electronic integration has increased. Initially metallic [25–28] or Ag/AgCl external electrodes [20,21,24,41] were used, later a glove with an integrated electrodermal response sensor was manufactured [23], and an eventually gloves with textrodes integrated in the garment have been produced [22].

2. Materials

Several textile-enabled measurement devices and sensorized garments have been implemented for recording physiological variables that would allow to study the response of the ANS during stressful tasks in a non-invasive manner e.g., parameters from cardiac activity, GSR dynamics, skin temperature and RespR [10,13,29,30]. Some details relevant to the following Sections: Section 2.1 Measuring Devices and Section 2.2 Sensorized Garments have been published elsewhere [42,43] and validate the measurement performance of the wearable biomedical measurement system produced during the 1st phase of the ATREC project.

2.1. Wearable Biomedical Measurement Devices

For the 1st phase, two non-invasive physiological measurement devices have been built: One to measure GSR and skin temperature and a second device to record cardiogenic biopotentials and impedance thoracic measurements. Both are battery operated with 900 mAh lithium-ion batteries, and are provided with an internal 4GB SD memory card to allow long-term recording and off-line data analysis.

2.1.1. GSR and Body Temp

One of the devices enables skin impedance monitoring as well as ambient and body temperature monitoring. The reduced dimensions (50 × 35 × 15 mm) enable its integration in a wearable biomedical measurement system in a straightforward manner. In this case, this device is intended to be used with the sensorized glove and/or the arm-strap that will be explained in the following Sections, see Figure 2.

Figure 2. GSR device with a drawing of the connection with the sensorized glove.

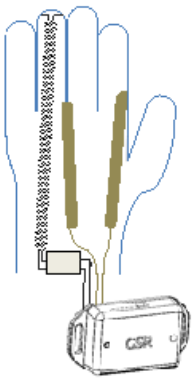

For the GSR measurements a Wheatstone bridge topology with constant voltage excitation of 0.5 V is implemented. The voltage is applied to the skin through a resistor of 2 KΩ that limits the maximum current. The Wheatstone bridge differential voltage is measured by an instrumentation amplifier that it is connected to the input of an Analog-to-Digital Converter (ADC) available in the microcontroller in order to obtain the GSR value. The GSR is measured with a sampling frequency of 250 Hz.

The temperature measurements are performed through a 1-wire DS1825 digital thermometer manufactured by Maxim Integrated (San Jose, CA, USA). The 1-Wire® communication protocol

implemented in the DS1825 allows the use of only one data line and ground for the communications with the microprocessor as well as for the power supply. The DS1825 incorporates a hardware 4-bit identification code that allows the connection of several temperature sensors to the same data line. The GSR measuring unit is provided with two temperature sensors, one external temperature sensor that is in contact with the skin and one internal temperature sensor placed in the microcontroller board. A sampling frequency of 1 Hz is used to measure both temperatures.

2.1.2. ECG amplifier and EBI Plethysmographer

This device records both the ECG biopotential signal as well as Thoracic Electrical Bioimpedance at a single frequency of 50 kHz. Its reduced dimensions (50 × 35 × 20 mm), makes the device suitable for easy integration with the chest strap electrode system described in the following section. The intended use for this ECG/EBI sensing unit is to record cardiogenic biopotentials to compute the HR from the acquired ECG and measure the impedance change caused during breathing to extract the RespR from the recorded changing TEB signal. In Figure 3 it is possible to observe the device with a typical electrode connection for ECG and TEB.

Figure 3. Drawing of the ECG/ICG measuring device indicating the connection with the biopotential and the TEB textrodes placed on the torso for performing ECG and respiration measurements.

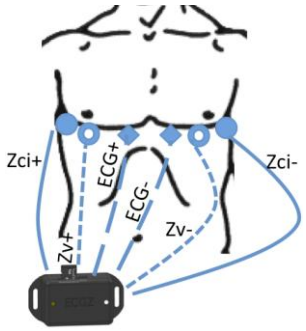

The ECG signal is measured by a 1-lead instrumentation amplifier topology suggested by Merritt *et al.* [44], the output voltage is connected to an ADC input in the microcontroller and recorded with a sampling frequency of 250 Hz. The TEB measurement is obtained using an excitation frequency of 50 kHz and a sampling frequency of 100 Hz. The impedance estimation core is based in the SOC AD5933 manufactured by Analog Devices (Norwood, MA, USA), implementing an analog front-end customized for four-electrode measurements [45].

2.2. Sensorized Garments and Textrodes

The following garments have been confectioned with several types of textile materials including conductive fabrics used for the textrodes and electrical connections. The conductive fabric used is the Shieldex® Fabric P130+B manufactured by STATEX GmbH, (Bremen, Germany). All the sensorized garments and their different supporting elements required to operate with the textile-enabled instrumentation mentioned in the previous section are described in this section.

2.2.1. Glove for GSR and Skin Temperature

Two textile electrodes have been integrated inside of the glove in the proximal phalanx of the index and middle fingers on the inside of the glove for measuring the GSR, and a temperature sensor has been placed in the tip of the ring finger of the glove to sense the peripheral skin temperature, see Figure 4 for details.

Figure 4. Drawing of the sensorized glove. (**a**) Upper view of the glove. (**b**) Cross-sectional view of the glove at the proximal phalanx in a perpendicular plane to the palm. (**c**) Palm view.

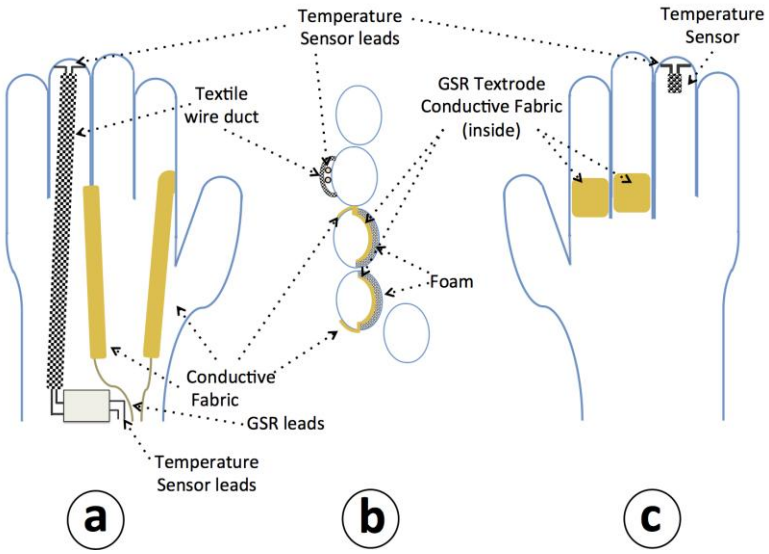

The textrodes and the temperature sensors are connected through 4 cables with the measuring device that is fastened with Velcro to a wristband as shown in Figure 5.

Figure 5. Sensorized glove connected to the measuring unit fasten to the wristband.

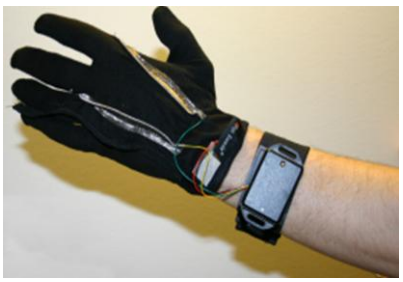

2.2.2. Upper-Arm Strap for GSR and Superficial Temperature

An upper arm strap has been confectioned with two integrated textrodes to sense the galvanic skin response in the skin surface. A DS1825 sensor is also integrated in the inner lining of the strap in order to contact the skin and in this way measure the skin surface temperature. Figure 6 shows the design of the confectioned sensorized garment and Figure 7a shows the confectioned sensorized upper arm strap and Figure 7b shows the same arm strap connected to the measurement unit for GSR and body temp measurement while worn on the arm.

Figure 6. Drawing of the confectioned sensorized upper arm strap. (**a**) Inside view, showing the sensors. (**b**) Outside side, where the sensing device is placed and connected. (**c**) Detail of the textile-electronic interconnection achieved by using conductive fabrics, yarn and sewing them through a ring-shaped end.

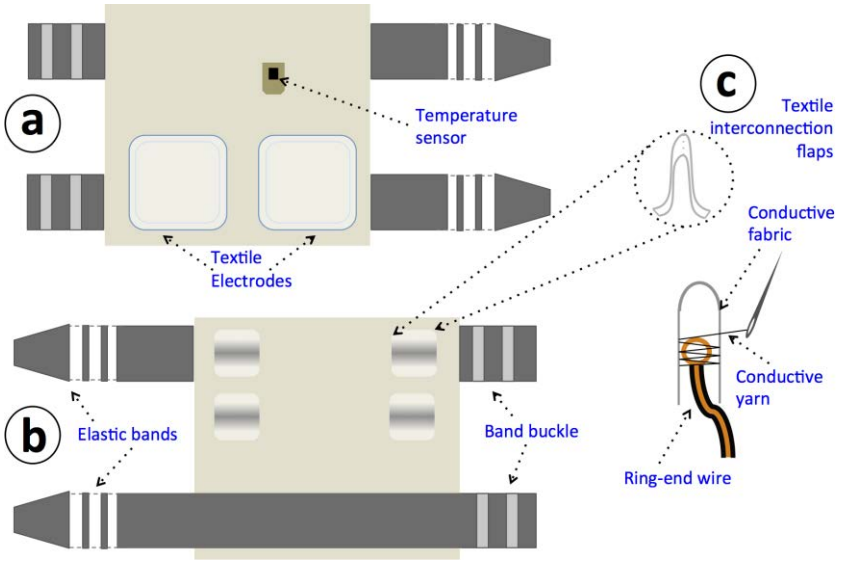

Figure 7. (**a**) Confectioned upper arm strap. (**b**) Measuring device and strap worn on the upper arm.

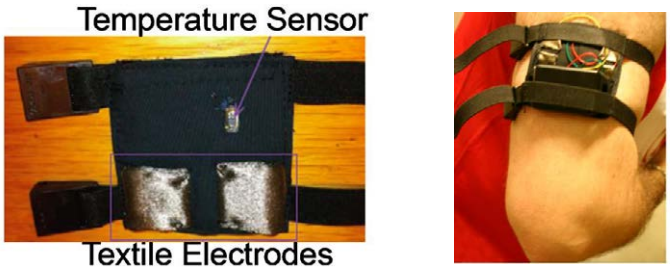

(**a**) (**b**)

2.2.3. Chest Straps System for Cardiac and Respiration Recordings

A chest strap garment with repositionable textile electrodes to record 1-lead ECG from two textrodes and tetrapolar TEB measurements with another four textrodes has been developed. The possibility of placing the electrodes in any place along the horizontal and vertical straps enables to test different measurement configurations for ECG and TEB measurements, see Figure 8a. Depending on the placement of the textrodes around the surface of the thorax and abdomen, the TEB measurement will have more or less cardiac and respiratory components allowing us to perform a multi-parametric signal recording if required.

Figure 8. (**a**) Chest straps system confectioned for placement of ECG and TEB electrodes. (**b**) Detail of the elastic perforated band. (**c**) Fixation between straps through chef jacket button.

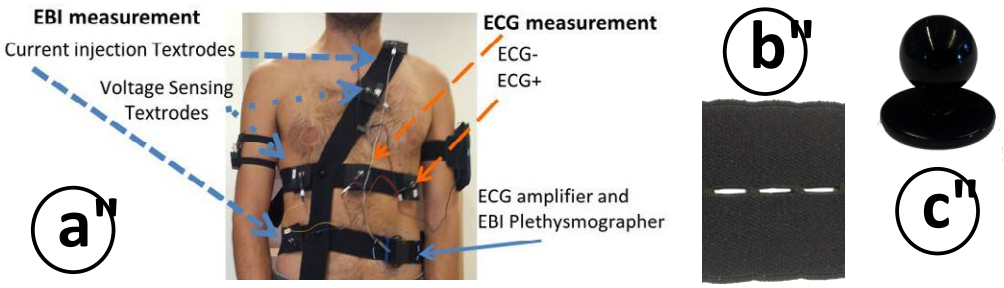

Each strap is made with a highly elastic band with 1 cm perforations every 2 mm, see Figure 8b. These perforations enable the reposition of the textrodes along the straps and fixation between straps using chef jacket buttons, see Figure 8c.

2.2.4. Repositionable Textrodes

The textile electrodes have an approximate surface of 25 cm^2 and are confectioned with a textile structure that is folded over itself creating a clamp through a male-female pair of press-studs, as shown in Figure 9. Note that the connection between the measurement leads and the textrode is achieved through a third press-stud, male.

Figure 9. (**a**) Schematic of the repositionable textrode. Notice that when folded the electrode is clamped using its male and female press-studs, thus creating an electrical and mechanical connection. (**b**) Confectioned repositionable textrode.

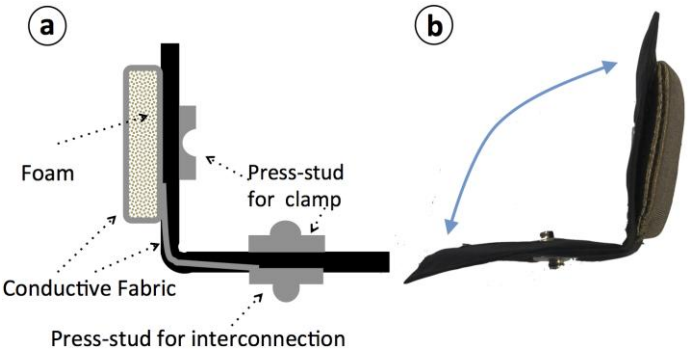

2.3. Voice Recording

In order to record the voice during the experiments of the first phase of the project, a smartphone was custom programmed for such purpose. The selected device was the BRVAR909 manufactured by Bravus Europe AMISL (Andorra), an Android 2.2 based rugger device, IP67 specifications complaint including water and shock resistant. An 8 GB SD card was used as main storage system.

A customized Android application was designed and programmed, to allow the synchronized recording of the speakers' speech at 22.5 kHz. The local clock of the smartphone was also registered in this way, once the clock was synchronized with the rest of the measurement devices, the recordings of the speech could use the same time frames.

3. Methods

3.1. Activities for Assessment of Stress

In order to evaluate the performance of the prototype designed in the first phase of the project, an experiment was designed with the purpose of generating different types of stress in a set of subjects. The main purpose of this experiment was the controlled generation of emotional, mental and physical stress, through a set of stages. A PC-based application was created to induce stress situations in a controlled manner. The main tools used to generate stress are described in the following sections for each different type of stress.

3.1.1. Emotional Stress

In order to generate emotional stress, a set of different videos was used. The videos used were selected to specifically generate several types of emotions, including neutral, sadness, anger and disgust. In a first step, the videos were viewed without the interaction of the subject, and in a second step, they were repeated and the subject had to click under the emotion perceived in any moment. For this purpose, a circle of emotions inspired in the Plutchick circle was used [46]. Each video used in the experiment was based on a set of segments of movies with a total duration of approximated 10 min, and the movies used were Earth (2007), Life is Beautiful (1997) and Cannibal Holocaust (1980).

3.1.2. Mental Stress

In a different way, mental stress was generated through two different games. These games were selected in order to put the subject at the limits of mental calculus. The first game consists in making a set of quick mental sums. A set of digits to be added appears on the screen, and the subject has to click on the correct solution. The time available to solve each problem varies along the experiment, being decreased when the subject answers right, and increased when he/she answers wrong. The idea is to put the subject in a high level of mental activity, independently of his/her calculus ability. This game was played since 80 sums from two to five digits were carried out. The second game consists in a Tetris-based game, in which again the objective is to seek the limit of the mental ability of the subject. For this purpose, the speed of the game was controlled so the difficulty could be adapted during the exercise.

3.1.3. Physical Stress

Finally, physical stress was generated making the subject go up and down in the main stairs of a three level building during 5 min. This activity was selected due to its simplicity and since it quickly generates a high physical stress level.

3.1.4. Surveys and Questionnaires for Stress Assessment

Both socio-demographical and psychological computer-based surveys were included in the experiments. The socio-demographical survey aimed at registering all the relevant information from each subject, including personal data, main biometrics, sport activities, any toxic habits and details about what the subject did during the hour previous to the experiment.

Concerning the psychological surveys, their purpose was to monitor the stress level and typology during the different parts of the experiments. The Self-Assessment Manikin [47] and the Profile of Mood States [48] were carried out after the visualization of each video in the emotional stress stages.

Short computer-based control surveys were also carried out after every stage of the experiment, in order to determine if the subject was concentrated on each task or if, by the contrary, he/she got bored during the experiment. The aim was to determine the effectiveness of the stress situations along the experiment.

3.1.5. Baseline and Sequence of Experimental Setup

The total duration of the experiment was around 75 min. In a first step after starting the recording of the different devices of the prototype, the subject fills out a sociocultural questionnaire. The aim is to establish a baseline in the register. Once the sociocultural questionnaire is completed, the different stages of the experiment are carried out. It is important to highlight that several surveys are also carried out in order to monitor the real stress level of the subject during the experimental process. The sequence of the experiment is described as follows:

(1). Sociocultural survey.
(2). Neutral stage: neutral video.
(3). First mental stage: sum game.
(4). First emotional stage: sad video.
(5). Second mental stage: Tetris game.
(6). Second emotional stage: disgusting video.
(7). Physical stage: stair running.

3.2. Operational Test of the Wearable Biomedical Measurement Devices and Sensorized Garments

A total number of 12 measurement devices and sensorized garments have been produced for each modality. The correct operation of the measuring devices and the corresponding sensorized garments has been validated at least on two different healthy volunteers obtaining at least 2 min of GSR recordings with the glove and the arm strap as well as ECG and respiration activity. In addition, to such test performed systematically prior to the initiation of each measurement session of 75 min, non-systematic test have been carried out all through the implementation of the project. e.g., battery life test, where the systems were used continuously for more than 2 h.

3.3. Speech Analysis

Voice was recorded during the experiments with the aim of studying its use in order to assess emotional status. Several features were successfully calculated from the speech recordings, with the aim of implementing those more useful to determine the stress level. The features extracted in the voice analysis were statistical parameters from Mel Frequency Cepstral Coefficients, short time energy, pitch, pitch perturbation quotient, amplitude perturbation quotient, jitter, voice turbulence index, and soft phonation index.

3.4. Experimental Recordings Performed with the Wearable Biomedical Measurement Systems

Non-invasive recordings have been carried out with the 12 sets of wearable measurement devices and sensorized garments in 42 volunteers undergoing the battery of stress test described in previous sections. This way over 3,000 min of multichannel recordings have been produced.

3.5. Analysis of Multi-Sensorial Data

A total of 724 features from seven different signals were used to extract the information derived from the stress levels of the subjects. Time-Frequency and Statistical analysis has been performed on each of the different type of the signals. Several time configurations were tested in order to determine the best time frames for the stress analysis. For this purpose, two parameters were taken into account: the frame length and the frame overlap. Frame lengths of 10, 30, 60, 180 and 300 s were evaluated, and time overlaps of 0, 10, 30 and 60 were considered. From the preliminary results, we selected a frame length of 60 s and a time overlap of 10 s, so that a decision was taken every 10 s using information from the last 60 s of each signal. These values represented a tradeoff between time resolution and performance.

4. Results

4.1. Validation of Sensorized and Wearable Biomedical Measurements Systems

This section presents the measurements recorded with the measuring devices described and the sensorized garments in Sections 2.1 and 2.2, respectively. More specifically, this section presents a set of measurements obtained during the validation test with the one measurement device and garment of each kind for a single subject. More detailed information has been presented in [42].

4.1.1. GSR and Temperature

Skin temperature and GSR were recorded in several subjects. While skin temperatures produced very stable measurements around 34 °C with both garments producing flat recordings, GSR measurements exhibited larger variance, see Figure 10. Note that the GSR data has been filtered with a moving average window of 5 s as in [49].

Figure 10. Galvanic skin response measurements. (**a**) Glove. (**b**) Upper arm strap.

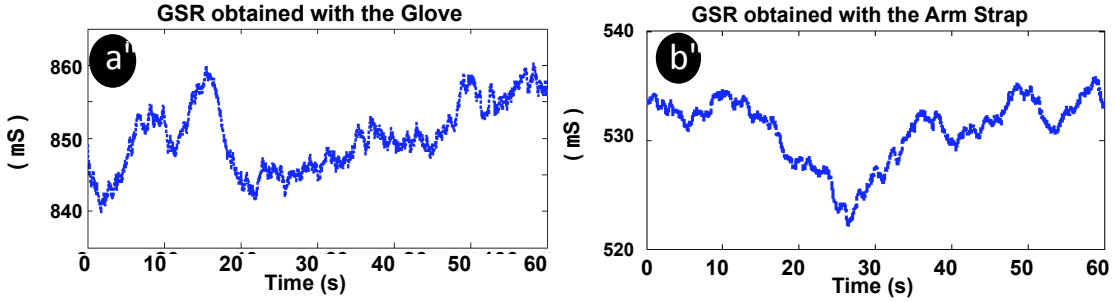

4.1.2. ECG Recordings

Surface cardiac biopotentials were recorded in several subjects with the wearable measurement system presented in Figure 8a. The ECG recording plotted in Figure 11a shows 60 s of an ECG record. As shown in the 4 second-long zoomed segment the recording is very fair, allowing for a straight detection of the R complex for heart rate assessment. The first 25–30 s show slow activity related with respiratory movement. In the plot it is possible to see that during the seconds 60 to 80 while the subject kept the breath, the ECG recording was completely stable.

Figure 11. (**a**) ECG recording. (**b**) Transthoracic Electrical Bioimpedance recording.

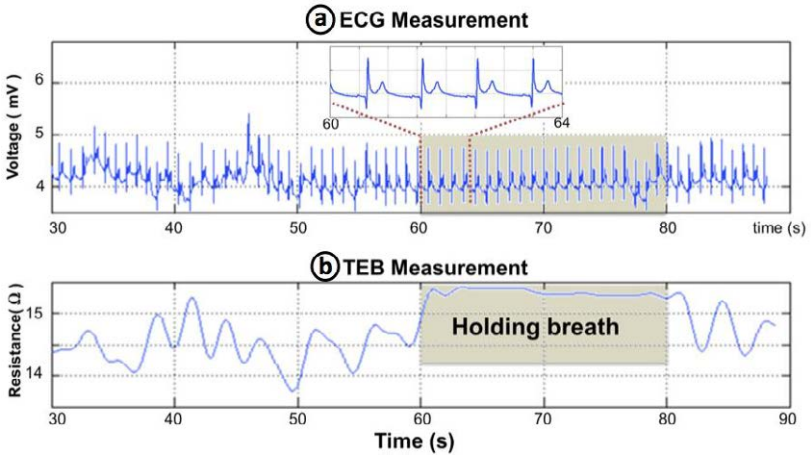

4.1.3. Thoracic EBI Recordings

TEB recordings were obtained simultaneously to the ECG recording, see Figure 11, using the wearable measurement system presented in Figure 8a for several subjects. A 60-second segment of the TEB recording is shown in Figure 11b. The respiration activity is easily observable in this plot as the resistance increases and decreases according to the respiration cycle. Note that the changes stop between 60 and 80 s on the plot while the subject was holding his or her breath.

Figure 12. 90 s speech recording obtained with the BRVAR909 smartphone for one of the subjects of the experiments.

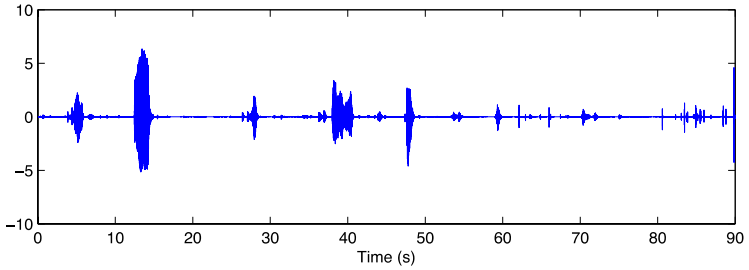

4.2. Voice Recordings

The recordings obtained with the BRVAR909 presented clear speech signals as shown in Figure 12, where a segment of 90 min is shown.

4.3. Measurement Database

The experimental test produced full recordings for 42 subjects from February 2013 to May 2013; generating more than 50 h of multisensorial data, see Table 1. All signals were stored in raw data, and later processed to extract features potentially useful to implement detection algorithms and classifiers for assessment of the user's mental stress.

Table 1. Signals recorded on the database.

Signal	Site or Configuration	
Electrocardiogram	In thoracic region, in an axial plane	
Thoracic Electrical Bioimpedance	Transthoracic Respiration	
Galvanic Skin Response	Between Middle and Index Fingers	Back of Upper Arm
Temperature	Tip of Ring Finger	Back of Upper Arm
	Ambient Temperature	
Speech	Built-in Microphone on the Smartphone	

4.4. Preliminary Analysis of Acquired Data

It is important to recall that the aim of the experiments during the first phase was to establish the potential usefulness of the different type of recordings measured with the implemented prototypes. Notice that, for such analysis work, the database was split in two: the first 25 subjects were used for design and training, and the remaining 17 subjects were used to testing purposes to validate the performance of the classification algorithms.

For this purpose, a 4-class classification scenario was designed, with the aim of determining in which stage was the subject: neutral stage, emotional stress stage, mental stress stage and physical stress stage. As previously indicated, a time window with a length of 60 s and a time overlap of 10 s was used, *i.e.*, a decision was produced every 10 s using data from the last 60 s of each recording. These values represented a tradeoff between time resolution and performance.

From the 724 evaluated 192 were selected using a genetic algorithm [50] that were run through a Linear Discriminant Classifier (LDC).

Table 2 shows the results obtained with the implemented classifiers. Both the number of features selected by the genetic algorithm and the error rate obtained by the LDC are included. Results show the best performance of the electrocardiogram signals and the thoracic impedance signals, when compared to the other signals recorded in the experiments. The 10 features selected from the ECG recording and the 20 selected from the TEB measurement are enumerated in two lists in Appendix, respectively. It is important to highlight the performance of the speech analysis that resulted in a very high error rate. This is mainly caused by the absence of voice in most of the recorded data, making the speech-based classifier to achieve higher error rates.

5. Discussion

5.1. Wearable Biomedical Measurement Devices and Sensorized Garments

Small sized measurement devices were made specifically to facilitate the integration with the sensorized garments. State-of-the-art techniques were used for textile-electronic integration like press-studs, which pressed through a conductive fabric is the most used approach to perform such type of textile-electronic interconnections and it can be found in commercial products [5,7] as well as in research prototypes [51,52]. Sewing with conductive yarn through conductive fabrics has been used before to establish an electrical connection [53]. The sensorized garments have fulfill their intended purpose in Phase 1 allowing the acquisition of several different physiological measurements during exercises designed to specifically target assessment of stress. The performance of the measurement devices and the sensorized garments was previously validated in [42,43].

5.2. Preliminary Observations from Stress Experiments

It is clearly noticed from the error rate reported in Table 2, that the biosignals producing the best classification of mental status are the ECG, mainly heart rate and the respiration rate. Such results may be expected since both respiration and heart rate are highly mediated by the ANS and also it is relatively easier to obtain robust ECG and TEB measurements with tight garments on the thorax than GSR or temperature from fingers or arms. A detail description of the multiparametric and classification work performed on the database will be reported elsewhere.

Table 2. Signals recorded on the database.

Signal	Nr of Extracted Features	Selected Features	Error Rate
Electrocardiogram	244	10	23.72%
Thoracic Electrical Bioimpedance	244	20	24.40%
Temperature (Arm)	16	7	44.53%
Speech	44	15	48.44%
Galvanic Skin Response (Fingers)	80	40	48.48%
Temperature (Finger)	16	4	56.80%
Galvanic Skin Response (Arm)	80	20	57.85%

Note: Ordered according to classification performance.

The obtained error rates in detection of stress from heart rate and the respiration rate, 23.72% and 24.40%, respectively, are slightly better than 31% error rate obtained from HR variability analysis as shown in [54]. The performance exhibit by heart rate and the respiration rate is also superior than the performance obtained from analysis of the electroculogram with an error rate >25% [55], while they are comparable to the performance obtained from ECG analysis [55] and significantly worse than the performance obtained from EEG analysis, with error rates as low as 6% [55].

5.3. Voice Recording

The classification error obtained with the analysis of the recorded speech (>48%) is slightly over what other authors have reported in [56] for automatic classification of stress from speech analysis (46% & 44%, using Hidden Markov Models and Vector Quantification, respectively). When comparing the 48% error rate obtained in this study with the error rates obtained with traditional Teager Energy Operator-based feature vector with a Hidden Markov Model-trained classifier (22.5% error), or using a weighted sub-band detection scheme (4.7%) [57] the differences are significant.

In either case the error rate obtained based on ECG or TEB features was significantly lower. The relatively larger error rate produced when using speech-based features might be due to the fact that while voice recordings were performed in every experiment for the duration of the experiment, unfortunately the test activities did not produce enough speech content to be able to characterize the different states properly. Hopefully during the final validation test planned for the end of the second phase, the voice recordings will contain more speech information useful for classification purpose.

5.4. Lessons Learned

Executing this project has given us the opportunity to obtain new experiences and learn from them. One issue that we find important is judging what is enough, otherwise the production of excess data, samples or data might increase the requirements of the project unnecessarily and can have undesired consequences. Considering the exploratory nature of the first phase, manufacturing 12 different sets of measurement devices and sensorized garments was completely unnecessary and not efficient since it required more financial and staff resources. The fact is that the experiments were never done simultaneously, which means that a few measurement sets would have been enough.

Another lesson learnt that had a significant influence on the realization of the experiments was the use of a SD card for data storage and also for data access, instead than an alternative method for data access like Bluetooth. The lack of this feature meant that prior to the execution of each experiment to perform a operational test, the SD card had to be removed and read in the PC and despite this fact, there were always doubts about whether the measurements were being recorded properly because the access to the recorded data could not be done until the experiment was finalized. This limitation has been overcome in the measurement device implemented during Phase 2.

6. Conclusions and Outlook

The wearable measurement systems and the voice recording system have allowed the execution of activities specifically targeted to evaluate the influence of stress on several physiological variables.

Therefore the 1st phase of the ATREC project has been completed and the preliminary analysis from the experimental results suggest that for the 2nd phase, it is very likely that a sensorized vest or T-shirt with integrated textrodes for biopotential recordings and trans-thoracic bioimpedance measurements will be manufactured, similar to the one reported in [58].

Acknowledgments

The ATREC project is funded by the Spanish Ministry of Defense through the ―OINCIDENTE" program (DGAM DNR 1003211003500) and it is executed under the supervision of the Metrology and Human Factors Department, of ―La Marñosa" Institute of Technology.

Author Contributions

F.S., J.F. and R.B. have implemented the sensorized garments and performed the functional tests. F.S. have conceived the Wearable Measurement Systems. F.G. has developed the measurement instrumentation. F.S. and J.F. have integrated electronic the measurement devices with the textile and wearable sensors. I.M.-H., D.A., C.L. and R.G.-P. have participated in the execution of the stress test and have performed the analysis of the recordings. F.S. and R.G.-P. have supervised both the technical and experimental activities. F.S. and R.G.-P. have written the initial manuscript and I.M.-H., J.F., L.A., R.B., D.A. and C.L. have participated in the revision of the manuscript supporting the writing process.

Conflicts of Interest

The authors declare no conflict of interest.

References

1. Chan, M.; Esteve, D.; Fourniols, J.Y.; Escriba, C.; Campo, E. Smart wearable systems: Current status and future challenges. *Artif. Intell. Med.* **2012**, *56*, 137–156.
2. Lanata, A.; Scilingo, E.P.; de Rossi, D. A multimodal transducer for cardiopulmonary activity monitoring in emergency. *IEEE Trans. Inf. Technol. Biomed.* **2010**, *14*, 817–825.
3. Di Rienzo, M.; Rizzo, F.; Meriggi, P.; Castiglioni, P.; Mazzoleni, P.; Ferrarin, M.; Ferratini, M. MagIC: A textile system for vital signs monitoring. Advancement in design and embedded intelligence for daily life applications. In Proceedings of 29th Annual International Conference of the IEEE Engineering in Medicine and Biology Society, Lyon, France, 22–26 August 2007; pp. 3958–3961.
4. Reiter, H.; Muehlsteff, J.; Sipila, A. Medical application and clinical validation for reliable and trustworthy physiological monitoring using functional textiles: Experience from the HeartCycle and MyHeart project. In Proceedings of IEEE-EMBC, Boston, US, 30 August–3 September, 2011;pp. 3270–3273.
5. Polar Electro Oy. Polar H6 Hear Rate Sensor. Available online: http://www.polarusa.com/us-en/products/accessories/H6 (accessed on 10 March 2014).

6. Vivonoetics. The Equivital TnR Product Range. Available online: http://vivonoetics.com/wp-content/downloads/Brochures/General TnR Brochure Vivonoetics contact.pdf (accessed on 10 March 2014).
7. Nuubo. nECG shirt L1. Available online: http://www.nuubo.com/sites/default/themes/nuubo2/pdf/DATASHEETS_EN_shirt.pdf (accessed on 10 March 2014).
8. Sloan, R.P.; Shapiro, P.A.; Bagiella, E.; Boni, S.M.; Paik, M.; Bigger, J.T., Jr.; Steinman, R.C.; Gorman, J.M. Effect of mental stress throughout the day on cardiac autonomic control. *Biol. Psychol.* **1994**, *37*, 89–99.
9. Jovanov, E.; Lords, A.O.; Raskovic, D.; Cox, P.G.; Adhami, R.; Andrasik, F. Stress monitoring using a distributed wireless intelligent sensor system. *IEEE Eng. Med. Biol. Mag.* **2003**, *22*, 49–55.
10. Bernardi, L.; Wdowczyk-Szulc, J.; Valenti, C.; Castoldi, S.; Passino, C.; Spadacini, G.; Sleight, P. Effects of controlled breathing, mental activity and mental stress with or without verbalization on heart rate variability. *J. Am. Coll. Cardiol.* **2000**, *35*, 1462–1469.
11. Saidatul, A.; Paulraj, M.P.; Yaacob, S.; Mohamad, N.N.F. Automated system for stress evaluation based on EEG signal: A prospective review. In Proceedings of IEEE 7th International Colloquium on Signal Processing and Its Applications, Penang, Malaysia, 4–6 March 2011; pp. 167–171.
12. Setz, C.; Arnrich, B.; Schumm, J.; La Marca, R.; Troster, G.; Ehlert, U. Discriminating stress from cognitive load using a wearable EDA device. *IEEE Trans. Inf. Technol. Biomed.* **2010**, *14*, 410–417.
13. Villarejo, M.V.; Zapirain, B.G.; Zorrilla, A.M. A stress sensor based on Galvanic Skin Response (GSR) controlled by ZigBee. *Sensors* **2012**, *12*, 6075–6101.
14. Kataoka, H.; Kano, H.; Yoshida, H.; Saijo, A.; Yasuda, M.; Osumi, M. Development of a skin temperature measuring system for non-contact stress evaluation. In Proceedings of the 20th Annual International Conference of the IEEE Engineering in Medicine and Biology Society, Hong Kong, China, 29 October–1 November 1998; pp. 940–943.
15. Looije, R.; te Brake, G.; Neerincx, M. Geo-collaboration under stress. In Prodeedings of Workshop on Mobile HCI for Emergencies, Singapore, 9 September 2007.
16. Charfuelan, M.; Kruijff, G.-J. Analysis of Speech Under Stress and Cognitive Load in USAR Operations. In *Natural Interaction with Robots, Knowbots and Smartphones*; Mariani, J., Rosset, S., Garnier-Rizet, M., Devillers, L., Eds.; Springer: New York, NY, USA, 2014; pp. 275–281.
17. Rothkrantz, L.J.; Wiggers, P.; Wees, J.-W.A.; Vark, R.J. Voice Stress Analysis. In *Text, Speech and Dialogue*; Sojka, P., Kopefcek, I., Pala, K., Eds.; Springer: Berlin/Heidelberg, Germany, 2004; Volume 3206, pp. 449–456.
18. Ivonin, L.; Chang, H.-M.; Chen, W.; Rauterberg, M. Unconscious Emotions: Quantifying and Logging Something We Are not Aware of. *Personal Ubiquitous Comput.* **2012**, *17*, 663–673.
19. Kimmy, A.; Chen, W.; Lindsay, B. Smart Photo Frame for Arousal Feedback—Wearable sensors and intelligent healthy work environment. In Proceedings of Workshop on Smart Offices and Other Workplaces of the 7th International Conference on Intelligent Environments, Nottingham, UK, 25–28 July 2011; pp. 685–696.

20. Axisa, F.; Dittmar, A.; Delhomme, G. Smart clothes for the monitoring in real time and conditions of physiological, emotional and sensorial reactions of human. In Proceedings of the 25th Annual International Conference of the IEEE Engineering in Medicine and Biology Society, Valencia, Spain, 21–25 July 2003; pp. 3744–3747.
21. Axisa, F.; Gehin, C.; Delhomme, G.; Collet, C.; Robin, O.; Dittmar, A. Wrist ambulatory monitoring system and smart glove for real time emotional, sensorial and physiological analysis. In Proceedings of 26th Annual International Conference of the IEEE Engineering in Medicine and Biology Society (EMBC2004), San Francisco, CA, USA, 1–5 September 2004; pp. 2161–2164.
22. Valenza, G.; Lanata, A.; Scilingo, E.P.; de Rossi, D. Towards a smart glove: Arousal recognition based on textile electrodermal response. In Proceedings of Annual International Conference of the IEEE Engineering in Medicine and Biology Society (EMBC2010), Buenos Aires, Argentina, 31 August–4 September 2010; pp. 3598–601.
23. Katsis, C.D.; Katertsidis, N.; Ganiatsas, G.; Fotiadis, D.I. Toward emotion recognition in car-racing drivers: A biosignal processing approach. *IEEE Trans. Syst. Man Cybern. Part A Syst. Hum.* **2008**, *38*, 502–512.
24. Strauss, M.; Reynolds, C.; Hughes, S.; Park, K.; McDarby, G.; Picard, R.W. The handwave bluetooth skin conductance sensor. In *Affective Computing and Intelligent Interaction*; Springer Berlin Heidelberg: Beijing, China, 22–24 October 2005; pp. 699–706.
25. Scheirer, J.; Picard, R. The Galvactivator: A Glove that Senses and Communicates Skin Conductivity. In Proceedings of the 9th International Conference on Human-Computer Interaction, LA, USA, 5–10 August 2001.
26. Fletcher, R.R.; Dobson, K.; Goodwin, M.S.; Eydgahi, H.; Wilder-Smith, O.; Fernholz, D.; Kuboyama, Y.; Hedman, E.B.; Poh, M.-Z.; Picard, R.W. iCalm: Wearable sensor and network architecture for wirelessly communicating and logging autonomic activity. *IEEE Trans. Inf. Technol. Biomed.***2010**, *14*, 215–223.
27. Poh, M.-Z.; Swenson, N.C.; Picard, R.W. A wearable sensor for unobtrusive, long-term assessment of electrodermal activity. *IEEE Trans. Biomed. Eng.* **2010**, *57*, 1243–1252.
28. Ouwerkerk, M. Unobtrusive Emotions Sensing in Daily Life. In *Sensing Emotions*; Westerink, J.; Krans, M.; Ouwerkerk, M., Eds.; Springer Netherlands: Eindovhen, Netherlands, 2011; Volume 12, pp. 21–39.
29. De Santos Sierra, A.; Avila, C.S.; Guerra, C.J.; del Pozo, G.B. A Stress-Detection System Based on Physiological Signals and Fuzzy Logic. *IEEE Trans. Ind. Electron.* **2011**, *58*, 4857–4865.
30. Zhai, J.; Barreto, A.B.; Chin, C.; Chao, L. Realization of stress detection using psychophysiological signals for improvement of human-computer interactions. In Proceedings of IEEE SoutheastCon 2005, Ft. Lauderdale, FL, USA, 8–10 April 2005; pp. 415–420.
31. Liu, G.-Z.; Huang, B.-Y.; Wang, L. A wearable respiratory biofeedback system based on generalized body sensor network. *Telemed. e-Health* **2011**, *17*, 348–357.
32. Braecklein, M.; Tchoudovski, I.; Moor, C.; Egorouchkina, K.; Pang, L.; Bolz, A. Wireless telecardiological monitoring system for the homecare area. In Proceedings of 27th Annual International Conference of the IEEE Engineering in Medicine and Biology Society (EMBC2005), Shanghai, China, 1 April 2005; pp. 3793–3795.

33. Gargiulo, G.; Bifulco, P.; Cesarelli, M.; Ruffo, M.; Romano, M.; Calvo, R.A.; Jin, C.; van Schaik, A. An ultra-high input impedance ECG amplifier for long-term monitoring of athletes. *Med. Devices* **2010**, *3*, 1–9.
34. De Rossi, D.; Carpi, F.; Lorussi, F.; Mazzoldi, A.; Paradiso, R.; Scilingo, E.P.; Tognetti, A. Electroactive fabrics and wearable biomonitoring devices. *Autex Res. J.* **2003**, *3*, 180–185.
35. Grossman, P. The LifeShirt: A multi-function ambulatory system monitoring health, disease, and medical intervention in the real world. *Stud. Health Technol. Inform.* **2004**, *108*, 133–141.
36. Weber, J.; Blanc, D.; Dittmar, A.; Comet, B.; Corroy, C.; Noury, N.; Baghai, R.; Vaysse, S.; Blinowska, A. Telemonitoring of vital parameters with newly designed biomedical clothing. *Stud. Health Technol. Inform.* **2004**, *108*, 260–265.
37. Zhang, Y.-T.; Poon, C.C.; Chan, C.-H.; Tsang, M.W.; Wu, K.-F. A health-shirt using e-textile materials for the continuous and cuffless monitoring of arterial blood pressure. In Proceedings of 3rd IEEE/EMBS International Summer School on Medical Devices and Biosensors, Cambridge, MA, USA, 5–6 September 2006; pp. 86–89.
38. Yoo, J.; Yan, L.; Lee, S.; Kim, H.; Yoo, H.-J. A wearable ECG acquisition system with compact planar-fashionable circuit board-based shirt. *IEEE Trans. Inf. Technol. Biomed.* **2009**, *13*, 897–902.
39. Linz, T.; Kallmayer, C.; Aschenbrenner, R.; Reichl, H. Fully untegrated EKG shirt based on embroidered electrical interconnections with conductive yarn and miniaturized flexible electronics. In Proceedings of International Workshop on Wearable and Implantable Body Sensor Networks (BSN 2006), Boston, MA, USA, 3–5 April 2006; pp. 26–30.
40. Paradiso, R.; Loriga, G.; Taccini, N.; Gemignani, A.; Ghelarducci, B. Wealthy, a wearable health-care system: new frontier on etextile. *J. Telecommun. Inf. Technol.* **2005**, *4*, 105–113.
41. Picard, R.W. Future affective technology for autism and emotion communication. *Phil. Trans. Roy. Soc. B Biol. Sci.* **2009**, *364*, 3575–3584.
42. Seoane, F.; Ferreira, J.; Alvarez, L.; Buendia, R.; Ayllón, D.; Llerena, C.; Gil-Pita, R. Sensorized Garments and Textrode-Enabled Measurement Instrumentation for Ambulatory Assessment of the Autonomic Nervous System Response in the ATREC Project. *Sensors* **2013**, *13*, 8997–9015.
43. Ferreira, J.; Álvarez, L.; Buendía, R.; Ayllón, D.; Llerena, C.; Gil-Pita, R.; Seoane, F. Bioimpedance-Based Wearable Measurement Instrumentation for Studying the Autonomic Nerve System Response to Stressful Working Conditions. *J. Phys. Conf. Ser.* **2013**, *434*, 012015.
44. Merritt, C.R.; Nagle, H.T.; Grant, E., Fabric-based active electrode design and fabrication for health monitoring clothing. *IEEE Trans. Inf Technol Biomed.* **2009**, *13*, 274–80.
45. Seoane, F.; Ferreira, J.; Sanchéz, J.J.; Bragós, R. Analog Front-End Enables Electrical Impedance Spectroscopy System On-Chip for Biomedical Applications. *Physiol. Meas.* **2008**, *29*, S267–S278.
46. Plutchik, R.; Kellerman, H.; Conte, H.R. A structural theory of ego defenses and emotions. In *Emotions in personality and psychopathopathology*; Izard, C.E., Ed.; Springer US: New York, NY, USA, 1979; pp. 227–257.
47. Bradley, M.M.; Lang, P.J. Measuring emotion: The Self-Assessment Manikin and the Semantic Differential. *J. Behav. Ther. Exp. Psychiat.* **1994**, *25*, 49–59.
48. McNair, D.; Lorr, M.; Droppleman, L. *Manual for the Profile of mood states (POMS)*; Educational and Industrial Testing Service: San Diego, CA, USA, 1971; pp. 1–27.

49. Wu, S.; Lin, T. Exploring the use of physiology in adaptive game design. In Proceedings of International Conference on Consumer Electronics, Communications and Networks (CECNet), 16–18 April 2011; pp. 1280–1283.
50. Raymer, M.L.; Punch, W.F.; Goodman, E.D.; Kuhn, L.A.; Jain, A.K. Dimensionality reduction using genetic algorithms. *IEEE Trans. Evol. Comput.* **2000**, *4*, 164–171.
51. Marquez, J.C.; Seoane, F.; Välimäki, E.; Lindecrantz, K. Comparison of Dry-Textile Electrodes for Electrical Bioimpedance Spectroscopy Measurements. *J. Phys. Conf. Ser.* **2010**, *224*, 012140.
52. Marquez, J.C.; Seoane, F.; Lindecrantz, K. Textrode functional straps for bioimpedance measurements—Experimental results for body composition analysis. *Eur. J. Clin. Nutr.* **2013**, *67*(Suppl 1), doi:10.1038/ejcn.2012.161.
53. Bouwstra, S.; Wei, C.; Feijs, L.; Oetomo, S.B. Smart Jacket Design for Neonatal Monitoring with Wearable Sensors. In Proceedings of Sixth International Workshop on Wearable and Implantable Body Sensor Networks (BSN2009), Berkeley, CA, USA, 3–5 June 2009; pp. 162–167.
54. Jongyoon, C.; Gutierrez-Osuna, R. Using Heart Rate Monitors to Detect Mental Stress. In Proceedings of Sixth International Workshop on Wearable and Implantable Body Sensor Networks (BSN2009), Berkeley, CA, USA, 3–5 June 2009; pp. 219–223.
55. Laurent, F.; Valderrama, M.; Besserve, M.; Guillard, M.; Lachaux, J.-P.; Martinerie, J.; Florence, G. Multimodal information improves the rapid detection of mental fatigue. *Biomed. Signal. Process. Control* **2013**, *8*, 400–408.
56. Namdeo, P.R.; Mishra, A.K. Speech analysis under stress. *World J. Sci. Technol.* **2012**, *2*, 174–177.
57. Hansen, J.; Kim, W.; Rahurkar, M.; Ruzanski, E.; Meyerhoff, J. Robust Emotional Stressed Speech Detection Using Weighted Frequency Subbands. *Eur. J. Adv. Signal Process.* **2011**, *2011*, 906789.
58. Marquez, J.C.; Rempfler, M.; Seoane, F.; Lindecrantz, K. Textrode-enabled Transthoracic Electrical Bioimpedance Measurements. Towards Wearable Applications of Impedance Cardiography. *J. Electr. Bioimpedance* **2013**, *4*, 45–50.

Appendix

Features Selected for the Obtained Error Rates

A1. From Electrocardiogram

Mean value of the heart rate

- Standard deviation of the heart rate
- Third quartile of the heart rate
- Logarithm of the spectrum in mid frequencies (0.08 Hz–0.15 Hz) of the heart rate
- Ratio of the logarithm of the low frequency energy (0.04 Hz–0.08 Hz) *vs.* Logarithm of the high frequency energy (0.15 Hz–0.5 Hz) of the heart rate
- First quartile of the heart rate variability
- Harmonic mean of the heart rate variability
- Logarithm of the standard deviation of the heart rate variability
- Average number of consecutive RR intervals separated more than 50 ms (pNN50)
- Mean value of the ultra-low frequency band (0 Hz–0.04 Hz) of the heart rate

A2. From Thoracic Electrical

- First quartile of the low frequency component (0.04Hz–0.08Hz) of the TEB
- Mode of the mid frequency component (0.08 Hz–0.15 Hz) of the TEB
- Minimum value of the high frequency component (0.15 Hz–0.5 Hz) of the TEB
- Mean value of the ultra-low frequency band (0 Hz–0.04 Hz) of the TEB
- Mean value of the respiratory rate
- Standard deviation of the respiratory rate
- Third quartile of the respiratory rate
- Kurtosis coefficient of the respiratory rate
- Sample entropy of the second differentiation of the respiratory rate
- Sample entropy of the third differentiation of the respiratory rate
- Variance coefficient of the inspired respiratory flux
- Mean value of the total respiratory time
- Standard deviation of the total inspiration time
- Harmonic mean of the respiratory rate
- Trimmed mean of the total respiratory time
- First LPC coefficient of the total respiratory volume
- Mean value of the inspired respiratory flux
- Variation coefficient of the inspired respiratory flux
- Mean value of the ultra low frequency band (0–0.04 Hz) of the inspiration time
- Mean value of the ultra low frequency band (0–0.04 Hz) of the total respiratory volume

PAPER VII

Assessment of mental, emotional and physical stress through analysis of physiological signals using smartphones

Inma Mohino-Herranz, Roberto Gil-Pita, Javier Ferreira, *et al.*

Published in Sensors 2015, 15(10), 25607-25627; doi:10.3390/s151025607

Sensors **2015**, *15*, 25607-25627; doi:10.3390/s151025607

OPEN ACCESS
sensors
ISSN 1424-8220
www.mdpi.com/journal/sensors

Article

Assessment of Mental, Emotional and Physical Stress through Analysis of Physiological Signals Using Smartphones

Inma Mohino-Herranz [1,*], Roberto Gil-Pita [1], Javier Ferreira [2,3], Manuel Rosa-Zurera [1] and Fernando Seoane [2,3]

[1] Department of Signal Theory and Communications, University of Alcala, Madrid 28871, Spain; E-Mails: roberto.gil@uah.es (R.G.-P.); manuel.rosa@uah.es (M.R.-Z.)
[2] Faculty of Care Sciences, Working Life and Welfare, University of Boras, Boras 50190, Sweden; E-Mails: javier.ferreira@hb.se (J.F.); fernando.seoane@hb.se (F.S.)
[3] School of Technology and Health, Royal Institute of Technology, Stockholm 14152, Sweden

* Author to whom correspondence should be addressed; E-Mail: inmaculada.mohino@uah.es; Tel.: +34-91-8856-662; Fax: +34-91-8856-699.

Academic Editor: Vittorio M. N. Passaro

Received: 31 July 2015 / Accepted: 29 September 2015 / Published: 8 October 2015

Abstract: Determining the stress level of a subject in real time could be of special interest in certain professional activities to allow the monitoring of soldiers, pilots, emergency personnel and other professionals responsible for human lives. Assessment of current mental fitness for executing a task at hand might avoid unnecessary risks. To obtain this knowledge, two physiological measurements were recorded in this work using customized non-invasive wearable instrumentation that measures electrocardiogram (ECG) and thoracic electrical bioimpedance (TEB) signals. The relevant information from each measurement is extracted via evaluation of a reduced set of selected features. These features are primarily obtained from filtered and processed versions of the raw time measurements with calculations of certain statistical and descriptive parameters. Selection of the reduced set of features was performed using genetic algorithms, thus constraining the computational cost of the real-time implementation. Different classification approaches have been studied, but neural networks were chosen for this investigation because they represent a good tradeoff between the intelligence of the solution and computational complexity. Three different application scenarios were considered. In the first scenario, the proposed system is capable of distinguishing among different types of activity with a 21.2% probability error, for activities coded as neutral, emotional, mental and physical. In the second scenario,

the proposed solution distinguishes among the three different emotional states of neutral, sadness and disgust, with a probability error of 4.8%. In the third scenario, the system is able to distinguish between low mental load and mental overload with a probability error of 32.3%. The computational cost was calculated, and the solution was implemented in commercially available Android-based smartphones. The results indicate that execution of such a monitoring solution is negligible compared to the nominal computational load of current smartphones.

Keywords: physiological measurements; smart textiles; smartphone; ECG; bioimpedance; stress detection; ergonomics

1. Introduction

The literature includes numerous definitions for "stress". This term was coined by Hans Selye [1,2], who defined it as "the non-specific response of the body to any demand for change". In several studies, Selye observed that laboratory animals exposed to different noxious physical and emotional stimuli (e.g., extremes of heat or cold, perceptual frustration) all exhibited the same pathological changes or alterations, including enlargement of the adrenals and shrinkage of lymphoid tissue. In subsequent studies, Selye demonstrated that persistent stress could cause these animals to develop selected diseases similar to those observed in humans, such as stroke, heart attacks or kidney disease. This phenomenon is studied in detail by the American Institute of Stress [3].

To relate the stress and the physiological signals, it is necessary to examine the sympathetic nervous system, which is closely related to stress [4]. The sympathetic nervous system (SNS) is one of the three major components of the autonomicnervous system (ANS) in addition to the enteric and parasympathetic systems. The main focus of the SNS is to mobilize the body's nervous system in what is known as the fight-or-flight response [5,6]. This response is a physiological reaction that occurs in response to a perceived harmful event, attack or threat to survival [7]. Moreover, this process is recognized as the first stage of a general adaptation syndrome that regulates stress response among vertebrates and other organisms. Therefore, the SNS is responsible for up- and down-regulating different homeostatic mechanisms. Certain reactions are provided by the SNS in such organs as the eyes, heart, lungs, blood vessels, sweat glands and digestive tract [8].

The knowledge derived from the real-time analysis of the stress level of a subject could be of special interest in the monitoring of many professional activities, such as those of soldiers, pilots, emergency personnel and other professionals responsible for human lives. Furthermore, assessment of professionals' current mental fitness for executing the task at hand might avoid unnecessary risks. To obtain this knowledge, two physiological measurements were recorded in this work using customized non-invasive wearable instrumentation for electrocardiogram (ECG) and thoracic electrical bioimpedance (TEB) signals. In a previous work [9], the responses provided by the heart, sweat glands, temperature and the thoracic electrical bioimpedance signals were studied, and it was demonstrated that

the best results were obtained for ECG and TEB measurements. For this reason, we use only these two physiological measurements in this study.

The designed customized wearable instrumentation consists of a vest, a recorder and a smartphone. The vest is comfortable, discreet and easy to wear and contains several electrodes that measure the ECG and TEB signals, which are recorded and transmitted in real time via Bluetooth by an ECGZ2 device to the smartphone, which is responsible for processing the data and estimating parameters related to monitoring of the SNS activity, such as the heart rate or the breathing rate.

Relevant information from both the ECG and TEB measurements is extracted by evaluation of a reduced set of selected features. These features are primarily obtained from filtered and processed versions of raw ECGZ2 measurements, which calculate selected statistical and descriptive parameters. The selection of the reduced set of features was performed using genetic algorithms, thus constraining the computational cost of the real-time implementation. Different classification approaches have been studied, but neural networks were chosen for this work because they represent a good tradeoff between the intelligence of the solution and computational complexity.

Three different analyses of application scenarios were performed to assess the performance of the proposed system. In the first scenario, the proposed system is capable of distinguishing among different types of activities that are neutral, emotional, mental and physical. In the second scenario, the proposed solution distinguishes among the three different emotional states of neutral, sadness and disgust. In the third scenario, the system is able to distinguish between low mental load and mental overload. The computational cost was calculated, and the solution was implemented in commercially available Android-based smartphones. The results indicate that the execution of such a monitoring solution is negligible compared to the nominal computational load of current smartphones.

The remainder of this paper is structured as follows. The hardware system is described in Section 2, and the software design is covered in Section 3. The generation and analysis of the experimental database are described in Section 4. Section 5 summarizes the results obtained by the proposed system with the generated database, and Section 6 provides conclusions for the paper.

2. Hardware System Overview

This section describes the different components of the designed system. The textrodes, the vest itself, the recorder unit and the smartphone.

- Textrodes: The textrodes are electrodes constructed with a textile structure that have an approximate surface of 60 $\times$ 40 mm and are used to measure both the ECG and TEB signal, using only four electrodes. These measurements are strongly related to the mental, emotional and physical state of the subject [10,11]. Figure 1 shows one of the textrodes that is included in the vest.
- Vest: The vest design is illustrated in Figure 2. Both comfort and usability were important characteristics in the design of the vest. To ensure a good grip, all contours of the vest are fitted with silicone bands. Furthermore, different sizes were created, and each vest includes adjustable options, as shown in Figure 3. Using these details, we provided a garment that is comfortable for both men and women.

- Recorder: To record the ECG and TEB measurements acquired by the textrodes, a device known as ECGZ2 was specifically designed to record and send data to the smartphone. The ECGZ2 allows sampling of each measurement with a different sampling frequency. For the ECG measurement, the sampling frequency is 250 Hz, and for the TEB, the sampling frequency is 100 Hz. This device is connected to the textrodes through wires included inside the vest. The device is placed in a pocket of the vest, and the design of this device is shown in Figure 4.
  In the previous version, the information was stored in Micro SD. However, in the new version, we send the information via Bluetooth to the smartphone, which is responsible for receiving and processing data and obtaining results in real time. Additional technical specifications can be found in [9].
- Smarthphone: The final component of the designed system is a smartphone, which is responsible for processing the information transmitted in real time by the ECGZ2 unit and estimating those parameters related to the monitoring of the SNS activity. In our design, the selected device was the "Samsung Galaxy Pocket" with an 832-MHz CPU, 512 MB RAM and a 1200-mAh battery. Section 3 describes the software included in the smartphone.

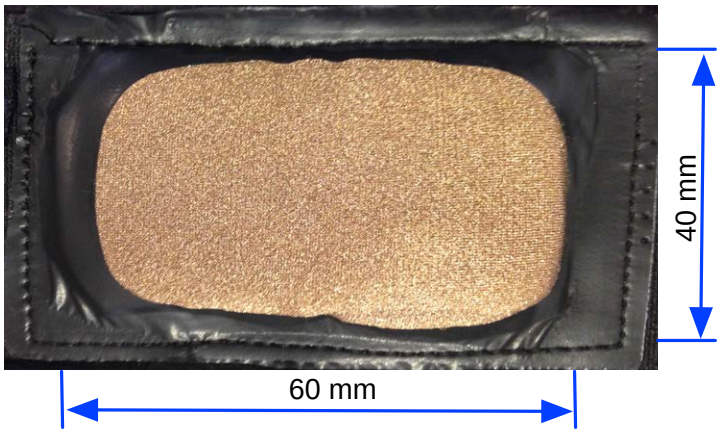

Figure 1. Textrode.

Figure 2. Vest: (**A**) front view; (**B**) back view.

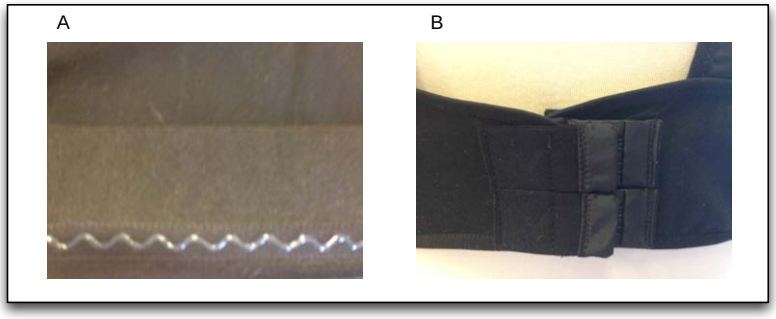

Figure 3. Vest: (**A**) anti-slip band; (**B**) adjustable fastener.

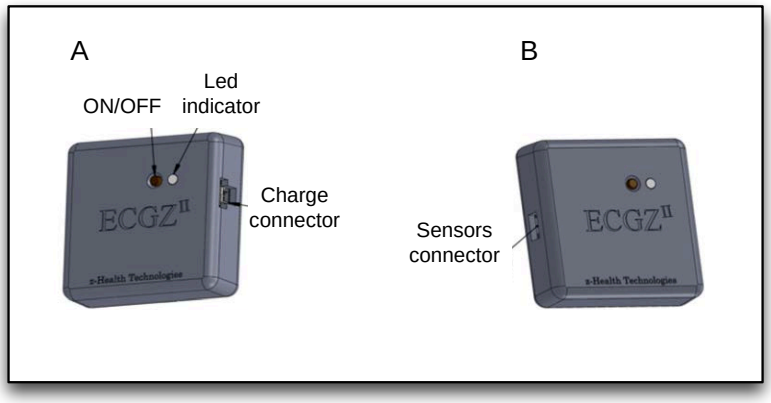

Figure 4. ECGZ2 device design: (**A**) left device view; (**B**) right device view.

3. Software System Design

This section explains the details necessary for understanding the software system implemented in the smartphone and also describes the feature calculations for each measurement, the algorithms used to select the best reduced set of features, the performance of the classifiers with the selected set of features and each tool used to optimize the results.

The scheme used to obtain the complete software system is illustrated in Figure 5. The figure demonstrates that both the ECG and the TEB signals are the inputs of the system, and a reduced set of features is extracted from these signals, which is subsequently used as inputs to the classifier. In this work, the features are determined using a window of 60 s, and the classifier gives an output decision every 10 s.

It is important to note that to determine the set of features, both the performance of the classifier (in terms of error rate) and the computational complexity of the global system must be taken into account. For this purpose, a genetic algorithm tailored to this problem was selected. For simplicity, we consider the number of simple operations per second N_{op} as an indicator of the computational complexity of the real-time implementation of a given set of features, because this value is proportional to the CPU load of the final implementation.

Thus, this section is structured as follows. First, the feature extraction process is described; the classifier specifications are explained; and a description of the algorithm is provided for the selection of the reduced set of features.

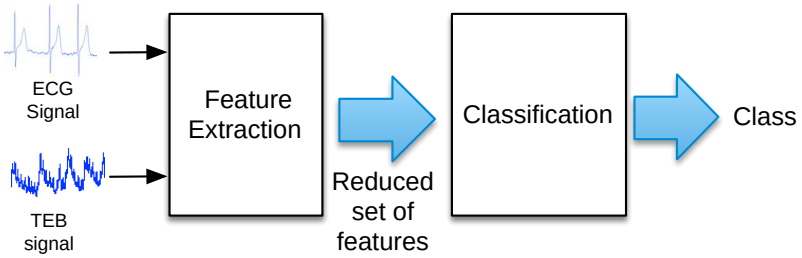

Figure 5. General scheme of the classifier.

3.1. Feature Extraction

This section describes how the features are extracted from ECG and TEB measurements. This process refers to the block referred to as "feature extraction" in Figure 5. Special attention is focused on the description of the computational cost associated with the extraction of each feature. Therefore, all of the possible features are described, taking into account that the final real-time implementation extracts only a reduced number of features.

3.1.1. Features for ECG Measurement

Numerous types of features are commonly used to study ECG measurements, including heart rate variability (HRV) [12–14] or the power ratios of several frequency bands [15–17]. In this work, we use signals obtained and processed in three steps. Figure 6 shows the process used to calculate the ECG-based features in which three different steps can be distinguished: filtering, processing and calculating the parameters and baseline.

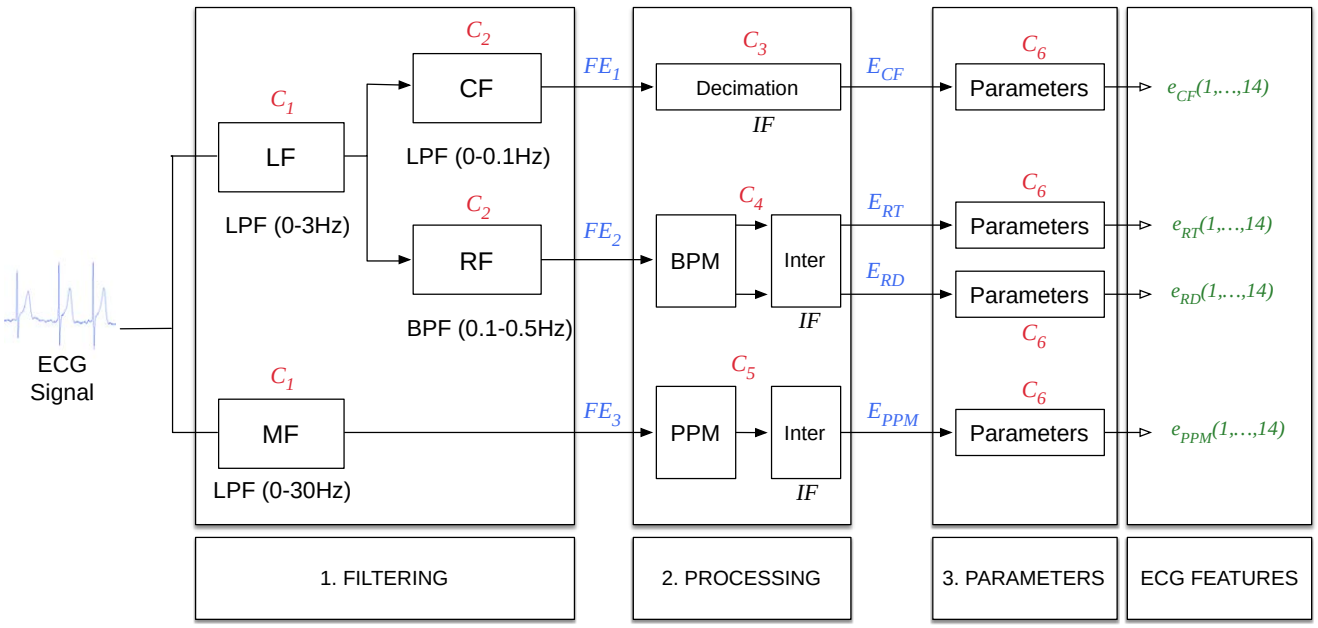

Figure 6. ECG-based feature extraction scheme.

- Step 1: Filtering. The filtering step, as its name indicates, is a step in which the raw ECG measurement is filtered into different frequency bands. First, the signal is low-pass filtered with a

cutoff frequency of 0.5 Hz (Low Frequency (LF) block) and then low-pass filtered with a cutoff frequency of 30 Hz (Medium Frequency (MF) block). In both cases, the filter order is $N_1 = 100$. The first filter is an anti-aliasing filter, which allows the use of interpolated finite impulse response (IFIR) filters [1]. Thus, the output of this anti-aliasing filter is applied to two different IFIR filters with a stretch factor of $SF = 25$, both with order $N_2 = 1150$.

The first IFIR (Continuous Frequency (CF) block) is a low-pass filter with a cutoff frequency of 0.1 Hz, and from this block, we obtain the first filtered signal FE_1.The second block (Respiration Frequency (RF) block) is a band-pass filter with cutoff frequencies of 0.1 Hz and 0.5 Hz, from which the filtered signal FE_2 is obtained. Finally, the last obtained filtered signal is FE_3.

Each filter in this step has a different computational cost due to the specific structure and the filter order. This computational cost is measured in the number of simple operations per second and affects the global number of operations in the features of the final system N_{op}. In this case, we use a filter with an order of $N_1 = 100$ for the LF and MF blocks. Thus, if the sampling frequency for the ECG measurement F_{ECG} is 250 Hz, then the number of simple operations per second is $C_1 = N_1 * F_{ECG} = 25,000$ operations per second. For the IFIR filters, the number of operations per second is denoted as C_2, and it is different due to the filter structure, because this filter is an IFIR filter, as shown in Equation (1):

$$C_2 = \frac{N_2 \cdot F_{ECG}}{SF} \tag{1}$$

Thus, we obtain $C_2 = 11,500$ operations per second.

- Step 2: Processing. In this step, we used different algorithms for each signal obtained in Step 1. The signal FE_1 is decimated to an intermediate frequency $IF = 50$ Hz, using $C_3 = 3750$ operations per second. We selected this value because it is sufficient for extracting all information from the signal and allows standardization of the blocks in the next step.

  The signal known as FE_2 is processed to obtain information from the breath. For this purpose, we use the block denominated beats per minute (BPM). This block considers the signal to be sine shaped, and it periodically determines the minimum and the maximum values of the signal, thus allowing estimation of the number of breaths per minute and the amplitude of these breaths. These values are used by the next block, denominated as "inter", that interpolates the signals by generating two Intermediate Frequency (IF)signals using piecewise constant interpolation to the last known value. The first signal known as E_{RT} represents the breaths per minute interpolated to the IF, and the second signal known as E_{RD} represents the amplitude for each breath interpolated to the IF. This process takes $C_4 = 9050$ operations per second.

  The last signal provided by Step 2 is known as E_{PPM} and is obtained through evaluation of the pulsations per minute (PPM). The PPM block uses a simple algorithm based on thresholding of the five-sample differentiation of the signal FE_3, thus estimating the position of the pulses using $C_5 = 8800$ operations per second.

  For the computational complexity of the blocks of this step, the number of simple operations required was evaluated for each block of the step.

- Step 3: Parameters. This step is necessary for obtaining the parameters that contain relevant information for monitoring the SNS. For this purpose, we calculated the 13 different parameters,

listed in Table 1 with the corresponding required number of instructions per second C_6. It is important to note that in the case of the trimmed mean, the median and percentiles data must be sorted, which consumes nearly all of the operations required for the cases ($C_6 = 27,580$). Therefore, in the case in which several parameters of this type are evaluated for the same signal, the data must be sorted only once, thus reducing the number of operations.
Furthermore, with the aim of characterizing the baseline of each signal, the last parameter denominated as baseline was calculated, totaling 14 parameters per signal. This baseline represents the long-term mean value of the signal and is calculated using a first order low-pass IIR (Infinite Impulse Response) filter. Because we use four signals (E_{CF}, E_{RT}, E_{RD} and E_{PPM}) and 14 possible parameters, the number of available features for ECG measurement is 56.

Table 1. List of parameters and the number of operations per second required.

Parameter	C_6 **(Operations Per Second)**
Mean	300
Standard deviation	1201
Trimmed mean of 25%	27,805
Median	27,580
Skewness	2101
Kurtosis	2701
Maximum	300
Minimum	300
Percentile 25%	27,580
Percentile 75%	27,580
Geometric mean	3901
Harmonic mean	3301
Mean absolute deviation	1200
Baseline	550

3.1.2. Features for TEB Measurement

For this second measurement, the procedure used to obtain the features is quite similar to the one used in the case of the ECG measurement, producing a total of 56 TEB-based features. Figure 7 shows the TEB features scheme, that again contains three different steps with a structure similar to that described for ECG.

For the sake of simplicity, only two significant differences in the blocks of the ECG are detailed. These differences are:

- The filters in the first step are different due to the use of a different sampling rates of $F_{TEB} = 100$ Hz. All signals from this step are determined using IFIR filters because the estimation of the PPM from the TEM is performed in a different manner.
- Because the shape of the pulse-related component in the TEB is completely different from the typical shape of the ECG signal, the algorithm for determining the PPM uses the BMP block, with parameters adapted to the properties of the signal.

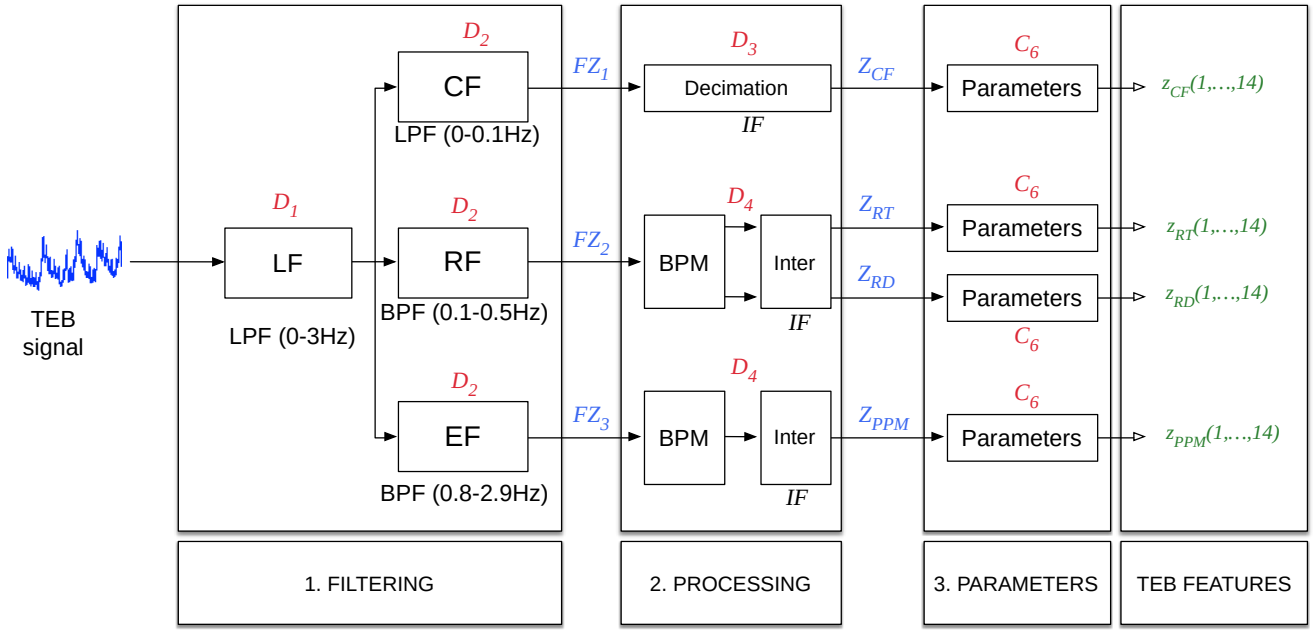

Figure 7. Thoracic electrical bioimpedance (TEB)-based feature extraction scheme.

This computational cost is different from the one obtained for the ECG-based features, because the sampling frequency is different, but equations similar to those described above can be used: $D_1 = N_1 \cdot F_{TEB}$ and $D_2 = N_2 \cdot F_{TEB}/SF$, where now $SF = 10$, $N_1 = 100$ and $N_2 = 400$. Thus, in the case of TEB, $D_1 = 10,000$, $D_2 = 4000$, $D_3 = 900$ and $D_4 = 2116$.

3.2. Classification

The classification process corresponds to the second block of Figure 5. The classifier block uses the input vector composed of the selected features in order to estimate the associated class, and several types of classifiers can be used for this purpose. In this work, we tested the use of linear classifiers [18], quadratic classifiers [19] and neural networks [20]. After several tests, we observed that the best results for this specific study were obtained using neural networks, specifically a multilayer perceptron (MLP) with 10 neurons, which represents a good tradeoff between computational cost after training and performance in terms of classification error rate. Figure 8 shows an example of the use of an MLP. An input vector $\mathbf{x} = [x(1), \ldots, x(N)]$ composed of a set of N extracted features is used as the input. In this work, we use one hidden layer composed of 10 tan-sigmoidal neurons, and the number of components M of the output vector $\mathbf{y} = [y(1), \ldots, y(M)]$ depends on the experiment and matches the number of classes in the problem at hand. The decision is a function of which term $y(m)$ is maximal. The MLPs were trained using the Levenberg–Marquardt algorithm and using a validation set that provides an early stop in the training process to minimize the loss of generalization due to overtraining.

The proposed MLP classifier and the feature extraction system were implemented in the smartphone described in Section 2 using the full set of features, to assess whether the system is suitable for real-time applications using currently available smartphones. After four hours of full performance, the battery level decreased by an additional 10%, compared to the standard decrease of the battery level in sleep mode, using less than 6% of the CPU resources of the smartphone. Further experiments demonstrated

that the battery consumption was primarily due to the Bluetooth communication with the ECGZ2 device, because similar results were obtained in the case of switching off the feature extraction and the classification blocks.

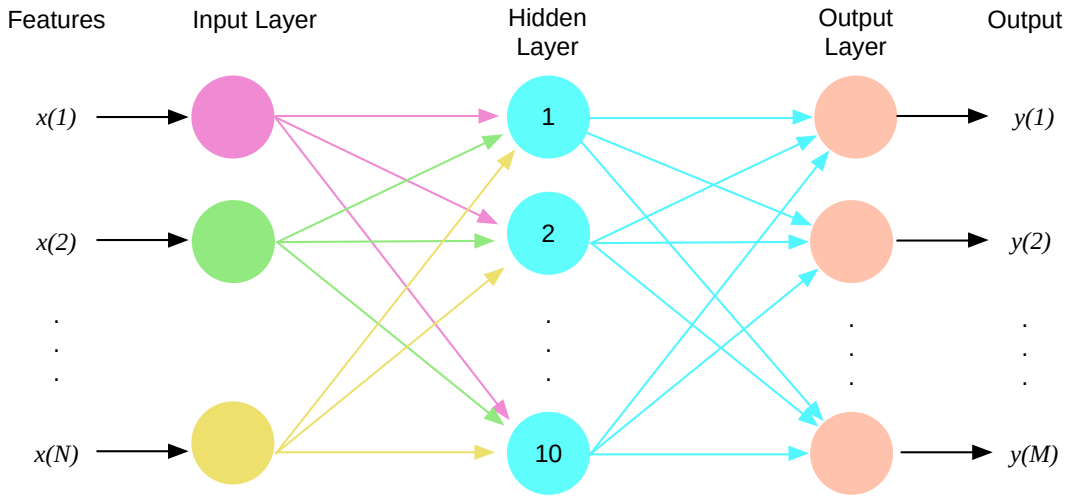

Figure 8. Multilayer perceptron scheme.

3.3. Feature Selection

Selection of a suitable reduced set of features is one of the key points in the design of classification systems for real-time stress analysis. The use of a large set of features (even the full set composed of 56 ECG-based features and 56 TEB-based features, totaling 112 features) might cause problems in the generalization ability of the obtained results, resulting in degraded system performance in real scenarios. For this purpose, we reduced the amount of features used in the classification based on the objectives: first, improving the performance to avoid overtraining and, second, reducing the computational complexity of the final solution.

Numerous algorithms are available that are aimed at selecting the best features from a global set, and in recent years, evolutionary algorithms have became a standard solution for solving this type of problem. These algorithms apply evolutionary laws to a generic population of possible solutions to meta-heuristically find the best possible solution [21,22]. In particular, genetic algorithms can be successfully applied to the problem of feature selection [23], and they have been successfully used in different research areas, such as speech processing [24] or optimization of an economic dispatch problem [25]. With these algorithms, it is possible to find the best features that achieve the maximum efficiency, which in our work is defined by low classification error with a constrained global number of operations per second N_{op}.

In our problem, we seek the best reduced set of features that aids the system in performing proper classification. For this purpose, a "population" of possible sets of features is evaluated with the goal of maximizing the percentage of correct classification. Because several possible solutions must be tested, we use linear classifiers that allow training and testing to be performed much faster than with NNs. Moreover, constraints can be easily added to genetic algorithms. In this case, we limited the maximum number of operations per second ($N_{op} < N_{max}$). Therefore, the algorithm must find the best set of features using less than N_{max} operations per second.

To avoid loss of generalization in the results while maximizing accuracy in the estimation of the error rate, k-fold cross-validation was used in the experiments, with k set equal to the number of subjects available in the design database. Thus, the data were divided into k folds or subsets containing data from each subject, and each time, the registers from one given subject are used as a test set, with the data from the remaining $k-1$ subjects used for the design tasks. Thus, the design and test process for the global system (feature selection, classifier design and error estimation using k-fold cross-validation) is performed following the described procedure:

- In each iteration of the k-fold cross-validation process, the recordings from the i-th subject are selected as a test set, and the recordings from the remaining $k-1$ subjects are used as a design set.
- The design test is used to determine the best subset of features by applying a genetic algorithm. In this process, the following steps are described:
    1. A "population" of 200 combinations of features is randomly generated.
    2. If there are two combinations with exactly the same set of features, one of them is modified by randomly replacing one of the features.
    3. For each combination in the population, if the associated number of instructions per second N_{op} is greater than the maximum N_{max}, then a feature is randomly removed. This step is repeated as many times as necessary. If all of the features of a given combination are removed, then one feature is added at random until the condition $N_{op} < N_{max}$ is satisfied.
    4. Each combination is ranked using the mean squared error of a least squares linear classifier measured using a $(k-1)$-fold cross-validation process over the corresponding design set.
    5. The best 20 combinations of the population are selected as "survivals" and are used to generate a new population of 200 new solutions using the random crossover of two parents.
    6. Mutations are added to the population by changing a feature with a probability of 10%. It is important to highlight that the best individual of each population remains unaltered. The process iterates in Step 2 until 100 generations are evaluated.
- To avoid a local minimum in the optimization method, the feature selection process using the genetic algorithm is repeated five times with random initial populations. The final combination is selected as the best combination of all final populations. This solution renders exceptionally good results with a required number of operations per second N_{op} that is less than the constraining value N_{max}.
- Once the best combination is finally selected, the obtained reduced set of features is used to train an MLP with 10 neurons. The design set is randomly subdivided into a training set containing the recordings of 90% of the individuals in the database, and the remaining data are used as a validation set to control the training process using an early stop constraint. To avoid local minima, the full training process is repeated five times, and the best network in terms of error over the design set is selected.

4. Description of the Experiments

To evaluate the performance of our system, a complete database was created in which stress and emotions were elicited through different methods. The experiments used to create the database were run

with $k = 40$ subjects. The subjects consisted mainly of students and climbers aged 20 to 49 and included 12 females and 28 males. The total duration of the complete experiment was approximately 90 min. The experiments were recorded in a laboratory and used to generate a database.

All of the experiments were performed under the conditions of respect for individual rights and ethical principles that govern biomedical research involving humans, and written informed consent was obtained from all participants. The experiments were approved by the Research Ethics Committee at the University of Alcala, and the protocol number assigned to this experiment is CEI: 2013/025/201130624.

A set of segments extracted from several validated movies was used to elicit emotion/emotional stress [26], and a set of games based on mental arithmetic were used to elicit mental load [27–29]. Finally, to elicit physical load, the participant climbed up and down stairs for five minutes.

The experiment consists of six stages in which the subject must follow instructions given by a computer, with each stage consisting of a different task. Figure 9 shows the different stages, which are explained as follows:

- Stage 1: In this stage, the subject must watch a fragment of the nature BBC documentary film "Earth" two times. The fragment lasts from the timestamp 00:00:45 to 00:07:06. The first time, the subject simply watches the movie, and the second time, he/she must continuously note the felt emotion from a set of emotions, with the aim of assessing the elicited emotion. We labeled this stage as the neutral state.
- Stage 2: A game based on addition was specifically developed for the second stage. A sum of two digits is shown on the screen; the subject must do the sum mentally and click the correct solution from a set of possible solutions. The number of digits in the to sum increases from two to five every 25 sums. The difficulty of the task is automatically adapted to the ability of the user, such that if the subject responds correctly, less time is available for the next sum, and if he/she does not complete the sum in the time estimated, the time available for the next sum is increased. Each time that the user fails, a disgusting and stressful sound is played. The duration of this stage varies from five and seven minutes depending on the skill of the subject.
- Stage 3: In this stage, the subject has the option to choose among three different films, validated to elicit sadness:
  - "American History X" (1998) by Savoy Pictures, The Turman-Morriset Company (Christian, MO, USA) [30]. This movie is assumed to elicit strong emotional arousal in participants [31].
  - "I Am Legend" (2007) by Warner Bross. This movie is a post-apocalyptic science fiction/horror film [32]. The selected movie fragments were the most impactful such that they could induce a loaded emotional charge.
  - "Life is beautiful" (1997) by Miramax [33]. Again, the fragments used were representative in order to induce sadness [34].

In all cases, scenes with a total duration of approximately 12 min were selected, and each participant watched the selected movie twice. The first time, the subject simply watches the movie, and the second time, he/she must continuously note the felt emotion from a set of emotions, with the aim of assessing the elicited emotion.

- Stage 4: In this stage, the subject must play the well-known game "Tetris". This game was used to elicit a workload in several papers, such as [35]. To intensify the mental load, we added stressful sounds and increased the rhythm of the game. The difficulty of the game varies from easiest to hardest and attempts to apply the highest work load to the subject. Thus, when the participant removes rows, the speed is slightly increased, and when he/she loses, the game restarts again with a speed slightly slower than the speed at the end of the previous game. The duration of this stage varies from 5 to 7 min depending on the skill of the subject.
- Stage 5: The last film fragment was selected from "Cannibal Holocaust" (1980) by F.D Cinematografica [36] and was intended to generate disgust, which represents a strong emotional load [37]. The duration of the fragments is close to three minutes, and again, each participant watches the selected movie twice.
- Stage 6: The aim of this stage is to check the functionality of the system (vest + algorithms) with the moving subject and to elicit physical workload. The experiment was performed at university facilities in a location with three floors. For this test, the subject must climb up and down the stairs quickly for 5 min.

As we can see in Figure 9, before each stage of the experiment, there is a baseline stage, denominated "instructions/resting", which was primarily used to rest and to read the instructions of the next stage. This way, the subjects are not continuously experiencing mental, emotional or physical load, which could lead to a decrease in the performance. The length of this inter-stage interval was about 5 min approximately, the time required to achieve a stable hemodynamic condition [38]. Longer resting times have not been considered, since they would suppose an excessive total length of the experiment, which might fatigue the subjects.

To study the ability of the sensor-based system to analyze stress load, three different analyses of the generated database were considered:

- Analysis 1: In the first analysis, classification of the type of activity was used as the target of the analysis. For this purpose, four different situations were used as classes ($M = 4$):
  - Neutral activity, which was registered during the last 140 s of the first movie, *i.e.*, the documentary; thus, considering that each individual watched each movie twice, we obtained a total of 280 s for each individual in the database.
  - Emotional activity, which was characterized during viewing of the last 70 s of the second and third movies; therefore, we again obtained a total of 280 s per individual.
  - Mental activity, which was registered during the last 140 s of both games, produced 280 s in total.
  - Physical activity was registered during the last 280 s of the physical activity stage.
- Analysis 2: In the second analysis, the objective was to distinguish among the emotional states during the viewing of the movies, according to three different emotions ($M = 3$): neutral emotion, sadness and disgust. For this purpose, recordings from the last 200 s of each movie were used, generating 400 s for the neutral emotion (the documentary), 400 s for sadness (the second movie) and 400 s for disgust (the third movie).

- Analysis 3: In the third analysis, the objective was to distinguish between low mental activity at the beginning of the games and high mental load at the end of the games ($M = 2$). The first 110 s of each game were labeled as low mental activity, and the last 110 s of each game were labeled as high mental activity (mainly due to the different difficulty of the games from the beginning to the end).

Therefore, the database is fully balanced in all three analyses.

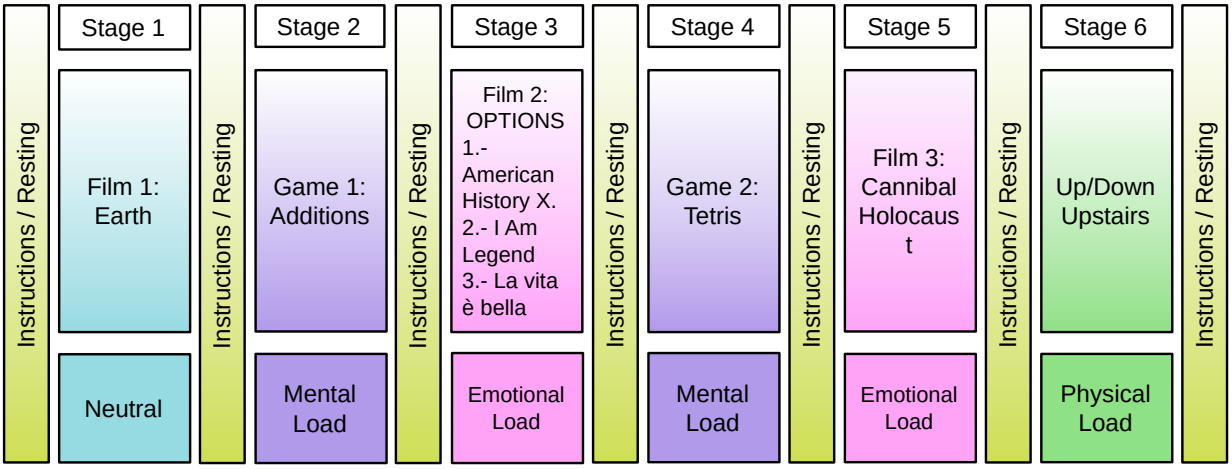

Figure 9. Scheme describing the stages of the experiment used to generate the database.

To assess elicitation of the SNS activity in the different analyses, Table 2 shows the average values for the IF signals in the different classes defined in the three analyses: type of activity, emotional state and mental activity. The two-sample Kolmogorov–Smirnov test, one of the most useful and general nonparametric methods for comparing two samples, was performed for each combination of two classes and for each IF signal. Statistically-significant differences ($p < 0.01$, significance level of 0.05) were found in all comparisons performed for the E_{RT}, E_{RD}, Z_{CF} and Z_{RT} signals in the case of Analysis 1 and the E_{RD}, Z_{CF} and Z_{RT} signals in the case of Analysis 2. These results demonstrate the correct elicitation of the emotions in the database.

Table 2. Average values for the eight IF signals in the different classes defined in the three analyses: type of activity, emotional state and mental activity.

IF Signal	Analysis 1 Type of Activity				Analysis 2 Emotional State			Analysis 3 Mental Activity	
	Neutral	**Emotional**	**Mental**	**Physical**	**Neutral**	**Sad**	**Disgust**	**Low**	**High**
E_{CF}	4.92	4.93	4.92	5.36	4.92	4.93	4.92	4.92	4.92
E_{RT}	28.17	29.62	27.69	24.75	27.95	29.53	28.46	28.76	27.59
E_{RD}	0.32	0.40	0.45	1.20	0.32	0.43	0.43	0.44	0.45
E_{PPM}	72.07	70.99	74.62	130.43	72.10	70.21	71.12	74.37	74.77
Z_{CF}	5.61	6.33	5.74	7.89	5.60	5.74	6.89	5.75	5.72
Z_{RT}	19.44	20.10	20.50	27.17	19.45	19.85	20.27	20.97	20.46
Z_{RD}	0.09	0.16	0.27	0.67	0.09	0.09	0.23	0.19	0.25
Z_{PPM}	74.36	71.99	74.30	93.86	74.03	72.62	71.80	74.34	74.35

5. Results

This section discusses the results obtained by the proposed system in the different analyses. In the first approach, the results are shown as a function of classification error probability *versus* number of operations per second (N_{op}), for different values of N_{max} (maximum number of operations per second).

5.1. Analysis 1: Activity Identification

In the first analysis, we used four different types of activities: neutral, emotional, mental and physical. The algorithm described in Section 3.3 was applied 100 times, for values of N_{max} from 20,000 to 200,000 in steps of 20,000. Figure 10 shows the box plot of the obtained results, which represent the classification error probability *versus* the number of operations per second N_{op}, for different values of N_{max}. We observe that for 20,000 N_{op}, the mean error probability obtained is approximately 33%. The error probability decreases as the value of N_{op} increases up to 80,000.

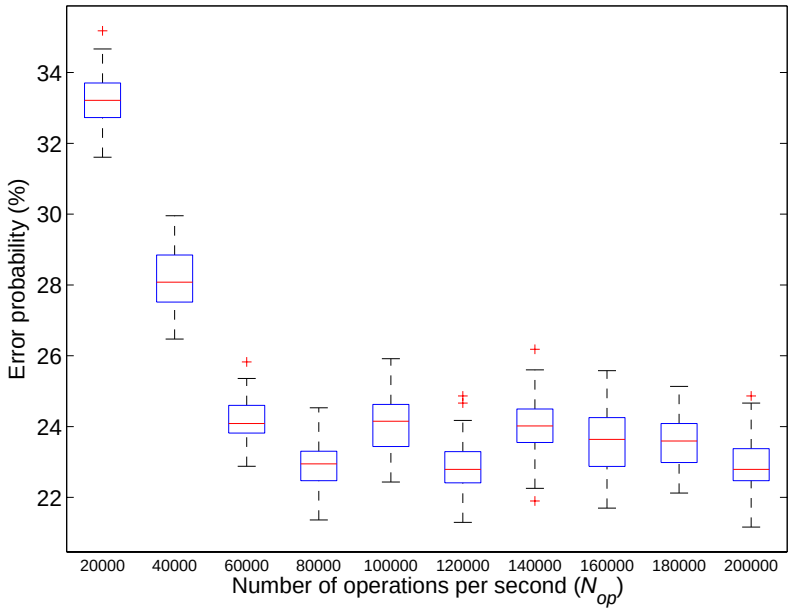

Figure 10. Box plot of the probability of error obtained by the classifiers for different values of the maximum number of operations per second (N_{op}) particularized for Analysis 1: type of activity.

To illustrate the obtained results and the differences of classification errors between classes in detail, Table 3 shows the confusion matrix and percentage of classification error (error probability) for each class defined in Analysis 1 using a maximum number of 80,000 operations per second ($N_{op} < 80,000$). The confusion matrix shows how the classifier encounters additional difficulty in distinguishing between emotional and mental classes, with physical activity as the most easily recognizable class.

The average error obtained with 80,000 N_{op} is approximately 21.23%, corresponding to the use of approximately 12 features. All features selected by the genetic algorithm are based on the ECG measurement. More concretely, the main features used are the mean, the standard deviation, the kurtosis, the minimum, the skewness and the baseline of the E_{CF} signal, and the mean, the standard deviation, the harmonic mean and the baseline of the E_{PPM} signal.

Table 3. Confusion matrix and percentage of classification error (error probability) for each class using a maximum number of 80,000 operations per second ($N_{op} < 80,000$), particularized for Analysis 1: type of activity.

True Class	Predicted Class				% Error Probability
	Neutral	Emotional	Mental	Physical	
Neutral	971	3	146	0	13.30%
Emotional	12	881	199	28	21.34%
Mental	128	374	604	14	46.07%
Physical	0	37	10	1073	4.20%
		Average			21.23%

For this first analysis, the obtained average error rate in this real-time activity identification is 21.23%, which is slightly better than those obtained from the heart rate (23.72%) and the respiration rate (24.40%) in [9] and significantly better than the 31% error rate obtained from HRV analysis in [39].

5.2. Analysis 2: Emotional State

In the second analysis, the objective was to distinguish among three emotions: neutral emotion, sadness and disgust. Again, the algorithm described in Section 3.3 was performed 100 times for values of N_{max} from 20,000 to 200,000 in steps of 20,000. Figure 11 shows the box plot of the obtained results and represents the classification error probability for different values of N_{max}. We observe that the mean error probability obtained is the lowest for 60,000 N_{op}.

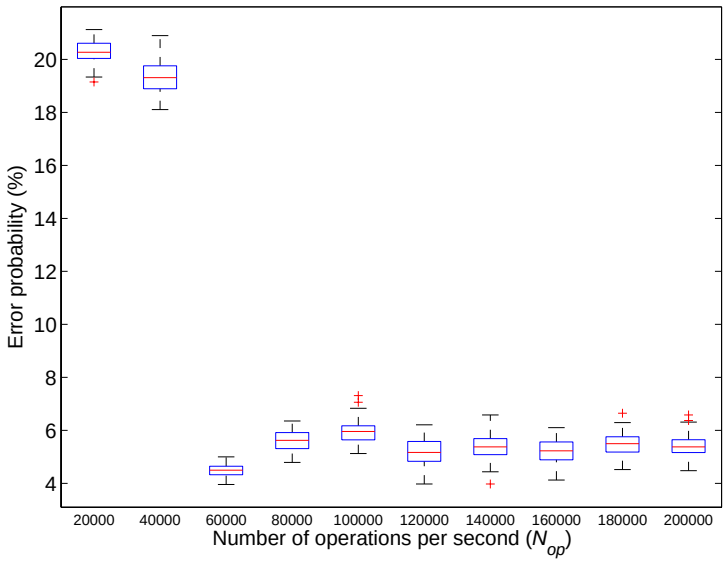

Figure 11. Box plot of the probability of error obtained by the classifiers for different values of the maximum number of operations per second (N_{op}) particularized for Analysis 2: emotional state.

Table 4 shows the confusion matrix and percentage of classification error (error probability) for each class of the second analysis using a maximum of 60,000 operations per second ($N_{op} < 60,000$). In this

case, the average error probability obtained is 4.77%, and the confusion between sadness and disgust is highlighted. The main features selected by the genetic algorithm in this case are the mean and the baseline of the E_{CF} signal and the mean and the baseline of the Z_{PPM} signal.

Table 4. Confusion matrix and percentage of classification error (error probability) for each class using a maximum number of 60,000 operations per second ($N_{op} < 60,000$), particularized for Analysis 2: emotional state.

True Class	Predicted Class			% Error Probability
	Neutral	Sadness	Disgust	
Neutral	1584	16	0	1.00%
Sadness	12	1496	92	6.50%
Disgust	0	109	1491	6.81%
Average				4.77%

For this analysis, the obtained error rate is 4.77%, which is a result considerably lower than the 14% error rate obtained in [40], in which facial electromyogram, respiration, electrodermal activity and electrocardiogram signals are used to classify five emotional classes (high stress, low stress, disappointment, euphoria and neutral face).

5.3. Analysis 3: Mental Activity

This analysis contains two different classes: low and high mental activity. Figure 12 displays the obtained results. Once again, low N_{op} produces the highest error and an increase of N_{op} reduces the error. In this case, the best performance is obtained for 80,000 N_{op}.

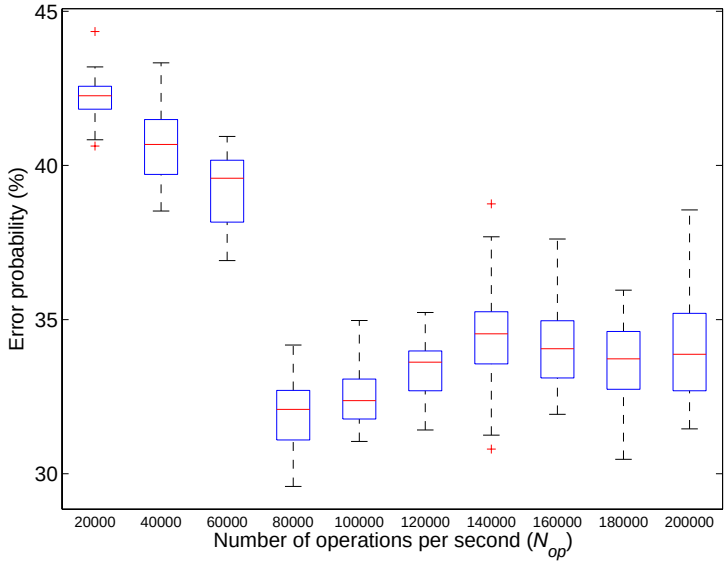

Figure 12. Box plot of the probability of error obtained by the classifiers for different values of the maximum number of operations per second (N_{op}) particularized for Analysis 3: mental activity.

Table 5 shows the confusion matrix and percentage of classification error (error probability) for each class using a maximum number of 80,000 operations per second ($N_{op} < 80,000$), specific to Analysis 3: mental activity. In this case, the average error probability obtained is 32.33%. The main features selected by the genetic algorithm in this case are the minimum and the maximum of the signal Z_{RT}; the mean, the skewness, the harmonic mean and the baseline of Z_{CF}; the minimum, the maximum, the skewness, the kurtosis and mean absolute deviation of Z_{RD}; and the baseline of E_{CF}.

Table 5. Confusion matrix and percentage of classification error (error probability) for each class using a maximum number of 80,000 operations per second ($N_{op} < 80,000$), particularized for Analysis 3: mental activity.

True Class	Predicted Class		% Error Probability
	Low Mental Load	High Mental Load	
Low mental load	572	308	35.00%
High mental load	261	619	29.66%
	Average		32.33%

In this third analysis, the obtained average error rate is 32.33%. The error rate for a similar analysis was higher using ECG or EOG (Electrooculogram) signals [41], but significantly lower (14% error rate) when the EEG signal was used.

6. Conclusions

Analysis of the ECG and TEB measurements recorded with sensorized instrumentation can be highly useful for detecting high levels over long periods of time or sudden increases in mental overload, emotional response or physical activity for workers in professions with associated risks, such as fire-fighters, first responders, police and soldiers, among others. The designed software performs quite well with $N_{op} = 60,000$ operations per second for the emotional state experiments (approximately 5% of estimated classification error) and with $N_{op} = 80,000$ operations per second for the determination of the type of activity (approximately 21% of estimated classification error) and mental overload (approximately 32% of estimated classification error). In two out of the three classification task, the feature selection algorithm selected features obtained from both ECG and TEB physiological measurement. For task identification, only information from the ECG measurement was selected. This real-time solution was successfully implemented in an actual smartphone.

The current wearable biomedical measurements and smartphone technologies allow realistic implementation of personalized monitoring systems for the detection of stress, mental overload and emotional status in real time. The combination of these currently existing technologies could potentially enable solutions for monitoring of signs related to the development of stress-related diseases at work or prompt detection of acute increases in stress levels in specifically dangerous job scenarios. Such specialization would require further investigations to trim the classification engine to target the new required specifications. Although, these tasks are certainly not trivial, from the current stand point, they appear completely feasible.

Acknowledgments

This work has been funded by the Spanish Ministry of Defense through the "COINCIDENTE" (*COoperación en INvestigación CIentífica y Desarrollo EN TecnologíasEstratégicas*—Cooperation in Scientific Research and Development in Strategic Technologies) program (DGAM DNR 1003211003500).

Author Contributions

Inma Mohino-Herranz and Roberto Gil-Pita developed the database, the classifications algorithms and features. Fernando Seoane and Javier Ferreira implemented the sensorized garments. Fernando Seoane conceived of the wearable measurement system. Inma Mohino-Herranz wrote this manuscript, and Fernando Seoane and Manuel Rosa-Zurera participated in the revision of the manuscript, supporting the writing process.

Conflicts of Interest

The authors declare no conflicts of interest.

References

1. Mehrnia, A.; Willson, A.N., Jr. On optimal IFIR filter design. In Proceedings of the 2004 IEEE International Symposium on Circuits and Systems, Vancouver, BC, Canada, 23–26 May 2004 ; pp. 111–133.
2. Le Fevre, M.; Matheny, J.; Kolt, G.S. Eustress, distress, and interpretation in occupational stress. *J. Manag. Psychol.* **2003**, *18*, 726–744.
3. The American Institute of Strees. What is Stress? Available online: http://www.stress.org/what-is-stress/ (accessed on 29 September 2015).
4. Sloan, R.P.; Shapiro, P.A.; Bagiella, E.; Boni, S.M.; Paik, M.; Bigger, J.T.; Gorman, J.M. Effect of mental stress throughout the day on cardiac autonomic control. *Biol. Psychol.* **1994**, *37*, 89–99.
5. Jansen, A.; van Nguyen, X.; Karpitskiy, V.; Mettenleiter, T.C.; Loewy, A.D. Central command neurons of the sympathetic nervous system: Basis of the fight-or-flight response. *Science* **1995**, *270*, 644–646.
6. Taylor, S.E.; Klein, L.C.; Lewis, B.P.; Gruenewald, T.L.; Gurung, R.; Updegraff, J.A. Biobehavioral responses to stress in females: Tend-and-befriend, not fight-or-flight. *Psychol. Rev.* **2000**, *107*, 411–429.
7. Cannon, W. *The Wisdom of the Body*; W.W. Norton: New York, NY, USA, 1932.
8. Silverthorn, D.U.; Ober, W.C.; Garrison, C.W.; Silverthorn, A.C.; Johnson, B.R. *Human Physiology: An Integrated Approach*; Pearson/Benjamin Cummings: San Francisco, CA, USA, 2009.
9. Seoane, F.; Mohino, I.; Ferreira, J.; Alvarez, L.; Buendia, R.; Ayllón, D.; Llerena, C.; Gil-Pita, R. Wearable biomedical measurement systems for assessment of mental stress of combatants in real time. *Sensors* **2014**, *14*, 7120–7141.

10. Gullette, E.C.; Blumenthal, J.A.; Babyak, M.; Jiang, W.; Waugh, R.A.; Frid, D.J.; Krantz, D.S. Effects of mental stress on myocardial ischemia during daily life. *Jama* **1997**, *277*, 1521–1526.
11. Agrafioti, F.; Hatzinakos, D.; Anderson, A.K. ECG pattern analysis for emotion detection. *IEEE Trans. Affect. Comput.* **2012**, *3*, 102–115.
12. Healey, J.; Picard, R. Detecting stress during real-world driving tasks using physiological sensors. *IEEE Trans. Intell. Trans. Syst.* **2005**, *6*, 156–166.
13. Healey, J. Wearable and Automotive Systems for Affect recognition From Physiology. Ph.D. Thesis, Department of Electrical Engineering and Computer Science, Massachusetts Institute of Technology, Cambridge, MA, USA, 2000.
14. McCraty, R.; Atkinson, M.; Tiller, W.A.; Rein, G.; and Watkins, A.D. The effects of emotions on short-term power spectrum analysis of heart rate variability. *Am. J. Cardiol.* **1995**, *76*, 1089–1093.
15. Lee, C.; Yoo, S.K.; Park, Y.; Kim, N.; Jeong, K.; Lee, B. Using neural network to recognize human emotions from heart rate variability and skin resistance. In Proceedings of the 27th Annual International Conference of the Engineering in Medicine and Biology Society, Shanghai, China, 17–18 January 2006; pp. 5523–5525.
16. Billman, G.E. The LF/HF ratio does not accurately measure cardiac sympatho-vagal balance. *Front. Physiol.* **2013**, doi:10.3389/fphys.2013.00026.
17. Piccirillo, G.; Vetta, F.; Fimognari, F.L.; Ronzoni, S.; Lama, J.; Cacciafesta, M.; Marigliano, V. Power spectral analysis of heart rate variability in obese subjects: Evidence of decreased cardiac sympathetic responsiveness. *Int. J. Obes. Relat. Metab. Disord.* **1996**, *9*, 825–829.
18. Mladenić, D.; Brank, J.; Grobelnik, M.; Milic-Frayling, N. Feature selection using linear classifier weights: Interaction with classification models. In Proceedings of the 27th Annual International ACM SIGIR Conference on Research and Development in Information Retrieval, Sheffield, UK, 25–29 July 2004; pp. 234–241.
19. Sharma, N.; Pal, U.; Kimura, F.; Pal, S. Recognition of off-line handwritten devnagari characters using quadratic classifier. In *Computer Vision, Graphics and Image Processing*; Springer Heidelberg: Berlin, Germany, 2006; pp. 805–816.
20. Hagan, M.T.; Demuth, H.B.; Beale, M.H; Orlando, D.J. *Neural Network Design*; Pws Pub Co.: Boston, MA, USA, 1996.
21. Haupt, R.L.; Haupt, E. *Practical Genetic Algorithms*; John Wiley and Sons Inc.: Hoboken, NJ, USA, 2004.
22. Chambers, L.D. Practical Handbook of Genetic Algorithms: Complex Coding Systems; CRC Press: Boca Raton, FL, USA, 1998.
23. Davis, L. *Handbook of Genetic Algorithms*; Van Nostrand Reinhold: New York, NY, USA, 1991.
24. Mohino, I.; Goni, M.; Alvarez, L.; Llerena, C.; Gil-Pita, R. Detection of emotions and stress through speech analysis. In Proceedings of the Signal Processing, Pattern Recognition and Application-2013, Innsbruck, Austria, 12–14 February 2013.
25. Walters, D.C.; Sheble, G.B. Genetic algorithm solution of economic dispatch with valve point loading. *IEEE Trans. Power Syst.* **1993**, *8*, 1325–1332.
26. Gross, J.J.; Levenson, R.W. Emotion elicitation using films. *Cogn. Emot.* **1995**, *9*, 87–108.

27. Pellouchoud, E.; Smith, M.E; McEvoy, L.; Gevins, A. Mental effort-related EEG modulation during video-game play: Comparison between Juvenile subjects with Epilepsy and normal control subjects. *Epilepsia* **1999**, *40*, 38–43.
28. Turner, J.R.; Carroll, D. Heart rate and oxygen consumption during mental arithmetic, a video game, and graded exercise: Further evidence of metabolically-exaggerated cardiac adjustments? *Psychophysiology* **1985**, *22*, 261–267.
29. Carroll, D.; Turner, J.R.; Rogers, S. Heart rate and oxygen consumption during mental arithmetic, a video game, and graded static exercise. *Psychophysiology* **1987**, *24*, 112–118.
30. Smith, P. American history X. In *America First: Naming the Nation in US Film*; Routledge: Abingdon, UK, 2007; pp. 244–258.
31. Giesbrecht, T.; Geraerts, E.; Merckelbach, H. Dissociative experiences are related to commissions in emotional memory. *Psychiatry Res.* **2003**, *150*, 277–285.
32. Clasen, M. Vampire Apocalypse: A Biocultural Critique of Richard Matheson's I Am Legend. *Philos. Lit.* **2010**, *34*, 313–328.
33. Von Jagow, B. *Representing the Holocaust, Kertész's Fatelessness and Benigni's La vita è bella*; Purdue University Press: West Lafayette, IN, USA, 2002.
34. Fernández, C.; Pascual, J.C.; Soler, J.; García, E. Validación española de una batería de películas para inducir emociones. *Psicothema* **2011**, *23*, 778–785. (In Spanish)
35. Denot-Ledunois, S.; Vardon, G.; Perruchet, P.; Gallego, J. The effect of attentional load on the breathing pattern in children. *Int. J. Psychophysiol.* **1998**, *29*, 13–21.
36. Fenton, H.; Grainger, J.; Castoldi, G.L. *Cannibal Holocaust: And the Savage Cinema of Ruggero Deodato*; Fab Press: Surrey, UK, 1999.
37. Jackson, N. *Cannibal Holocaust, Realist Horror, and Reflexivity*; Post Script: Jacksonville, FL, USA, 2002; pp. 32–45.
38. Palatini, P. Recommendations on how to measure resting heart rate. *Medicographia* **2009**, *31*, 414–419.
39. Choi, J.; Gutierrez-Osuna, R. Using heart rate monitors to detect mental stress. In Proceedings of the 6th IEEE International Workshop on Wearable and Implantable Body Sensor Networks, Berkeley, CA, USA, 3–5 June 2009; pp. 219–223.
40. Katsis, C.D.; Ganiatsas, G.; Fotiadis, D.I. An integrated telemedicine platform for the assessment of affective physiological states. *Diagn. Pathol.* **2006**, *1*, doi:10.1186/1746-1596-1-16.
41. Laurent, F.; Valderrama, M.; Besserve, M.; Guillard, M.; Lachaux, J. P.; Martinerie, J.; Florence, G. Multimodal information improves the rapid detection of mental fatigue. *Biomed. Signal Process. Control* **2013** , *8*, 400–408.